

Alma Mater Studiorum – Università di Bologna

**DOTTORATO DI RICERCA IN
Meccanica e Scienze Avanzate dell'Ingegneria**

Ciclo XXVIII

Settore Concorsuale di afferenza: 09/C2

Settore Scientifico disciplinare: ING-IND/18

**FUNCTIONAL MODIFICATION OF MATERIALS AND SYNTHESIS OF
NANOSTRUCTURES BY NON-EQUILIBRIUM ATMOSPHERIC PRESSURE
PLASMA PROCESSES**

Presentata da: Anna Liguori

Coordinatore Dottorato

Relatore

Prof. Vincenzo Parenti Castelli

Prof. Vittorio Colombo

Esame finale anno 2016

I like the scientific spirit—the holding off, the being sure but not too sure, the willingness to surrender ideas when the evidence is against them: this is ultimately fine—it always keeps the way beyond open—always gives life, thought, affection, the whole man, a chance to try over again after a mistake—after a wrong guess.

Walt Whitman

Introduction	7
Outline	8
 <i>Part I</i>	
1. Conventional strategies for functional surface modification of materials	
1.1 Surface modification of biomedical polymers	22
1.2 Conventional methods for the functionalization of polymers	24
1.3 Conventional methods for the crosslinking of polymers	26
1.3.1 <i>Chemical methods</i>	27
1.3.2 <i>Physical methods</i>	29
1.4 Strategies for the fabrication of antibacterial surfaces	32
References	33
2. Plasma assisted processes for the modification of materials	
2.1 Non-equilibrium atmospheric pressure plasma for the functional modification of polymers	38
2.2 Non-equilibrium atmospheric pressure plasma sources	41
2.3 Functionalization of polymers by means of non-equilibrium plasma	44
2.3.1 <i>Plasma functionalization to improve cell adhesion</i>	45
2.3.2 <i>Plasma functionalization for biomolecules immobilization</i>	46
2.3.3 <i>Plasma preparation of antibacterial surfaces</i>	48
2.3.4 <i>Ageing of plasma functionalized polymers.</i>	40
2.4 Plasma deposition	50
2.5 Plasma induced crosslinking	52
References	53
3. Non-equilibrium atmospheric pressure plasma functionalization of electrospun scaffolds for fibroblast adhesion	
3.1 Introduction	61
3.2 Experimental part	62
3.2.1 <i>Scaffolds fabrication</i>	63
3.2.2 <i>Plasma treatment for the surface modification</i>	64
3.2.3 <i>Scaffolds characterization</i>	64
3.2.4 <i>Cell culture on scaffolds and immucytochemistry</i>	66
3.3 Results and Discussion	66
3.4 Conclusions	71

References	71
4. Non-equilibrium atmospheric pressure plasma for the immobilization of biomolecules on biomaterials	
4.1 Introduction	75
4.2 Experimental part	76
4.2.1 <i>PLLA mats fabrication</i>	76
4.2.2 <i>PLLA mats functionalization</i>	77
4.2.3 <i>Antibody conjugation</i>	79
4.2.4 <i>Characterization techniques</i>	79
4.3 Results and Discussion	80
4.4 Conclusions	85
References	85
5. Non-equilibrium atmospheric pressure plasma for materials decontamination and prevention of biofilm formation	
5.1 Introduction	88
5.2 Experimental part	89
5.2.1 <i>Specimens preparation</i>	89
5.2.2 <i>Plasma sources</i>	90
5.2.3 <i>Mechanical characterization</i>	91
5.2.4 <i>In vitro plasma antibacterial activity</i>	91
5.2.5 <i>In vitro cytocompatibility</i>	92
5.3 Results and Discussion	93
5.3.1 <i>Mechanical characterization</i>	94
5.3.2 <i>Evaluation of plasma activity in reducing bacteria adhesion</i>	95
5.3.3 <i>Evaluation of plasma activity in decontaminating early and mature biofilm</i>	98
5.3.4 <i>Evaluation of cytocompatibility of plasma treated soft reline specimens</i>	101
5.4 Conclusions	102
References	103
6. Non-equilibrium atmospheric pressure plasma for polymeric coatings deposition and nanocomposite coatings co-deposition	
6.1 Introduction	107
6.2 Experimental part	107
6.2.1 <i>Materials</i>	107
6.2.2 <i>Non-Equilibrium Atmospheric Pressure Dual Gas Plasma Jet</i>	108

6.2.3	<i>Experimental setup and operating conditions for the pPAA coating deposition</i>	109
6.2.4	<i>Experimental setup and operating conditions for the pPAA/AgNPs coating co-deposition</i>	111
6.2.5	<i>Water Contact Angle (WCA) Measurements</i>	112
6.2.6	<i>Attenuated Total Reflectance-Fourier Transform Infrared (ATR-FTIR) Spectroscopy</i>	112
6.2.7	<i>X-ray Photoelectron Spectroscopy (XPS)</i>	112
6.2.8	<i>Optical Microscope Analysis</i>	113
6.2.9	<i>Scanning Electron Microscopy</i>	113
6.2.10	<i>Antimicrobial Assay</i>	113
6.3	Results and Discussion	114
6.3.1	<i>pPAA coating deposition</i>	114
6.3.2	<i>pPAA/AgNPs coating co-deposition</i>	124
6.4	Conclusions	134
	References	135

7. Non-equilibrium atmospheric pressure plasma for crosslinking of biopolymers

7.1	Introduction	140
7.2	Experimental part	140
7.2.1	<i>Fabrication of pullulan electrospun mats</i>	141
7.2.2	<i>Fabrication of gelatin and genipin containing gelatin electrospun mats</i>	141
7.2.3	<i>Non-equilibrium atmospheric pressure DBD and crosslinking protocols</i>	142
7.2.4	<i>Characterization of pullulan crosslinked mats</i>	144
7.2.5	<i>Characterization of gelatin and genipin containing gelatin crosslinked mats</i>	145
7.3	Results and Discussion	146
7.3.1	<i>Crosslinking of pullulan electrospun mats</i>	146
7.3.2	<i>Crosslinking of gelatin and genipin containing gelatin electrospun mats</i>	151
7.4	Conclusions	158
	References	159

Part II

8. Conventional methods for the synthesis of nanoparticles	
8.1 Introduction	162
8.2 Top-down processes	162
8.3 Bottom-up processes	163
References	165
9. Cold plasma assisted processes for the synthesis of nanoparticles	
9.1 Introduction	169
9.2 Non-equilibrium atmospheric pressure plasma for nanomaterials fabrication	169
9.2.1 <i>Microplasma systems</i>	170
9.2.2 <i>Microplasmas for synthesis of nanostructures in gas and solid phase</i>	173
9.2.3 <i>Microplasmas for synthesis of nanostructures in a liquid environment</i>	175
9.2.4 <i>Microplasma for surface engineering of nanostructures in liquid phase</i>	175
9.3 Atmospheric pressure DC microplasma for the synthesis of CuO QDs	177
9.3.1 <i>Experimental part</i>	178
9.3.2 <i>Results and Discussion</i>	179
9.3.3 <i>Conclusions</i>	182
References	182
Acknowledgments	186

Introduction

Widely employed for a steadily increasing number of industrial processes and experimental studies, plasma can be considered as one of the most pervasive and promising technologies of our time.

Concerning the branch of thermal plasmas, the efforts carried out in the last two centuries have pushed this technology to assume a key role in several processes, i.e. metals cutting and welding, nanoparticles synthesis, waste reforming, leading to an accurate and almost complete knowledge on the exploitability of thermal plasmas in the industrial sector.

Conversely, the potentialities offered by non-equilibrium plasmas, especially if working at atmospheric pressure, are still far away to be totally understood, since the surprising and, sometimes, unpredictable results coming from studies carried out all over the world bring out the growing versatility of this technology and its suitability for many applications intersecting our daily lives.

Promising results in several fields, i.e. materials modification, coatings deposition, decontamination of solid and liquid substrates, stimulate the vision of the successful use of non-equilibrium atmospheric plasma, also called cold atmospheric plasma (CAP), technology, known to be highly environmentally friendly, flexible, easily scaling up or down, in substitution of conventional techniques.

Furthermore, besides the applications of CAP in the industrial sector, the results of the experimental studies performed in the field placed at the front edge of plasma research activities and referred as *Plasma medicine* highlighted that these plasmas are endowed of unique properties and characteristics, which make them suitable also for biomedical applications and medical therapies.

All these mentioned applications are made possible by specific mechanisms occurring during the interactions between plasma and treated substrate (solid, liquid, polymeric or biologic). Unfortunately, the knowledge gained so far is not enough to provide an exhaustive interpretation to these mechanisms, which are generally quite different from those of conventional processes, and an interdisciplinary approach is strongly required to improve the understanding of the plasma induced effects.

To answer to the challenging questions about the way in which plasma and its components interact with all the different substrates would enable to better control each plasma process and to further widen the fields of possible applications. Further studies are then needed, but the worthy results so far achieved jointly to the increasing number of scientific groups involved in this research field allow being optimistic regarding the achievement of this aim.

Outline

During my Ph.D studies at Alma Mater Studiorum – Università di Bologna, I have been thoroughly involved in the activities of the Research Group for Industrial Application of Plasmas (IAP group) headed by Prof. Colombo.

I focused my studies mainly on the setup and optimization of CAP-assisted processes for materials modification, coating deposition, crosslinking of polymers and synthesis of nanostructures in liquid phase. I also had the opportunity to take part to other research activities dealing with the investigation of the physical characteristics of the plasma discharge by means of the employment of diagnostic techniques and with interesting applications of CAP in the field of *Plasma medicine*.

The present dissertation, organized in two parts, is focused to present and discuss the results obtained from the research activities carried out in the wide and interesting field of plasma and materials.

The first part of the work is mainly aimed at investigating the potentialities of CAP for the modification of materials, coating deposition and crosslinking of polymers. In the first two chapters, I will briefly summarize the conventional techniques and the CAP approaches most employed to carry out the processes I dealt with during my studies. In the other chapters, organized by topic, the results achieved during my research activities in the fields of surface material modification, coating deposition and crosslinking of polymers will be presented and discussed. As reported in the respective chapters of the first part of the dissertation, some of the presented research activities and achieved results were made possible thanks to the fruitful and instructive collaborations between the IAP Group and Research Groups at University of Bologna, University of Piemonte Orientale and University of Catania. In particular, the collaborations with the Research Groups of Prof. Maria Letizia Focarete (Alma Mater Studiorum - Università di Bologna), Prof. Adriana Bigi (Alma Mater Studiorum - Università di Bologna), Prof. Laura Calzà (Alma Mater Studiorum - Università di Bologna), Prof. Lia Rimondini (University of Piemonte Orientale) and Prof. Antonino Pollicino (University of Catania) are gratefully acknowledged.

The second part of the dissertation is linked to the research activities I performed during my short term scientific mission (STSM), granted by the CMST COST Action TD1208 – Electrical Discharge with Liquids for Future Application, undertaken in Prof Mariotti's research group at Ulster University, Northern Ireland, UK. As reported in the related chapters, the STSM and the collaboration with Prof. Mariotti enabled to garner useful knowledge on the potentialities of plasma-induced chemistry in a liquid environment for the synthesis of nanostructures. Similarly to the first one, the

second part of the dissertation will first present an overview on the conventional methods for nanostructures synthesis, while the last chapter will be devoted at illustrating the plasma assisted processes for nanoparticles production and the experimental activities I performed during the STSM, aimed at synthesising nanostructures in liquid phase by means of CAP.

The presented activities were developed in the framework of the European networking projects MPNS COST Action MP1101 - Biomedical Applications of Atmospheric Pressure Plasma Technology and CMST COST Action TD1208 - Electrical Discharge with Liquids for Future Application and the FARB (Alma Mater Studiorum – Univeristà di Bologna grant for fundamental research) project PLASMAT “Plasma-assisted preparation and modification of molecular and macromolecular materials for biomedical, pharmaceutical and energy applications”, within the activities of IAP Group at Alma Mater Studiorum - Università di Bologna).

The achieved results have been reported in the following papers published or submitted to international journal:

1. A. Liguori, E. Traldi, E. Toccaceli, R. Laurita, A. Pollicino, M. L. Focarete, V. Colombo, M. Gherardi, Co-deposition of plasma-polymerized polyacrylic acid and silver nanoparticles for the production of nanocomposite coatings using a non-equilibrium atmospheric pressure plasma jet, *Plasma Processes and Polymers* 2015, DOI: 10.1002/ppap.201500143.
2. A. Liguori, A. Pollicino, A. Stancampiano, F. Tarterini, M. L. Focarete, V. Colombo, M. Gherardi, Deposition of plasma-polymerized polyacrylic acid coatings by a nonequilibrium atmospheric pressure nanopulsed plasma jet, *Plasma Processes and Polymers* 2016, 13, 375.
3. A. Liguori, L. Paltrinieri, A. Stancampiano, C. Gualandi, M. Gherardi, V. Colombo, M. L. Focarete, Solid-State Crosslinking of Polysaccharide Electrospun Fibers by Atmospheric Pressure Non-Equilibrium Plasma: A Novel Straightforward Approach, *Plasma Processes and Polymers* 2015, 12, 1195.
4. L. S. Dolci, S. D. Quiroga, M. Gherardi, R. Laurita, A. Liguori, P. Sanibondi, A. Fiorani, L. Calzà, V. Colombo, M. L. Focarete, Carboxyl Surface Functionalization of Poly(L-lactic acid) Electrospun Nanofibers through Atmospheric Non-Thermal Plasma Affects Fibroblast Morphology, *Plasma Processes and Polymers* 2012, 11, 203.
5. A. Liguori, A. Bigi, V. Colombo, M. L. Focarete, M. Gherardi, C. Gualandi, M. Oleari, S. Panzavolta, Crosslinking of gelatine by means of atmospheric pressure non-equilibrium plasma: a green and easy method, to be submitted.

6. A. Liguori, A. Cochis, A. Stancampiano, R. Laurita, B. Azzimonti, R. Sorrentino, E. Varoni, M. Petri, V. Colombo, M. Gherardi, L. Rimondini, Cold atmospheric plasma affects early bacteria adhesion and decontamination of soft relined palatal obturators, submitted to Journal of Biomedical Materials Research Part B.
7. T. Velusamy, A. Liguori, M. Macias-Montero, M. Gherardi, V. Colombo, P. Maguire, D. Mariotti, One-Step Rapid Synthesis of CuO Quantum Dots with tailored energy-band diagram for all-inorganic solar cells, submitted to Nature Communications.
8. L. S. Dolci, A. Liguori, A. Merlettini, L. Calzà, M. Gherardi, V. Colombo, M. L. Focarete, Antibody immobilization on poly(L-lactic acid) nanofibers advantageously carried out by means of a non-equilibrium atmospheric plasma process, submitted to Journal of Physics D: Applied Physics.
9. C. Gualandi, N. Bloise, N. Mauro, P. Ferruti, A. Manfredi, M. Sampaolesi, A. Liguori, R. Laurita, M. Gherardi, V. Colombo, L. Visai, M. L. Focarete, E. Ranucci, Poly-L-lactic acid nanofiber–polyamidoamine hydrogel composites: preparation, properties and preliminary evaluation as scaffolds for human pluripotent stem cell culturing, submitted to Macromolecular Bioscience.

Furthermore, I took part into other research in the field of *Plasma medicine* and diagnostic of plasma discharges, which led to the following scientific works:

1. E. Simoncelli, D. Barbieri, R. Laurita, A. Liguori, A. Stancampiano, L. Viola, R. Tonini, M. Gherardi, V. Colombo, Preliminary investigation of the antibacterial efficacy of a handheld plasma gun source for endodontic procedures, *Clinical Plasma Medicine* 2015, 3, 2.
2. M. Boselli, V. Colombo, M. Gherardi, R. Laurita, A. Liguori, E. Simoncelli, A. Stancampiano, Characterization of a cold atmospheric pressure plasma jet device driven by nanosecond voltage pulses, *IEEE Transactions on Plasma Science* 2015, 43, 3.
3. D. Barbieri, M. Boselli, F. Cavrini, V. Colombo, M. Gherardi, M. P. Landini, R. Laurita, A. Liguori, A. Stancampiano, Investigation of the antimicrobial activity at safe levels for eukaryotic cells of a low power atmospheric pressure inductively coupled plasma source, *Biointerphases* 2015, 10, 029519.
4. M. Gherardi, E. Turrini, R. Laurita, E. De Gianni, L. Ferruzzi, A. Liguori, A. Stancampiano, V. Colombo, C. Fimognari, Atmospheric Non-Equilibrium Plasma Promotes Cell Death and Cell-Cycle Arrest in a Lymphoma Cell Line, *Plasma Processes and Polymers* 2015, DOI: 10.1002/ppap.201500033.

5. M. Boselli, V. Colombo, M. Gherardi, R. Laurita, A. Liguori, P. Sanibondi, A. Stancampiano, High-Speed Multi-Imaging of Repetitive Unipolar Nanosecond-Pulsed DBDs, *IEEE Transactions on Plasma Science, Images in Plasma Science* 2014, 42, 10.
6. S. Bianconi, F. Cavrini, V. Colombo, M. Gherardi, R. Laurita, A. Liguori, P. Sanibondi, A. Stancampiano, ICCD imaging of the transition from uncoupled to coupled mode in a plasma source for biomedical and materials treatment applications, *IEEE Transactions on Plasma Science, Images in Plasma Science* 2014, 42, 10.
7. M. Boselli, F. Cavrini, V. Colombo, E. Ghedini, M. Gherardi, R. Laurita, A. Liguori, P. Sanibondi, A. Stancampiano, High-speed and Schlieren imaging of a low power inductively coupled plasma source for potential biomedical applications, *IEEE Transactions on Plasma Science, Images in Plasma Science* 2014, 42, 10.
8. M. Boselli, V. Colombo, E. Ghedini, M. Gherardi, R. Laurita, A. Liguori, P. Sanibondi, A. Stancampiano, Schlieren high-speed imaging of a nanosecond pulsed atmospheric pressure non-equilibrium plasma jet, *Plasma Chemistry and Plasma Processes* 2014, 34, 4.

The results have been also presented at international conferences:

1. Non-equilibrium nanopulsed plasma jet for the synthesis of copper-based nanostructures in liquid environments, oral presentation at International Conference on Electrical Discharges with Liquids (ICEDL 16), Kocaeli University, Turkey, 13-17 March 2016.
2. Plasma treatment of materials and for materials synthesis, oral presentation at (Micro)Plasma & Microstructures, Ghent University, Belgium, 26-27 November 2015.
3. Atmospheric non-equilibrium plasma sources and processes with a focus on plasma medicine and antibacterial applications, oral presentation at GEC-68/ICRP-9/SPP-33, Honolulu, USA, 12-16 October 2015.
4. Effective decontamination of soft relin-based oral cancer shutters by means of non-thermal atmospheric plasma, poster presentation at Joint meeting of COST Actions CMST TD1208 and MPNS MP1101, Bertinoro, Italy, 13-16 September 2015
5. Investigation of the antimicrobial activity at safe levels for eukaryotic cells of a low power atmospheric pressure inductively coupled plasma source, poster presentation at Joint meeting of COST Actions CMST TD1208 and MPNS MP1101, Bertinoro, Italy, 13-16 September 2015

6. Atmospheric pressure non-thermal plasma for imparting water resistance properties to pullulan electrospun non-woven mats, poster presentation at Joint meeting of COST Actions CMST TD1208 and MPNS MP1101, Bertinoro, Italy, 13-16 September 2015
7. Investigation of antibacterial efficacy of a plasma gun source for endodontic applications, oral presentation at Joint meeting of COST Actions CMST TD1208 and MPNS MP1101, Bertinoro, Italy, 13-16 September 2015.
8. Single step process for deposition on nanocomposite antibacterial coatings using a non-equilibrium atmospheric pressure plasma jet, poster presentation at Joint meeting of COST Actions CMST TD1208 and MPNS MP1101, Bertinoro, Italy, 13-16 September 2015.
9. Non-equilibrium atmospheric pressure plasma jet driven by a nanosecond pulse generator for acrylic acid plasma-polymerization, poster presentation at Joint meeting of COST Actions CMST TD1208 and MPNS MP1101, Bertinoro, Italy, 13-16 September 2015.
10. PlasmMi-Plasma Mobile Inactivator: cold plasma smartphone sanitizer to reduce hospital and community-acquired bacterial diseases, poster presentation at Joint meeting of COST Actions CMST TD1208 and MPNS MP1101, Bertinoro, Italy, 13-16 September 2015.
11. Atmospheric pressure DC microplasma for the surfactant-free synthesis of CuO nanoparticles in a liquid environment, oral presentation at Joint meeting of COST Actions CMST TD1208 and MPNS MP1101, Bertinoro, Italy, 13-16 September 2015.
12. In vivo investigation on the effects of plasma activated water against plant pathogenic bacteria, poster presentation at Joint meeting of COST Actions CMST TD1208 and MPNS MP1101, Bertinoro, Italy, 13-16 September 2015.
13. Characterization of a cold nanopulsed plasma jet in free-flow configuration and impinging on different substrates, poster presentation at Joint meeting of COST Actions CMST TD1208 and MPNS MP1101, Bertinoro, Italy, 13-16 September 2015.
14. Advanced investigation of electrical and fluid-dynamic parameters on a nanopulsed plasma jet impinging on a liquid substrate, poster presentation at Joint meeting of COST Actions CMST TD1208 and MPNS MP1101, Bertinoro, Italy, 13-16 September 2015.
15. Investigation of the antimicrobial activity at safe levels for eukaryotic cells of a low power atmospheric pressure inductively coupled plasma source, poster presentation at Sixth Central European Symposium on Plasma Chemistry (CESPC-6), Bressanone (Italy), September 2015
16. Multi-diagnostic investigation of a non-equilibrium atmospheric pressure plasma jet driven by nanosecond voltage pulses in free-flow configuration and while impinging on different substrate, oral presentation at Sixth Central European Symposium on Plasma Chemistry (CESPC-6), Bressanone (Italy), September 2015.

17. Surface characterization of plasma-polymerized polyacrylic acid thin film deposited by means of a nanosecond pulsed plasma jet, oral presentation at Sixth Central European Symposium on Plasma Chemistry (CESPC-6), Bressanone (Italy), September 2015.
18. Investigation of the efficacy of plasma gun decontamination of realistic root canal models for endodontic applications, oral presentation at Sixth Central European Symposium on Plasma Chemistry (CESPC-6), Bressanone (Italy), September 2015.
19. In vivo investigation on the effects of plasma activated water against plant pathogenic bacteria poster presentation at 22th ISPC, Antwerp, Belgium, July 2015.
20. Characterization of a cold nanopulsed plasma jet in free-flow configuration and impinging on different substrates poster presentation at 22th ISPC, Antwerp, Belgium, July 2015.
21. Advanced investigation of electrical and fluid-dynamic parameters on a nanopulsed plasma jet impinging on a liquid substrate, poster presentation at 22th ISPC, Antwerp, Belgium, July 2015.
22. Investigation of the antimicrobial activity at safe levels for eukaryotic cells of a low power atmospheric pressure inductively coupled plasma source, poster presentation at 22th ISPC, Antwerp, Belgium, July 2015.
23. Effective decontamination of soft relined oral cancer shutters by means of non-thermal atmospheric plasma, poster presentation at 22th ISPC, Antwerp, Belgium, July 2015.
24. Investigation of antibacterial efficacy of a plasma gun source for endodontic applications poster presentation at 22th ISPC, Antwerp, Belgium, July 2015.
25. Atmospheric pressure non-thermal plasma for imparting water resistance properties to pullulan electrospun non-woven mats, poster presentation at 22th ISPC, Antwerp, Belgium, July 2015.
26. Effective deposition of plasma-polymerized polyacrylic acid thin film by means of a plasma jet driven by nanosecond high voltage pulses, oral presentation at 22th ISPC, Antwerp, Belgium, July 2015.
27. Effective decontamination of soft relined oral cancer shutters by means of non-thermal atmospheric plasma ” poster presentation at Congresso Nazionale Biomateriali SIB, Portonovo, Ancona (Italy), June 2015
28. Characterization and evaluation of bactericidal effect and cytocompatibility of a low power ICP source for biomedical applications, oral presentation at the 42nd IEEE International Conference on Plasma Science (ICOPS) Belek, Antalya (Turkey), May 2015.

29. Investigation of antibacterial efficacy of a plasma gun source for endodontic applications, oral presentation at the 42nd IEEE International Conference on Plasma Science (ICOPS) Belek, Antalya (Turkey), May 2015.
30. Characterization of a cold atmospheric pressure plasma jet driven by nanosecond high-voltage pulses, oral presentation at the 42nd IEEE International Conference on Plasma Science (ICOPS) Belek, Antalya (Turkey), May 2015.
31. Atmospheric pressure non-thermal plasma for the production of composite materials, oral presentation at the 42nd IEEE International Conference on Plasma Science (ICOPS) Belek, Antalya (Turkey), May 2015.
32. Crosslinking of water-soluble pullulan nanofibrous mats through atmospheric plasma treatment, oral presentation at the 42nd IEEE International Conference on Plasma Science (ICOPS) Belek, Antalya (Turkey), May 2015.
33. Advanced investigation of the interaction between a plasma jet and a liquid surface: influence of electrical and fluid dynamic parameters, oral presentation at the 11th biennial Frontiers in Low Temperature Plasma Diagnostic (FLTPD) workshop, Porquerolles Island (France), May 2015
34. Advanced investigation of the interaction between a plasma jet and a liquid surface: influence of atmosphere and substrate composition, poster presentation at the 11th biennial Frontiers in Low Temperature Plasma Diagnostic (FLTPD) workshop, Porquerolles Island (France), May 2015.
35. Direct and indirect treatment of prokaryotic and eukaryotic cells in liquid medium by means of a low power inductively coupled plasma (icp) torch: evaluation of antibacterial effects and cytocompatibility, oral presentation at the 2nd Annual meeting of COST Action TD1208, Barcelona, Spain, 2015.
36. Plasma gun decontamination of bacteria in liquid suspensions, poster presentation at the 2nd Annual meeting of COST Action TD1208, Barcelona, Spain, 2015.
37. Characterization of a non-equilibrium atmospheric pressure plasma jet driven by nanosecond voltage pulses, oral presentation at 20th Symposium on Application of Plasma Processes - SAPP XX, Tatranská Lomnica, Vysoké Tatry, Slovakia, 17-22 September 2014
38. Plasma gun decontamination of bacteria in liquid suspensions, poster presentation at 20th Symposium on Application of Plasma Processes - SAPP XX, Tatranská Lomnica, Vysoké Tatry, Slovakia, 17-22 September 2014

39. Investigation of the effectiveness of a gatling machine gun-like plasma source for biomedical applications and materials treatment, poster presentation at 14th International Conference on Plasma Surface Engineering, Garmisch-Partenkirchen, Germany, 15-19 September 2014
40. Non-equilibrium plasma sources and processes with a focus on antibacterial applications and sterilization, keynote lecture at 14th International Conference on Plasma Surface Engineering, Garmisch-Partenkirchen, Germany, 15-19 September 2014
41. Atmospheric plasma surface modification of electrospun poly(l-lactic acid): effect on mat properties and cell culturing, poster presentation at 26th Annual Conference of the European Society for Biomaterials (ESB), Liverpool, UK, 31 August – 3 September 2014
42. Atmospheric plasma surface modification of electrospun poly(L-lactic acid): effect on mat properties and cell culturing, poster presentation at 3rd International Conference on Electrospinning, San Francisco, USA, 4 - 7 August 2014
43. Processes and sources for biomedical and material applications in UNIBO, poster presentation at Gordon Research Conference on Plasma Processing Science - Many Scales, Many Applications, One Discipline, Bryant University, Smithfield, USA, 22-27 July 2014
44. Processes and sources for biomedical and material applications in UNIBO, oral presentation at Gordon Research Seminar on Plasma Processing Science: Non-Equilibrium Plasma Diagnostics, Modeling, and Applications, Bryant University, Smithfield, USA, 26-27 July 2014
45. Non-thermal plasma promotes apoptosis and cell-cycle arrest in a lymphoma cell line, oral presentation at 5th International Conference on Plasma Medicine (ICPM5), Nara, Japan, 18 - 23 May 2014
46. Investigation of the effectiveness of a low power inductively coupled plasma source for biomedical applications, oral presentation at 5th International Conference on Plasma Medicine (ICPM5), Nara, Japan, 18 - 23 May 2014
47. Plasma source for fast and continuous purification of water flows, poster presentation at 5th International Conference on Plasma Medicine (ICPM5), Nara, Japan, 18 - 23 May 2014
48. A novel plasma based teeth whitening technology, poster presentation at 5th International Conference on Plasma Medicine (ICPM5), Nara, Japan, 18 - 23 May 2014
49. Diagnostics of a low power inductively coupled plasma source for potential biomedical applications, poster presentation at 5th International Conference on Plasma Medicine (ICPM5), Nara, Japan, 18 - 23 May 2014

50. Antimicrobial activity of a low power inductively coupled plasma source at safe levels for eukaryotic cells, poster presentation at 5th International Conference on Plasma Medicine (ICPM5), Nara, Japan, 18 - 23 May 2014
51. Atmospheric pressure non-equilibrium plasma for the production of composite materials, poster presentation at 5th International Conference on Plasma Medicine (ICPM5), Nara, Japan, 18 - 23 May 2014
52. Investigation of the effectiveness of a Gatling machine gun-like plasma source for biomedical applications and materials treatment, poster presentation at 5th International Conference on Plasma Medicine (ICPM5), Nara, Japan, 18 - 23 May 2014
53. Comparison of the growth inhibition potential of different dielectric barrier discharge operating regimes, poster presentation at 5th International Conference on Plasma Medicine (ICPM5), Nara, Japan, 18 - 23 May 2014
54. Plasma as a new odontoiatric tool to improve implants adhesion, poster presentation at 5th International Conference on Plasma Medicine (ICPM5), Nara, Japan, 18 - 23 May 2014
55. Investigation of the effectiveness of a low power inductively coupled plasma source for biomedical applications, invited presentation at COST TD1208 Annual meeting, Lisboa, Portugal, 10 – 13 March 2014
56. Investigation of the effectiveness of a gatling machine gun-like plasma source for biomedical applications and materials treatment, poster presentation at COST TD1208 Annual meeting, Lisboa, Portugal, 10 – 13 March 2014
57. Plasma-assisted electrospinning: the many facets of a process, oral presentation at Workshop on Atmospheric Plasma Processes and Sources, EU COST MP1101, Bohinjaska Bistrica, Slovenia, 22 – 23 January 2014
58. Processes and sources for biomedical and surface treatment applications in UNIBO, invited presentation at Workshop on Atmospheric Plasma Processes and Sources, EU COST MP1101, Bohinjaska Bistrica, Slovenia, 22 – 23 January 2014
59. Atmospheric plasma surface modification of electrospun poly(L-lactic acid): effect on mat properties and cell culturing, oral presentation at MiMe-Materials in Medicine 2013, Faenza, Italy, 8-11 October 2013
60. Surface modification of poly(L-lactic acid) electrospun scaffold by atmospheric plasma: scaffold properties and fibroblast morphological response, oral presentation at ISSIB-IV, Roma, Italy, 24-28 September 2013
61. Increasing cell viability of 3D scaffolds for tissue engineering by means of an atmospheric pressure plasma jet, poster presentation at ISPC21, Cairns, Australia, 4-9 August 2013

62. Effect of atmospheric pressure non-equilibrium plasma treatment on poly-L-lactic acid electrospinnability, poster presentation at ISPC21, Cairns, Australia, 4-9 August 2013
63. Study of the effect of atmospheric pressure plasma treatment on electrospinnability of poly-L-lactic acid solutions: voltage waveform effect, poster presentation at ISPC21, Cairns, Australia, 4-9 August 2013
64. High speed imaging characterization of a Dielectric Barrier Discharge Roller plasma source, poster presentation at ISPC21, Cairns, Australia, 4-9 August 2013
65. Characterization of a plasma jet for biomedical applications: composition, temperature, fluid dynamics and plasma structure, poster presentation at ISPC21, Cairns, Australia, 4-9 August 2013
66. Atmospheric plasma surface modification of electrospun poly(L-lactic acid): effect on mat properties and cell culturing, oral presentation at ISPC21, Cairns, Australia, 4-9 August 2013
67. Study of the effect on human mesenchymal and epithelial cells of an atmospheric pressure plasma source driven by different voltage waveforms, poster presentation at ISPC21, Cairns, Australia, 4-9 August 2013
68. Parametric study on the effectiveness of treatment of polyethylene (PE) foils for pharmaceutical packaging with a large area atmospheric pressure plasma source, poster presentation at ISPC21, Cairns, Australia, 4-9 August 2013
69. Plasma-assisted electrospinning: the many facets of a process, oral presentation at ISPC21, Cairns, Australia, 4-9 August 2013
70. Study of the role of dielectric material in a dielectric barrier discharge (DBD) plasma source for dermatological application, poster presentation at ISPC21, Cairns, Australia, 4-9 August 2013
71. Comparison of localized treatment effectiveness on biocompatible glass with different atmospheric pressure plasma sources, poster presentation at ISPC21, Cairns, Australia, 4-9 August 2013
72. Study of the role of dielectric material in a dielectric barrier discharge (DBD) plasma source for dermatological applications, poster presentation at 11th ICSD, Bologna, Italy, 30 June - 4 July 2013
73. Parametric study on the effectiveness of treatment of polyethylene (PE) foils for pharmaceutical packaging with a large area atmospheric pressure plasma source, poster presentation at PPS 2013, San Francisco, USA, 16-21 June 2013

74. Atmospheric plasma surface modification of electrospun poly(L-lactic acid): effect on mat properties and cell culturing, oral presentation at PPPS 2013, San Francisco, USA, 16-21 June 2013
75. Comparison of localized treatment effectiveness on biocompatible glass with different atmospheric pressure plasma sources, poster presentation at PPPS 2013, San Francisco, USA, 16-21 June 2013
76. Plasma meets electrospinning: the many facets of a process, oral presentation at Congresso AIV, Catania, Italy, 15-17 May 2013
77. Bioplasma: on the industrial and social potential of cold atmospheric plasma applications, keynote presentation at Congresso AIV, Catania, Italy, 15-17 May 2013
78. Characterization of the plasma structure of a Dielectric Barrier Discharge roller plasma source for material treatment at atmospheric pressure, poster presentation at FLTPD-X, Kerkrade, the Netherlands, 28 April - 2 May 2013
79. Characterization of a plasma jet for biomedical applications: composition, temperature, fluid dynamics and plasma structure, poster presentation at FLTPD-X, Kerkrade, the Netherlands, 28 April - 2 May 2013
80. Multi-imaging techniques for the characterization of a nanopulsed DBD system for biomedical applications, oral presentation at Plasma to Plasma!, Leiden, The Netherlands, 7-11 January 2013

Finally, I have been co-supervisor for the following MA and BA thesis:

1. Tommaso Gallingani, “Ottimizzazione di processi assistiti da sorgenti di plasma atmosferico di non equilibrio per la funzionalizzazione di polimeri, la deposizione di coating e la sintesi di nanostrutture” Alma Mater Studiorum – Università di Bologna.
2. Matteo Ulivi, “Ottimizzazione funzionale di una sorgente plasma jet di non-equilibrio per processi di polimerizzazione e sintesi di nanoparticelle in liquido”, Alma Mater Studiorum-Università di Bologna.
3. Matteo Castellucci, “Realizzazione ed analisi sperimentale di una sorgente DBD innovativa per il trattamento di elettrofilati di PLLA”, Alma Mater Studiorum – Università di Bologna
4. Elena Toccaceli, “Messa a punto sperimentale di un processo di deposizione di film nanocompositi con plasma atmosferico di non equilibrio”, Alma Mater Studiorum - Università di Bologna

5. Alessandra Lepore, “Funzionalizzazione, deposizione e caratterizzazione di film polimerici via plasma atmosferico di non equilibrio”, Alma Mater Studiorum - Università di Bologna
6. Alice Patria, “Analisi dell'efficacia antibatterica di sorgenti di plasma di non equilibrio per applicazioni medicali”, Alma Mater Studiorum - Università di Bologna
7. Emanuele Simoncelli, “Progettazione, realizzazione e caratterizzazione di una sorgente Plasma Gun”, Alma Mater Studiorum - Università di Bologna
8. Giovanni Anceschi, “Sviluppo di processi di inattivazione batterica assistiti da sorgenti di plasma freddo a pressione atmosferica”, Alma Mater Studiorum - Università di Bologna
9. Filippo Marani, “Realizzazione e caratterizzazione chimico-fisica di una sorgente di plasma di non equilibrio operante a pressione atmosferica per la modifica superficiale di materiali polimerici in ambiente controllato”, Alma Mater Studiorum - Università di Bologna
10. Simone Bianconi, “Progettazione, realizzazione e caratterizzazione di fasci di sorgenti microplasma (gatling plasma) per applicazioni biomedicali e di modificazione superficiale”, Alma Mater Studiorum - Università di Bologna

Part I

CHAPTER 1
CONVENTIONAL STRATEGIES FOR FUNCTIONAL
SURFACE MODIFICATION OF MATERIALS

1.1 Surface modification of biomedical polymers

Polymers have been successfully applied in several fields such as biomedical applications, fabrication of protective coatings, composite materials and microelectronic devices, thin-film technology, and so on [1]. Generally, specific surface properties such as chemical composition, hydrophilicity, roughness, conductivity, lubricity, crosslinking density, are required for the success of these applications [1]. Polymers, although being characterized by excellent bulk physical and chemical properties, low manufacturing cost and ease of process, very often are not able to meet all the requirements needed for these applications. In order to overcome this limitation, the modification of surface properties of polymers are often required to transform inexpensive materials into highly valuable finished products [2].

Recently, the forefront sector of the tissue engineering has attracted a great interest; activities in this field, merging the principles of biology, medicine and engineering, aim at replacing damaged or missing biological tissues with functional artificial substitutes [2-4], named scaffolds, consisting in most cases in polymeric materials, selected for their strength and mechanical properties.

Since these scaffolds are required to be biocompatible, biodegradable, able to promote cells adhesion, growth and sometimes differentiation, without inducing any inflammatory responses, formation of undesired tissues or other deleterious reactions, the control of their surface properties is mandatory [5], even more than for other applications.

In order to properly modify the surface properties of the polymeric scaffolds, conferring them biocompatible properties and preventing the occurrence of unwanted inflammatory response, the interactions between material and cells must be understood [2, 6].

Generally, cells bind to the extra-cellular matrix (ECM) through the cell membrane receptors. There are several classes of these receptors, also called protrusions, which are micrometer-sized sheet-like structures composed of an actin filament mesh with, at their end, smaller hair-like protrusions, “filopodia”, consisting of long, thin actin filament bundles which act as sensors of the environment of the cell. When the filopodia find a suitable binding site, a so-called receptor binding site, the filopodia bind to this site, and a feedback signalling pathway within the cell allows more receptors to be localized in that region of the cell. One class of receptors include the integrins, which bind selectively to specific binding sites such as Arg-Gly-Asp (RGD) tripeptide found in cell adhesive proteins such as vitronectin, laminin, and fibronectin [2, 6].

Considering biomaterial-cell interactions, these receptors sense the surrounding environment of the cell, which is the biomaterial surface. If this surface contains binding sites, similar to the natural ECM, it can be referred as a biomimetic material. As a consequence, cells will interact with the

material and will recognize the implant as if it were a part of the body. The receptor binding to the ligands, present on the biomimetic material, determines the strength of the cell attachment, the cell migration rate, and the extent of cytoskeletal organization formation [2, 6].

The presence of the functional groups can be stated to directly influence the cell adhesion and differentiation [6]. Indeed, several papers demonstrated the surface-dependent differences in integrin binding in relation to the functional groups onto the material [6, 7]. For example, the presence of polar functionalities seems to exhibit intermediate levels of local adhesion components, while the hydrophobic substrates displayed the lowest levels, underlining the influence of the surface chemistry on the cells adhesion and differentiation [6, 8]. Besides the key role played by the chemical surface characteristics of the scaffold on the biocompatibility of the material, it is worth pointing out that also the morphology of the scaffolds requires to be considered with the aim to mimic the fibrous structure of the ECM due to the presence of proteins such collagen and fibronectin [6, 9-12].

The surface functionalization of polymers is not only required to promote cell adhesion and proliferation, but also to enable the immobilization of drugs, enzymes, antibodies or other biologically active species, leading to the fabrication of bio-active scaffolds, demanded for a variety of biomedical applications. While the end use of the bio-active polymer varies with each application, the overall concept for its fabrication is the same. It concerns the selection of the polymer presenting the bulk properties matching the end use, its surface functionalization in order to introduce the type and quantity of reactive functional groups, the covalent binding of the natural or synthetic bioactive compound onto the functionalized polymer surface, via an intermediary, as needed [13].

Another relevant aspect to take into account for the application of scaffolds and implants in the biomedical film is represented by the presence of bacteria in every biological environment. It is now widely accepted that bacteria survive by attaching to solid substrates, in sessile structured communities called biofilms, where they can persist for extended periods, acting as a reservoir of pathogens and multiplying their pathways of transmission [14, 15, 16]. Bacteria in biofilms are drastically more resistant to antibiotics and external forces and can withstand host immune responses [14, 17].

For the correct functioning of an implant, it is thus critical that the attachment of bacteria is prevented, by conferring antibacterial characteristics to the surface of the implant.

In this chapter, a quick overview of the conventional approaches and strategies, mainly based on chemical and physical methods, for the modification of the chemical characteristics of polymers as well as for the fabrication of antibacterial surfaces is reported.

1.2 Conventional methods for the functionalization of polymers

As already discussed, chemical and physical surface modifications of the polymeric materials are generally required to confer biomimetic characteristics to the implant. Several strategies have been investigated and tested over time and despite being different, under a chemical point of view, all of them aim at the introduction of polar functional groups onto the material surface. Indeed, polar groups such as carboxyl, hydroxyl, amine groups are expected to confer hydrophilic characteristics to the surface and, moreover, they can also be used for the immobilization of biomimetic molecules.

As reviewed and deeply documented by Desmet et al, in their work “Nonthermal Plasma Technology as a Versatile Strategy for Polymeric Biomaterials Surface Modification: A Review” published on *Biomaterials* in 2009, the techniques for the introduction of functional groups onto polymeric substrates can be subdivided in different classes [6].

The first class of techniques refers to the wet-chemical methods and concerns the reactions between a chemical compound in solution and the surface of a solid material. Examples of this technique include aminolysis, a chemical reaction in which a molecule is split into two parts by reacting with a molecule of ammonia or an amine, and alkaline or acidic hydrolysis, which relies on the cleavage of chemical bonds by the addition of water. When a polyester is hydrolyzed via autocatalytic cleavage of main-chain ester-bonds, hydroxyl and carboxyl end-groups are generated, with an increase of roughness and hydrophilicity of the surface [6, 18, 19]. In some cases, both enhanced cell attachment and spreading are obtained. In general, subsequent immobilization of natural proteins tends to increase cell adhesion and viability.

Wet chemical methods are very effective, but they present relevant drawbacks linked to the fact that they are not green technology and they can lead to non-specific reactions, irregular surface etching and surface degradation with a reduction of the mechanical properties [6, 20].

A second strategy implies oxidization of the surface of a biomaterial by exposing it to ozone. Ozone can be used as such, but it was found that a combination of ozone and UV irradiation significantly increased the kinetics of the process [6, 21]. This observation could be attributed to the different pathways for both methods. As for wet-chemical treatment, this is a non-specific technique and dependant on the UV/ozone procedure adopted for the functionalization and cleaning of the surface

[6, 22]. UV treatment has been used for surface graft polymerization of polymers in the presence of a photoinitiator or photosensitizer [6, 23, 24]. Depending on the chemical structure of the grafted polymer, different functionalities are introduced into the surface. UV can be applied while the sample is kept under vacuum conditions (VUV), or submerged in an inert gas such as argon, or covered with monomer solution [6].

The most common radiation types, used in industry, include γ -radiation and e-beam radiation [6, 138]. Ion beams are used in order to achieve ion implantation in the outer surface layer or to deposit coatings. Many different ions have been employed for irradiating polymers such as hydrogen and helium atoms, as well as ions of gold or uranium. Ion implantation does not directly introduce functional groups onto the surface but the surface chemistry, and thus the surface properties, are changed. For the treatment of polymers, the high energy irradiation can cause additional chemical effects: free radicals can recombine, leading to cross-linking, and chains can be cleaved, leading to degradation of the polymer [6, 25, 26].

Self-assembly is a class of processes where a disordered system of components forms and organizes a structure or pattern as a consequence of specific, local interactions among the components themselves, without inputs from the outside of the system. In the case of surfaces, this implies that certain molecules are able to interact with a surface and form a self-assembled monolayer (SAM) on the surface. Depending on the chemical structure of the molecules making up the SAM-layer, different functionalities can be introduced onto the surface [6].

The polar groups introduced by means of the reported techniques lead to an increase of the hydrophilicity, inducing a surface modification of the chemical properties of the substrate. These functional groups can be exploited to promote the adhesion of cells directly onto the polymer or to induce the chemical immobilization of natural or synthetic compounds to the polymer surface, in order to achieve the desired biocompatibility or bio-activation of the material.

The major methods to immobilize a bioactive compound to a polymeric surface are adsorption via electrostatic interactions, ligand–receptor pairing, and covalent attachment. Non-covalent adsorption is sometimes desirable, as in certain drug delivery applications [13, 27]. It is also appropriate in the case of regenerable antimicrobial textiles. However, covalent immobilizations offer several advantages by providing the most stable bond between the compound and the functionalized polymer surface. In the biomedical field, a covalent immobilization can be used to extend the half-life of a

biomolecule or allow for continued bioactivity of in-dwelling devices (as in vascular devices, shunts, or catheters) [13, 28, 29]. In the case of active food packaging applications, a covalent linkage ensures that the bioactive compound will not migrate to the food and thus may offer the regulatory advantage of not requiring approval as a food additive [13]. Among the numerous bio-conjugation methods based on the covalent immobilization, one of the most common technique is the carbodiimide coupling of a carboxylic group with a primary amine, based on the reaction of the carbodiimide with the carboxylic group to form a reactive intermediate, which is stabilized by the addition of (sulfo)-N-hydroxysuccinimide (NHS) to form a reactive ester [6, 13].

1.3 Conventional methods for the crosslinking of polymers

Among the wide range of polymers, an interesting class is represented by the so-called biopolymers, which being produced by living organisms (plants, microorganisms, etc) represents a sustainable and renewable resource, in contrast with the quickly depletable feedstocks of polymers deriving from petrochemicals or chemical processes.

Like polymers, biopolymers are chain-like molecules made up of repeating chemical blocks. Biopolymers can be classified in three groups, depending on the nature of the repeating unit they are made of: (i) polysaccharides are made of sugars, (ii) proteins of amino acids, and (iii) nucleic acids of nucleotides. The following substances are example-biopolymers for each group: cellulose (found in plants), gelatin (obtained from a controlled hydrolysis of collagen), and DNA (genetic material of a given organism). In contrast to synthetic polymers, which have a simpler and more randomic structure, biopolymers are complex molecular assemblies that adopt precise and defined 3D shapes and structures. This feature is essential to make these biopolymers active molecules *in vivo*.

Due to their high biocompatibility and biodegradability, biopolymers find a wide range of applications in the pharmaceutical and biomedical fields, being also ideal excipients, building blocks, carrier and protective agents to improve the performances of other biologically active molecules in a product.

Despite their interesting properties, the range of the possible applications of these biopolymers is not so high as expected, since the majority of them turn out to be extremely soluble upon water contact, bringing out the necessity of a crosslinking step to ensure manufacture stability during their storage and use in case of contact with water.

Crosslinking, which refers to the linking of polymeric chains, can be defined, according to the IUPAC definition, as a small region in a macromolecule from which at least four chains are emanate, and

formed by reactions involving sites or groups on existing macromolecules or by interactions between existing macromolecules. The small region of the macromolecule may be an atom, a group of atoms, or a number of branch points connected by bonds or oligomeric chains. In the majority of cases, a crosslinking is a covalent structure but the term can be also used to describe sites of weaker chemical interactions, portions of crystallites, and even physical interactions and entanglements.

As reported by Hennink *et al* in their work “Novel crosslinking methods to design hydrogels” published on *Advanced Drug Delivery Reviews* in 2012, different chemical and physical approaches have been developed for polymer crosslinking [30]. The most relevant methods and techniques are here reported and briefly described.

1.3.1 Chemical methods

Crosslinking by radical polymerization

Chemically crosslinked gels can be obtained by radical polymerization of low molecular weight monomers in the presence of crosslinking agents. Poly(2-hydroxyethyl methacrylate) (pHEMA) is a well known and frequently studied hydrogel system by polymerization of HEMA in the presence of a suitable crosslinking agent (e.g. ethylene glycol dimethacrylate). Using similar procedures, a great variety of other hydrogel systems has been synthesized [30, 31]. The hydrogel characteristics, among which the swelling, can be modulated by the amount of crosslinker. Moreover, stimuli-sensitive materials can be obtained by the addition of e.g. methacrylic acid (pH-sensitive gels [32]) or N-isopropylacrylamide (temperature-sensitive gels [33]). Besides the radical polymerization of mixtures of vinyl-monomers, chemically crosslinked hydrogels can also be obtained by radical polymerization of water-soluble polymers derivatized with polymerizable groups. Different water-soluble (synthetic, semi-synthetic and natural) polymers have been used for the design of hydrogels via this route.

Crosslinking by chemical reaction of complementary groups

The method exploits the presence of functional groups (mainly OH, COOH, NH₂) in the chemical structure of water-soluble polymers to create covalent linkages between the polymeric chains through inducing reactions between functional groups with complementary reactivity, such as an amine-carboxylic acid or an isocyanate-OH/NH₂ reaction.

Water-soluble polymers with hydroxyl groups (e.g. poly(vinylalcohol)) can be crosslinked using glutaraldehyde [13, 34, 35]. In order to establish crosslinking, rather drastic conditions have to be applied (low pH, high temperature, methanol added as quencher). In contrast, amine-containing polymers can be crosslinked with the same reagent under mild conditions whereby so-called Schiff

bases are formed. This has especially been investigated for the preparation of crosslinked proteins and amine containing polysaccharides [30, 36]. Because glutaraldehyde is a toxic compound that even at low concentration shows cell-growth inhibition, alternatives have been developed. Crosslinking of gelatin using polyaldehydes obtained by partial oxidation of dextran has been reported [30, 37]. These gels were designed for application in wound treatment and epidermal growth factor (EGF) was incorporated to promote wound healing. The release rate of EGF decreased with increasing storage time, due to the ongoing processes of both chemical crosslinking and physical structuring of the hydrogel matrix.

Water-soluble polymers can be converted into hydrogels using bis (or higher) functional crosslinking agents, which react with functional groups of water-soluble polymers via addition reactions. Polysaccharides can be crosslinked with 1,6-hexamethylenediisocyanate, divinylsulfone, or 1,6-hexanedibromide and many other reagents [30]. The network properties can be easily tailored by the concentration of the dissolved polymer and the amount of crosslinking agent. The crosslinking reactions are preferably carried out in organic solvents, because water can also react with the crosslinking agent. Furthermore, since the crosslinking agents are generally very toxic, the gels have to be extracted to remove traces of unreacted agents. If these matrices are aimed for the release of pharmaceutically active agents, they have to be loaded after the gel formation and extraction process [30, 38, 39].

Condensation reactions between hydroxyl groups or amines with carboxylic acids or derivatives are frequently applied for the synthesis of polymers to yield polyesters and polyamides, respectively. These reactions can also be used for the preparation of crosslinked hydrogels. A very efficient reagent to crosslink water-soluble polymers with amide bonds is N,N-(3-dimethylaminopropyl)-N-ethyl carbodiimide (EDC) [30, 40]. During the reaction N-hydroxysuccinimide is added to suppress possible side-reactions and to have a better control over the crosslink density of the gels. The gels were designed as a delivery device for the release of antibacterial proteins and were incorporated in a Dacron prosthetic valve. Lysozyme was loaded in the gels after their formation and released both in vitro and in vivo for a period of 2 days. To improve the loading capacity, a negatively charged polysaccharide, (chondroitin sulfate) was incorporated in the hydrogels network [30, 41]. Indeed, the loading capacity was substantially increased and the release was retarded with increasing chondroitin content of the gels mostly due to electrostatic interactions between the cationic protein and anionic polysaccharide.

Crosslinking by high-energy radiation

High energy radiation, in particular gamma and electron beams, can be used to polymerize unsaturated compounds. This means that water-soluble polymers derivatized with vinyl groups can be converted into hydrogels using high energy irradiation. During irradiation (gamma or electron-beam) of aqueous solutions of polymers, radicals can be formed on the polymer chain by e.g. the scission of C–H bonds. Additionally, radiolysis of water molecules generates the formation of hydroxyl radicals, which can attack polymer chains also resulting in the formation of macroradicals [30, 42]. Recombination of the macroradicals on different chains results in the formation of covalent bonds and finally in a crosslinked structure. Since the generated macroradicals can react with oxygen, radiation is normally performed in an inert (nitrogen, argon) atmosphere.

Although the great number of chemical approach set up for the crosslinking of hydrogel and water soluble polymers, new methods are required for conferring stability to the biopolymers that will be employed in the fields of biomedicine and tissue engineering. The main reason lies in the fact that these methods are based in the use of crosslinking chemical agents to prepare such hydrogels. These agents do not only affect the integrity of the substances to be entrapped (e.g. proteins, cells), but they are often toxic compounds to be removed/extracted from the gels before they application [30]. In order to overcome the drawback of the chemical approach, alternative methods for obtaining physically crosslinked polymers are demanded.

1.3.2 Physical methods

Crosslinking by ionic interactions

Alginate is a well-known example of a polymer that can be crosslinked by ionic interactions. Alginate is a polysaccharide with mannuronic and glucuronic acid residues and can be crosslinked by calcium ions [30, 43]. Crosslinking can be carried out at room temperature and physiological pH. Therefore, alginate gels are frequently used as matrix for the encapsulation of living cells [30, 44] and for the release of proteins [30, 45]. Interestingly, the gels can be destabilized by extraction of the Ca-ions from the gel by a chelating agent. The release of proteins from alginate microparticles, obtained by spraying a solution of sodium alginate into an aqueous solution of calcium chloride, can be modulated by coating the particles with cationic polymers, e.g. chitosan and polylysine [30, 46, 47].

Crosslinking by crystallization

Poly(vinyl alcohol) (PVA) is a water-soluble polymer. When aqueous solutions of PVA are stored at room temperature they gradually form a gel with, however, a low mechanical strength. Interestingly, once aqueous solutions of this polymer undergo a freeze–thawing process, a strong and highly elastic gel is formed [30, 48]. The properties of the gel depend on the PVA molecular weight, the PVA concentration in water, the temperature and time of freezing and the number of freezing cycles. Gel formation is ascribed to the formation of PVA crystallites, which act as physical crosslinking sites in the network [30, 48].

Crosslinking from amphiphilic block and graft copolymers

Amphiphilic block and graft copolymers are able to self-assemble in water to form organized structures like polymeric micelles and hydrogels, in which the hydrophobic segments of the polymers are aggregated. Amphiphilic diblock copolymers typically form micelles, lamellar phases, etc. [30, 49]. Physically crosslinked hydrogels are generally obtained from multiblock copolymers or graft copolymers. The latter can be composed of a water-soluble polymer backbone, for example a polysaccharide, to which hydrophobic units are attached, or hydrophobic chains containing water-soluble grafts.

The biodegradability of poly(lactic acid) (or its copolymer with glycolic acid) and the biocompatibility of poly(ethylene glycol) prompted several researchers to prepare block copolymers composed of these segments, and to develop hydrogels from them for drug delivery purposes. Drug release can be driven by both passive diffusion and degradation phenomena. Triblock polymers with the hydrophobic PL(G)A segment in the middle have been prepared by coupling of two PEG–PL(G)A diblock copolymers [30, 50-52]. Micelles are formed at low concentrations in water, and at higher concentrations thermoreversible gels are formed. The critical gel concentration and gel-to-sol transition temperature strongly depend on the molecular weights and the composition of the blocks [132].

Multiblock copolymers of PEG and another hydrophobic polyester, poly(butylene terephthalate) (PBT), were investigated [30, 53, 54]. These biocompatible polymers are prepared by melt polycondensation of PEG, butanediol and dimethyl terephthalate. To load polymers with lysozyme as a model protein, polymer solutions were prepared in a mixture of chloroform and hexafluoroisopropanol (6:1) and subsequently a water-in-oil emulsion, containing the protein in the aqueous phase, was prepared. These emulsions were either cast to form a film, or microspheres were prepared using a water-in-oil-in-water emulsion method. The equilibrium swelling ratio, the

estimated mesh size of the hydrogel network and the release rate of lysozyme increased with the weight percentage and molecular weight of the PEG blocks [30, 53, 54].

Crosslinking by hydrogen bonds

Poly(acrylic acid) and poly(methacrylic acid) form complexes with poly(ethylene glycol). These complexes are held together by hydrogen bonds between the oxygen of the poly(ethylene glycol) and the carboxylic group of poly((meth)acrylic acid), whereas for poly((meth)acrylic acid) hydrophobic interactions also play a role [30, 55]. Hydrogen bonding does not only occur between poly((meth)acrylic acid) and poly(ethylene glycol), but has also been observed in poly(methacrylic acid-g-ethylene glycol) [30, 56, 57]. The hydrogen bonds are only formed when the carboxylic acid groups are protonated. This implies that the swelling of these gels is strongly dependent on the pH.

Crosslinking by proteins interactions

Protein engineering is a recent branch of materials chemistry, a field which was pioneered by Tirrell and Cappello [30, 58, 59]. The major advantage is that the sequence of peptides, and thereby its physical and chemical properties, can be precisely controlled by the proper design of the genetic code in synthetic DNA sequences. Even synthetic amino acids, which normally do not occur in nature, can be synthesised [30, 60]. By genetic engineering, Cappello and colleagues prepared sequential block copolymers containing a repetition of silk-like and elastine-like blocks, in which the insoluble silk-like segments are associated in the form of aligned hydrogen bonded beta strands or sheets [30, 59, 62].

These biocompatible so-called ProLastins are fluid solutions in water which can be mixed with drugs, and undergo an irreversible sol-to-gel transition with time under physiological conditions due to crystallization of the silk-like domains. The rate of gelation and subsequent drug release depends on various factors like concentration, polymer composition, and temperature. The release rates are related to water content of the gels and the molecular weights of the incorporated compounds and follow first-order like kinetics [30].

As reported, many crosslinking methods have been investigated to physically crosslink biopolymer and the fundamentals studies so far performed have greatly contributed to the understanding of the phenomenon [30]. However, more effective technologies are demanded, since all the presented processes turn out to be very high time-consuming and the final results is strongly dependent on the kind of biopolymers subjected to the process as well as to the characteristics of the environment in which the process is performed.

Finally, it is worth underlining that all the chemical and physical crosslinking methods here briefly reported are based on processes performed in liquid state. The possibility to induce the crosslinking of the biopolymers directly in the solid state is strongly required to relevantly decrease the process time and to scale up the fabrication of materials with the desired properties.

1.4 Strategies for the fabrication of antibacterial surfaces

As mentioned above, the contamination of scaffolds by bacterial biofilm definitely has to be prevented in order to guarantee the success of its application onto biological tissues. As documented by Campoccia *et al.* [62], the earliest step in the pathogenesis of foreign-body-related infections is bacterial adhesion and, clearly, there is no possibility for colonisation to occur if bacteria cannot adhere to a solid surface. Bacterial adhesion on biomaterial surfaces is known to occur through multiple mechanisms, spanning from passive adsorption due to the physic-chemical interactions between the solid surface and the bacteria cells to active mechanisms of adhesion mediated by specific bacteria structures [62, 63, 64].

Considering the early phases of microbial adhesion on the biomaterial surface, the strategies to contrast bacterial colonisation strongly depend on the route of contamination. Indeed, while the contamination in a dry state can be contrasted by an adequate sterility of the operating room, the contamination due to wet conditions is harder to prevent. In aqueous solutions, bacterial adhesion on biomaterial surfaces is influenced by numerous variables, including the type of pathogens and the nature of the physiological fluids, since the presence of proteins can lead to the formation of proteinaceous layer onto the surface of the biomaterial, supporting the adhesion of bacteria.

Bacterial adhesion in these circumstances is driven by: mass transport, electrostatic interactions, Van der Waals forces, hydrophobic interactions, hydrogen bonding. Bacterial behaviour varies especially as a function of material hydrophobicity and electrostatic charge. Chemico-physical properties and functional groups exhibited by the biomaterial surface interact with those of the bacterial cells determining the kinetics of microbial adhesion. The adsorption of proteins on a surface can be reduced either by altering the interaction potential (so that protein-surface interactions are suppressed) or by slowing down the rate of adsorption through high potential barriers for the interaction. This latter way of controlling the kinetic of adsorption can be achieved by polymer grafting resulting in the introduction of long range repulsive forces [62, 65]. Other strategies to achieve lower bacterial adhesion in biomaterials exposed to protein solutions rely on conditioning the surfaces. Heparin coatings have long been used to reduce bacterial adhesion to catheters and artificial lenses [62, 66, 67]. Heparin, in this case, was introduced to increase hydrophilicity, forming a highly hydrated layer

between the bacteria and the surface. In fact it has been proved that just heparin in solution can interfere with *S. epidermidis* adhesion [62, 68, 69]. Increased hydrophilicity of contact lenses can lead to a decreased bacterial adhesion [62, 70].

A critical point when developing new coatings concerns the way of the depositing and stabilizing the coating on the biomaterial. Current approaches to achieve functional antifouling coatings rely on different strategies including, among others, production of self-assembled mono- or multilayers, polymer brushes, surface grafting, zwitterionic polymers, hydrogels, and so on. The great difficulties in demonstrating the efficacy of anti-adhesive inert surfaces under real clinical conditions poses serious limitations to the assessment of the best anti-adhesive surfaces as well as to the correlation of in vitro, in vivo preclinical, and clinical data. Furthermore, it is worth taking into account that the antifouling properties conferred to the biopolymers require to be selected in relation to the application and in order to prevent bacteria adhesion, guaranteeing at the same time the desirable interactions with the host tissue. Indeed, for instance, low adhesiveness of antifouling surfaces is certainly a great advantage for catheters, but in other internal applications could possibly hinder tissue adhesion and integration of the implant. The achievement of selective adhesion properties has therefore become a relevant target of study [71].

References

- [1] C. M. Chan, T. M. Ko, H. Hiraoka, Surf. Sci. Rep. 1996, 24, 1.
- [2] T. Jacobs, R. Morent, N. De Geyter, P. Dubruel, C. Leys, Plasma Chem. Plasma Process. 2012, 32, 1039.
- [3] Y. Tabata, Drug Discov. Today 2001, 6, 483.
- [4] R. Vasita, K. Shanmugam, D. Katti, Curr. Top. Med. Chem. 2008, 8, 341.
- [5] Y. P. Jiao, F. Z. Cui, Biomed. Mater. 2007, 2, R24.
- [6] T. Desmet, R. Morent, N. De Geyter, C. Leys, E. Schacht, P. Dubruel, Biomacromolecules 2009, 10, 9.
- [7] B. G. Keselowsky, D. M. Collard, A. J. Garcia, Proc. Natl. Acad. Sci. U.S.A. 2005, 102, 5953.
- [8] B. G. Keselowsky, D. M. Collard, A. J. Garcia, Biomaterials 2004, 25, 5947.
- [9] L. Moroni, J. R. De Wijn, C. A. Van Blitterswijk, J. Biomater. Sci., Polym. Ed. 2008, 19, 543.
- [10] L. Moroni, R. Licht, J. de Boer, J. R. de Wijn, C. A. Van Blitterswijk, Biomaterials 2006, 27, 4911.
- [11] J. Y. Lim, H. J. Donahue, Tissue Eng. 2007, 13, 1879.

- [12] M. W. Moon, S. H. Lee, J. Y. Sun, K. H. Oh, A. Vaziri, J. W. Hutchinson, *Scr. Mater.* 2007, 57, 747.
- [13] J. M. Goddard, J. H. Hotchkiss, *Prog. Polym. Sci.* 2007, 32, 698.
- [14] M. Cloutier, D. Mantovani, F. Rosei, *TIBTEC* 2015, 33, 11.
- [15] J. W. Costerton, P. S. Stewart, E. P. Greenberg, *Science* 1999, 284, 1318.
- [16] A. Kramer, I. Schwebke, G. Kampf, *BMC Infect. Dis.* 2006, 6, 130.
- [17] K. Glinel, P. Thebault, V. Humblot, C. M. Pradier, T. Jouenne, *Acta Biomater.* 2012, 8, 1670.
- [18] Y. P. Jiao, F. Z. Cui, *Biomed. Mater.* 2007, 2, R24.
- [19] Y. Cao, W. Liu, G. Zhou, L. Cui, *Handchirurgie Mikrochirurgie Plastische Chirurgie* 2007, 39, 156.
- [20] M. S. K. Chong, C. N. Lee, S. H. Teoh, *Mater. Sci. Eng. C: Biomimetic Supramol. Syst.* 2007, 27, 309.
- [21] M. J. Walzak, S. Flynn, R. Foerch, J. M. Hill, E. Karbasheski, A. Lin, M. Strobel, *J. Adhes. Sci. Technol.* 1995, 9, 1229.
- [22] B. Singh, N. Sharma, *Polym. Degrad. Stab.* 2008, 93, 561.
- [23] K. Kato, E. Uchida, E. T. Kang, Y. Uyama, Y. Ikada, *Prog. Polym. Sci.* 2003, 28, 209.
- [24] J. Deng, L. Wang, L. Liu, W. Yang, *Prog. Polym. Sci.* 2009, 34, 156.
- [25] U. Edlund, M. Kallrot, A. C. Albertsson, *J. Am. Chem. Soc.* 2005, 127, 8865.
- [26] A. Sodergard, *J. Bioact. Compat. Polym.* 2004, 19, 511.
- [27] T. Richey, H. Iwata, H. Oowaki, E. Uchida, S. Matsuda, Y. Ikada, *Biomaterials* 2000, 21, 1057.
- [28] I. S. Alferiev, J. M. Connolly, S. J. Stachelek, A. Ottey, L. Rauova, R. J. Levy, *Biomacromolecules* 2006, 7, 317.
- [29] J. M. Harris, New York: Plenum Press, 1992.
- [30] W. E. Hennink, C. F. van Nostrum, *Adv. Drug Deliver. Rev.* 2012, 64, 223.
- [31] R. S. Langer, N. A. Peppas, *Biomaterials* 1981, 2, 201.
- [32] R. Bettini, P. Colombo, N. A. Peppas, *J. Controlled Release* 1995, 37, 105.
- [33] H. Cicek, A. Tuncel, *J. Polym. Sci., Part A Polym. Chem.* 1998, 36, 543.
- [34] W. S. Dai, T. A. Barbari, *J. Membr. Sci.* 1999, 156, 67.
- [35] N. Willmott, H. M. H. Kamel, J. Cummings, J. F.B. Stuart, A. T. Florence, *Microspheres and Drug Therapy. Pharmaceutical, Immunological and Medical Aspects*, Elsevier, Amsterdam, 1984, pp. 189–205.
- [36] S. R. Jameela, A. Jayakrishnan, *Biomaterials* 1995, 16, 769.

- [37] J. P. Draye, B. Delaey, A. van de Voorde, A. van den Bulcke, B. Bogdanov, E. Schacht, *Biomaterials* 1998, 19, 99.
- [38] S. H. Gehrke, L. H. Uhden, J. F. McBride, *J. Controlled Release* 1998, 55, 21.
- [39] T. Coviello, M. Grassi, G. Rambone, E. Santucci, M. Carafa, E. Murtas, F.M. Riccieri, F. Alhaique, *J. Controlled Release* 1999, 60, 367.
- [40] A. J. Kuijpers, P. B. van Wachum, M. J.A. van Luyn, G. H. M. Engbers, J. Krijsveld, S. A. J. Zaat, J. Dankert, J. Feijen, *J. Controlled Release* 2000, 67, 323.
- [41] A. J. Kuijpers, G. H. M. Engers, T. K. L. Meyvis, S. C. de Smedt, J. Demeester, J. Krijsveld, S.A.J. Zaat, J. Dankert, J. Feijen, *Macromolecules* 2000, 33, 3705.
- [42] N. A. Peppas, A. G. Mikos, Preparation methods and structure of hydrogels, in: N.A. Peppas (Ed.), *Hydrogels in Medicine and Pharmacy*, Vol. I, CRC Press, Boca Raton, FL, 1986, Chapter 1.
- [43] P. Gacesa, *Carbohydr. Polym.* 1988, 8, 161.
- [44] M. F. A. Goosen, G. M. O'Shea, H. M. Gharapetian, S. Chou, A. M. Sun, *Biotechnol. Bioeng.* 1985, 27, 146.
- [45] W. R. Gombotz, S. F. Wee, *Adv. Drug Deliv. Rev.* 1998, 31, 267.
- [46] A. Polk, B. Amsden, K. de Yao, T. Peng, M. F. A. Goosen, *J. Pharm. Sci.* 1994, 83, 178.
- [47] L. S. Liu, S. Q. Liu, S. Y. Ng, M. Froix, T. Ohno, J. Heller, *J. Controlled Release* 1997, 43, 65.
- [48] F. Yokoyama, I. Masada, K. Shimamura, T. Ikawa, K. Monobe, *Colloid Polym. Sci.* 1986, 264, 595.
- [49] S. Forster, M. Antonietti, *Adv. Mater.* 1998, 10, 195.
- [50] D. S. Lee, B. Jeong, Y. H. Bae, S.W. Kim, *Proc. Int. Symp. Controlled Release Bioact. Mater.* 1996, 23, 228.
- [51] B. Jeong, Y. H. Bae, S. W. Kim, *Macromolecules* 1999, 32, 7064.
- [52] B. Jeong, D. S. Lee, J. I. Shon, Y. H. Bae, S. W. Kim, *J. Polym. Sci. Part A Polym. Chem.* 1999, 37, 751.
- [53] J. M. Bezemer, D. W. Grijpma, P. J. Dijkstra, C. A. van Blitterswijk, J. Feijen, *J. Controlled Release* 1999, 62, 393.
- [54] J. M. Bezemer, R. Radersma, D. W. Grijpma, P. J. Dijkstra, J. Feijen, C. A. van Blitterswijk, *J. Controlled Release* 2000, 64, 179.
- [55] D. Eagland, N. J. Crowther, C. J. Butler, *Eur. Polym. J.* 1994, 30, 767.
- [56] C. L. Bell, N. A. Peppas, *J. Controlled Release* 1996, 39, 201.
- [57] A. M. Mathur, K.F. Hammonds, J. Klier, A. B. Scanton, *J. Controlled Release* 1998, 54, 177.
- [58] K. P. McGrath, M.J. Fournier, T. L. Mason, D. A. Tirrell, *J. Am. Chem. Soc.* 1992, 114, 727.

- [59] J. Cappello, J. Crissman, M. Dorman, M. Mikolajczak, G. Textor, M. Marquet, F. Ferrari, *Biotechnol. Prog.* 1990, 6, 198.
- [60] E. Yoshikawa, M. J. Fournier, T. Mason, D. A. Tirrell, *Macromolecules*, 1994, 27, 5471.
- [61] J. Cappello, J. W. Crissman, M. Crissman, F. A. Ferrari, G. Textor, O. Wallis, J. R. Whitley, X. Zhou, D. Burman, L. Aukerman, E. R. Stedronsky, *J. Controlled Release*, 1998, 53, 105.
- [62] D. Campoccia, L. Montanaro, C. R. Arciola, *Biomaterials* 2013, 34, 8533.
- [63] P. Speziale, G. Pietrocola, S. Rindi, M. Provenzano, G. Provenza, A. Di Poto A, *et al. Future Microbiol* 2009, 4, 1337.
- [64] D. Campoccia, P. Speziale, S. Ravaioli, I. Cangini, S. Rindi, V. Pirini, *et al. Biomaterials* 2009, 30, 6621.
- [65] F. Poncin-Epaillard, T. Vrlinic, D. Debarnot, M. Mozetic, A. Coudreuse, G. Legeay, *et al., J Funct Biomater* 2012, 3, 528.
- [66] M. R. Ruggieri, P. M. Hanno, R. M. Levin, *J Urol* 1987, 138, 423.
- [67] S. Nagaoka, H. Kawakami, *ASAIO J* 1995, 41, M365.
- [68] C. R. Arciola, Y. Bustanji, M. Conti, D. Campoccia, L. Baldassarri, B. Samorì B, *Biomaterials* 2003, 24, 3013.
- [69] Y. Bustanji, C. R. Arciola, M. Conti, E. Mandello, L. Montanaro, B. Samorì, *Proc Natl Acad Sci U S A* 2003, 100, 13292.
- [70] C. R. Arciola, L. Montanaro, R. Caramazza, V. Sassoli, D. Cavedagna, *J Biomed Mater Res* 1998, 42, 1.
- [71] L. G. Harris, S. Tosatti, M. Wieland, M. Textor, R. G. Richards, *Biomaterials* 2004, 25, 4135.

CHAPTER 2

PLASMA ASSISTED PROCESSES FOR THE MODIFICATION OF MATERIALS

2.1 Non-equilibrium atmospheric pressure plasma for the functional modification of polymers

In the previous chapter, polymers surface modification and crosslinking techniques mainly based on the use of chemical and physical methods have been reported with a focus on their possible advantages and drawbacks. The documented investigation allowed concluding that innovative, flexible and effective techniques, based on environmentally friendly and less time-consuming approaches, able to guarantee better, or at least the same, results than that achieved by means of conventional processes in the fields of biomaterials functionalization, polymers crosslinking and antibacterial surfaces preparation are demanded.

CAP technology can be considered as an effective alternative to conventional techniques and, even more, a suitable solution to overcome the above reported issues. Indeed, the plasma processes enable to effectively functionalize the surface layer of the polymers with short treatment times (from some seconds to few tens of minutes); to choose the chemical characteristics to confer to the treated polymer by varying the gas used for the plasma generation; to uniformly modify the whole surface and, importantly, without the use of chemical solvents.

Plasma is sometimes referred to as the fourth state of matter and is a partly ionized gas, defined as a quasi-neutral particle system in the form of gaseous or fluid-like mixtures of electrons, ions and radicals, generally also containing neutral particles (atoms, molecules). Since certain electrons are free, rather than bound to molecules or atoms, positive and negative charges can move independently from each other. There are two main categories of plasma: equilibrium and non-equilibrium plasmas. Equilibrium plasmas cannot be used for the surface treatment of polymers because of their high gas temperature, while non-equilibrium plasmas have a much lower gas temperature but relatively high electron temperature. Non-equilibrium plasmas do not induce any thermal damage of the surface of heat sensitive materials, although the reactive species can lead to chemical functionalization and, in some cases, physical modifications of the surface [1].

Since plasma contains a wide range of active species, different interactions of the plasma with the surface can occur. During exposure, different chemical functional groups can be implanted at the surface, in relation to the gas used for the plasma generation [2], and as a side effect the crosslinking can occur. This is often referred to as plasma functionalization or plasma treatment and the most used gases are oxygen or nitrogen containing gases or inert gases. The incorporated groups change the surface properties, mainly the surface wettability and thus the surface energy, but also the surface roughness [3]. The plasma-treated surfaces can be used to directly promote the cell adhesion and differentiation or to immobilize (or to graft) biologically active ligands. One major and important

drawback of plasma treatment is the durability of the treatment effect, since the surface undergoes a hydrophobic recovery after treatment losing part of the generated effect [4, 5].

Besides the plasma functionalization, CAPs have been greatly employed in the plasma polymerization process, basically a deposition technique where a gaseous or liquid monomer is introduced inside the plasma and converted into active fragments [6-9], which, reacting with each other and with the surface of the substrate, enable the formation of plasma polymer coating. These coatings are characterized by chemical and physical properties, which make them slightly different than conventionally fabricated polymer coatings. As a matter of fact, plasma polymer coatings generally are pinhole-free, highly crosslinked and are therefore insoluble, thermally stable, chemically inert and mechanically tough. Furthermore, these films often are highly coherent and adherent to a variety of substrates including conventional polymer, glass and metal surfaces [10].

A schematic representation of the CAP assisted processes, which can be carried out onto polymeric materials is reported in Figure 1.

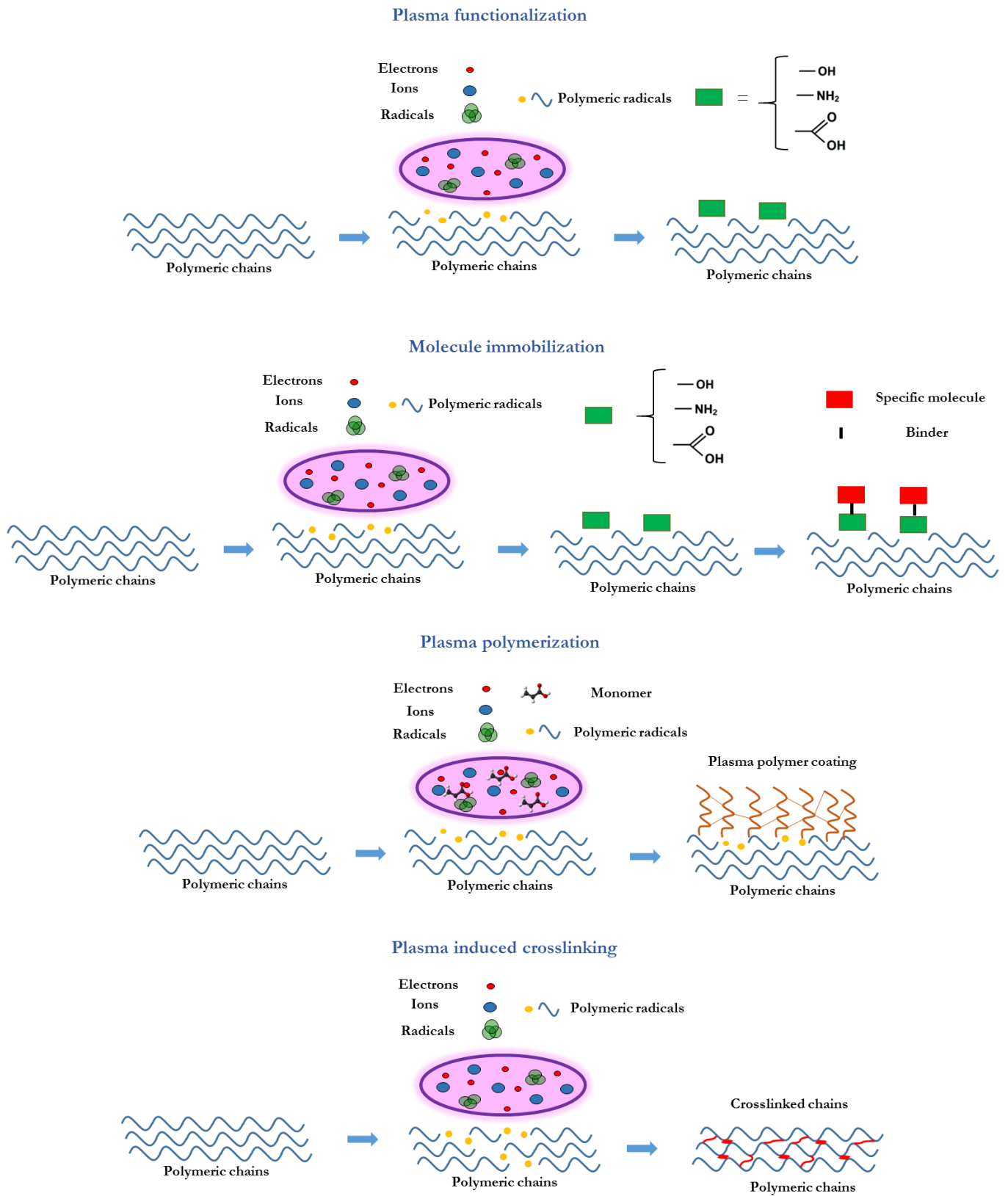


Figure 1. Surface modification processes assisted by non-equilibrium plasmas

In this chapter, after a brief overview on the most used CAP sources, some studies from scientific literature reporting the use of CAP for the surface modification of biomaterials, by means of plasma functionalization or polymerization, and the crosslinking of polymers are reported and discussed.

2.2 Non-equilibrium atmospheric pressure plasma sources

Non-equilibrium plasmas are generated by the application of an electric field to a neutral gas, which ensures the ionization in the gas volume and the production of charged particles, accelerated in the applied electric field. Electrons are particularly affected by the electric field, due to their mass, while the heavy ions efficiently exchange their energy by collisions with the background gas, remaining cold and guaranteeing a temperature suitable for the treatment of thermo-sensitive materials, such as biopolymers. The collisions between energetic electrons and neutral molecules lead to the creation of radicals, which are crucial for the chemical activity of the plasma.

An effective and proven technology in the field of plasma modification of materials is represented by low pressures plasmas, which operating with a pressure in a range of 10^{-8} - 10^{-2} bar are very stable and characterized by highly controllable reactions, also due to the long mean free path of the gas particles.

The challenging request for developing flexible and easy to scale-up processes has encouraged and accelerated the evolution of the plasma technology, leading to the design and optimization of processes based on the use of non-equilibrium plasma sources working at atmospheric pressure, which, for the absence of the vacuum pump, can also be cost-effectively integrated in industrial in-line processes for the production of both high- and low value-added materials.

The difficulty in operating with atmospheric pressure plasmas is represented by the instabilities of the discharge, linked to the short mean free path. Indeed, if not properly controlled and prevented, these instabilities can induce the transition to thermal arc discharge, greatly undesired because of the loss of homogeneity as the discharge is constricted to narrow current channels, with a subsequent increase of the gas temperature [11].

Different solutions have been optimized to prevent this transition at atmospheric pressure [12, 13]. Pulsed corona employed at atmospheric pressure limit the discharge maintenance time by working in a pulsed regime; Dielectric Barrier Discharges (DBDs) prevent the transition by autopulsation of the discharge with a dielectric barrier covering one or both the electrodes; in the direct current (DC) glow discharges, the instabilities are prevented by the application of a fast gas flow.

In the following, the most significant properties of the non-equilibrium atmospheric pressure plasma discharges employed in the experimental activities reported in the present thesis are briefly discussed.

Corona discharge

A corona is a weakly luminous discharge, which appears at atmospheric pressure near sharp points, edges, or thin wires, where the electric field is sufficiently large. Corona discharges are always non-uniform: a strong electric field, ionization, and luminosity are located in the vicinity of one electrode [14]. Charged particles are dragged by the weak electric fields from one electrode to another to close the electric circuit [14]. Applications of the continuous coronas are limited by low current and power, which results in a low rate of treatment of materials and exhaust streams. Increasing the corona power without transition to sparks becomes possible by using pulse-periodic voltages. Therefore, for the pulsed corona discharges, the key is the development of the pulse power supplies generating sufficiently short voltage pulses with a steep front and short rise times. As an example, nanosecond pulse power supplies generate pulses with duration 100–300 nsec, sufficiently short to avoid the corona-to-spark transition [14].

Despite the small active volume, corona discharges are often applied for treatment of polymers [15–18], even though it was suggested that corona-discharge treatment could possibly influence the biodegradability of certain polymers [19].

Dielectric Barrier Discharge (DBD)

The transition to equilibrium plasma is prevented in a pulsed corona by employing nanosecond pulse power supplies. Another approach to avoid this transition is based on the use of a dielectric barrier in the discharge gap that stops the current flow and prevents spark formation. Such a discharge is called DBD. The presence of a dielectric barrier precludes DC operation of DBD, which usually operates at frequencies of 0.05–500 kHz. DBD has numerous applications because it can be operated in strongly non-equilibrium conditions at atmospheric pressure and using different gases, including air, at reasonably high power levels and (in contrast to the pulsed corona) without requiring the use of sophisticated pulse power supplies [14].

DBD plasma sources can be characterized by several configurations and in one of the most common configuration least one of the electrodes is covered by a dielectric layer (Figure 2). The dielectric, as reported, is the essential part of the discharge. Indeed, after ionization at a certain location in the discharge gap, the transported charge accumulates at the dielectric surface, generating an electrical field that reduces the field in the gap and interrupts in this way the current flow after a few nanoseconds [11]. When an AC voltage (typical frequencies: 1–100 kHz) with an amplitude sufficient for breakdown is applied, a large number of microdischarges are induced, randomly distributed in time and space. The dielectric layer limits the amount of charge transported by a single microdischarge and distributes the microdischarges over the entire area of the electrode [11].

DBDs have been applied for a wide variety of applications such as ozone generation, in UV sources, in polymer treatment, for pollution control, for biological and medical application, in plasma-assisted combustion and so on [14].

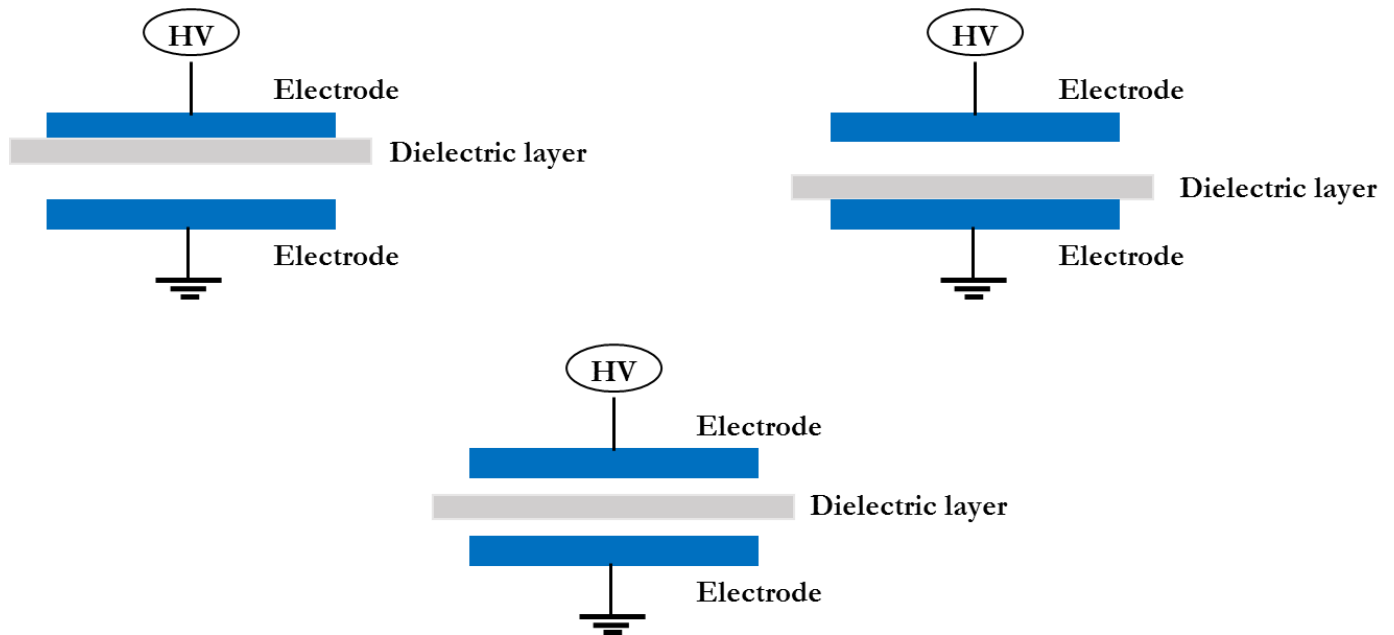


Figure 2. Schematic representations of dielectric-barrier discharges (DBDs). (The schematic refers to the DBD representation reported in [14])

Plasma Jet for remote plasma treatment

In recent years, non-equilibrium atmospheric pressure plasma jets (APPJs) have been raising a significant interest because of their broad range of applications, among which the decontamination and sterilization of surfaces [20, 21], surface modification of polymers [22-24], thin film deposition [25, 26], nanomaterials fabrication and modification [27-31], medical therapies [32, 33, 34]. One of the reasons of the diffuse interest toward APPJs is their versatility, granted by the diverse possible combinations of driving power supply, gas employed, and source architecture [35]. Among this ample number of plasma sources, APPJs notable for their scientific and historical relevance, characteristic architecture, or extensive application are the plasma needle [36], the plasma gun [37], the plasma pencil [38], the kINPen [39], the plasma jet array or Gatling machine gun-like plasma jet [40, 41], and the plasma jet with the porous alumina layer between anode and cathode [42].

In the field of the treatment of thermo-sensitive polymers, plasma jets are often employed since they allow performing a remote plasma treatment [11]. Differently from the active plasma treatment where the substrate to be treated is placed between the electrodes, in the remote configuration (or afterglow treatment) the substrate is located outside the region of plasma generation, but it comes in contact with the gas stream loaded with radicals and other active species. While the active plasma treatment

has the advantage of a higher concentration of active species near the surface of the substrate, in the remote plasma treatment the concentration of species reaching the substrate decreases as a function of distance from the plasma generation region and depends on the lifetime of the active species [43]. The remote plasma configuration is generally chosen to prevent damages from the discharge and to treat the surface of materials of any thickness and any geometry (3D objects) [11].

2.3 Functionalization of polymers by means of non-equilibrium plasma

The functionalization of polymers is strictly connected to the modification of the chemical characteristics of the surface layer in relation to the gas used for the plasma generation and treatment. Oxygen and oxygen-containing plasmas are commonly employed to produce a variety of oxygen functional groups, including C-O, C=O, O-C=O, C-O-O and CO₃ at the polymer surface, through the reactions between the active species from the plasma and the surface atoms [44]. Nitrogen and nitrogen-containing plasmas are widely used to improve wettability, printability, bondability and biocompatibility of polymer surfaces [45]. The introduction of amino groups on the surface of polystyrene films with ammonia-plasma treatment was reported to improve cell affinity [46]. Ammonia and nitrogen plasmas have been used to provide surface amino binding sites for immobilization of heparin on a variety of polymer surfaces [47]. Despite the use of nitrogen containing gas for the plasma generation, oxygen functionalities are always incorporated on the polymer surfaces, mainly due to the presence of oxygen inside the plasma chamber and the creation during the plasma process of free radicals on the polymer surface, which are able to react with the oxygen when the surface is exposed to the atmosphere [44]. Polymers that are treated with inert gas, such as Ar or He, plasmas will not be subjected to the incorporation of new functionalities on their surface during the process, however, free radicals, which can interact with the oxygen from the atmosphere, will be created [48].

In light of these considerations, it can be stated that unfortunately plasma functionalization does not result in a unique functionality, which means it can not be considered as a selective technique [11]. In order to overcome this limitation, the deposition of coatings, containing the desired functional groups, onto the substrates by means of plasma-polymerization processes is performed, as described in the following.

The functionalization of the polymer surfaces can be devoted to the fabrication of biocompatible polymers, which can be exploited as substrate for the direct adhesion of eukaryotic cells or for the preparation of bioactive surfaces through the immobilization, by means of chemical reactions, of biomolecules onto the functionalized substrate. It is worth underlining that, contextually to the

increase of the biocompatibility, plasma functionalization, when performed in properly selected operating conditions, can also confer antibacterial characteristics to the surface, leading to the fabrication of materials highly suitable for biomedical applications and regenerative medicine.

2.3.1 Plasma functionalization to improve cell adhesion

Several efforts in the field of plasma modification of materials have been devoted to document the effectiveness of non-equilibrium plasma in increasing the surface biocompatibility of polymers by means of processes based on the use of non-polymerizable gas, with the aim to promote cells adhesion, proliferation and differentiation. Furthermore, interesting reviews, such as the works of Leys and co-workers [11, 49], have deeply abridged the state of the art, providing a complete overview on the plasma processes up to now implemented and on the achieved results. In the frame of atmospheric pressure processes, some interesting works are here reported and discussed.

Nakagawa *et al.* [50] and Teraoka *et al.* [51] modified PLA surfaces with an atmospheric air plasma jet. The X-ray photoelectron spectroscopy (XPS) underlined the introduction of oxygen-containing groups such as C–O, C=O and O–C=O on the top layer of the substrate surface were incorporated. Cell culture tests performed with mouse osteoblast-like MC3T3-E1 cells highlighted the improvement of both cells adhesion and proliferation onto the plasma treated PLA. Furthermore, the authors demonstrated the surface modification method of PLLA using the low-temperature plasma treatment apparatus at atmospheric pressure is a clinically useful method, where the bonding of the cell can be easily controlled by varying the gas to employ during the process [50]. Yildirim *et al.* [52] employed an atmospheric pressure DBD plasma operated in oxygen to treat PCL samples and observed that the oxygen plasma treatment not only enhances the hydrophilicity and increases solid surface energy, surface roughness of PCL but also improves the initial attachment and the proliferation of osteoblasts on the PCL substrate. Lee *et al.* also used an atmospheric pressure DBD operating in air to modify PCL films [53]. Fourier Transform Infrared (FT-IR) spectroscopy and XPS detected a higher amount of oxygen containing hydrophilic groups (C–O, COOH, C=O and OH) on the plasma-treated films and the cell attachment and proliferation of human prostate epithelial cells (HPECs) was found to be ten times higher on plasma-treated PCL films compared to untreated film. The same authors used different gas mixtures [54] for plasma treatment and observed that when Ar+H₂ was used as gas discharge, the contact angle increased after treatment. Opposite results were found for Ar+N₂, Ar and Ar+O₂. The increase in the hydrophobicity of the Ar + H₂ plasma-treated PCL film resulted in a lower cell loading in the initial step of cell culture as well as a decrease in the level of cell attachment and proliferation compared with the pristine film. However, the hydrophilic

properties of the Ar + N₂, Ar and Ar + O₂ plasma-treated PCL film improved the adhesion properties. Therefore, the Ar + N₂, Ar and Ar + O₂ plasma-treated PCL films showed a better cell distribution and growth than that of the pristine PCL film.

Recently, Kuzminova *et al.* [55] reported about the use of an atmospheric pressure DBD operated in air for the modification of surface properties of PET foils, observing that the exposure to the plasma led to a rapid change of the surface chemical composition, with an increase of the amount of –COOH groups. This was in turn responsible for the fast increase of the polar part of surface energy and consequently for the increase of PET wettability. However, both changes in surface chemical composition and wettability were found to be independent on the DBD plasma treatment duration: no significant differences were observed for PET foils treated 1 and 32 s. The biological tests, performed by using two cell types (Saos-2 human osteoblast-like cells and HUVEC human umbilical vein endothelial cells), highlighted that the result in terms of cell adhesion is also linked to the kind of cell. In fact, whereas endothelial cells were found to rapidly attach and grow on treated PET foils, only slight enhancement in cells count was observed for osteoblast-like cells. This finding underlines that it is not possible to generalize the results obtained for a particular cell type on other cell types and, thus, each cell type has to be considered separately. Trizio *et al.* [56] dealt with the functionalization of a 3D porous PCL scaffold by means of an atmospheric pressure plasma jet fed with a mixture of He and O₂. The results highlighted that plasma can functionalize the outer and inner surface of the scaffold with a consequent improvement of the cytocompatibility. Indeed the cytocompatibility assays revealed that Saos-2 cells could adhere to and colonize better the porous structure of plasma treated PCL scaffolds, reaching a polygonal shape and developing their typical cluster aggregation.

2.3.2 Plasma functionalization for biomolecules immobilization

Besides the introduction of chemical groups to promote cell adhesion and proliferation directly onto the functionalized surface, plasmas can also be used for the covalent immobilization of bioactive molecules, in order to promote the interaction of cells with the grafted molecules rather than with the underlying surface. In this case, plasma is mainly used to pretreat the surface before the immobilization of the selected biomolecule, carried out by means of chemical or physical techniques. This approach has been implemented for the immobilization of biomolecules like insulin, chitosan, gelatin, Arg-Gly-Asp (RGD) or Arg-Gly-Asp-Cys (RGDC), enabling to obtain the enhancing of cell-material interaction [57–60]. The immobilization of insulin on PHBV led to an increased cell proliferation of human fibroblast cells and full cell spreading on the surface [57]. By using the spacer

arm bNH₂PEG (O,O'-bis-(2-aminopropyl)-polyethylene glycol 500), the RGDC peptide were immobilized on the surface of acrylic acid grafted poly(tetrafluoroethylene) (PTFE) [58]. The attachment amount of HUVECs was observed to be four times higher for the modified polymer than for the pristine one. Besides the covalent immobilization, some authors have been immersing plasma pretreated biomedical polymers into protein containing solutions leading to non-covalent linking of proteins to the surface. Although these proteins can be easily removed, they also lead to a better cell attachment and proliferation onto the modified surface [59–62]. It can be inferred that plasma functionalized surfaces with amine, carboxyl, hydroxyl and aldehyde groups can provide a suitable platform for the interfacial immobilization of bioactive molecules. The ability of plasma technology in introducing functional groups onto the surface of polymers, also by employing atmospheric pressure plasma processes, have been widely documented, as above reported. Moreover, in this context, with the aim to further discuss the potentialities of CAPs in introducing functional groups for biomolecules immobilization, two other studies are reported. Kostov *et al.* [63] investigated the surface modification of different polymers performed by means of an Ar plasma jet operated in different operating conditions; moreover, the comparison between the polymer surface modifications induced by the plasma jet and a Dielectric Barrier Discharge (DBD) treatment was carried out [63]. The achieved results brought out that both the plasma sources are efficient tools for the surface modification, even though, in the optimized operating conditions, the plasma jet can enable the introduction of a higher amount of –COOH groups than the DBD treatment, suggesting the occurrence of a more intense surface oxidation [63]. Sarra-Bournet *et al.* [64] proposed the filamentary dielectric barrier discharge (FDBD) and the atmospheric pressure glow discharge (APGD) as interesting alternatives to the low pressure plasma sources. N₂ + H₂ and N₂ + NH₃ plasmas were applied on poly(tetrafluoroethylene) to determine the relative influence of both the discharge regime and the gas nature on the surface transformations. From XPS analysis, it was shown that the discharge regime had a significant effect on the surface transformation; FDBDs operating in H₂/N₂ led to a high concentration of amino-groups with high specificity but also important damaging on the surface. Glow discharges in both H₂/N₂ and NH₃/N₂ led to lower concentrations of amino-groups with lower specificity but lower surface damaging. Therefore, this simple surface treatment turned out to be an effective, low cost method for the production of uniform surface modification with amino-groups that can subsequently be used to graft various chemical functionalities used for biomaterial compatibility [64].

2.3.3 Plasma preparation of antibacterial surfaces

The surface functionalities that arise as a result of plasma treatment can serve as a platform for further surface modification processes, such as cell adhesion, grafting of biomolecules and other functional structures. Among the spectrum of the possible applications, the functionalization of the polymers surface can be properly controlled to confer antibacterial properties to the substrate. As previously mentioned, bacterial attachment to a solid surface is highly dependent on the surface properties of the material, such as its chemical composition and reactivity, surface energy and hydrophobicity [65], surface roughness [66, 67], and porosity. Furthermore, bacterial attachment is a competitive process, in which microorganisms race against host proteins and cells for the colonisation of the surface [68], as inferred by using a microfluidic device for real time imaging of the behaviour of osteoblasts in response to the presence of a very limited numbers of *S. epidermidis* on an alloy surface. During the early stages of culture, osteoblast adhesion, spreading, and proliferation were not adversely affected. Towards the end of the culture, however, the osteoblasts became damaged because *S. epidermidis* actively proliferated in the co-culture channels and formed small clusters on the alloy surface, changing the microenvironment so that it was no longer favorable for the sustenance of osteoblasts [69].

Since most pathogens are hydrophilic under physiological conditions, decreasing the water contact angle of the material may improve its antibacterial properties. Indeed, a DC oxygen treatment of medical grade poly(vinyl chloride) resulted in a 70% reduction in bacterial adhesion for the four strains of *P. aeruginosa* [70]. However, this reduction was unlikely to be sufficient to prevent *P. aeruginosa* colonisation of endotracheal intubation devices [71]. Treatment of polyethylene terephthalate with helium and 20% oxygen in helium (He/O₂) plasma were demonstrated to significantly reduce *S. epidermidis* bacterial adhesion compared with the untreated material [72]. Furthermore, exposure to plasma was shown to irreversibly damage bacterial cells, allowing in situ sterilisation of the biomaterial during the surface modification process.

Besides the preparation of antibacterial surfaces, another great challenge in designing materials intended for biological environments is the production of surfaces that resist nonspecific protein adsorption. When a biomaterial is implanted in vivo, in fact, after a few minutes a layer of nonspecific adsorbed proteins is formed. Subsequently, many events which generate the so called “foreign body reaction”, such as cytokine production or macrophage attack, will occur to develop the formation of a thin collagenous capsule which isolates the implant from the body [73, 74]. Proteins randomly adsorbed at the biomaterial surface will not specifically interact with receptors, proteins, or

glycoproteins located at the cell membrane, in order to drive a cell-specific response. The only possibility to drive a specific cell–surface interaction (e.g. a specific function) is therefore to avoid a nonspecific protein adsorption, which may occur immediately after the implantation [74]. As an example, to prevent protein adsorption poly(ethylene glycol) (PEG), also known as poly(ethylene oxide) (PEO), a synthetic, water-soluble polymer has been largely employed on plasma activated substrates with or without coupling agents for several practical applications ranging from chemistry to biomedical and cosmetics [74]. The large interest that PEO coatings generate in these applications is mainly due to its low degrees of protein adsorption [74, 75], together with low cell and bacterial adhesion [74, 76].

2.3.4 Ageing of plasma functionalized polymers

In general, the concentration of functional groups introduced on a polymer surface by plasma treatment could change as a function of time depending on the environment and temperature. This phenomenon is due to the greater mobility of the polymer chains at the surface than in the bulk, allowing the surface to reorient in response to different environments. Surface orientation can be accomplished by the diffusion of low molecular weight oxidized components into the bulk. When a polymer is exposed to an oxygen-containing plasma, the surface changes to a higher energy state as a result of the formation of polar groups and of the increase of the surface energy. Various surface studies have indicated that the decrease in the surface energy when the treated surface is placed in a low energy medium, such as air or vacuum, is caused by the rotation of the polar groups in the bulk or the migration of low molecular weight fragments to the surface to reduce the interfacial energy [44]. Conversely, when a low energy surface formed by treating a polymer in a fluorine-containing plasma is placed in a high energy medium such as water, the apolar groups will tend to minimize the interfacial energy by moving away from the surface into the bulk [44].

This phenomenon is usually described as ageing of a treated surface and in light of the previous considerations, it is a very complex phenomenon affected by the storage conditions of the substrate. In this respect, Nakamatsu *et al.* [77] observed that poly(tetrafluoroethylene) treated with air plasma and kept in water did not lose the functionalization achieved with the plasma treatment, as the polar hydrophilic groups remained on the surface, even for 180 days after the treatment. On the contrary, the surface chemical composition of a N₂ plasma treated polyethylene surface, monitored as a function of storage time in air, was subjected to a rapid loss of nitrogen and a significant increase in oxygen during the first few days.

Another important factor affecting the aging characteristics of a plasma treated polymeric surface is the storage temperature. Indeed, it has been demonstrated that a lower storage temperature reduces the rate of ageing [78]. The rapid change of the contact angle at high temperatures supports the idea that the changes in the surface are caused by polymer chain motion, reorienting the polar groups into the bulk [78].

2.4 Plasma deposition

In order to overcome the recovery of the functionalities introduced by the plasma treatment onto the surface of the polymeric substrates, plasma polymerization is generally preferred to the functionalization, especially when the elapsing time between the surface chemical modification and the use of the substrate is too high to prevent the total or partial loss of the induced functionalities.

Differently from the immobilization of molecules, plasma deposition is not based on the covalent binding of species onto a previously activated polymer surface, but it enables, in a single step process, to coat a substrate by exploiting the contextual activation of both the monomeric units introduced inside the plasma region and the substrate subjected to the plasma discharge.

A wide variety of substrates and monomers has been applied so far [11] and, depending on the nature of the monomer and on the operating conditions used to carry out the process, the coatings are characterized by different chemical and physical properties, mainly due to the fact that the monomer can react in different ways with the plasma [79, 80].

In the frame of biomedical applications, great efforts have been devoted to the plasma polymerization of acrylic acid (AA), since it enables to produce coatings containing carboxylic acid (—COOH) groups [81], which are known to favor cell adhesion and can also be exploited for biomolecule immobilization [82].

Low-pressure plasma enhanced chemical vapour deposition (PECVD) is nowadays one of the most widespread tools for the effective coatings deposition on substrates [83]. Several studies have been already performed with the aim to investigate the characteristics of plasma-polymerized acrylic acid (pPAA) films deposited by means of PECVD technology. The obtained results show that the plasma operating conditions can strongly influence the chemical composition, the morphology and the homogeneity of the pPAA coatings, as well as their water stability [84, 85].

In recent years, many efforts have been dedicated to develop coating processes relying on non-equilibrium plasma sources working at atmospheric pressure [86-88]; as an example, the possibility to employ atmospheric pressure DBD to obtain functional surfaces with chemically reactive moieties such as amino [89] or carboxylic groups [90] was demonstrated.

Results of previous works on pPAA deposition [91-93] showed that in these systems the effect of monomer fragmentation on the retention of –COOH groups turns out to be relevant: the higher the monomer fragmentation, the lower the amount of –COOH groups on the coated substrate [91, 93], as also experimentally evidenced by Palumbo *et al.* [94] through a correlation of Optical Emission Spectroscopy and X-ray Photoelectron Spectroscopy results.

With the aim to contribute to overcome the problem of the monomer fragmentation, recent studies were performed on the polymerization of an allyl monomer containing phosphorus [95] and the deposition of glycidyl methacrylate layer [96] with a nanosecond square-pulsed AP-DBD, in order to maximize the structural retention of monomers and preserve their functional groups. In fact, thanks to its very high slew rate, the ultra-short square pulses enable the generation of a short and homogeneous discharge with a large proportion of high energy electrons, which efficiently induce the creation of free radicals able, in turn, to initiate the free radical polymerization reactions, responsible of the high retention of the monomer functional groups [96].

Differently from the AP-DBD systems, non-equilibrium atmospheric pressure plasma jet (APPJ) are well suited for localized treatment and coating of complex 3D geometries, since the substrate does not have to be placed in the gap between electrodes. Furthermore, the possibility to scale down the dimension of the jet to the submillimeter range widens the field of application of the process. The studies performed with this kind of sources demonstrated the effectiveness of non-equilibrium APPJs in depositing polymeric films by means of monomer polymerization.

With regard to AA plasma-polymerization, Donegan *et al.* [97] investigated the water stability, the chemical/morphological characteristics and the level of protein adhesion of pPAA coatings deposited onto silicon substrates by using two different plasma jet deposition systems. Chen *et al* [98] highlighted the possibility to deposit pPAA coatings onto the surfaces of silk fibers (SF) using an atmospheric pressure glow discharge in order to immobilize antimicrobial peptide onto the SF surface. Carton *et al.* [99] employed a pulsed-arc atmospheric pressure plasma jet for the AA plasma polymerization and the deposition of organic coatings suitable for biomedical applications. The same plasma source was also used to perform the polymerization of AA and methylene-bis-acrylamide [100]. The latter compound was added as crosslinking agent to the precursor in order to improve the water stability of the deposited coatings. Ward *et al.* [101] performed the deposition, by introducing ultrasonic atomization of AA into an APGD, of pPAA layers characterized by good adhesive and gas barrier properties.

Besides the fabrication of plasma polymer coatings, in recent years the efficacy of CAPs in depositing nanocomposite coatings, characterized by nanoparticles (NPs) embedded in a polymeric matrix,

widely required for a great range of industrial applications, has been successfully demonstrated [102-112]. The first work on his topic was published in 2009 by Bardon *et al.* [113] and reported on the deposition of a nanocomposite coating where AlCeO₃NPs were embedded in an organosilicon matrix; the process was performed injecting in a DBD reactor a NPs dispersion in a liquid organosilicon precursor. Later, Dembele *et al.* [114] reported on the deposition of a nanocomposite coatings (organosilicon polymer and TiO₂NPs) obtained by introducing a dispersion of NPs in tetramethoxysilane in a plasma jet having a point to plane corona configuration. Some studies were also performed on the synthesis of organo-inorganic nanocomposite coatings by means of atmospheric pressure cold plasma. In particular, Uygun *et al.* [115] deposited different coatings by introducing a dispersion of polymer precursor (either pyrrole, thiophene, or furan monomers), TiO₂NPs, and LiClO₄ in acetonitrile in an atmospheric pressure RF uniform glow discharge. Michel *et al.* [116] investigated the deposition of plasma-polymerized polyaniline (PANI) coatings including mercaptoaniline functionalized PtNPs, by introducing a dispersion of functionalized NPs in ethanol and aniline in the plasma region of a DBD. Fanelli *et al.* [117] reported on the deposition of ZnONPs/hydrocarbon polymer nanocomposite coatings using an atmospheric pressure DBD, fed with He and with an aerosol of oleate-capped ZnONPs dispersed in a hydrocarbon solvent. Recently, cold plasma deposition of nanocomposite coatings with antibacterial properties has also been investigated, exploiting the well known antimicrobial properties of AgNPs [118]. Indeed, Beier *et al.* [119] reported on a process where hexamethyldisiloxane, used as silicon containing precursor for the matrix, and a dispersion containing either AgNO₃ or AgNPs were simultaneously injected in the plasma region of a DC pulsed arc discharge plasma jet. A different process, relying on the use of DC plasma jet, was proposed by Deng *et al.* [25]; N₂ was used to sustain the plasma discharge and an admixture of O₂, tetramethyldisiloxane, as organosilicon precursor for the matrix, N₂ and AgNPs was fed to the plasma region. To date, only one work, published by Humud *et al.* [120] proposed the fabrication of coatings containing AgNPs in a polymeric matrix using an atmospheric pressure plasma; the process, performed with a DBD plasma jet, was aimed at improving the conductivity of a polyaniline matrix by means of the introduction of AgNPs. As precursor, a dispersion of AgNPs in aniline was carried, in form of aerosol, by an Ar flow and injected into the plasma region [120].

2.5 Plasma induced crosslinking

As reported in the previous chapter, the crosslinking of water soluble biopolymer can be performed by using either physical methods or chemical agents [121-123]. However, the most common crosslinking agents often give rise to cytotoxicity problems, and are therefore not suitable for

biomedical applications. Many efforts have been devoted to develop less cytotoxic chemical agents, as well as new methods able to crosslink biopolymers without using chemical compounds [124-128]. Non-equilibrium plasma, being an environmentally friendly technology, can represent a suitable solution for the achievement of the proposed aim. Some studies have been recently performed to evaluate the possibility of employing a single-step plasma process to induce the crosslinking of water soluble polymers in liquid phase, since non-equilibrium plasma treatment is able to induce the formation of radicals, which may recombine producing unsaturation and polymer crosslinking [129-131].

Prasertsung *et al.* [132], pointed out that the generation of pulsed electrical discharges in gelatin solutions enables: (i) to increase the solution viscosity; (ii) to enhance the gel strength; (iii) to produce films characterized by a higher crosslinking degree with respect to that obtained by untreated gelatin solutions. Recently, Molinas *et al.* [133] reported about the possibility to use an atmospheric dielectric barrier discharge (DBD) plasma to induce in-situ liquid phase gelation of an aqueous solution of chitosan in order to obtain a crosslinked hydrogel.

To the best of our knowledge, only few studies have reported the use of plasma to confer water resistance and improve the mechanical properties of water soluble polymers directly in the solid state [134, 135]. These studies, which were carried out by subjecting electrospun polymeric fibres to low pressure plasma treatments, were not successful in stabilizing the polymer against water dissolution, probably because the plasma treatment affected only the surface of the fibres resulting in a limited crosslinking degree.

Therefore, further studies are required to optimize the non-equilibrium plasma processes in order to induce crosslinking directly in the solid state

References

- [1] M. Zenkiewicz, P. Rytlewski, R. Malinowski, *Polimery* 2011, 56, 185.
- [2] N. De Geyter, R. Morent, C. Leys, L. Gengembre, E. Payen 2007, 201, 7066.
- [3] N. Y. Cui, N. M. D. Brown 2002, *Appl Surf Sci* 189, 31.
- [4] R. Morent, N. De Geyter, C. Leys, E. Payen 2007, *Surf Coat Technol* 201, 7847.
- [5] N. De Geyter, R. Morent, C. Leys 2008, *Nucl Instrum Meth B* 226, 3086.
- [6] R. Morent, N. De Geyter, S. Van Vlierberghe, A. Beaurain, P. Dubruel, E. Payen 2011, *Prog Org Coat* 70, 336.
- [7] N. De Geyter, R. Morent, S. Van Vlierberghe, *Prog Org Coat* 70, 293.

- [8] R. Morent, N. De Geyter, S. Van Vlierberghe, P. Dubruel, C. Leys, L. Gengembre, E. Schacht, E. Payen 2009, *Prog Org Coat* 64, 304.
- [9] R. Morent, N. De Geyter, S. Van Vlierberghe, E. Vanderleyden, P. Dubruel, C. Leys, E. Schacht 2009, *Plasma Chem Plasma Process* 29, 103.
- [10] F. Arefi, V. Andere, P. Montazer-Rahmati, J. Amouroux 1992, *Pure Appl Chem* 64, 715.
- [11] T. Desmet, R. Morent, N. De Geyter, C. Leys, E. Schacht, P. Dubruel, *Biomacromolecules* 2009, 10, 9.
- [12] A. N. Bhoj, M. J. Kushner, *Plasma Sources Sci. Technol.* 2008, 17, 3.
- [13] A. Fridman, A. Chirokov, A. Gutsol, *J. Phys. D: Appl. Phys.* 2005, 38 R1.
- [14] A. Fridman, *Plasma Chemistry*, Cambridge University Press, 2008.
- [15] S. M. Desai, R. P. Singh, *Long-Term Prop. Polyolefins* 2004, 169, 231.
- [16] I. Novak, V. Pollak, I. Chodak, *Plasma Processes Polym.* 2006, 3, 355.
- [17] L. P. Zhu, B. K. Zhu, L. Xu, Y. X. Feng, F. Liu, Y. Y. Xu, *Appl. Surf. Sci.* 2007, 253.
- [18] D. Walsh, T. Furuzono, J. Tanaka, *Biomaterials* 2001, 22, 1205.
- [19] S. Osawa, T. Yokoyama, M. Hanada, T. Ogawa, *Kobunshi Ronbunshu* 2001, 581.
- [20] K. D. Weltmann *et al.*, *J. Phys. D, Appl. Phys.* 2008, 41, 194008.
- [21] J. Shen *et al.*, *Appl. Phys. Exp.* 2012, 5, 036201.
- [22] U. Lommatzsch, D. Pasedag, A. Baalman, G. Ellinghorst, H. E. Wagner, *Plasma Process. Polym.* 2007, 4, S1041.
- [23] C. Cheng, Z. Liye, R. J. Zhan, *Surf. Coat. Technol* 2006., 200, 6659.
- [24] E. J. Szili, S. A. Al-Bataineh, P. M. Bryant, R. D. Short, J. W. Bradley, D. A. Steele, *Plasma Process. Polym.* 2011, 8, 38–50.
- [25] X. Deng, C. Leys, D. Vujosevic, V. Vuksanovic, U. Cvelbar, N. De Geyter, R. Morent, Anton Nikiforov, *Plasma Process. Polym.* 2014, 11, 921.
- [26] H. Fakhouri, D. B. Salem, O. Carton, J. Pulpytel, F. Arefi-Khonsari, *J. Phys. D, Appl. Phys.* 2014, 47, 265301.
- [27] D. Mariotti, M. Sankaran, *J. Phys. D, Appl. Phys.* 2011, 44, 174023.
- [28] D. Mariotti, J. Patel, V. Svrcek, P. Maguire, *Plasma Process. Polym.* 2012, 9, 1074.
- [29] S. Mitra, V. Svrcek, D. Mariotti, T. Velusamy, K. Matsubara, M. Kondo, *Plasma Process. Polym.* 2014, 11, 158.
- [30] S. W. Lee, D. Liang, X. P. A. Gao, R. M. Sankaran, *Adv. Funct. Mater.* 2011, 21, 2155.
- [31] S. W. Lee, C. Mattevi, M. Chhowalla, R. M. Sankaran, *J. Phys. Chem. Lett.* 2012, 3, 772
- [32] I. E. Kieft, M. Kurdi, E. Stoffels, *IEEE Trans. Plasma Sci.* 2006, 34, 1331.
- [33] G. Fridman *et al.*, *Plasma Chem. Plasma Process.* 2006, 26, 425.

- [34] L. Brulle *et al* PLoS ONE 2012, 7, e52653.
- [35] X. Lu, M. Laroussi, V. Puech, Plasma Sour. Sci. Technol. 2012, 21, 034005.
- [36] E. Stoffels, A. J. Flikweert, W. W. Stoffels, G. M. W. Kroesen, Plasma Sour. Sci. Technol. 2002, 11, 383.
- [37] E. Robert *et al.*, Plasma Process. Polym. 2009, 6, 12, 795.
- [38] M. Laroussi, X. Lu, Appl. Phys. Lett. 2005, 87, 11, 113902.
- [39] K. D. Weltmann *et al.*, Contrib. Plasma Phys. 2009, 49, 631.
- [40] J. Y. Kim, J. Ballato, S.-O. Kim, Plasma Process. Polym. 2012, 9, 253.
- [41] S. Bianconi, F. Cavrini, V. Colombo, M. Gherardi, R. Laurita, A. Liguori, P. Sanibondi, A. Stancampiano, 2014, IEEE Trans. Plasma Sci., 42, 2746.
- [42] K. Kim, G. Kim, Y. C. Hong, S. S. Yang, Microelectron. Eng. 2010, 87, 1177.
- [43] E. Temmerman, Y. Akishev, N. Trushkin, C. Leys, J. Verschuren, J. Phys. D: Appl. Phys. 2005, 505.
- [44] C. M. Chan, T. M. Ko, H. Hiraoka, Surf. Sci. Rep. 1996, 24, 1.
- [45] P.J.C. Chappel, J.R. Brown, G.A. George, H.A. Willis, Surf. Interf. Anal. 1991, 17, 43.
- [46] Y. Nakayama, T. Takahagi, F. Soeda, K. Hatada, S. Nagaoka, J. Suzuki and A. Ishitani, J. Polym. Sci. A 1988, 26, 559.
- [47] D.T. Clark, A. Dilks, J. Appl. Polym. Sci. Polym. Sci. 1977, 15, 2321.
- [48] R. M. France, R. D. Short, J. Chem. Soc., Faraday Trans. 1997, 93, 3173.
- [49] T. Jacobs, R. Morent, N. De Geyter, P. Dubruel, C. Leys, Plasma Chem. Plasma Process. 2012, 32, 1039.
- [50] M. Nakagaw, F. Teroaka, S. Fujimoto, Y. Hamada, K. Kibayashi, J. Takahashi, J Biomed Mater Res A 2006, 77A, 112.
- [51] F. Teraoka, M. Nakagawa, M. Hara Dent Mater J 2006, 25, 560.
- [52] E. D. Yildirim, H. Ayan, V. N. Vasilets, A. Fridman, S. Gucer, W. Sun, Plasma Process Polym 2008, 5, 58.
- [53] H. U. Lee, Y. S. Jeong, K. N. Koh, S. Y. Jeong, H. G. Kim, J. S. Bae, C. R. Cho, Current Appl Phys 2009, 9, 219.
- [54] H. U. Lee, Y. S. Jeong, S. Y. Jeong, S. Y. Park, J. S. Bae, H. G. Kim, C. R. Cho, Appl Surf Sci 2008, 254, 5700.
- [55] A. Kuzminova, M. Vandrovcová, A. Shelemin, O. Kylián, A. Choukourov, J. Hanus, L. Bacáková, D. Slavínská, H- Biederman, Appl. Surf. Sci. 2015, 357, 689.
- [56] I. Trizio, F. Intraruovo, R. Gristina, G. Dilecce, P. Favia, Plasma Process. Polym. 2015, DOI: 10.1002/ppap.201500104.

- [57] I. K. Kang, S. H. Choi, D. S. Shin, S. C. Yoon *Int J Biol Macromol* 2001, 28, 205.
- [58] C. Baquey, F. Palumbo, M. C. Porte-Durrieu, G. Legeay, A. Tressaud, R. D'Agostino, *Nucl Instrum Meth B* 1999, 151, 255.
- [59] H. S. Seo, Y. M. Ko, J. W. Shim, Y. K. Lim, J. K. Kook, D. L. Cho, B. H. Kim, *Appl Surf Sci* 2010, 257, 596.
- [60] Y. Xia, F. Boey, S. S. Venkatraman, *Biointerphases* 201, 5, 32.
- [61] H. Shen, X. Hu, F. Yang, J. Bei, S. Wang, *Biomaterials* 2007, 28, 4219.
- [62] J. Yang, J. Bei, S. Wang, *Biomaterials* 2002, 23, 2607.
- [63] K.G. Kostov, T.M.C. Nishime, A.H.R. Castro, A. Toth, L.R.O. Hein, *Appl. Surf. Sci.* 2014, 314, 367.
- [64] C. Sarra-Bournet, S. Turgeon, D. Mantovani, G. Laroche, *J. Phys. D: Appl. Phys.* 2006, 39, 3461.
- [65] J. Piglowski, I. Gancarz, J. Staniszewska-Kus, D. Paluch, M. Szymonowicz, A. Konieczny, *Biomaterials* 1994, 15, 909.
- [66] R. Bos, H. C. Van Der Mei, H. J. FEMS *Microbiol Rev* 1999, 23, 179.
- [67] Y. H. An, R. J. Friedman, R. A. Draughn, E. A. Smith, J. H. Nicholson, J. F. John, *J Microbiol Methods* 1995, 24, 29.
- [68] G. Subbiahdoss, B. Pidhatika, G. Coullerez, M. Charnley, R. Kuijter, H. C. van der Mei *et al.* *Eur Cell Mater* 2010, 19, 205.
- [69] J. H. Lee, H. Wang, J. B. Kaplan, W. Y. Lee, *Acta Biomater* 2010, 6, 11.
- [70] D. J. Balazs, K. Triandafillu, Y. Chevolut, B. O. Aronsson, H. Harms, P. Descouts P, *et al.* *Surf Interface Anal* 2003, 35, 301-
- [71] K. Triandafillu, D. J. Balazs, B. O. Aronsson, P. Descouts, P. Tu Quoc, C. van Delden, *et al.* *Biomaterials* 2003, 24, 1507.
- [72] M. Katsikogianni, E. Amanatides, D. Mataras, Y. F. Missirlis, *Colloids Surf B Biointerphases* 2008, 65, 257.
- [73] J. M. Anderson, *Annu. Rev. Mater. Res.* 2001, 31, 81.
- [74] R. d'Agostino, P. Favia, Yoshinobu Kawai, H. Ikegami, N. Sato, F. Arefi-Khonsari, *Advanced Plasma Technology*, John Wiley & Sons, 08 set 2008.
- [75] J. D. Andrade, S. Nagaoka, S. Cooper, T. Okano, S. W. Kim, *Trans. ASAIO* 1987, 33, 75.
- [76] W. R. Gombotz, W. Guanghui, T. A. Horbett, A. S. Hoffman, *J. Biomed. Mater. Res.* 1991, 25, 1547.
- [77] J. Nakamatsu, L. F. Delgado-Aparicio, R. Da Silva, F. Soberón, *J. Adhesion Sci. Technol.* 1999, 13, 753.
- [78] S. Morita, S. Hattori, *Pure Appl. Chem.* 1985, 57, 1277.

- [79] D. C. Guerin, D. D. Hinshelwood, S. Monolache, F. S. Denes, V. A. Shamamian, *Langmuir* 2002, 18, 4118.
- [80] D. L. Cho, P. M. Claesson, C. G. Golander, K. Johansson, *J. Appl. Polym. Sci.* 1990, 41, 1373.
- [71] M. R. Alexander, T. M. Duc, *Polymer* 1999, 40, 5479.
- [82] Y. Arima, H. Iwata, *Biomaterials* 2007, 28, 3074.
- [83] H. Jiang, L. Hong, N. Venkatasubramanian, J. T. Grant, K. Eyink, K. Wlacek, S. Fries-Carr, J. Enlow, T. J. Bunninn, *Thin Solid Films* 2007, 515, 3513.
- [84] R. Jafari, M. Tatoulian, W. Morscheidt, F. Arefi-Khonsari, *React. Funct. Polym.* 2006, 66, 1757.
- [85] D. Hegemann, E. Korner, S. Guimond, *Plasma Process. Polym.* 2009, 5, 246.
- [86] P. Heyse, R. Dams, S. Paulussen, K. Houthoofd, K. Janssen, P. A. Jacobs, B. F. Sels, *Plasma Process Polym.* 2007, 4, 145.
- [87] G. Borgia, N. M. D. Brown, *J. Phys. D Appl. Phys.* 2007, 4, 145.
- [88] I. P. Vinogradov, A. Lunk, *Surf. Coat. Technol.* 2005, 200, 695.
- [89] C. P. Klages, A. Grishin, *Plasma Process. Polym.* 2008, 5, 368.
- [90] K. Lachmann, M. C. Rehbein, M. Jansch, M. Thomas, S. O. Klages, *Plasma Med.* 2012, 2, 127.
- [91] R. Morent, N. De Geyter, S. Van Vlierberghe, E. Vanderleyden, P. Dubruel, C. Leys, E. Schacht, *Plasma Chem. Plasma Process.* 2009, 29, 103.
- [92] I. Topala, N. Dumitrascu, G. Popa, *Nucl. Instrum. Methods Phys. Res. B* 2009, 267, 442.
- [93] A. J. Beck, R. D. Short, A. Matthews, *Surf. Coat Technol* 2008, 203, 822.
- [94] F. Palumbo, P. Favia, A. Rinaldi, M. Vulpio, R. d'Agostino, *Plasmas Polym.* 1999, 4, 133.
- [95] F. Hilt, N. D. Boscher, D. Duday, N. Desbenoit, J. Levalois-Grutzmacher, P. Choquet, *ACS Appl. Mater. Inter.* 2014, 6, 18418.
- [96] N. D. Boscher, F. Hilt, D. Duday, G. Frache, T. Fouquet, P. Choquet, *Plasma Process. Polym.* 2015, 12, 66.
- [97] M. Donegan, D. P. Dowling, *Surf. Coat. Technol.* 2013, 234, 53.
- [98] G. Chen, M. Zhou, Z. Zhang, G. Lv, S. Massey, W. Smith, M. Tatoulian, *Plasma Process. Polym.* 2011, 8, 701.
- [99] O. Carton, D. B. Salem, S. Bhatt, J. Pulpytel, F. Arefi-Khonsari, *Plasma Process. Polym.* 2012, 9, 984.
- [100] D. B. Salem, O. Carton, H. Fakhouri, J. Pulpytel, F. Arefi-Khonsari, *Plasma Process. Polym.* 2014, 11, 269.
- [101] L. J. Ward, W. C. E. Schofield, J. P. S. Badyal, A. J. Goodwin, P. J. Merlin, *Chem. Mater.* 2003, 15, 1466.

- [102] S. Kango, S. Kalia, A. Celli, J. Njuguna, Y. Habibi, R. Kumar, *Prog. Polym. Sci.* 2013, 38, 1232.
- [103] S. Li, M. M. Lin, M. S. Toprak, D. K. Kim, M. Muhammed, *Nano Rev.* 2010, 1, 5214.
- [104] I. Y. Jeon, J. B. Baek, *Materials* 2010, 3, 3654.
- [105] G. Schmidt, M. M. Malwitz, *Curr. Opin. Colloid Interface Sci.* 2003, 8, 103.
- [106] M. Groenewolt, M. Antonietti, *Adv. Mater.* 2005, 17, 14.
- [107] A. A. Voevodin, J. S. Zabinski, *Compos. Sci. Technol.* 2005, 65, 741.
- [108] Z. Guo, K. Lei, Y. Li, H. W. Ng, S. Prikhodko, H. T. Hahn, *Compos. Sci. Technol.* 2008, 68, 6.
- [109] C. Aymonier, D. Bortzmeyer, R. Thomann, Rolf Mulhaupt, *Chem. Mater.* 2003, 15, 4874.
- [110] Z. H. Mbhele, M. G. Salemane, C. G. C. E. van Sittert, J. M. Nedeljkovic, V. Djokovic, A. S. Luyt, *Chem. Mater.* 2003, 15, 5019.
- [111] C. J. Weng, J. Y. Huang, K. Y. Huang, Y. S. Jhuo, M. H. Tsai, J. M. Yeh, *Electrochim. Acta* 2010, 55, 8430.
- [112] X. Shi, T. A. Nguyen, Z. Suo, Y. Liu, R. Avci, *Surf. Coat. Technol.* 2009, 204, 237.
- [113] J. Bardon, J. Bour, D. Del Frari, C. Arnoult, D. Ruch, *Plasma Process. Polym.* 2009, 6, S655.
- [114] A. Dembele, M. Rahman, I. Reid, B. Twomey, J. M. Don MacElroy, D. P. Dowling, *J. Nanosci. Nanotechnol.* 2011, 11, 1.
- [115] A. Uygun, L. Oksuz, A. G. Yavuz, A. Gulec, S. Sen, *Curr Appl Phys.* 2011, 11, 250.
- [116] M. Michel, J. Bour, J. Petersen, C. Arnoult, F. Ettingshausen, C. Roth, D. Ruch, *Fuel Cells* 2010, 10, 932.
- [117] F. Fanelli, F. Fracassi, *Plasma Chem. Plasma Process.* 2014, 34, 473.
- [118] Q. Feng, J. Wu, G. Chen, F. Cui, T. Kim, J. Kim, *J. Biomed. Mater. Res.* 2000, 52, 662.
- [119] O. Beier, A. Pfuch, K. Horn, J. Weisser, M. Schnabelrauch, A. Schimanski, *Plasma Process. Polym.* 2013, 10, 77.
- [120] H. R. Humud, A. K. Abass, Z. Wheeb, *Asian J. Appl. Sci. Eng.* 2014, 3, 25.
- [121] I. Rault, V. Frei, D. Herbage, N. Abdul-Malak N, A. Huc, *J Mater Sci Mater Med* 1996, 7, 215.
- [122] E. Khor, *Biomaterials* 1997, 18, 95.
- [123] L. H. Olde Damink, P. J. Dijkstra, M. J- A. Van Luyn, P. B. Van Wachem, P. Nieuwenhuis, J. Feijen, *J Mater Sci Mater Med* 1995, 6, 460.
- [124] A. Bigi, G. Cojazzi, S. Panzavolta, N. Roveri N, K. Rubini, *Biomaterials* 2002, 23, 4827.
- [125] S Amadori, P. Torricelli, K. Rubini, M. Fini, S. Panzavolta, A. Bigi, *J Mater Sci: Mater Med* 2015, 26, 69.

- [126] S. Panzavolta, M. Gioffrè, M. L. Focarete, C. Gualandi, L. Foroni, A. Bigi, *Acta Biomater.* 2011, 7 1702.
- [127] S. Torres-Giner, J. V. Gimeno-Alcanaiz, M. J. Ocio, J. M. Lagaron, *ACS Appl. Mater. Interfaces* 2009, 1, 218.
- [128] Y. Z. Zhang, J. Venugopal, Z. M. Huang, C. T. Lim, S. Ramakrishna, *Polymer* 2006, 47, 2911.
- [129] B. Vallon, B. Drevillon, F. Poncin-Epaillard, *Appl. Surf. Sci.* 1997, 108, 177.
- [130] B. Dong, S. Manolache, E. B. Somers, A. C. Lee Wong, F. S. Denes, *J. Appl. Polym. Sci.* 2005, 97, 485.
- [131] S. Tajima, K. Komvopoulos, *Appl. Phys. Lett.* 2006, 89, 124102.
- [132] I. Prasertsung, S. Damrongsakkul, N. Saito, *Plasma Process. Polym.* 2013, 10, 792.
- [133] R. Molina, P. Jovancic, S. Vilchez, T. Tzanov, C. Solans, *Carbohydr. Polym.* 2014, 103, 472.
- [134] J. Ratanavaraporn, R. Rangkupan, R. Jeeratawatchai, S. Kanokpanonta, S. Damrongsakkula, *Int. J. Biol. Macromol.* 2010, 47, 431.
- [135] K. Sisson, C. Zhang, M. C. Farach-Carson, D. B. Chase, J. F. Rabolt, *Biomacromolecules* 2009, 10, 7.

CHAPTER 3

NON-EQUILIBRIUM ATMOSPHERIC PRESSURE PLASMA FUNCTIONALIZATION OF ELECTROSPUN SCAFFOLDS FOR FIBROBLAST ADHESION

3.1 Introduction

As overviewed in the previous chapters, among the various techniques available for surface modification and functionalization of biomaterials, non-equilibrium plasma treatment has been proven to enhance biomaterial cellular acceptance and to increase cell viability and proliferation [1–3]. This solvent-free versatile process can provide a uniform physical and chemical modification of the scaffold surface without altering its bulk properties; indeed, the typical thickness of the region affected by plasma treatment ranges from several hundreds of angstrom to several hundreds of nanometers [4]. Potentialities of CAP are greatly expressed in surface modification of polymers and biomaterials. However, only few works report about the use of atmospheric plasma to functionalize porous nanofibrous scaffolds fabricated through electrospinning technology [5–9]. Indeed, most of the available data in this field are related to low-pressure plasma processes [10–20].

Electrospun assemblies are ideal candidates for the production of scaffolds to be used for tissue engineering, since they mimic the fibrillar arrangement of the extracellular matrix, fulfilling specific topographical, morphological, and mechanical requirements of different tissues and organs [21].

In this chapter, the experimental studies and activities carried out to assess the capability of atmospheric pressure non-equilibrium plasma to improve the hydrophilicity of electrospun poly(L-lactic acid) scaffolds by means of the introduction of carboxyl groups on scaffold surface are reported. Results concerning the evaluation of the thermo-mechanical properties, morphology, hydrophilicity, and water uptake of the plasma-treated scaffolds, as well as the amount of carboxyl functional groups on the scaffold surface are reported. Finally, the effect of plasma treatment on mouse embryonic fibroblast morphology is presented and discussed.

Studies and results, here reported and deeper described in the scientific work [22], were carried out and obtained thanks to the collaboration among three scientific research groups at the Alma Mater Studiorum - Università di Bologna : the IAP Group headed by Prof. Colombo, the group headed by Prof. Laura Calzà from the Health Sciences and Technologies - Center for Industrial Research (HST-ICIR) and the group headed by Prof. Maria Letizia Focarete from the Department of Chemistry ‘G. Ciamician’.

3.2 Experimental part

In this session, the processes for the fabrication of electrospun scaffolds and for their modification by means of non-equilibrium atmospheric pressure plasma treatment are briefly described. Some information regarding the characterization techniques performed to evaluate the effects of the plasma treatment in terms of morphological, thermo-mechanical and chemical modification induced onto the

scaffolds, along with the procedure adopted to investigate the behaviour of the cell culture onto the scaffold, are reported. All the details concerning the employed protocols can be found in the scientific work published on Plasma Processes and Polymers [22].

3.2.1 Scaffolds fabrication

The scaffolds were fabricated in poly(L-lactic acid) (PLLA), typically used in the fabrication of bioresorbable scaffolds for wound dressings [23], neural tissue engineering [24], cardiac repair [25], and other tissue-engineered implants [26].

The electrospun PLLA (ES-PLLA) scaffolds fabrication was carried out by Prof. Focarete's group by using a home-made electrospinning apparatus schematically depicted in Figure 1, where the main components are shown. The system is composed of a high-voltage power supply, a syringe pump, a glass syringe, a stainless-steel blunt-ended needle connected with the power supply electrode and a rotating cylindrical collector.

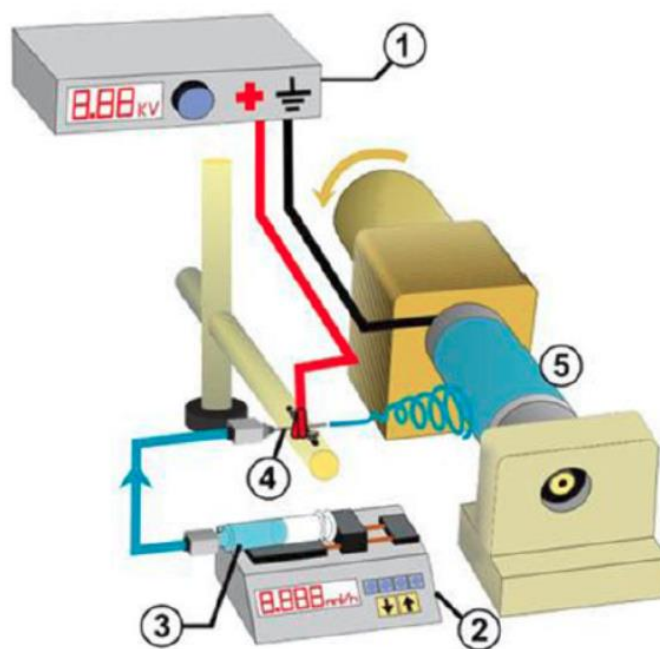


Figure 1. Schematic 3D view of the electrospinning apparatus: (1) high voltage power supply, (2) syringe pump, (3) syringe (4) stainless-steel needle, (5) rotating cylindrical collector [22].

3.2.2 Plasma treatment for the surface modification

The plasma functionalization of the ES scaffolds was performed by the IAP Group. The plasma treatment of PLLA scaffolds was carried out by means of a Linear Corona (LC) plasma source mounted on a shaft moved at a controlled speed by a motorized linear stage (Figure 2).

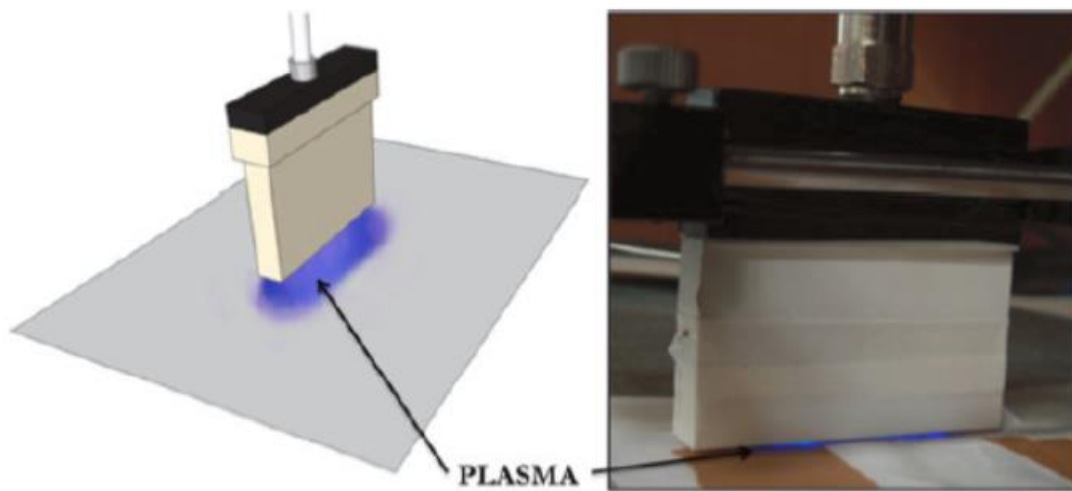


Figure 2. Schematic (left) and picture (right) of the LC plasma treatment of PLLA scaffolds [22]

The LC plasma source, made by the IAP Group, is composed of a housing made of dielectric material and a sharp stainless steel blade, 36 mm wide and 0.1 mm thick, as the high-voltage electrode. The housing is provided of a gas inlet, a compensation chamber and two parallel gas channels to feed a uniform gas flow to the electrode region, as reported in Figure 3.

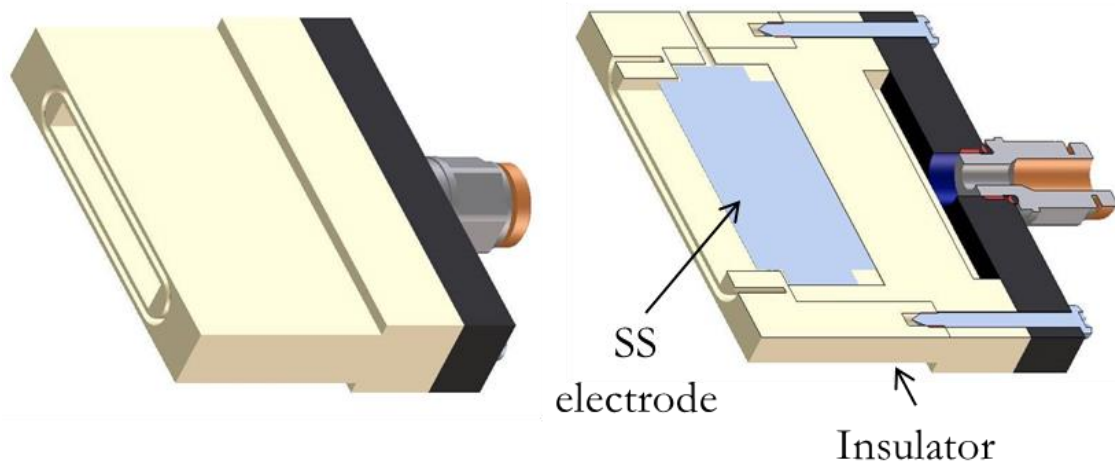


Figure 3. 3D drawings of the LC plasma source

In order to generate a uniform glow discharge and to deliver a uniform treatment of ES-PLLA scaffolds and PLLA-film, the LC plasma source was driven by a nanosecond pulsed generator having peak voltage (PV) 7–20 kV into a 100–200 Ohm load, pulse repetition frequency (PRF) 83–1 050 Hz, pulse width 12 ns and rise time 3 ns.

Plasma treatments were carried out at PV 20 kV, PRF 1 kHz; N₂ was employed as the plasma gas with a 5 slpm flow rate; the treatments were performed after flushing the gas line for 5 min. The

distance between source and substrate was kept constant at 2 mm, the plasma treatment time was 20 s. After plasma treatment all materials were kept at RT in air.

3.2.3 Scaffolds characterization

The characterization of the pristine and plasma treated scaffolds was performed by means of scanning electron microscope (SEM), thermogravimetric analysis (TGA), differential scanning calorimetry (DSC) and stress strain test. The effects of the plasma treatment on the scaffolds hydrophilicity were investigated by means of water contact angle and water absorption measurements.

SEM observations were carried out using a Philips 515 SEM at an accelerating voltage of 15 kV, on samples sputter-coated with gold. TGA analysis measurements were performed with a TA Instruments TGA2950 from RT to 600 °C. DSC measurements were carried out using a TA Instruments Q100 DSC equipped with the liquid nitrogen cooling system (LNCS) accessory. Stress–strain measurements were carried out with an Instron 4465 tensile testing machine on rectangular sheets cut from electrospun mats (5mm wide).

Static WCA measurements were performed soon after plasma treatment and after selected ageing times at RT under ambient conditions by using an optical contact angle and surface tension meter KSV's CAM 100 (KSV, Espoo, Finland). Milli-Q water was used for measurements. The water drop profile images were collected in a time range of 0–90 s, every 1 s.

Water adsorption was determined by weighing the scaffold before and after soaking in deionized water for 24 h at RT. Prior to weighing, excess of adsorbed water was removed from the scaffold by gently blotting with filter paper. Scaffolds were immediately weighted in wet conditions with an electronic balance, to avoid water evaporation. The percentage water adsorption was calculated according to the following equation:

$$\text{Water adsorption (\%)} = \frac{W_e - W_d}{W_d} \cdot 100\%$$

where W_e is the wet weight and W_d is the dry weight (initial weight) of the scaffold. In order to improve the statistics, the experiments were performed using scaffolds with predefined size (2.5cm x 2.5 cm) and with thickness between 30 and 60mm.

The chemical characterization of the pristine and plasma treated ES-PLLA scaffolds, performed by Prof Calzà's group, was carried out with the aim to evaluate the amount of carboxyl groups onto the scaffolds surface by using the chemical surface conjugation with fluorescein isothiocyanate (FITC) and a fluorescence characterization technique.

The ES-PLLA scaffolds plasma treated (ES-PLLA-LC) and untreated (ES-PLLA-untreated) were washed with EtOH 30% and subsequently the carboxyl groups were activated by incubation with EDC and sNHS, in buffer MES 0.1 M pH 5 for 1 h at RT by shaking. The fibres were incubated with 0.01M diaminobutane in carbonate buffer and incubated with FITC. The controls were obtained by using the same protocol adopted for plasma treated and untreated scaffolds, but avoiding the incubation step in presence of EDC and sNHS reagents. In order to evaluate stability of plasma treatment and ageing, ES-PLLA-untreated and ES-PLLA-LC scaffolds were conjugated at different times after plasma treatment (0, 6, 24, 48,

72, and 144 h) and the fluorescence of FITC was considered as a function of storage time at 48 °C; the ES-PLLA-LC scaffold fluorescence was also compared with that obtained on plasma ES-PLLA untreated nanofibres.

FITC conjugate ES-PLLA-untreated, ES-PLLA-LC were observed by means of Nikon eclipse E600 (Nikon, Italy) equipped with digital CCD camera Qimaging Retiga 20002V.

A schematic representation of the employed chemical protocol for the FITC conjugation is reported in Figure 4.

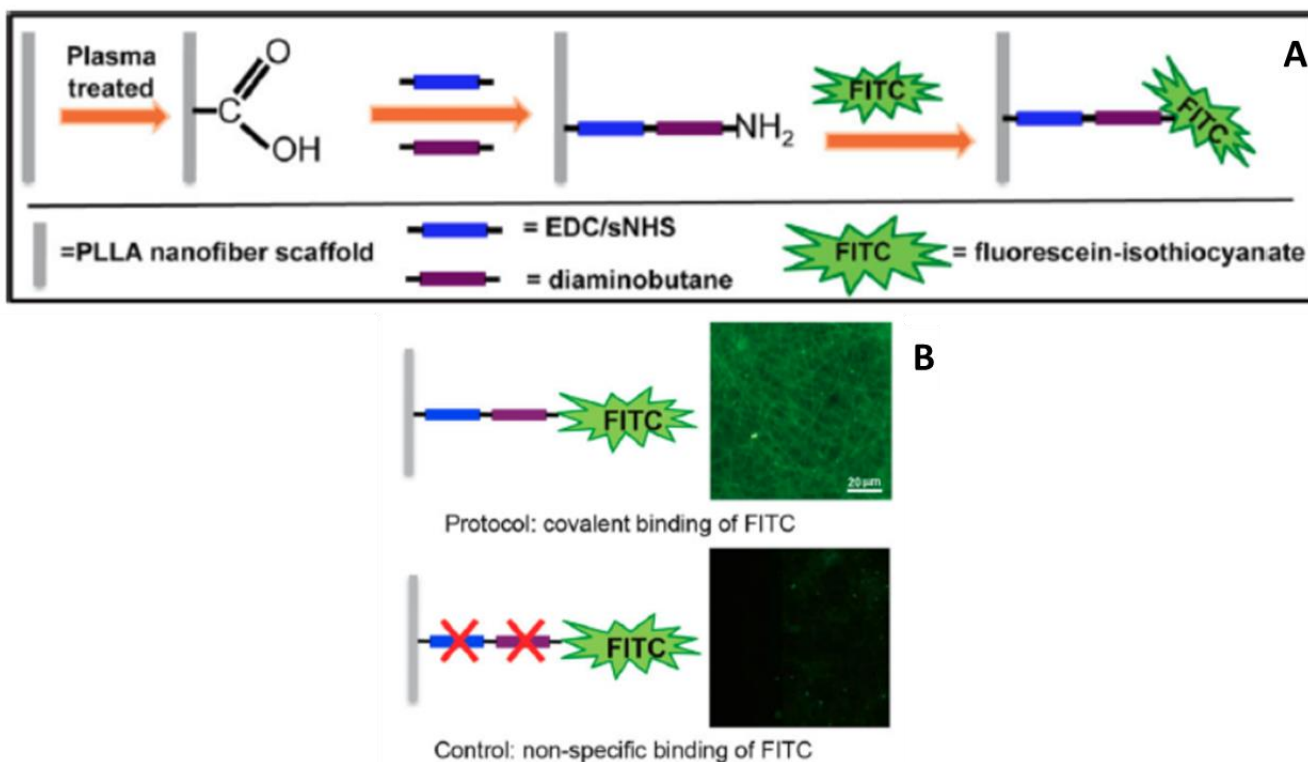


Figure 4. A) Scheme of chemical conjugation reaction; B) Fluorescence microscope images for ES-PLLA-LC and ES-PLLA-untreated [22].

3.2.4 Cell culture on scaffolds and immucytochemistry

Cell culture on scaffolds was performed by Prof. Calzà's group. Mouse embryonic fibroblasts (MEF) cultured for 24, 48 and 72 h were fixed in 4% PFA in 0.1 M phosphate buffer for 20 min at RT, washed with PBS and incubated with blocking buffer for 1 h at RT in order to minimize non-specific absorption of antibody. Subsequently, the cells were incubated with anti-actin primary antibodies in PBS 0.3% triton overnight at 4 °C. The cells were rinsed with PBS and incubated with DyLight488-labeled secondary antibodies (1:1 000) 30 min at 37 °C followed by rinses with PBS (2x10 min). To identify pyknotic and fragmented nuclei, nuclear staining was performed, using the nuclear dye Hoechst 33258 for 20 min at RT and washed with PBS. More than 150 cells were counted. Finally, the cells were mounted with glycerol 0.1% 1,4-phenyldiamine. Negative controls were performed by primary antibody absence. Cells were observed by means of Nikon eclipse E600 (Nikon, Italy) equipped with digital CCD camera Qimaging Retiga 20002V.

3.3 Results and Discussion

Morphology of pristine ES-PLLA (ES-PLLA-untreated) and plasma-treated PLLA fibres (ES-PLLA-LC) is shown in the SEM micrographs of Figure 5. No morphological modifications, in terms of fibre shape, uniformity, and diameter were observed in the sample exposed to the LC plasma source.

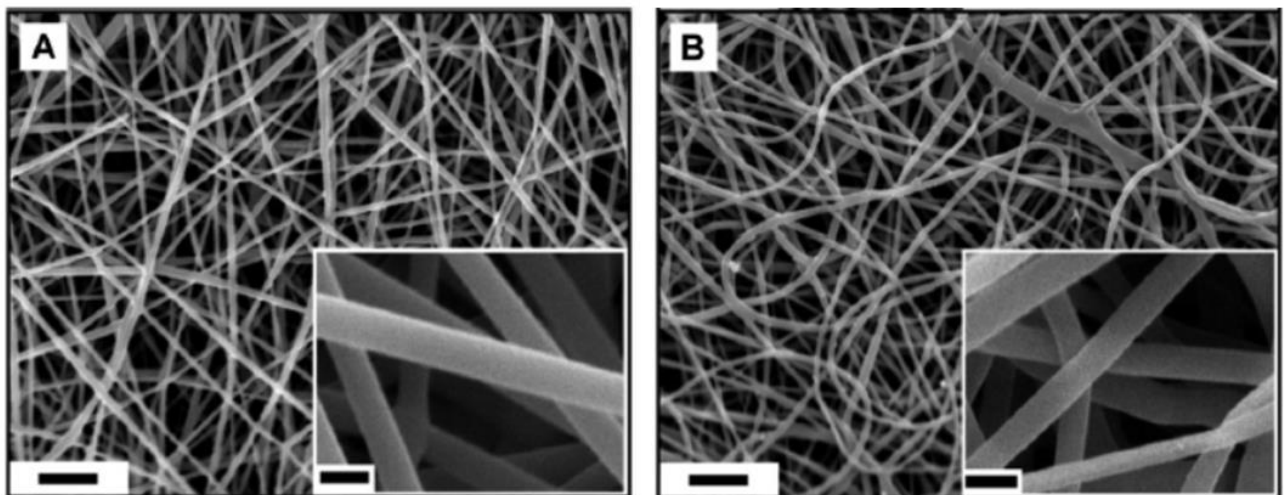


Figure 5. SEM micrographs of: A) ES-PLLA-untreated and B) ES-PLLA-LC (scale bar: 10mm).

Insets: higher magnification (scale bar: 1mm) [22].

The thermo-mechanical characterization pointed out the ES-PLLA-untreated scaffold presented a glass transition at a temperature (T_g) around 65 °C and a cold crystallization process followed by a melting process of the same entity. This result indicates that the melting phenomena regards only the

PLLA crystal phase developed in the cold crystallization process during the heating scan, thus demonstrating that completely amorphous PLLA mats were obtained through the electrospinning process, as previously reported [27, 28]. The plasma treatment did not modify the thermal properties of the polymer that remained amorphous. As expected, similarity of thermal properties led to mechanical properties not significantly different for the two scaffolds. The only appreciable effect of the plasma treatment was a slight decrease of the elastic modulus associated with a small increase of deformation at break, attributing to a slight loss of rigidity.

The WCA measurements highlighted that LC plasma treatment dramatically lowered the contact angle of the scaffold and its wettability with respect to the untreated scaffold (Figure 6A). Indeed, in the plasma-treated scaffold, the water drop was spread out instantaneously and immediately penetrated into the mesh, resulting in a change of the WCA from about 120° to about 20° (or lower) within 60 s, as revealed by the evolution of water drop profile reported in Figure 6B.

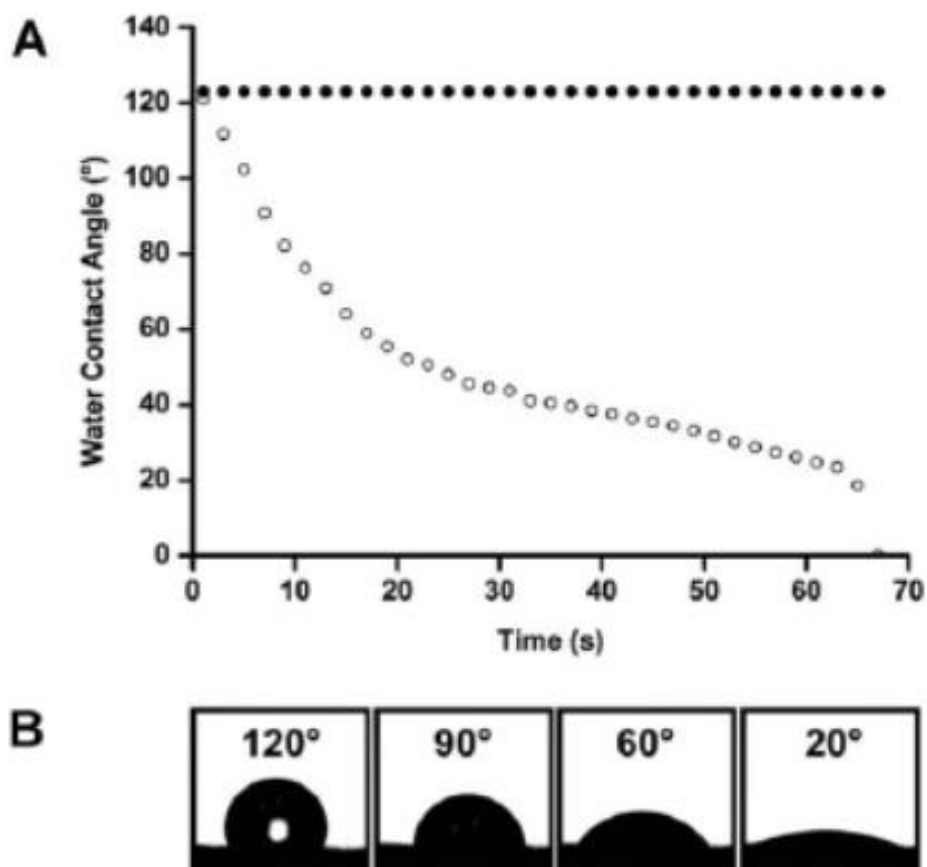


Figure 6. A) Water contact angle behavior of ES-PLLA-untreated (black circles) and ES-PLLA-LC soon after plasma treatment (white circles); B) evolution of water drop profile obtained on ES-PLLA-LC with time [22].

WCA values obtained for electrospun scaffolds were compared with those obtained for PLLA compression molded films, both untreated and subjected to the same plasma treatment performed on electrospun scaffolds. Data listed in Table 1 show that, as expected, untreated ES-PLLA fibrous meshes display enhanced hydrophobicity compared to PLLA planar films given their porous structure that increases air entrapment. The porous structure of the electrospun scaffolds is also responsible for the rapid penetration of the water drop inside the plasma treated construct, which was observed over an ageing time of at least 48 h at RT (Table 1). Such rapid water penetration did not occur for films. In the case of PLLA-film-LC, the decrease of WCA was not so pronounced as in the case of the fibrous meshes; however data confirm an increase of hydrophilicity also for PLLA-film-LC, which is maintained for at least 48 h.

Table 2. Effect of ageing time at RT on WCA values of PLLA electrospun scaffolds and films [22].

Sample	Time after plasma treatment [h]	WCA [°]
ES-PLLA-untreated	-	121.5 ± 1.7
ES-PLLA-LC	3	Instantaneous water absorption
	24	Instantaneous water absorption
	48	Instantaneous water absorption
PLLA film untreated	-	90.3 ± 5.8
PLLA film LC	3	46.4 ± 3.9
	24	48.6 ± 3.4
	48	45.8 ± 4.0

The ageing effects on electrospun samples exposed to LC plasma and stored for different periods of time in air at RT were also studied through water uptake measurements. The results reported that LC plasma treatment dramatically increased the ability of retaining water into the construct of ES-PLLA-LC: the average percentage of water uptake was around 10% and around 400% for ES-PLLA-untreated and ES-PLLA-LC, respectively. In addition, this ability was preserved for different ageing times, up to at least 120 h.

The presence of carboxyl (—COOH) functional groups, introduced on the surface of PLLA fibres by LC plasma treatment, was studied by means of chemical conjugation reactions via the FITC fluorophore. The carboxyl groups were activated with water-soluble carbodiimide to covalently attach FITC molecules. Figure 7 displays the mean fluorescence intensity after background subtraction

(signal – background normalized to ES-PLLA-untreated) of both ES-PLLA-untreated and ES-PLLA-LC subjected to conjugation reaction. The signal of ES-PLLA-LC increased more than five times if compared with that of ES-PLLA-untreated.

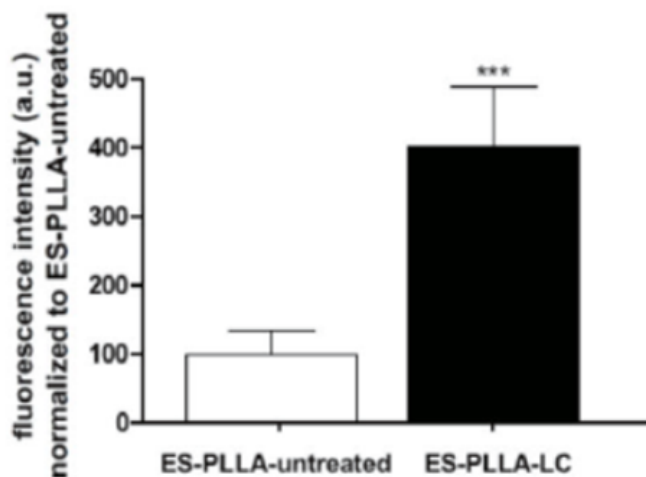


Figure 7. Mean fluorescence intensity normalized to ES-PLLA-untreated, error bars expressed as mean \pm SD of four independent measurements (statistical analysis: t-test *** $p < 0.0001$) [22]

It is worth noting that fluorescence signal of ES-PLLA-untreated is not completely lacking, possibly due to the presence of terminal carboxyl groups in the macromolecular chains of PLLA.

Finally, fluorescence intensity of ES-PLLA-LC was measured as a function of time at RT, observing that the intensity of FITC fluorescence remained almost constant over a period of 6 days, in agreement with the above reported results on scaffold wettability and water uptake.

In order to explore the LC plasma treatment effect on cell–material interactions, MEF morphology was investigated as a function of surface chemical composition, by seeding the cells on glass, BME-coated glass (as control), ES-PLLA-untreated, and ES-PLLA-LC, for 24, 48, and 72 h, in order to analyse cell morphology [26].

Results obtained from cells seeded on glass and on BME-coated glass were overlapping, therefore the BME-coated glass was chosen as the control substrate. At all investigated times the cell body of fibroblasts seeded on BME-coated glass showed the classical round and “spread” shape (Figure 8A) and no significant time-dependent variation of shape was observed. Conversely, fibroblast shape factors were mostly different when cultured on ES-PLLA-untreated and ES-PLLA-LC. Notably, fibroblasts seeded on ES-PLLA-untreated (Figure 8B) were small, rounded, and star-like with short cell processes, while those grown on ES-PLLA-LC (Figure 8C) were elongated and with “dendritic” morphology.

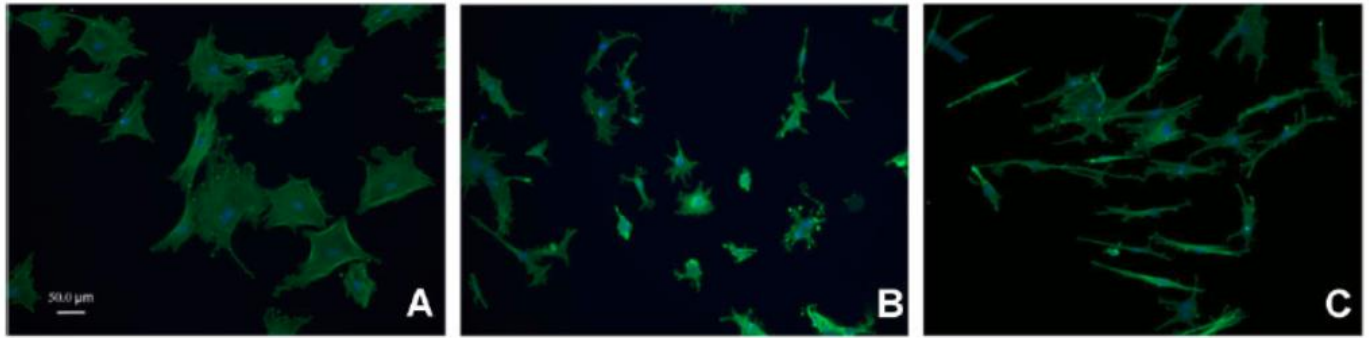


Figure 8. Mouse embryonic fibroblast cells (MEF) cultured on A) BME-coated glass, B) ES-PLLA-untreated and C) ES-PLLA-LC [22].

The applied atmospheric pressure plasma treatment remarkably changed the chemical surface properties of the scaffold. While ES-PLLA-untreated was highly hydrophobic (with a measured WCA of about 120°), the ES-PLLA-LC showed a dramatic decrease of WCA (from 120° to below than 20° within 60 s after drop deposition).

Water uptake experiments confirmed WCA results: LC plasma treatment increased the average percentage of water uptake by the scaffold, from about 10% up to about 400% for ES-PLLA-untreated and ES-PLLA-LC, respectively. The obtained results demonstrate that the applied treatment is an effective method to increase the surface hydrophilicity and wettability of ES-PLLA. The increase of hydrophilicity of the plasma-treated PLLA scaffolds can be interpreted considering that oxygen containing functionalities are introduced on the scaffold surface, enhancing its hydrophilic behaviour. It is well known that the common treatments to introduce oxygen based groups onto polymeric material surface are oxygen or air plasma treatments, where the oxidation is mainly caused by radical reactions between the polymeric chains and the atomic oxygen in the plasma, or inert gases plasmas followed by a post-plasma exposure to air [29]. In all cases, the introduction of oxygen-containing functionalities leads to various functionalities such as hydroxyl, hydroperoxides, carbonyls, carboxylic acids, and peracids [29]. In fact, a higher content of oxygen containing groups (namely —COOH groups) was detected on ES-PLLA-LC, through the chemical conjugation reactions [30] followed by functionalization with fluorescent FITC molecule. The interest toward carboxyl groups is also related to the possibility of further exploitation of such functionalities through conjugation reactions to introduce specific bioactive molecules on the biomaterial surface.

The investigation of the plasma functionalization on the biocompatibility of PLLA-scaffold surface was carried out by evaluating the survival and morphology of fibroblasts grown on untreated and LC treated ES-PLLA. A main result of this study is that plasma-treatment significantly improved the biocompatibility of ES-PLLA, as underlined by the elongated shape of fibroblasts seeded onto plasma

treated mats. This results is a further proof of the fact that a surface chemical modification could deeply affect cell biology. In fact, fibroblast shape is a complex phenomenon strictly regulated by transmembrane proteins (like integrins) linking binding domains of the extracellular matrix to the cell cytoskeleton [31], which is highly influenced by cell adhesion and mechanical forces [32]. The increase in carboxyl groups derived from plasma treatment could actively participate in the reshaping of fibroblast, as suggested also for silk fibroin surface treated with low energy plasma [33].

3.4 Conclusions

Non-thermal atmospheric pressure plasma was successfully applied for surface modification of ES-PLLA scaffolds that mimic the extracellular matrix. The plasma treatment was effective in modifying surface chemical properties of the scaffolds without altering their morphological characteristics and thermo-mechanical properties. A notable increase of scaffold hydrophilicity and wettability was observed and measured as a decrease of WCA and water absorbance capacity. The functionalization of the fibres surface occurred through the introduction of carboxylic functional groups. Chemical derivatization and conjugation with FITC were used to evaluate the amount of carboxyl functional groups and a relevant increase of —COOH concentration was registered. In vitro experiments were performed using MEF cells to assess the effect of plasma treatment on cells. Cells cultured on ES-PLLA-LC showed a more elongated and “dendritic” morphology than cells cultured on untreated ES-PLLA. Moreover, cells cultured on ES-PLLA-LC showed a higher vitality than cells grown on ES-PLLA-untreated. These results demonstrated that the treatment applied was successful to make the scaffold more compatible with fibroblast cells.

References

- [1] P. K. Chu, J. Y. Chen, L. P. Wang, N. Huang, *Mater. Sci. Eng. R Rep.* 2002, 36, 143.
- [2] T. Desmet, R. Morent, N. De Geyter, C. Leys, E. Schacht, P. Dubruel, *Biomacromolecules* 2009, 10, 2351.
- [3] R. Morent, N. De Geyter, T. Desmet, P. Dubruel, C. Leys, *Plasma Process. Polym.* 2011, 8, 171.
- [4] V. N. Vasilets, A. V. Kuznetsov, V. I. Sevast'yanov, *High Energy Chem.* 2006, 40, 79.
- [5] P. P. Tsai, J. R. Roth, C. Weiwei, *Text. Res. J.* 2005, 75, 819.
- [6] F. Sun, X.-S. Li, J.-K. Xu, P.-T. Cao, *Chin. J. Polym. Sci.* 2010, 28, 705.
- [7] Y. H. Kang, K. Ahn, S. Y. Jeong, J. S. Bae, J. S. Jin, H. G. Kim, S. W. Hong, C. R. Cho, *Thin Solid Films* 2011, 519, 7090.

- [8] L. Hyun-Uk, K. Yoon-Hee, J. Se-Young, K. Kwangnak, K. Jong-Pil, B. Jong-Seong, C. Chae-Ryong, *Polym. Degrad. Stabil.* 2011, 96, 1204.
- [9] G.-Y. Heo, S.-J. Park, *Carbohydr. Polym.* 2012, 88, 562.
- [10] K. Park, Y. M. Ju, J. S. Son, K. D. Ahn, D. K. Han, *J. Biomater. Sci.-Polym. E* 2007, 18, 369.
- [11] H. Park, K. Y. Lee, S. J. Lee, K. E. Park, W. H. Park, *Macromol. Res.* 2007, 15, 238.
- [12] A. Martins, E. D. Pinho, S. Faria, I. Pashkuleva, A. P. Marques, R. L. Reis, N. M. Neves, *Small* 2009, 5, 1195.
- [13] H. S. Yoo, T. G. Kim, T. G. Park, *Adv. Drug Deliv. Rev.* 2009, 61, 1033.
- [14] A. Polini, S. Pagliara, R. Stabile, G. Stefano Netti, L. Roca, C. Prattichizzo, L. Gesualdo, R. Cingolania, D. Pisignano, *Soft Matter* 2010, 6, 1668.
- [15] H. Park, J. W. Lee, K. E. Park, W. H. Park, K. Y. Lee, *Colloid Surf. B* 2010, 77, 90.
- [16] R. Wyrwa, B. Finke, H. Rebl, N. Mischner, M. Quaas, J. Schaefer, C. Bergemann, J. B. Nebe, K. Schroeder, K.-D. Weltmann, M. Schnabelrauch, *Adv. Eng. Mater.* 2011, 13, B165.
- [17] J.-P. Chen, C.-H. Su, *Acta Biomater.* 2011, 7, 234.
- [18] C. Zanden, M. Voinova, J. Gold, D. M€orsdorf, I. Bernhardt, J. Liu, *Eur. Polym. J.* 2012, 48, 472.
- [19] Q. Cheng, B. L. Lee, K. Komvopoulos, Z. Yan, S. Li, *Tissue Eng. A* 2013, 19, 1188.
- [20] F. Taraballi, S. Zanini, C. Lupo, S. Panseri, C. Cunha, C. Riccardi, M. Marcacci, M. Campione, L. Cipolla, *J. Colloid Interface Sci.* 2013, 394, 590.
- [21] Q. P. Pham, U. Sharma, A. G. Mikos, *Tissue Eng.* 2006, 12, 1197.
- [22] L. S. Dolci, S. D. Quiroga, M. Gherardi, R. Laurita, A. Liguori, P. Sanibondi, A. Fiorani, L. Calzà, V. Colombo, M. L. Focarete, “Carboxyl Surface Functionalization of Poly(L-lactic acid) Electrospun Nanofibers through Atmospheric Non-Thermal Plasma Affects Fibroblast Morphology”, *Plasma Process. Polym.* 2014, 11, 203, Copyright Wiley-VCH Verlag GmbH & Co. KGaA. Reproduced with permission.
- [23] S. P. Zhong, Y. Z. Zhang, C. T. Lim, *WIREs Nanomed. Nanobiotechnol.* 2010, 2, 510.
- [24] F. Yang, R. Murugan, S. Wang, S. Ramakrishna, *Biomaterials* 2005, 26, 2603.
- [25] S. Mukherjee, C. Gualandi, M. L. Focarete, R. Ravichandran, J. R. Venugopal, M. Raghunath, S. Ramakrishna, *J. Mater. Sci.: Mater. Med.* 2011, 22, 1689.
- [26] D. W. Hutmacher, *Biomaterials* 2000, 21, 2529.
- [27] X. Zhong, K. Kim, D. Fang, S. Ran, B. S. Hsiao, B. Chu, *Polymer* 2002, 43, 4403.
- [28] C. Gualandi, M. Govoni, L. Foroni, S. Valente, M. Bianchi, E. Giordano, G. Pasquinelli, F. Biscarini, M. L. Focarete, *Eur. Polym. J.* 2012, 48, 2008.
- [29] C. M. Chan, T. M. Ko, H. Hiraoka, *Surface Sci. Rep.* 1996, 24, 1.

- [30] G. T. Hermanson, *Bioconjugate Techniques*, 2nd ed., Academic Press, New York 2008.
- [31] E. Zamir, B. Geiger, *J. Cell Sci.* 2001, 20, 3583.
- [32] B. Greig, J. P. Spatz, A. D. Bershadsky, *Nat. Rev. Mol. Cell Biol.* 2009, 10, 21.
- [33] P. Amornsudthiwat, R. Mongkolnavin, S. Kanokpanont, J. Panpranot, C. S. Wong, S. Damrongsakkul, *Colloids Surf. B, Biointerfaces* 2013, 111, 579.

CHAPTER 4

NON-EQUILIBRIUM ATMOSPHERIC PRESSURE PLASMA FOR THE IMMOBILIZATION OF BIOMOLECULES ON BIOMATERIALS

4.1 Introduction

As reported and documented in chapter 2, the covalent immobilization of bioactive compounds such as drugs, enzymes and antibodies, onto polymeric surfaces has been widely investigated in the last decades for applications in different fields spanning from medical diagnostics, drug delivery, tissue engineering, bioprocessing and food packaging [1-9]. Polymeric biomaterials used in tissue engineering and regenerative medicine field need to be modified with biochemical cues, through surface chemistry, to achieve bioactivity and to provide cell signaling. Surface modification of polymeric scaffolds with molecules targeting biological functions allows the regulation of cellular behavior, promoting adhesion, proliferation, differentiation [10,11], and the conjugation of biomolecules, which, presenting a high affinity with cell receptors, are exploitable for cells binding [12,13]. In the wide range of methods for the introduction of functional groups onto the surface of polymeric substrates, wet-chemical methods have been deeply investigated and employed [1,8, 14,15]. Well-known examples of wet-chemical methods include alkaline or acidic hydrolysis and aminolysis, both based on the autocatalytic cleavage of the main-chain ester-bonds to generate carboxyl and amine end-groups respectively, onto the surface of the polymer. As a consequence of the autocatalytic cleavage, the roughness and the wettability of the polymeric surface turned out to increase [8]. Although chemical approaches for surface functionalization do not require any specialized equipment and are more capable of penetrating porous 3D substrates than other physical techniques [1], the wet-chemical methods present some relevant drawbacks related to the fact that polyesters are susceptible of degradation by chain scission with loss of mechanical properties and, since they are sensitive towards solvents, irregular etching of the surface might occur [1,8]. Moreover, the use of hazardous chemicals requires also extended treatment in concentrated corrosive solutions [1]. In light of these considerations, wet-chemical methods are not suitable for industrial applications and more flexible, environmentally friendly solutions are sought.

In this chapter the comparison between a conventional wet-chemical method and a CAP process for the functionalization of poly(L-lactic acid) (PLLA) electrospun fibers with carboxylic groups, required for the subsequent chemical conjugation of an antibody onto the fibres surface, is reported. The wet-chemical method is performed by means of alkaline hydrolysis at room temperature (RT), while the plasma process is carried out by means of a DBD operated at atmospheric pressure in a controlled atmosphere of a He/air mixture. After functionalization, the physico-chemical and morphological properties of the electrospun PLLA fibres were evaluated through water contact angle, gel permeation chromatography (GPC) and scanning electron microscopy (SEM), and compared to those of the untreated fibres. The amount of —COOH functional groups, created at the fibre surface

by both the wet chemical method and the atmospheric pressure plasma treatment, was assessed by means of fluorescence analysis after chemical derivatization with fluorescein isothiocyanate (FITC). In order to compare the efficiency of biomolecules immobilization for chemically- and plasma-treated fibres, the functionalization step was followed by the conjugation of an artificial antibody (anti-CD10) to PLLA fibres surface by exploiting the carbodiimide chemistry, via 1-ethyl-3-[3-dimethylaminopropyl] carbodiimide (EDC) and hydroxysulfosuccinimide (sNHS). Finally, the presence of the anti-CD10 antibody on the fibres surface was evaluated through a secondary antibody-FITC labeled by means of fluorescence intensity measurement.

The research activity, which led to a scientific work [16], submitted to Journal of Physics D: Applied Physics, was carried out in collaboration with Prof. Focarete's group from the Department of Chemistry 'G. Ciamician', which took care of the mats fabrication, their functionalization with the chemical method and their characterization.

4.2 Experimental part

In this session, the processes for the fabrication of electrospun scaffolds and for their functionalization by means of chemical method and CAP treatment are briefly described. Some information regarding the characterization techniques performed to evaluate the effects of the chemical method and plasma treatment in terms of morphological, thermo-mechanical and chemical modification induced onto the mats, along with the procedure adopted to investigate the immobilization of biomolecules on the functionalized mats, are reported.

4.2.1 PLLA mats fabrication

The fabrication of mats was carried out by Prof. Focarete's group by using an electrospinning apparatus, composed of a high voltage power supply (Spellman, SL 50 P 10/CE/230), a syringe pump (KD Scientific 200 series), a glass syringe, a stainless-steel blunt-ended needle (inner diameter: 0.84 mm) connected with the power supply electrode, and a rotating cylindrical collector (50 mm diameter; 120 mm length). PLLA was dissolved in a mixed solvent, DCM:DMF=65:35 v/v at a concentration of 13% w/v. The polymer solution was dispensed, through a Teflon tube, to the needle with a flow rate of 0.02 ml/min. The electrospinning process was performed by applying a potential of 20 kV, at RT with a relative humidity of 50%, collecting the electrospun fibres over a

rotating cylindrical collector (40 rpm) placed at a distance of 20 cm from the needle. The obtained PLLA electrospun fibrous mats were kept under vacuum over P₂O₅ at RT overnight in order to remove residual solvents.

4.2.2 PLLA mats functionalization

Alkaline hydrolysis of PLLA mats

The chemical functionalization of the PLLA mats was performed by Prof. Focarete's group. PLLA mats were fixed by means of CellCrown supports (Scaffdex, Tampere, Finland), in a 24-well and immersed in H₂O:EtOH=90:10 (v:v) for 10 minutes. Subsequently, electrospun mats were washed twice with distilled H₂O and then incubated with sodium hydroxide (NaOH) solution at different concentrations and for different times, as described in the Results section. Finally, the electrospun mats were abundantly washed with distilled H₂O.

Plasma treatment of PLLA mats

The plasma functionalization of the mats was carried out by the IAP group. The Dielectric Barrier Discharge (DBD) plasma source employed for the introduction of —COOH groups onto the surface of PLLA electrospun mats consisted of two aluminium parallel-plate electrodes; the upper electrode, having a surface of 13x8 cm² and a thickness of 0.13 mm, was covered by a dielectric POM-C plate, having a surface of 15x11 cm² and a thickness of 2.4 mm and was connected to the high voltage (HV) generator; while the lower electrode, with a surface of 13x9 cm² and a thickness of 0.13 mm, was grounded.

The plasma source was enclosed in a volume having a size of (21x17x3) cm³ (LxWxH) to perform the treatment in a controlled atmosphere by introducing specific gases or gas mixtures. The gas mixtures used for volume saturation and plasma discharge generation are introduced from the top of the plasma reactor through a rilsan tube (diameter 6 mm) connected to the gas flow meter. A bleed port (1 cm diameter) was placed on a side wall of the plasma reactor for removing the air at the beginning of the process and for keeping a constant pressure inside the close volume during the process. The DBD plasma source was driven by a commercial pulsed DC generator (FID GmbH-FPG 20-1NMK) producing high-voltage pulses with a slew rate of 3–5 kV ns⁻¹, a pulse duration around 30 ns, a peak voltage (PV) of 7–20 kV, and an energy per pulse of 50 mJ at maximum voltage amplitude into a 100–200V load impedance, with a maximum pulse repetition rate (RR) of 1000 Hz. During the plasma treatment, the mats were placed onto the grounded electrode and directly subjected to the plasma discharge, as reported in Figure 1. The plasma was generated by fixing the gap between the

grounded electrode and the POM-C plate at 0.5 mm and setting the PV and RR at 10.4 kV and 500 Hz, respectively. Treatment times of 5, 7.5 and 10 min were adopted. A mixture of 3 slpm of He and 1 slpm of air was used for the saturation of the chamber and for plasma generation. To produce the controlled atmosphere conditions, the gas mixture was initially flown for 4 min inside the close volume; following this phase, the chamber bleed port was opened and the plasma discharge was ignited while maintaining the flux of the gas mixture constant during the whole plasma treatment.

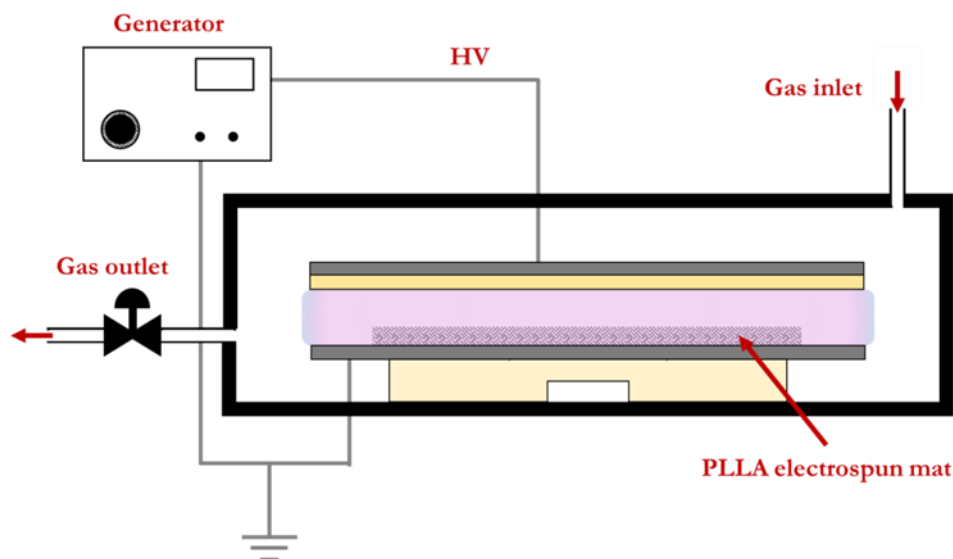


Figure 1. Experimental setup employed for the plasma functionalization of the PLLA mats [16]

Carboxylic groups evaluation

The evaluation of the obtained —COOH groups was carried out by means of fluorescence characterization [17]. Briefly, functionalized PLLA mats were fixed by means of CellCrown supports and activated by incubation with 10 mM EDC and 10mM sulfo-NHS in 0.1M MES buffer (pH 5) for 30 min at RT. The solution was removed and the mats were incubated with Diaminobutane (0.01 M) in 0.1M carbonate buffer (pH 9.8) for 1 h at RT and rinsed three times for 5 minutes with carbonate buffer. Finally, the mats were incubated with 10^{-4} M FITC in carbonate buffer for 2 hours at RT and rinsed three times in PBS for 5 minutes. Negative control was obtained by omitting the presence of reactive reagents (EDC and sNHS) in the above described procedure in order to evaluate non-specific binding of FITC to the fibre surface. The mean intensity fluorescence is shown after the subtraction of the negative control.

4.2.3 Antibody conjugation

Ab-FITC conjugation

PLLA mats carrying —COOH groups at their surface were activated with EDC/sNHS in 0.1M MES (pH 5.0) buffer and incubated with Ab-FITC at different concentrations and at different conditions of time, pH and temperature, as indicated in the results and discussion section. As a negative control, the reaction was performed on PLLA hydrolyzed or PLLA plasma-treated without EDC/sNHS activation to evaluate non-specific binding of Ab-FITC to the fibre surface. The data are shown after the subtraction of the negative control.

Anti-CD10 antibody conjugation

PLLA fibres functionalized with —COOH groups at their surface, by both wet chemical and plasma treatment, were conjugated with anti-CD10 antibody using the following optimized protocol. Briefly, the anti-CD10 antibody was conjugated, onto the activated PLLA substrate, at three different concentrations (1, 5, 10 μ g/mL) in 0.1M PBS overnight at 4°C. In order to verify the anti-CD10 antibody immobilization, Ab-FITC at 1:200 dilution in 0.1M PBS (2h at RT) was used.

4.2.4 Characterization techniques

Fibre morphology was observed with a Philips 515 scanning electron microscope (SEM) at an accelerating voltage of 15 kV. Prior to SEM analysis, samples were sputter-coated with gold. The distribution of fibre diameters was determined through the measurement of about 250 fibres by means of an acquisition and image analysis software (EDAX Genesis) and the results were given as the average diameter \pm standard deviation (SD).

Static water contact angle (WCA) measurements were performed at RT by using an optical contact angle and surface tension meter KSV's CAM 100 (KSV, Espoo, Finland), by recording the side profiles of Milli-Q water drops for image analysis. The water drop profile images were collected in a time range of 0-20 s, by recording an image every 1 s. Results were averaged on at least five measurements obtained in different areas of the sample.

Polymer molecular weight data were obtained by gel permeation chromatography (GPC) at 33°C using a KNAUER Advance Instruments system equipped with three columns (Agilent) connected in series as follow: two PLgel minimix C (PM range from 200-2000000 g/mol, 250 mm/4.6 mm length/i.d.) and a PLgel minimix E (PM range up to 30000 g/mol, 250 mm/4.6 mm length/i.d.). Polystyrene standards in the range of molecular weight 2000–100 000 g/mol were used and a

refractive index detector was employed. Chloroform was used as eluent with a 0.3 mL min^{-1} flow and sample concentration of about 10 mg mL^{-1} was applied.

Image analysis has been performed using a Nikon eclipse E600 microscope (Nikon, Italy) equipped with digital CCD camera Q Imaging Retiga 20002V (Q Imaging, Surry, BC, Canada). All images were taken with a 10x objective (10x/0.50 NIKON Plan Fluor). The images were analyzed using Imaging NIS Elements software. In order to obtain the mean fluorescence intensity, images of at least five different fields for each sample were taken; furthermore for each of these fields the average intensity of eight different areas were calculated. Data were expressed as mean \pm SD.

4.3 Results and Discussion

The electrospinning process parameters were optimized in order to obtain PLLA defect-free fibres, randomly oriented, and characterized by a mean fibre diameter of $574 \pm 190 \text{ nm}$.

The chemical functionalization of the PLLA fibres was carried out using different alkaline hydrolysis conditions, by varying the hydrolysis time and the NaOH concentration, in order to achieve the highest density of carboxylic groups at the fibre surface while minimizing possible damage of the fibres caused by PLLA hydrolysis. PLLA fibres were treated with NaOH at concentrations of 0.01M, 0.02M and 0.05M for treatment times of 5 and 10 minutes. In these experimental conditions, no modification of the fibre morphology was detected by SEM analysis, with respect to the as spun, not-hydrolyzed mat. On the contrary, for concentrations of NaOH higher than 0.05 M, or for reaction times longer than 10 min, the nanofibres started collapsing and breaking.

The plasma functionalization of the PLLA fibres was performed according to the operating conditions reported in the experimental part by testing three different treatment times (5, 7.5 and 10 min). SEM analysis (Figure 2) highlighted that the treatment time of 5 min did not induce any morphological change or visible degradation to the electrospun mat. Conversely, after both 7.5 min and 10 min of plasma exposure, a partial loss of the fibrous morphology and a macroscopic damage, i.e. the presence of little holes in the mat, probably due to the occurrence of polymer thermal degradation. Based on the obtained results, 5 min plasma treatment was chosen as the optimal condition for the functionalization and the subsequent antibody conjugation step.

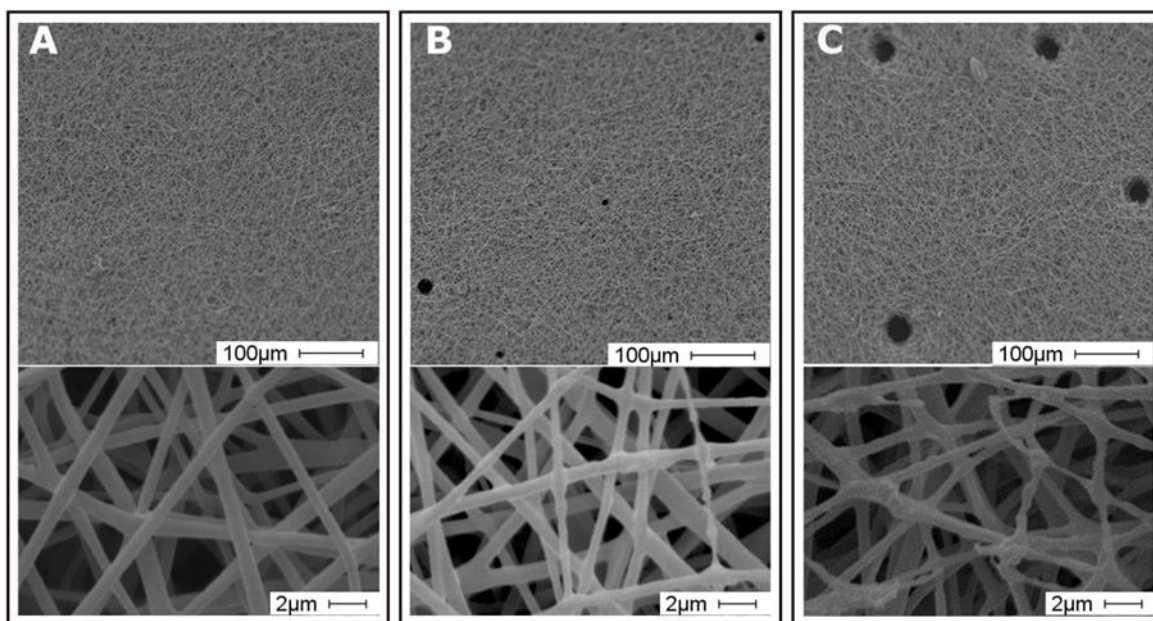


Figure 2. SEM images at two different magnifications of the plasma treated electrospun mats for 5 min (A), 7.5 min (B) and 10 min (C) [16].

The presence of carboxyl groups onto PLLA fibres was assessed, for both the chemically and the plasma functionalized mats, by means of conjugation reactions via the FITC fluorophore and measuring the —COOH-FITC mean fluorescence intensity [17]. Results of the alkaline hydrolysis protocol are displayed in Figure 3A, where the fluorescence intensity is reported as a function of NaOH concentration for the two different times investigated. As expected, the fluorescence intensity progressively increased as a function of NaOH concentration and incubation time. In light of the achieved results, the 10 min treatment with 0.05M NaOH was selected as the optimal condition for the subsequent conjugation step.

Figure 3B reports the comparison between the —COOH-FITC fluorescence intensities obtained for chemically and plasma functionalized mats, together with the results collected for the pristine PLLA mat. The fluorescence intensity of the mat after chemical hydrolysis was more than five times higher of that of untreated PLLA. Moreover, the chemical hydrolysis introduced a higher amount of carboxyl functionalities than the plasma treatment (Figure 3B). It is pointed out that, in order to evaluate any non-specific interactions, a control-reaction was performed on an electrospun PLLA mat without the EDC/sNHS reagents and the diaminobutane linker: in these conditions, i.e. in the absence of the conjugation reagents, the non-specific FITC fluorescence intensity resulted negligible.

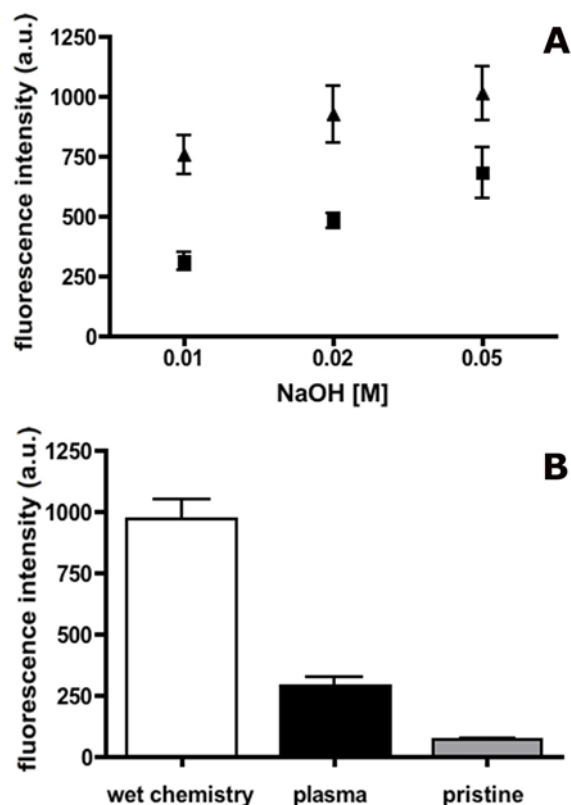


Figure 3. (A) COOH-FITC mean fluorescence intensity response (after negative control subtraction) as a function of NaOH concentration for 5min (■) and 10 min (▲) incubation time. (B) Comparison between COOH-FITC mean fluorescence intensity of pristine, chemically hydrolyzed (0.05M NaOH, 10 min) and plasma (5 min) functionalized PLLA mats [16].

Electrospun mats functionalized by means of the two selected protocols - i.e. 0.05M, 10min NaOH hydrolysis and 5min plasma treatment - were analyzed by the GPC to evaluate possible changes in PLLA molecular weight that was expected due to hydrolysis and scission of the ester linkages of the PLLA backbone chain to generate carboxylic and hydroxyl end-groups on polymer chains. GPC measurements demonstrated that molecular weight did not change for the chemically treated mat ($M_w = 129 \times 10^3 \text{ g mol}^{-1}$) whereas only a slight decrease was observed after the plasma treatment ($M_w = 121 \times 10^3 \text{ g mol}^{-1}$).

Surface hydrophilicity of the functionalized PLLA mat was evaluated through water contact angle measurements. A constant WCA value of 120° was obtained for pristine PLLA mat, indicating a hydrophobic behavior of the material. The carboxylic functionalization significantly lowered the WCA of the mats and increased mat wettability, allowing an almost instantaneous penetration of water. The reduction of WCA indicated that both the alkaline hydrolysis and the plasma treatment successfully improved the surface hydrophilicity.

In order to define the suitable conditions for the antibody conjugation, an antibody-FITC labeled (Ab-FITC) was used as a model compound. Ab-FITC was conjugated via EDC/sNHS to the surface of PLLA mat treated with NaOH 0.05M for 10 minutes. Different conjugation conditions were tested in order to optimize the covalent binding efficiency and to minimize the non-specific interactions between the antibody and the PLLA fibres. In particular, temperature, pH, time of reaction and Ab-FITC concentration were varied. The antibody was tested at concentrations of 1µg/mL, 5µg/mL and 10µg/mL in three different conditions: (I) carbonate buffer at pH 9.5 for 1 hour at RT; (II) carbonate buffer at pH 9.5 for 4 hours at 4°C; (III) PBS buffer at pH 7.5 for 20 hours at 4°C. As a negative control the reaction was performed on NaOH hydrolyzed PLLA without EDC/sNHS to evaluate the non-specific binding of the Ab-FITC to the fibre surface.

As expected, the results showed an increase of fluorescence intensity as a function of Ab-FITC concentration. Moreover, among the tested conditions, the reaction III was revealed to be the most favorable for the antibody conjugation.

As last step, the anti-CD10 antibody was covalently linked to the fibre surface of PLLA mats, both chemically and plasma functionalized, at the three different concentrations tested above, by using the selected optimal conjugation conditions (PBS buffer at pH 7.5 for 20 hours at 4°C). Subsequently, in order to saturate the unreacted sites and to avoid aspecific interactions with the molecules of the Ab-FITC used to recognize the anti-CD10, the mats were incubated with BSA 2% in PBS 0.1M pH7.5. Figure 4A shows the fluorescence intensity of the anti-CD10 / Ab-FITC system, as a function of anti-CD10 concentration. It is interesting to observe that, despite the different amount of —COOH groups introduced by the two functionalization methods, the chemically and the plasma treated PLLA mats displayed similar values of the mean fluorescence intensity due to anti-CD10 conjugation (Figure 4A). This result suggests that the larger amount of —COOH groups, detected on the chemically functionalized mats with respect to the plasma treated ones (as shown in Figure 3B), does not lead to a higher concentration of antibody conjugated onto the fibres.

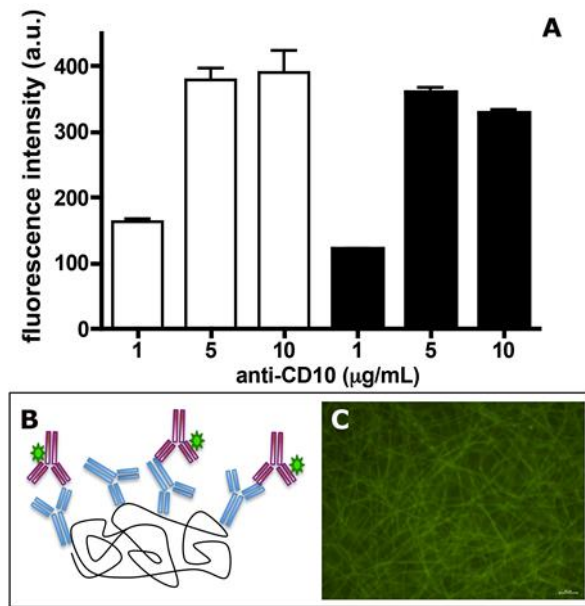


Figure 4. (A) Mean fluorescence intensity, after negative control subtraction, of the anti-CD10 conjugated at different concentrations onto the surface of PLLA mat (white bars = chemical functionalization; black bars = plasma treatment) and recognized by secondary antibody Ab-FITC labeled as schematized in (B). (C) Fluorescence microscope image of the PLLA fibres after anti-CD10 conjugation [16].

The two methods for PLLA fibres functionalization investigated in this work were optimized, by varying the experimental conditions, in order to minimize the fibre damage while generating the highest density of —COOH groups onto the fibres surface. Indeed, for both methods, optimal functionalization conditions, which did not cause any morphological change nor the reduction of polymer molecular weight, were found, demonstrating that in such conditions no appreciable polymer degradation occurred.

As expected, the formation of carboxylic groups at the fibre surface remarkably increased hydrophilicity of both chemically and plasma treated mats with respect to the pristine sample that was highly hydrophobic (with a measured WCA of about 120°). Interestingly, a dramatic decrease of WCA from 120° to below 20° in less than 20 s after drop deposition was observed for the two kinds of functionalized samples, even if chemically and plasma functionalized mats were characterized by a different amount of carboxylic groups. Indeed, although the fluorescence detection method revealed a higher amount of carboxyl functionalities onto the surface of mats subjected to the alkaline hydrolysis process with respect to the plasma treated ones (Figure 4B), the WCA results indicated that the concentration of —COOH groups introduced by the plasma functionalization was enough to greatly enhance hydrophilicity and wettability of the mat.

The ability of the chemically and plasma functionalized mats to covalently link an antibody was

assessed through two steps: (i) by optimizing the conjugation reaction using a FITC-labeled antibody as a model biomolecule, and (ii) by immobilizing an anti-CD10 antibody that was then revealed by a secondary antibody-FITC labeled. Interestingly, similarly to what underlined by the WCA analysis, despite the different amount of —COOH groups introduced by the two functionalization methods, the fluorescence analysis revealed that the chemically and plasma treated PLLA mats displayed similar values of the fluorescence intensity related to anti-CD10 conjugation (Figure 4A). The achieved result clearly highlights that no great differences in terms of antibody conjugation efficiency can be detected by comparing the wet-chemical method and the proposed plasma functionalization process. This effect can be explained by assuming that the amount of —COOH groups is in large excess with respect to the number of anti-CD molecules that can be conjugated onto the fibre surface, also due to the steric hindrance among the antibody molecules that limits their binding to neighboring sites.

4.4 Conclusions

In the present work, the efficacy of a CAP process for the conjugation of biomolecules onto the surface of PLLA electrospun fibres has been demonstrated. The comparison between a conventional wet-chemical method and the proposed plasma assisted approach for covalently linking biomolecules was carried out through the conjugation of an artificial antibody onto chemically and plasma functionalized mats. The results clearly highlighted that a high concentration of antibody was linked to chemically and plasma functionalized mats with respect to pristine PLLA fibres and, more interestingly, no great differences in terms of antibody conjugation efficiency was detected by comparing the chemically and plasma functionalized mats. The performed study brought out the possibility to replace a toxic chemical method with a highly flexible and eco-compatible non-equilibrium atmospheric plasma process for the effective immobilization of biomolecules onto biomaterials.

References

- [1] J. M. Goddard, J. H. Hotchkiss *J H Prog. Polym. Sci.* 2007, 32, 698
- [2] D. Falconnetta, G. Csucs, H. M. Grandina, M. Textor, *Biomaterials* 2006, 27, 3044
- [3] J. Glodek, P. Milka, I. Krest, M. Keusgen, *Sens Actuators B* 2002, 83, 82
- [4] T. Richey, H. Iwata, H. Oowaki, E. Uchida, S. Matsuda, Y. Ikada *Biomaterials* 2000, 21, 1057
- [5] Y. B. Zhu, C. Y. Gao, Y. X. Liu, J. C. Shen, *J. Biomed. Mater. Res. A* 2004, 69A 436

- [6] A. Oyane, M. Uchida, Y. Yokoyama, C. Choong, J. Triffitt, A. Ito, *J. Biomed. Mater. Res. A* 2005, 75A, 138
- [7] D. Briggs, D. M. Brewis, R. H. Dahm, I. W. Fletcher, *Surf. Interface Anal.* 2003, 35 156
- [8] T. Desmet, R. Morent, N. De Geyter, C. Leys, E. Schacht, P. Dubruel, *Biomacromolecules* 2009, 10, 2351
- [9] M. Zuwei, M. Zhengwei, G. Changyou, *Colloids and Surfaces B: Biointerfaces* 2007, 60, 137
- [10] F. Rossi, M. van Griensven, *Tissue Eng A* 2014, 20, 2043
- [11] S. Bierbaum, V. Hintze, D. Scharnweber, *Biomatter* 2012, 2, 132
- [12] Y. Yuan, M. Yin, J. Qiana, C. Liu, *Soft matter* 2011, 7, 7207
- [13] S. Petersen, A. Strohbach, R. Busch, S. B. Felix, K. P. Schmitz, K. Sternberg, *J Biomed Mater Res Part B: Appl Biomater* 2014, 102B, 345
- [14] T. I. Croll, A. J. O'Connor, G. W. Stevens, J. J. Cooper-White, *Biomacromolecules* 2004, 5, 463
- [15] K. B. Lee, K. R. Yoon, S. I. Woo, I. S. Choi, *J. Pharm. Sci.* 2003, 92, 933
- [16] L. S. Dolci, A. Liguori, A. Merlettini, L. Calzà, M. Gherardi, V. Colombo, M. L. Focarete, Antibody immobilization on poly(L-lactic acid) nanofibres advantageously carried out by means of a non-equilibrium atmospheric plasma process, submitted to *J. Phys. D: Appl. Phys.*
- [17] L. S. Dolci, S. D. Quiroga, M. Gherardi, R. Laurita, A. Liguori, P. Sanibondi, A. Fiorani, L. Calza, V. Colombo, M. L. Focarete, *Plasma Process. Polym.* 2013, 11, 203

CHAPTER 5

NON-EQUILIBRIUM ATMOSPHERIC PRESSURE PLASMA FOR MATERIALS DECONTAMINATION AND PREVENTION OF BIOFILM FORMATION

5.1 Introduction

Several studies in the frame of biomedical applications, clinical practices and surface decontamination have widely documented the capabilities of CAP as a suitable and effective tool for the reduction of bacterial load [1-8], thanks to its characteristic blend of several and synergic biologically active agents [8-11], which are effective in disrupting individual micro-organisms [3-7] and apparently are not influenced by mechanisms of microbial resistance to antibiotics (innate or acquired) [8].

Since among the biologically active components of plasma, charged particles and electric field are also included, it is proposed that these components can affect the cell membrane causing electrostatic disruption or at least permeabilization for a very short time [12-14]. As a consequence, plasma-derived ROS/RNS molecules can penetrate the cell membrane [15-16] inducing further chemical reactions inside the cytoplasm and leading to the oxidization of cellular proteins and microbial DNA [9, 17-19].

Some literature results report the effective use of plasma for biofilm disinfection or inactivation [20, 21]. The remarkable study carried out by Joaquin *et al.* [22], about the investigations of the effects induced by atmospheric plasma on living biofilm-forming bacterial cells, suggests these cells go through sequential physiological and morphological changes before becoming inactivated by plasma and that longer treatment time, even more than for the case of planktonic bacteria, are necessary to ensure a complete inactivation.

During my Ph.D activities, some efforts have been dedicated in evaluating the effects of CAP in decontaminating and preventing biofilm formation onto soft reline oral palatal obturators. The motivation to carry out the following study lies in the purpose to contribute in identifying a preventive and therapeutic approach to counteract or remove biofilm contamination from palatal obturators, widely used in plastic surgical reconstruction of tissues affected by cancer and resected by palate- and maxillectomy. Indeed, when the breach is wide, patients are required to temporarily or definitively wear custom-made removable palatal obturators, to replace the lacking tissues and restore masticatory, deglutition and speech functions [23].

Among the large number of materials suitable for this purpose, soft reline holds a relevant position since it is easily moldable and possesses, thanks to its sponge-like return, the mechanical characteristics required to sustain the typical values of the compressive oral forces.

Unfortunately, because of the sophistication of the raw material and the custom-made production process, soft reline oral palatal obturators are quite expensive; therefore, an eventual implant failure might be severely resource- (because of the implants cost) and time- (because of the long production

process) consuming. Severe bacteria biofilm contamination of the device is one of the major causes of failure of prosthetic rehabilitations in many body districts [24].

Conventional decontamination methods based on the use of antimicrobial agents have been already demonstrated to be often ineffective against bacteria within a biofilm; therefore, the ability to destroy these living organisms is critical and the development of an alternative technique is demanded.

In this chapter, the results concerning the treatment of soft relines oral shutters by means of two CAP sources, with the aim of evaluating their effectiveness in preventing biofilm adhesion and enabling biofilm decontamination, are presented. A wider description of the performed studies and of the achieved results is reported in the scientific work [25].

The ability of plasma in preventing biofilm adhesion was evaluated by contaminating with 24 h old biofilm sterile specimens previously exposed to plasma treatment, while the efficacy in reducing bacteria viability was tested treating with plasma specimens previously contaminated with 90 min (early) and 24 h (mature) old biofilm. In both cases, *Streptococcus mutans* and *Aggregatibacter actinomycetemcomitans* were chosen, since they are strongly related to biofilm formation in the oral cavity. Finally, since the soft relines palatal obturators are properly designed to replace resected tissues, the viability of human primary cells cultivated directly onto the surface of plasma treated specimens has been evaluated.

The work was carried out in collaboration with the group headed by Prof. Lia Rimondini, from the Laboratory of Biomedical Materials, Department of Health Sciences, Università del Piemonte Orientale, Novara, Italy.

5.2 Experimental part

In this session, first, the protocol used for soft relines specimens preparation, the characteristic of the plasma sources and the operating conditions adopted for plasma treatment are reported. The description of the techniques and methods employed to perform the mechanical characterization of the specimens before and after the plasma exposure and to evaluate the plasma antibacterial activity and the specimens cytocompatibility after the plasma exposure are presented.

5.2.1. Specimens preparation

Soft relines were prepared following the manufacturer's instructions (Reline Soft, GC Europe N.V., Leuven, Belgium); afterwards, polymers were cut in order to realize square specimens (5 mm per side) with a thickness of 2 mm. Prior to plasma treatment, specimens were sterilized by ethanol immersion overnight followed by three washes in phosphate buffered saline.

5.2.2. Plasma sources

The plasma treated of the specimens was performed by the IAP group. In order to evaluate the effectiveness of CAP in preventing bacteria adhesion and in biofilm decontamination, two dielectric barrier discharge (DBD) plasma sources were tested. Schematics and pictures of both adopted plasma sources are presented in Figure 1.

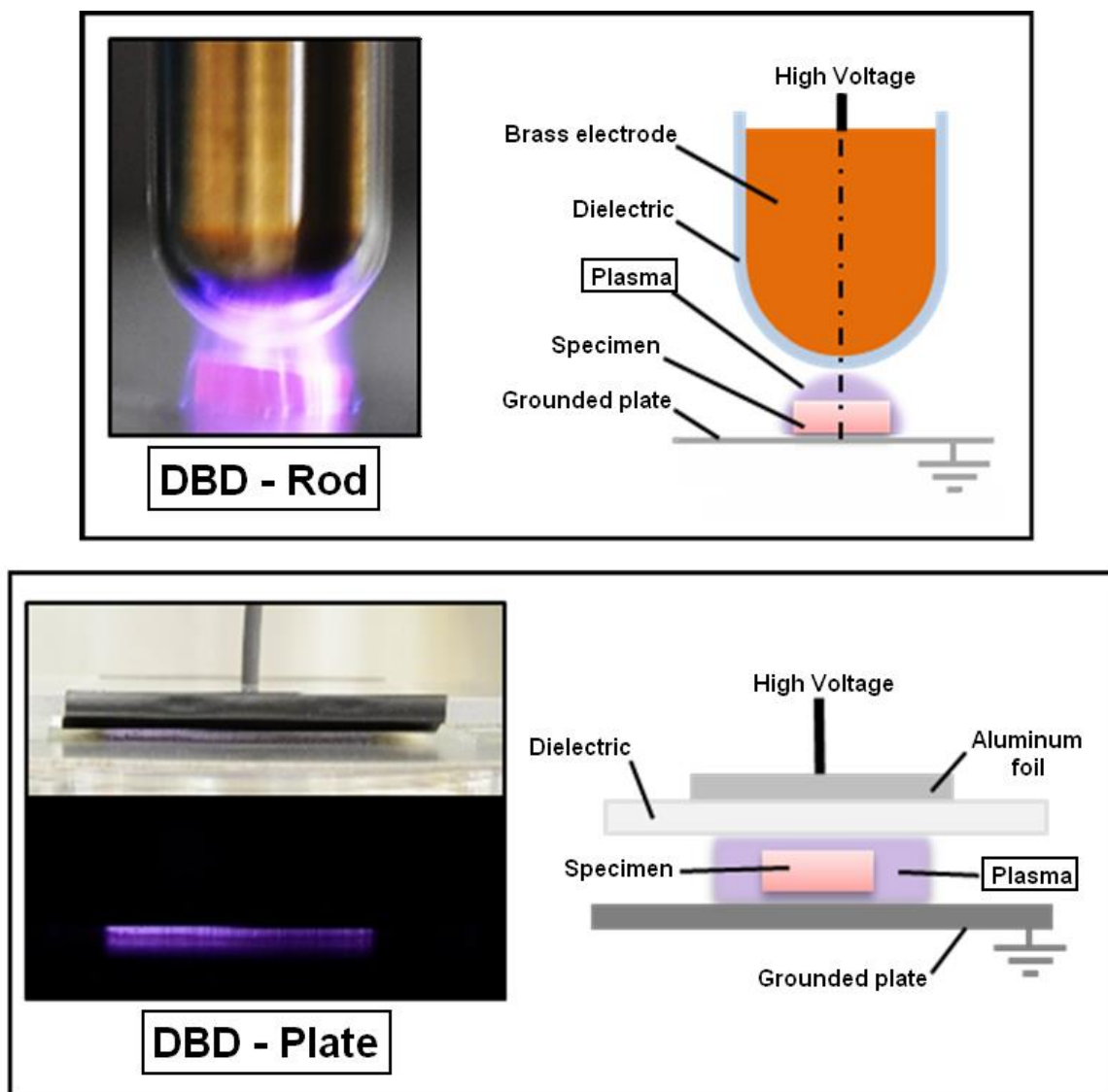


Figure 1. DBD-Rod (upper panel) and DBD-Plate (lower panel), pictures of the discharge during operation (left figures) and schematics representations of the sources (right figures) [25].

The first plasma source, named DBD-Rod, consists of a cylindrical brass electrode, with a 10 mm diameter, having a semispherical tip, with curvature radius of approximately 5 mm. The electrode is

covered with borosilicate glass (relative permittivity $\epsilon_r=4.7$) as dielectric layer with a thickness of 1 mm. When operated, the plasma source is positioned near, or even in contact with, a grounded electrode realised with an aluminium plate [26]. The DBD-Rod plasma source was driven by a micropulsed generator, producing high-voltage nearly sinusoidal pulses having a peak voltage (PV) of 15.4 kV, frequency (f) of 40 kHz, pulse duration of 250 μ s and fixed pulsed repetition frequency (PRF) of 1000 Hz.

The second plasma source used in this work, named DBD-Plate, is composed by a POM-C plate (1mm thickness, relative permittivity $\epsilon_r=3.4$), used as dielectric layer, and an aluminium foil (6x6 cm) adherent to the top surface of the dielectric plate as the high voltage electrode. The bottom surface of the dielectric barrier is parallel to an aluminium plate placed underneath and working as the grounded electrode. The DBD-Plate plasma source was driven by a micropulsed generator, producing high-voltage sinusoidal pulses having a peak voltage (PV) of 12 kV, frequency (f) of 20 kHz, pulse duration of 4 ms and fixed pulsed repetition frequency (PRF) of 100 Hz.

In this work, the distance between the dielectric surface and the grounded plate was kept constant and equal to 3 mm for both plasma sources. During the treatments, specimens were placed on the grounded plate.

5.2.3. Mechanical characterization

With the aim of evaluating the potential effects of plasma treatment on the mechanical properties of the relene polymer, stress-strain tests were carried out both on untreated and treated specimens. Stress-strain measurements were performed with an Instron 4465 (ITW Test and Measurements, Torino, Italy) tensile testing machine on rectangular samples (8 mm x 0.1 mm). The gauge length was 13 mm and the cross-head speed was 50 mm/min. At least five samples were tested for each condition and results were evaluated as the average value \pm standard deviation.

5.2.4. In vitro plasma antibacterial activity

The investigation of the antibacterial activity of the CAP treatments was carried out by the Prof Rimondini's group.

Bacteria Strains and Growth conditions

Two exponentially growing oral biofilm former strains were used for the evaluation of plasma induced antibacterial activity: i) *Streptococcus mutans* (DSMZ 20523, Leibniz Institute DSMZ-German Collection of Microorganisms and Cell Cultures, Braunschweig, Germany) and ii) *Aggregatibacter actinomycetemcomitans* (DSMZ 11123). Bacteria were cultivated in blood agar

plates (Sintak S.r.l., Corsico, Milan, Italy) at 37°C in aerobic conditions for 48 h until single round colonies were obtained. Single colonies were inoculated into fresh LB medium and grown at 37°C in a Gallenkamp orbital shaker incubator at 120 rpm until a 1x10⁷ cells/ml broth culture was obtained, according to McFarland 1.0 standard.

Evaluation of plasma activity in preventing bacteria adhesion

Sterile relined specimens were treated with both the DBD sources for 30, 60 and 120 s. Then, samples were placed into a 24 multiwell plate (Nunclon Delta Surface, Thermo Scientific, Rodano, Milan, Italy) and submerged with 1 ml of LB medium containing 1x10⁷ bacterial cells. Plate was incubated for 90 min at 37°C in agitation (120 rpm, adhesion phase) [27]. Finally, supernatants containing floating planktonic cells (separation phase) were removed and specimens were washed carefully with PBS. The number of biofilm viable colonies was evaluated by the Colonies Forming Unit (CFU) count, while bacteria viability was determined by the colorimetric metabolic 2,3-bis (2-methoxy-4-nitro-5-sulphophenyl)-5-[(phenyl amino) carbonyl]-2H-tetrazolium hydroxide assay (XTT, Sigma, Milan, Italy) assay, as previously described. Briefly, bacteria colonizing surface were detached by means of sonicator and vortex (30 s each, 3 times), collected in PBS and used to obtain 6 ten-fold dilutions; then, 20 ml of each dilutions were spotted onto LB agar plates and incubated for 24 h at 37°C. The final CFU number was calculated as follows [28]:

$$CFU = [(number\ of\ colonies \times dilution\ factor)^{(serial\ ten-fold\ dilution)}]$$

Bacteria viability was evaluated by adding 50 ml of XTT solution (3mg/ml in acetone containing 1µM menadione) to each well; plate was incubated for 4 h in the dark and the optical density was evaluated by a spectrophotometer (SpectraCount, Packard Bell, Chicago, USA) at 490 nm wavelength. Specimens not subjected to plasma treatment were used as control and bacteria viability onto these samples was considered as 100% and assumed to express the viability onto plasma treated specimens. Experiments were performed in triplicate.

Evaluation of plasma activity in decontaminating early biofilm

Sterile untreated specimens were placed into a 24 multiwell plate (Nunclon Delta Surface, Thermo Scientific) and submerged with 1 ml of LB medium containing 1x10⁷ bacteria cells. Plate was incubated for 90 min at 37°C in agitation at 120 rpm (adhesion phase). Then, supernatants were extracted in order to remove floating planktonic cells (separation phase) [27], and plasma treatment was directly performed onto 90 min bacteria cells (early biofilm) colonizing the surface of specimens for 30, 60 and 120 s by using both the DBD plasma sources. 20 min after the plasma treatment, CFU count and XTT assay were performed. Infected and untreated specimens were used as control and

bacteria viability onto these samples was considered as 100%. Experiments were performed in triplicate.

Evaluation of plasma activity in decontaminating mature biofilm

Sterile untreated specimens were infected as described. After the separation phase, samples containing biofilm were rinsed with 1ml of fresh medium and cultivated for 24 h at 37°C to promote biofilm maturation. Then, supernatants were removed and plasma treatment was directly performed onto 24 h bacteria cells (mature biofilm) colonizing the surface of the specimens for 30, 60 and 120 s by using both the plasma sources. After 20 min, CFU and XTT analysis were performed as described above. Infected and untreated specimens were used as control and bacteria viability onto these samples was considered as 100%. Experiments were performed in triplicate.

5.2.5. In vitro cytocompatibility

The investigation of the cytocompatibility of the CAP treatments was carried out by the Prof Rimondini's group.

Human Primary Cells

Cytocompatibility of plasma treated soft relin specimens was evaluated against pooled primary human gingival fibroblasts (HGFs) and skin keratinocytes (HEKs). HGFs were isolated from discarded normal human gingiva. Obtained cells were cultivated in α -MEM (Sigma) supplemented with 10% heat-inactivated foetal bovine serum FBS (Sigma-Aldrich, Italy) and 1% antibiotics-antimycotics (Anti-Anti, Sigma) at 37°C in a humidified 5% CO₂ atmosphere. HEK were obtained from Clonetics (Euroclone, Milan, Italy) and maintained in EpiLife® Medium (Invitrogen, Milan, Italy). Before confluence, both eukaryotic cell types were trypsinized, re-suspended, plated for the experiments and used within fifteen population doublings.

Evaluation of cytocompatibility of plasma treated soft relin specimens

Sterile specimens were plasma treated with both the DBD sources for 30 and 120 s. Then, a defined number (5×10^4 cells/specimen) of eukaryotic cells were seeded onto plasma treated relin surfaces; samples were incubated for 24 h at 37°C, 5% CO₂. After 24 h, eukaryotic cell viability was determined by the colorimetric metabolic assay 3-(4,5-dimethylthiazol-2-yl)-2,5-diphenyltetrazolium bromide (MTT, Sigma). Briefly, 20 μ L of MTT solution (3 mg mL⁻¹ in PBS) were spotted into each well; plates were incubated for 4 h in the dark in incubator at 37°C. Afterwards, medium was removed

and formazan crystals on the wells bottom were solved with 100 μ L of DMSO. Finally, 50 μ L aliquots were collected from each well and the optical density measured by the spectrophotometer at 570 nm. Eukaryotic cells were also cultivated onto untreated relin to confirm its cytocompatibility, while eukaryotic cells cultivated onto polystyrene wells were considered as 100% and assumed to express the viability onto plasma treated specimens. Furthermore, cells morphology, spread and density were visually checked by light microscope (Leica AF 6500, Leica Microsystems, Basel, CH). Experiments were performed in triplicate.

5.3 Results and Discussion

5.3.1. Mechanical characterization

The mechanical characterization was performed on untreated and 30, 60 and 120 s plasma treated soft relin polymers, with the aim to garner some knowledge about the possible variation induced in the material by plasma treatment in terms of elastic modulus, stress at break and deformation at break. Tensile mechanical properties of the samples treated with both the DBD plasma sources are reported in Table 1, where elastic modulus E , stress at break σ_b , and deformation at break ϵ_b are listed.

Table 1. Elastic modulus (E), stress at break (σ_b) and deformation at break (ϵ_b) for DBD-Rod and DBD-Plate plasma treated specimens. Data are expressed as means \pm standard deviations [25].

Specimen	E [MPa]	σ_b [MPa]	ϵ_b [%]
2 min DBD-Rod	2.90 \pm 0.87	3.13 \pm 1.38	143.91 \pm 32.99
1 min DBD-Rod	2.24 \pm 0.20	1.83 \pm 0.64	107 \pm 40,80
30 s DBD-Rod	2.40 \pm 0.52	2.14 \pm 0.84	111.58 \pm 32.54
2 min DBD-Plate	1.39 \pm 0.29	1.34 \pm 0.69	117.14 \pm 54.07
1 min DBD-Plate	1.70 \pm 0.12	2.13 \pm 0.41	158.2 \pm 27.14
30 s DBD-Plate	1.47 \pm 0.09	1.50 \pm 0.33	123.05 \pm 25.49
Untreated	2.05 \pm 0.56	2.20 \pm 0.97	132.99 \pm 34.99

Figure 2a and Figure 2b show a representative stress–strain curve of specimens treated by DBD-Rod and DBD-Plate, respectively. From the obtained results, no significant alteration of mechanical performances of the soft relin polymer was detectable even after 120 s of plasma treatment.

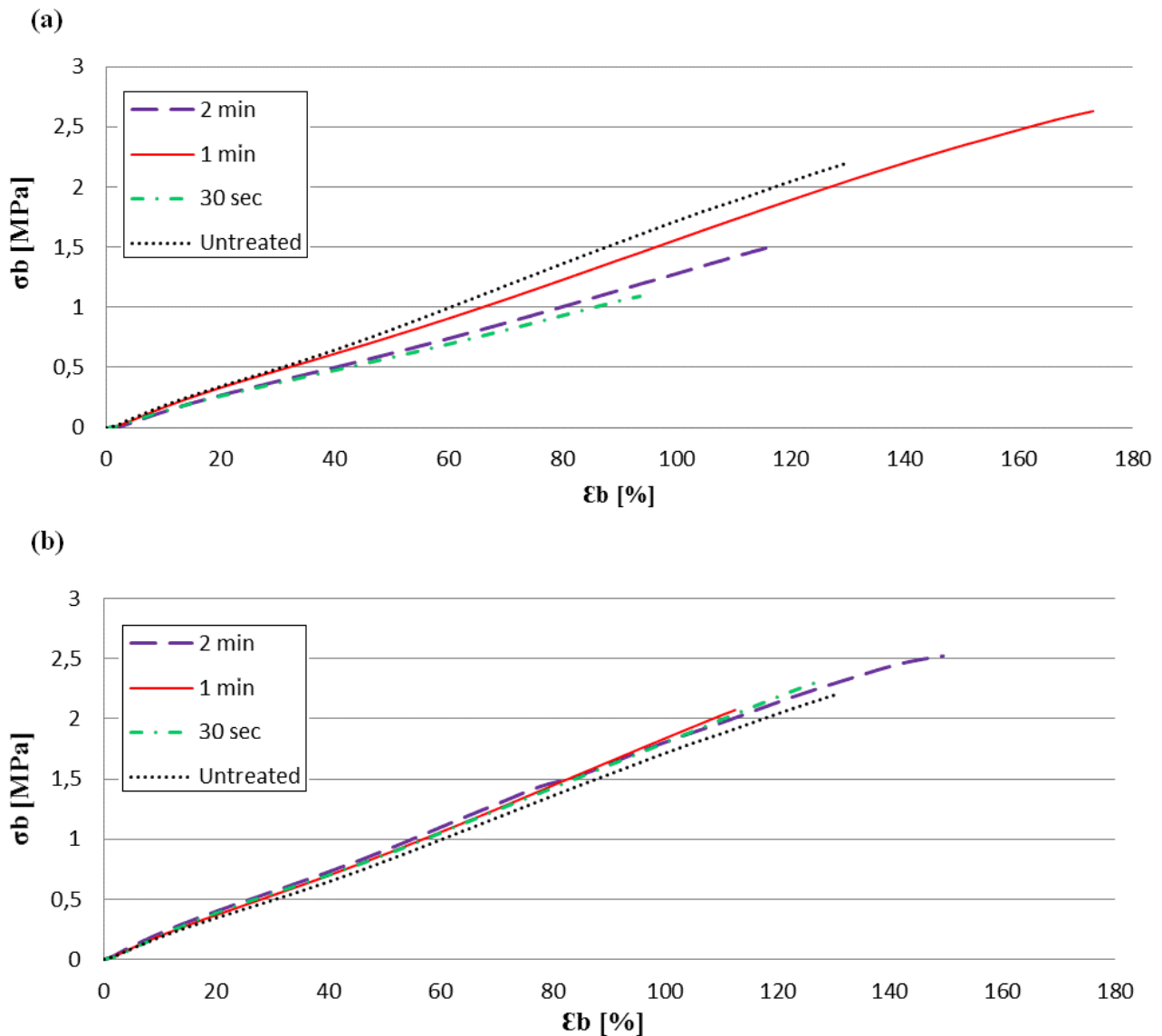


Figure 2 a-b. Stress-strain curves of DBD-Rod (a) and DBD-Plate (b) plasma treated samples for 30 s, 1 min and 2 min and untreated samples [25].

5.3.2. Evaluation of plasma activity in reducing bacteria adhesion

DBD-Rod and DBD-Plate sources, used to treat soft reline palatal obturators before bacterial contamination (as depicted in Figure 3a), turned out to be effective in preventing bacteria adhesion for both the selected biofilm formers.

In particular, the CFUs counts highlighted that on plasma treated samples the CFU number was approximately 2 logs lower than the one registered on untreated control (CNT) ($p < 0.05$, indicated by #), as reported in Figure 3b-e (left histograms). Moreover, as shown in Figure 3 b-e (right histograms), also the bacteria viability evaluated on the soft reline palatal obturators resulted to be affected by

plasma treatment, since a loss of bacteria viability of 40-60% for plasma treated samples with respects to the untreated ones ($p < 0.05$, indicated by *) was found.

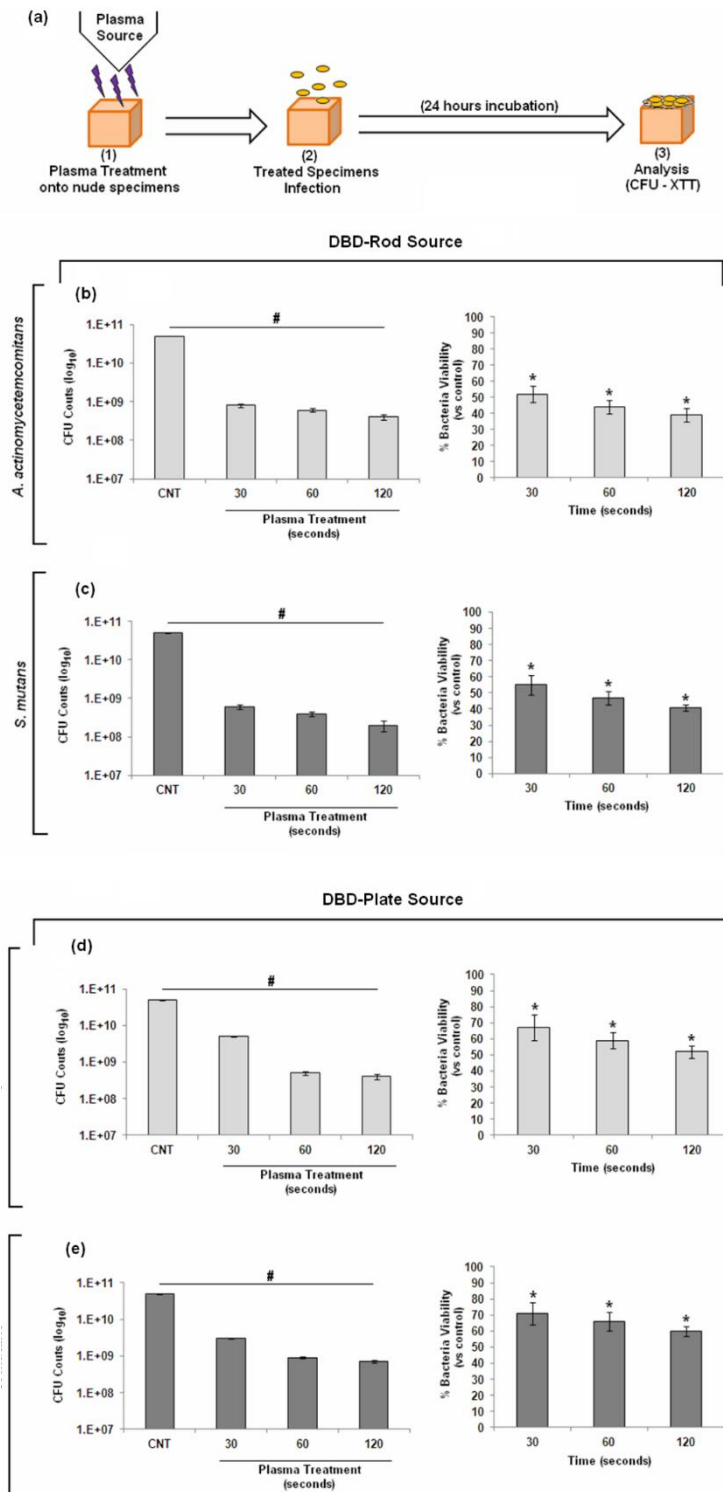


Figure 3a-e. Schematic representation of the experimental protocol (a); assessment of the capability of DBD-Rod and DBD-Plate plasma source in affecting *A.actinomycetemcomitans* (b and d) and *S.mutans* (c and e) adhesion, by means of CFUs counts (b-e left histograms) and evaluation of bacteria viability (b-e right histograms). Results were statistically significant in comparison with untreated controls (CNT) for both CFUs ($p < 0.05$, indicated by the #) and viability assessed by XTT ($p < 0.05$, indicated by the *). Bars represent mean values and standard deviations [25].

5.3.3. Evaluation of plasma activity in decontaminating early and mature biofilm

Plasma treatment of previously infected specimens (schematized in Figure 4a and Figure 5a) led to a significant decrease of CFU number and bacteria viability for both early and mature biofilm, even after a short treatment time (30-120 s). As it can be observed comparing Figure 4 and Figure 5, plasma treatment is more effective on early biofilm.

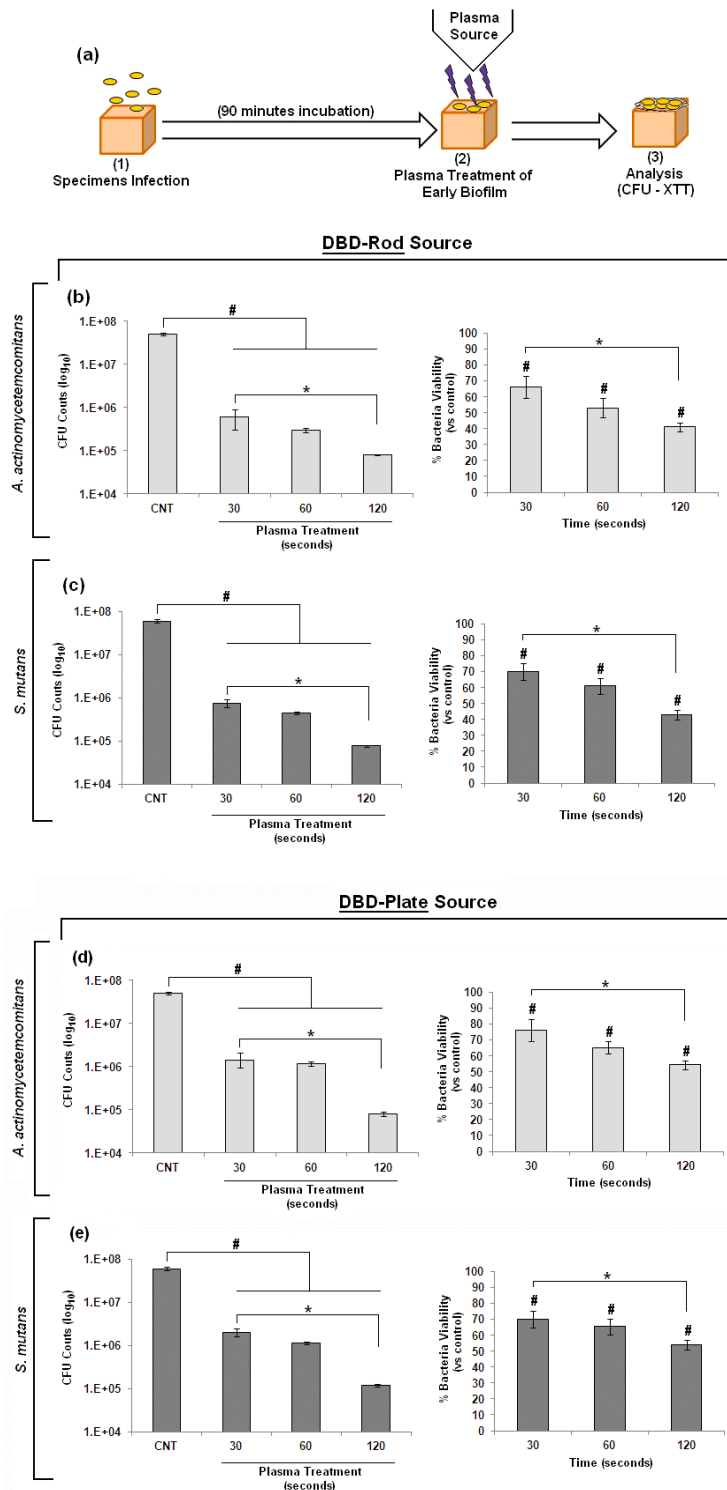


Figure 4a-e. Schematic representation of the experimental protocol (a); assessment of the effectiveness of DBD-Rod and DBD-Plate plasma source in decontaminating *A.actinomycetemcomitans* (b and d) and *S.mutans* (c and e) early biofilm, by means of CFUs counts (b-e left histograms) and evaluation of bacteria viability (b-e right histograms). Results were statistically significant in comparison with untreated controls (CNT) for both CFUs ($p < 0.05$, indicated by the #) and viability ($p < 0.05$, indicated by the *). Bars represent means and standard deviations [25].

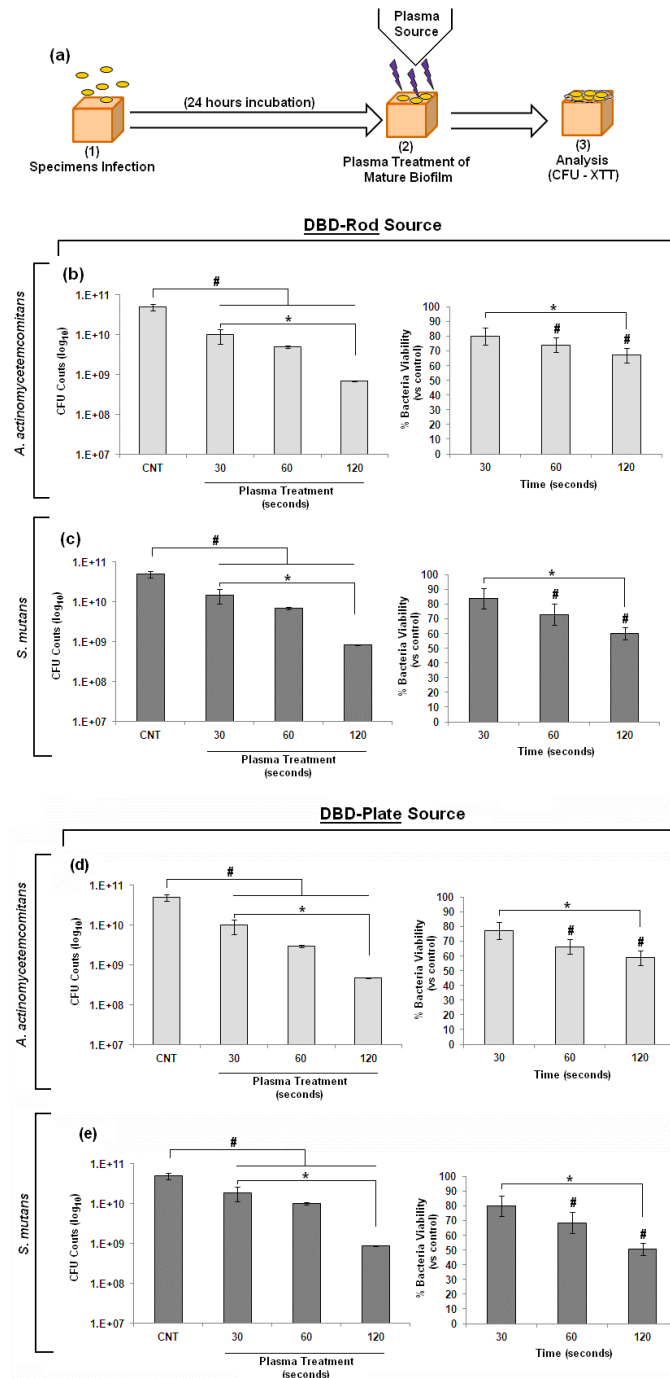


Figure 5 a-e. Schematic representation of the experimental protocol (A); assessment of the effectiveness of DBD-Rod and DBD-Plate plasma source in decontaminating *A.actinomycetemcomitans* (b and d) and *S.mutans* (c and e) mature biofilm, by means of CFUs counts (b-e left histograms) and evaluation of bacteria viability (b-e right histograms). Results were statistically significant in comparison with untreated controls (CNT) for both CFUs ($p < 0.05$, indicated by the #) and viability ($p < 0.05$, indicated by the *). Bars represent means and standard deviations [25].

In fact, both DBD-Rod (Figure 4b and c) and DBD-Plate (Figure 4d and e) induced at least a 3 Logs reduction of the CFUs number (b-e, left histograms) and a 40-60% loss in terms of bacteria viability (b-e, right histograms), for both the selected early biofilm formers. All the results obtained for plasma treated specimens were statistically significant in comparison to untreated controls ($p < 0.05$, indicated by the # for CFUs counts and by the * for viability assay).

Significant results were also obtained when plasma treatment was performed onto specimens infected by mature biofilm (Figure 5), even though the inhibition values resulted to be lower than the one obtained in the case of early biofilm. In fact, for the two considered biofilm formers, plasma treatment was able to induce 2 Logs reduction of the CFUs number (Figure 5 b-e left histograms) and 20-40% loss in terms of bacteria viability (Figure 5 b-e right histograms). Also in this case results were statistically significant in comparison to untreated controls ($p < 0.05$, indicated by the # for CFUs counts and by the * for viability assay). No differences were observed between DBD-Rod and DBD-plate sources.

5.3.4. Evaluation of cytocompatibility of plasma treated soft relin specimens

Cytocompatibility of untreated soft relin specimens (reported as polymer control in the Figure 6) was evaluated, considering eukaryotic cells cultivated onto polystyrene surface (reported as polystyrene control in Figure 6) as positive control and 100% viability. Results showed that both HEKs and HGFs were able to grow onto the specimens surface and no difference ($p > 0.05$) with respect to the polystyrene control was observed, as reported in Figure 6a-b and d-e. Also, relin specimens were subjected to plasma treatment performed under the same operating conditions implemented for bacterial decontamination, in order to assess the possible cytotoxic effects of plasma treated specimens. Results confirmed that plasma treatment of soft relin specimens did not affect their cytocompatibility; in fact, an almost insignificant, when compared to the controls (polystyrene and polymer, $p > 0.05$), decrease of the eukaryotic cells viability ratio was registered only after 120 s plasma treatment. Furthermore, also the visual observation confirmed that, after 24 h of cultivation, morphology, spread and density of both HEKs (Figure 6c) and HGFs (Figure 6f) cultured onto treated specimens were comparable with those of eukaryotic cells cultured on both the controls.

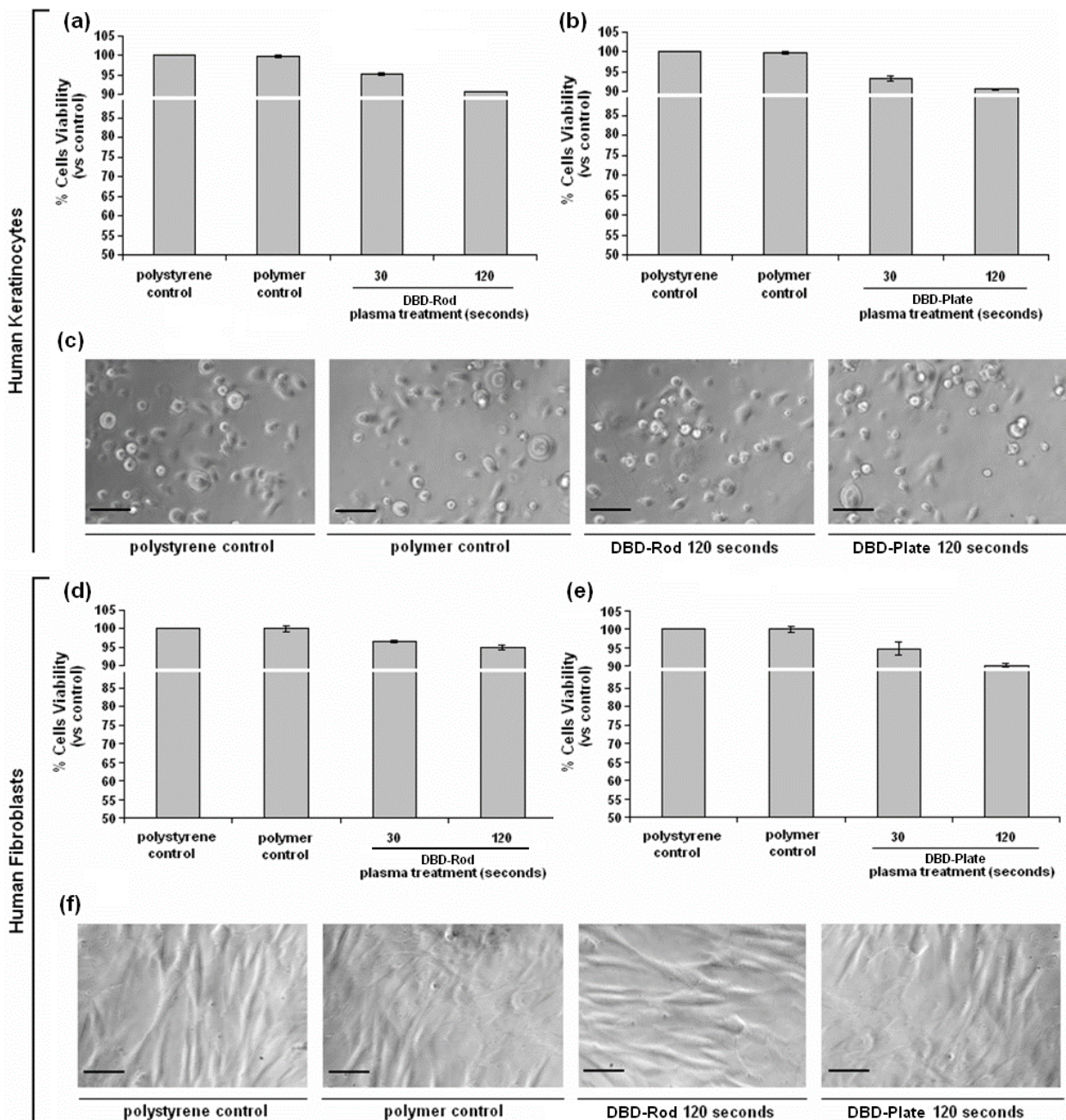


Figure 6a-f. Assessment of cytocompatibility of plasma treated soft relin specimens, by means of the evaluation of eukaryotic cell viability and visual observation. The viability and morphology of HEKs (a-c, upper panel) and HGFs (d-f, lower panel) grown onto plasma treated specimens were comparable towards controls cultivated onto untreated relin (polymer control) and polystyrene wells (polystyrene control). No statistically significant differences ($p > 0.05$) were detected between treated and control groups [25].

5.4 Conclusions

The possibility to effectively decontaminate soft relin palatal obturators, in order to prevent their failure and replacement, represents nowadays a challenge for clinicians. In the present work, the direct

application of cold atmospheric plasma has been demonstrated to represent an effective procedure able to significantly reduce bacterial contamination even in a single short time appliance. Indeed, plasma treatment can affect the chemical characteristics of the soft reline polymer surface, at least for the considered elapsing time between the plasma exposure and the contamination. As documented, bacterial adhesion onto surfaces is linked to the chemico-physical properties and functional groups exhibited by the material at its interface with the cells [29]. When polymeric surfaces are subjected to cold plasma treatment performed using oxygen containing gases, as in our case, the introduction of oxygenated functional groups occurs [30, 31], contributing to prevent the initial bacterial adhesion [32]. While effective in temporally modifying the surface chemical characteristics of the soft reline specimens plasma treatment did not induce any significant alteration of their bulk mechanical properties. This is of extreme importance since the choice of soft reline as constituting material is mainly based on its unique mechanical characteristics that are able to withstand compressive oral forces while granting comfort to the patients. Regarding the investigation of the capability of plasma in decontaminating biofilm infected surfaces, very promising results were observed towards early biofilm; in fact, both plasma sources were found to induce a strong decrease of bacteria number load and viability, suggesting that plasma was able to penetrate the biofilm matrix. However, since the obtained reduction in case of mature biofilm inactivation turned out to be less relevant than the one evaluated for the early biofilm, it can be supposed that the penetration of biologically active agents of plasma through the matrix of the mature biofilm is rather low and unable to eradicate all the mature biofilm layers with the adopted treatment times.

Since, the appliance of plasma onto reline prosthesis surface did not affect human cells viability or morphology, the reactive species anchored to the surface are assumed to be effective towards bacteria but not toxic for eukaryotic cells.

References

- [1] D. Barbieri, M. Boselli, F. Cavrini, V. Colombo, M. Gherardi, M. P. Landini, R. Laurita, A. Liguori, A. Stancampiano, *Biointerphases*, 2015, 10, 029519.
- [2] E. Simoncelli, D. Barbieri, R. Laurita, A. Liguori, A. Stancampiano, L. Viola, R. Tonini, M. Gherardi, V. Colombo, *Clin Plasma Med*, 2015, 10.1016/j.cpme.2015.11.001.
- [3] M. Laroussi, *IEEE T Plasma Sci* 2002, 30, 1409.
- [4] R. Brandenburg, J. Ehlbeck, M. Stielber, T. Woedtke, J. Zeymer, O. Schluter, K. D. Weltmann, *Contribution to Plasma Physics* 2007, 47, 72.
- [5] M. Cooper, G. Fridman, D. Staack, A. Gutsol, V. N. Vasilets, S. Anandan, Y. I. Cho, A. Fridman, A. Tsapin, *IEEE T Plasma Sci*. 2009, 37, 866.

- [6] Z. Machala, L. Chladekova, M. Pelach, *J. Phys. D.* 2010, 43, 222001.
- [7] X. Deng, J. Shi, M. G. Kong, *IEEE T Plasma Sci* 2006, 34, 1310.
- [8] M. Laroussi, M. G. Kong, G. Morfill, W. Stolz, editors. *Plasma medicine*. Cambridge: Cambridge University Press, 2012.
- [9] D. Dobrynin, G. Friedman, A. Fridman, A. Starikovskiy, *New J Phys* 2011, 13, 103033.
- [10] E. Stoffels, Y. Sakiyama, D. B. Graves, *IEEE T Plasma Sci* 2008, 36, 1441.
- [11] M. G. Kong, G. Kroesen, G. Morfill, T. Nosenko, T. Shimizu, J. van Dijk, J. L. Zimmermann, *New J Phys* 2009, 11, 115012.
- [12] M. Laroussi, D. A. Mendis, M. Rosenberg, *New J Phys* 2003, 5, 41.1.
- [13] T. G. Klampfl, G. Isbary, T. Shimizu, Y. F. Li, J. L. Zimmermann, W. Stolz, J. Schlegel, G. E. Morfill, H. U. Schmidt, *Appl Environ Microbiol* 2012, 78, 5077.
- [14] M. Leduc, D. Guay, R.L. Leask, S. Coulombe, *New J Phys* 2009, 11, 115021.
- [15] R. Pompl, F. Jamitzky, T. Shimizu, B. Steffes, W. Bunk, H.U. Schmidt, M. Georgi, K. Ramrath, W. Stolz, R. W. Stark, T. Urayama, S. Fujii, G. E. Morfill, *New J Phys* 2009, 11, 115023.
- [16] T. C. Montie, K. Kelly-Winterberg, J. Reece Roth, *IEEE T Plasma Sci* 2000, 28, 41.
- [17] K. Oehmigen, M. Hähnel, R. Brandenburg, C. Wilke, K. D. Weltmann, T. von Woedtke, *Plasma Process Polym* 2010, 7, 250.
- [18] S. G. Joshi, M. Cooper, A. Yost, M. Paff, U. K. Ercan, G. Fridman, G. Friedman, A. Fridman, A. D. Brooks, *Antimicrob Agents Chemother* 2011, 55, 1053.
- [19] M. Cooper, G. Fridman, A. Fridman, S. G. Joshi, *J Appl Microbiol* 2010, 6, 2039.
- [20] N. Abramzon, J. C. Joaquin, J. Bray, G. Brelles- Mariño, *IEEE T Plasma Sci* 2006, 34, 1304.
- [21] M. Y. Alkawareek, Q.T. Algwari, G. Laverty, S. P. Gorman, W. G. Graham, D. O'Connell, B. F. Gilmore, *PLoS One* 2012, 7, e44289.
- [22] J. C. Joaquin, C. Kwan, N. Abramzon, K. Vandervoort, G. Brelles-Mariño, *Microbiology* 2009, 155, 724.
- [23] G. Tirelli, R. Rizzo, M. Biasotto, R. Di Learda, B. Argenti, A. Gatto, F. Bullo, *Acta Otorhinolaryngol Ital* 2010, 30, 33.
- [24] M. Al Mohajer, R.O. Darouiche, *J Appl Biomater Funct Mater* 2014, 12, 1.
- [25] A. Liguori, A. Cochis, A. Stancampiano, R. Laurita, B. Azzimonti, R. Sorrentino, E. Varoni, M. Petri, V. Colombo, M. Gherardi, L. Rimondini, Cold atmospheric plasma treatment affects early bacterial adhesion and decontamination of soft relined palatal obturators, submitted to *Journal of Biomedical Materials Research Part B*.
- [26] M. Gherardi, E. Turrini, R. Laurita, E. De Gianni, L. Ferruzzi, A. Liguori, A. Stancampiano, V. Colombo, C. Fimognari, *Plasma Process Polym* 2015, DOI: 10.1002/ppap.201500033.

- [27] A. Cochis, B. Azzimonti, C. Della Valle, R. Chiesa, C. R. Arciola, L. Rimondini, *J Biomed Mater Res A* 2015, 103, 1176.
- [28] J. J. Harrison, C. A. Stremick, R. J. Turner, N. D. Allan, M. E. Olson, H. Ceri, *Nat Protoc* 2010, 5, 1236.
- [29] D. Campoccia, L. Montanaro, C. R. Arciola, *Biomaterials* 2013, 34, 8533.
- [30] T. Desmet, R. Morent, N. De Geyter, C. Leys, E. Schacht, P. Dubruel, *Biomacromolecules* 2009, 10, 2351.
- [31] T. Jacobs, R. Morent, N. De Geyter, P. Dubruel, C. Leys, *Plasma Chem. Plasma Process.* 2012, 32, 1039.
- [32] K. Triandafillu, D. J. Balazs, B. O. Aronsson, P. Descouts, P. Tu Quoc, C. van Delden, H. J. Mathieu, H. Harms, *Biomaterials* 2003, 24, 1507.

CHAPTER 6

NON-EQUILIBRIUM ATMOSPHERIC PRESSURE PLASMA FOR POLYMERIC COATINGS DEPOSITION AND NANOCOMPOSITE COATINGS CO-DEPOSITION

6.1 Introduction

The deposition of coatings performed by means of CAP enables to coat the substrate in a single step process by exploiting the contextual activation of both the monomeric units introduced inside the plasma region and the substrate subjected to the plasma discharge. Besides the production of a polymeric coatings by means of the deposition process, non-equilibrium atmospheric pressure has been also employed for the co-deposition of nanocomposite coatings, presenting nanoparticles (NPs) embedded in a polymeric matrix.

During the Ph.D activities, both the processes were setup and optimized in order to deposit plasma polymerized polyacrylic acid (pPAA) coatings, characterized by an high amount of carboxyl groups (-COOH) and nanocomposite coatings composed by Ag NPs into a pPAA matrix. The coating deposition and co-deposition were carried out by means of a CAP jet.

The characterization of the coatings was mainly performed by means of an attenuated total reflectance-Fourier transform infrared spectroscopy (ATR-FTIR) and with the X-ray photoelectron spectroscopy (XPS), in order to get information on the chemical structure of the coatings, while information about the thickness and morphology were garnered by means of optical microscopy for the pPAA coatings and by means of scanning electron microscopic (SEM) for the nanocomposite coatings. Finally, the antibacterial efficacy of the deposited nanocomposite coatings was preliminary assessed against a test microorganism by means of agar disk diffusion tests.

The results, reported in this chapter and thoroughly presented in the scientific papers [1, 2], published on Plasma Processes and Polymers, were obtained by the IAP Group head by Prof. Colombo in collaboration with Prof. Maria Letizia Focarete from the Department of Chemistry ‘G. Ciamician’ and with Prof. Antonino Pollicino, from the Department of Industrial Engineering of University of Catania, Italy.

6.2 Experimental part

In the present paragraph, the materials, the CAP source employed for the processes and the experimental setups, jointly with the performed chemical and morphological characterizations, are reported.

6.2.1 Materials

In order to obtain pPAA coatings, 99% anhydrous AA, containing 180–200ppm MEHQ as inhibitor was used as monomer precursor for the plasma polymerization process. For the fabrication of

nanocomposite coatings, a dispersion 5% w/w of AgNPs (mean diameter < 100 nm; Sigma–Aldrich) in anhydrous EtOH were used; the dispersion of AgNPs in EtOH was prepared by stirring the colloid at room temperature for 2 min. To support the discussion of the morphological analysis for the nanocomposite coatings, results will be also presented for films coated only with AgNPs, deposited using a dispersion of 5% w/w of AgNPs in EtOH. In the text, nanocomposite coatings and nanoparticle coatings are referred to as AgNPs/pPAA coating and AgNPs coating, respectively.

Multi-layer films, composed of a polyethylene (PE, approximately 50 mm thick), polyvinylidenechloride (PVDC, approximately 25 mm thick), and polyvinylchloride (PVC, approximately 200 mm thick) layers, were used as substrate.

The deposition of pPAA coatings was performed on PE and PVC layers, while the co-deposition of the nanocomposite coatings of AgNPs embedded in a pPAA matrix (AgNPs/pPAA) was performed onto the PE layer. The polymeric substrates were washed in ethanol before being subjected to the plasma polymerization process.

6.2.2. Non-Equilibrium Atmospheric Pressure Dual Gas Plasma Jet

The plasma source adopted for the deposition and co-deposition processes is a single electrode plasma jet, suitable for the treatment of different substrates such as metals, polymers, glasses, and biological materials (Figure 1), developed in our laboratory and previously reported in Refs [3-7].

The high-voltage single electrode is a 19.5 mm long stainless steel sharpened metallic needle with a diameter of 0.3 mm. The electrode protrudes from a quartz capillary (outer diameter of 1 mm) by 3 mm and for the case of plasma-polymerization process, described in this work, the plasma plume was ejected from the source tip through an orifice with a diameter of 4 mm. In this source, both a primary and a secondary gas can be introduced for specific applications. As can be observed in Figure 1c, the primary gas is injected through a diffuser with 12 channels (0.3 mm diameter) circularly disposed around the electrode and aimed at ensuring a uniform and laminar flow along the electrode tip. The secondary gas is instead introduced in the discharge region downstream the electrode tip through twelve 0.3 mm holes, tilted with respect to the plasma source axis [3, 4].

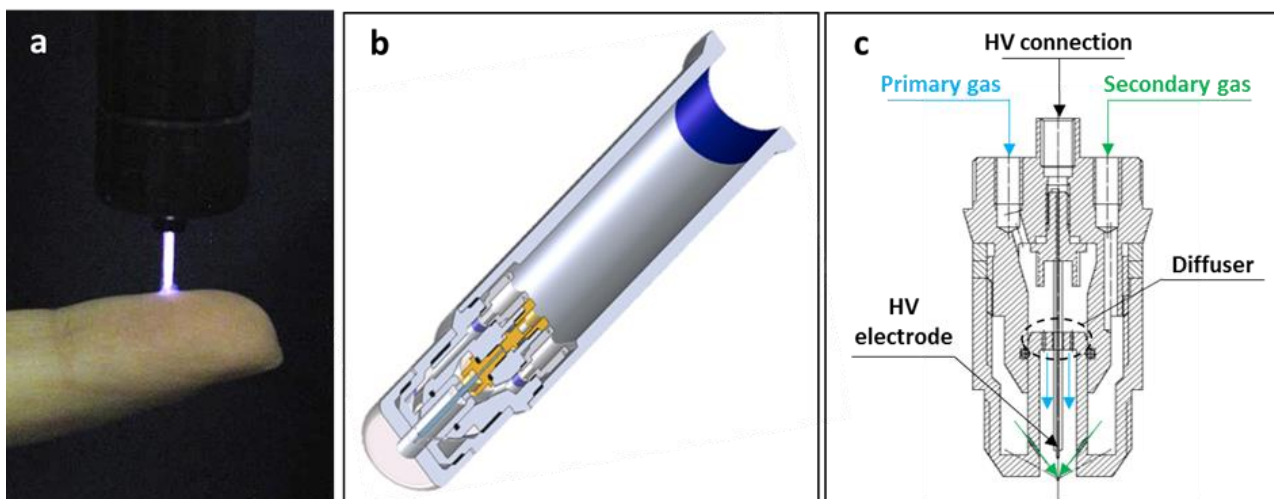


Figure 1. Non-equilibrium atmospheric pressure plasma jet: (a) picture while impinging on biological substrate; (b) assembly 3D rendering; (c) schematic of the head of the plasma jet with gas diffuser and gas pathways highlighted [1].

For the pPAA coating deposition, the plasma source was driven by a commercial pulsed DC generator (FID GmbH-FPG 20-1NMK) producing high-voltage pulses with a slew rate of $3\text{--}5\text{ kV ns}^{-1}$, a pulse duration around 30 ns, a peak voltage (PV) of 7–20 kV, and an energy per pulse of 50 mJ at maximum voltage amplitude into a 100–200V load impedance, with a maximum pulse repetition rate (RR) of 1000 Hz.

For the AgNPs/pPAA coating co-deposition, the plasma source was driven by a micropulsed generator producing high-voltage sinusoidal pulses having peak voltage (PV) of up to 40 kV, frequency (f) of 20–50 kHz, variable pulse duration, and fixed pulsed repetition frequency (PRF) of 100 Hz. During the plasma co-deposition process, PV, f and duty cycle were kept constant at 23.4 kV, 20 kHz, and 40%, respectively.

6.2.3 Experimental setup and operating conditions for the pPAA coating deposition

The effectiveness of the AA plasma polymerization process performed by means of the non-equilibrium atmospheric pressure nanopulsed plasma jet was investigated for the deposition of pPAA coatings stable upon water contact with a high retention of functional groups on PE and PVC substrates. The process was performed on both pristine and plasma pretreated polymeric films, as described in the following.

For the AA plasma polymerization process, only the primary gas was used, whereas no secondary gas was employed. In particular, Ar with a flow rate of 3 slpm was introduced at first inside a bubbler,

where the volume of the AA was kept constant at 35 ml, and then, carrying the monomer, to the plasma source. The mass flow rate of AA carried by the Ar flow was 0.05 ml min^{-1} . Two distinct operating conditions were selected, defined as “mild” and “strong:” the former was characterized by PV and RR of 10 kV and 330 Hz, respectively; the latter was characterized by PV and RR of 19.2 kV and 100 Hz, respectively. The treatment time varied from 3 to 20 min for the “mild” operating condition and from 5 to 20 min for the “strong” one. The AA plasma polymerization process was also performed on plasma pretreated PE and PVC substrates. The pretreatment of polymeric substrates (PE and PVC) was carried out by introducing 3 slpm Ar in the secondary channel of the plasma source, while the primary channel was kept closed. The 10 min long pretreatment was performed with a PV and RR of 12.7 kV and 500 Hz, respectively.

After the plasma pretreatment of the polymer substrate, the AA polymerization was carried out using the “strong” operating condition and a treatment time of 20 min. For all the above reported operating conditions, the gap between the plasma source and the polymeric substrate was kept constant at 2mm. The schematic representation of the experimental setup with the gas connections required for both the plasma polymerization process and the plasma pretreatment of the polymeric substrates is reported in Figure 2.

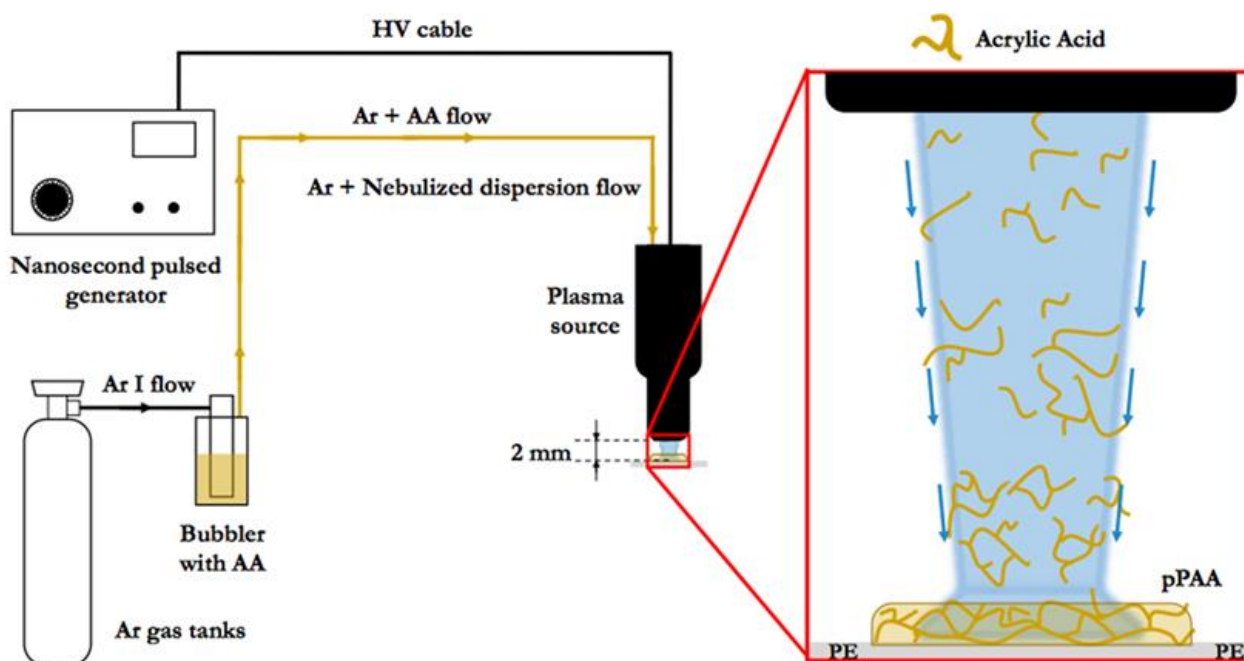


Figure 2. Experimental setup of the plasma polymerization processes with the gas connections required for both the plasma polymerization process and the plasma pretreatment of the polymeric substrates.

6.2.4 Experimental setup and operating conditions for the pPAA/AgNPs coating co-deposition

The experimental setup is schematically represented in Figure 3. For the AgNPs/pPAA deposition onto PE substrates, the plasma jet was operated in Ar and separately fed with the nanocomposite coating precursors, exploiting the two distinct gas channels of the plasma source. In particular, a flow of 2.5 slpm of Ar was introduced at first inside a bubbler containing the monomer and then, carrying the AA, injected into the plasma source through the primary channel. Simultaneously, a second flow of 2.5 slpm of Ar was introduced in a nebulizer system containing the dispersion of AgNPs in EtOH and the so formed aerosol was injected into the plasma source through the secondary gas channel. The mass flow rate of AA injected through the primary channel and of the AgNPs nebulized dispersion injected through the secondary channel, determined by the monomer and colloid consumption inside the flasks as reported in previous works [8, 9], were of 0.05 ml/min and 2.3 ml/min, respectively. For the deposition of AgNPs coatings, the primary gas channel was closed and only the aerosol of AgNPs in Ar was fed to the plasma region. During the deposition process, the distance between the plasma source and the PE substrate was kept constant at 2mm and a floating aluminum foil was placed under the PE film in order to facilitate the generation of the plasma discharge. For all the experiments, the treatment time was kept constant at 3 min.

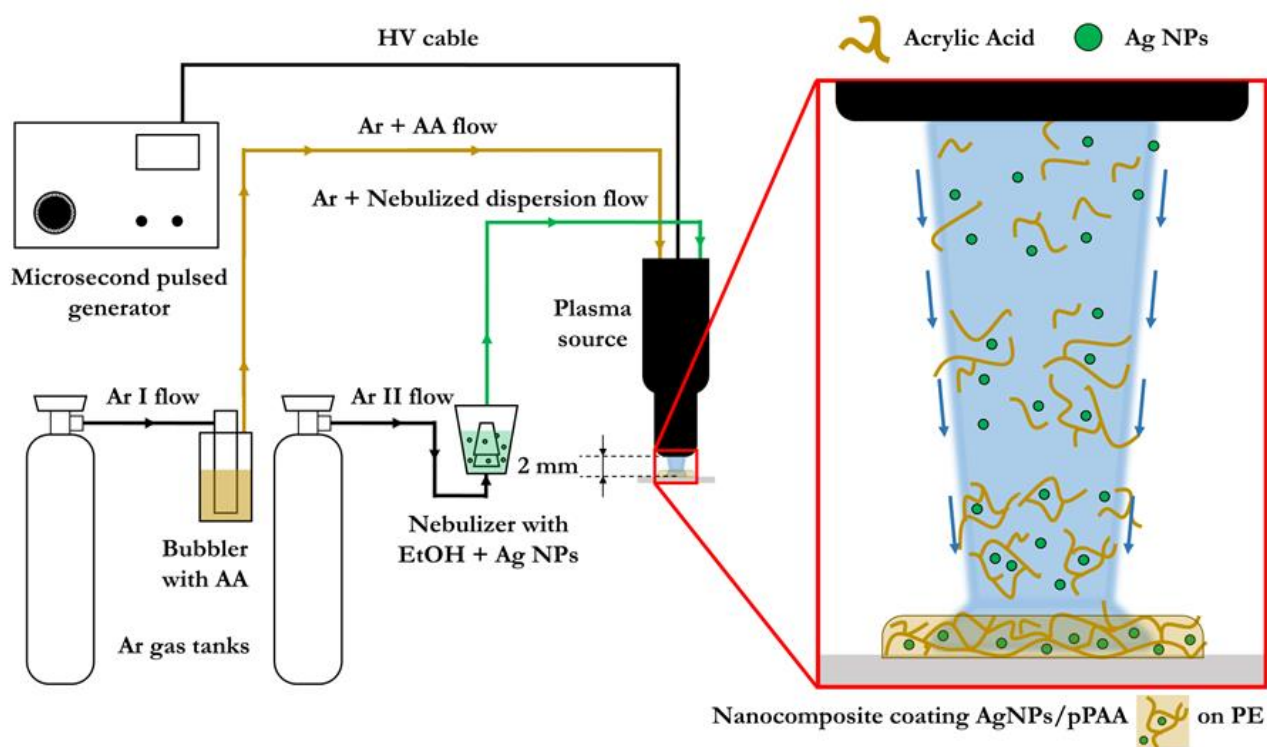


Figure 3. Experimental setup of the plasma co-deposition process [2].

6.2.5 Water Contact Angle (WCA) Measurements

WCA measurements were performed to evaluate the wettability of pPAA deposited coatings and to compare it with that of the pristine substrate. WCA measurements were carried out at RT by means of a commercial Kruss Drop Shape Analysis System DSA 30. Using the software provided with the instrument, measurements of the static WCA was automated. A distilled water drop of 2.0 ml was used as test liquid. Each measurement was run in triplicate and results are given as the average value \pm standard deviation.

6.2.6 Attenuated Total Reflectance-Fourier Transform Infrared (ATR-FTIR) Spectroscopy

ATR-FTIR was used to gather information on the chemical structure of the substrate before and after the deposition of the pPAA and pPAA/AgNPs films by the plasma polymerization process. The Agilent Cary 660 FTIR spectrometer was used to collect infrared absorption spectra of the pPAA films deposited on PE and PVC substrates and of pPAA/AgNPs coatings deposited on PE films. The spectrometer was equipped with an ATR sampling accessory, using a diamond crystal as internal reflection element. Spectra were acquired at RT in absorbance mode, from 3900 to 400 cm^{-1} with a resolution of 2 cm^{-1} ; a total of 32 scans were recorded for each spectrum.

6.2.7 X-ray Photoelectron Spectroscopy (XPS)

X-ray photoelectron spectroscopy measurements were carried out by Prof. Pollicino in order to evaluate the chemical composition of pPAA and AgNPs/pPAA coatings by means of a VG Instrument electron spectrometer using a Mg Ka_{1,2} X-ray source (1253.6 eV). The X-ray source in the standard conditions was operated at 300 W, 15 kV and 20 mA. The base pressure of the instrument was 5×10^{-10} Torr and an operating pressure of 2×10^{-8} Torr was adopted. A pass energy of 100 eV and 20 eV was used for widescans and narrowscans, respectively. The semi-quantitative surface analyses were carried out by the determination of the photoelectron peak areas obtained by multiplying the experimental values with the appropriate sensitivity factor. For acquiring the spectra, a take-off angle (t.o.a.) of 80° was used. Considering that the relationship between the depth of the analysed layer (d) and the t.o.a. (θ) is represented by the equation $d = 3l \sin\theta$, where l is the inelastic mean free path (IMFP) of the photoelectrons [10], it is possible to quantify the thickness of the analysed layer in about 40 Å. The calculation of the areas corresponding to the different photoelectron peaks was performed using VGX900x software; the curve fitting elaborations were done by means of PeakFit

software (version 4, from SPSS Inc.). The curve fitting of C1s envelope has been performed using the product of Gaussian and Lorentzian functions (80:20): the FWHM of the height of each curve was kept equal to 1.7 ± 0.1 eV. Binding energies were referred to the C-H level at 285 eV.

6.2.8 Optical Microscope Analysis

In order to garner some preliminary information about the average thickness of the pPAA deposited coatings, a digital three dimensional microscope Hirox Model KH-7700 characterized by high resolution optics 100–800X was employed. The instrument was equipped with a piezoelectric actuator on focus axis (z-axis), which enables a spatial resolution in the order of 0.5 μ m. The analysis was performed on PE and PVC substrates partially masked during the AA plasma-polymerization process, in order to allow the deposition of the pPAA only in a well-localized area, easily identifiable by the instrument. Measurements were obtained by performing a multi-focus digital reconstruction of the specimen in the area subjected to the plasma-polymerization process and by approximately evaluating the differences between each peak with respect to the level of the untreated area. The elaboration of the acquired data was performed using the proprietary instrument software. Each measurement was run in triplicate and results are given as the average value \pm standard deviation.

6.2.9 Scanning Electron Microscopy

Scanning electron microscopy was performed to investigate the morphology of the AgNPs/pPAA coatings deposited onto PE substrates; for comparison, SEM analysis was also performed on substrates where only AgNPs were deposited.

Scanning Electron Microscope observations were carried out using a Philips 515 SEM by applying an accelerating voltage of 15 kV, on samples sputter coated with gold; the SEM was also equipped with energy dispersive X-ray spectroscopy (EDS), which was used for elemental analyses of the samples.

6.2.10 Antimicrobial Assay

To evaluate the antibacterial properties of AgNPs/pPAA coatings, *Escherichia coli* (DSM 3083) was cultured on Tryptic soy agar (TSA) plates at 37 °C and a bacterial suspension was prepared in sterile distilled water from an overnight culture; the suspension was adjusted to approximately 1.5×10^8 CFU (Colony Forming Units) ml^{-1} based on McFarland turbidity standards, serially diluted and plated on TSA to quantify the bacterial concentration. The suspension was spread over the entire surface of the

TSA plate by swabbing uniformly across agar. Each plate was kept for 15 min at room temperature and then each sample to be tested (either pristine PE, PE coated with pPAA or PE coated with AgNPs/pPAA), having a surface 1 cm², was placed onto a contaminated agar plates. After incubation for 24 h at 37 °C, the presence/absence of a bacterial growth inhibition area was evaluated. Tests were performed in triplicate.

6.3 Results and Discussion

6.3.1 pPAA coating deposition

Since this work was aimed at depositing onto a polymer substrate, a pPAA coating containing carboxyl groups, strongly required in the frame of biomedical applications to promote cell adhesion or biomolecules immobilization, different operating conditions of the plasma polymerization process were evaluated.

As a first step, both PE and PVC substrates were subjected to the plasma polymerization process performed in “mild” operating condition, obtained by setting the PV and the RR at 10 kV and 330 Hz, for treatment times of 3, 5, and 20 min. The area of the polymeric substrate interested by the coating deposition was around 1 cm², significantly larger than the area of the plasma source orifice; this behavior is in agreement with the results presented by Onyshchenko *et al.* [11], who thoroughly investigated the dimension of the area functionalized by an atmospheric pressure plasma jet treatment. The ATR-FTIR spectra, shown in Figure 4, highlighted that after 3 min of the plasma polymerization process the characteristic peaks of the PE substrate could still be easily identified, whereas after 5 min only the spectrum of the pPAA film turned out to be detectable.

Similar results, even though less self-evident due to the characteristic peaks of the underlying substrate, were obtained when PVC was taken as the substrate for pPAA deposition (data not shown).

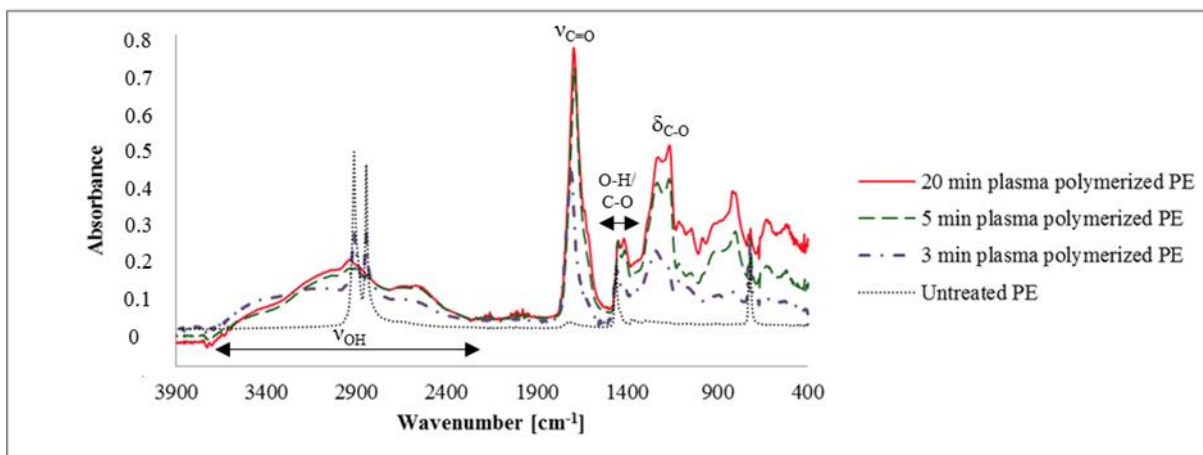


Figure 4. ATR-FTIR spectra of pristine PE and of PE substrates subjected to AA plasma polymerization process performed in “mild” operating conditions: 3, 5 and 20 min [1].

Taking into account the fact that with ATR-FTIR measurements the sampling depth is of the order of 600-700 nm [12], since the spectrum of the underlying PE substrate could not be detected after 5 min of AA plasma polymerization, it is reasonable to hypothesize that the obtained pPAA film was characterized by a thickness exceeding that dimension. The spectra collected for 5 and 20 min plasma polymerization processes exhibited a very strong absorption band at 1714 cm^{-1} which can be assigned to C=O stretching vibrations of the carboxylic functional groups. The ATR-FTIR spectra shown in Figure 3 also contain a very broad band in the region $3600\text{-}2400\text{ cm}^{-1}$, which can be attributed to OH stretching vibrations [13]. Superimposed on this broad peak, a band in the region $3000\text{-}2900\text{ cm}^{-1}$ due to CH_x stretching vibrations is noticeable [13]. At lower wavenumber, an absorption peak due to coupled C-O stretching and OH deformation between $1400\text{ and }1330\text{ cm}^{-1}$, and a strong C-O stretching absorption peak between $1332\text{ and }1135\text{ cm}^{-1}$ with the maximum around 1200 cm^{-1} can be found. Finally, the absorption band due to C(O)OH dimers appears between $999\text{ and }875\text{ cm}^{-1}$ [13,14]. Besides FTIR, the XPS technique can also provide useful information on the chemical composition of the pPAA deposited films and it is, differently from FTIR, a highly surface-sensitive technique. As known, the effective XPS sampling depth (d), which is the depth from which 95% of the electron signal arises, is calculated as $d = 3\lambda\sin\theta$, where θ is the electron take-off angle and λ is the electron mean free path. Thus, using λ of 1.4 nm, as determined by Clark *et al.*, [10] for C_{1s} photoelectrons, our results are representative of the composition of the approximately outermost 4 nm of the surface. XPS analysis was performed on the PVC substrate subjected to 3 min AA plasma polymerization in “mild” operating condition. This sample was selected in order to verify if chlorine atoms of the underlying PVC were or not detected after 3 min pPAA deposition since for this sample the characteristic peaks of the PVC substrate were still detected by the ATR-FTIR, similarly to the case

of PE substrate. Furthermore, in order to evaluate the role of the plasma polymerization time on the content of carboxylic acid ($-\text{COOH}$) and/or ester ($-\text{COOR}$) moieties, both characteristic of the pPAA chemical structure, the XPS investigation was also performed on 20 min plasma polymerized PVC samples. To obtain deeper insight into the chemical bonds on the surface of the samples, curve fitting of the high-resolution C_{1s} peak was performed. Figure 5 shows the C_{1s} peaks of the PVC samples subjected to 3 min (Figure 5a) and 20 min (Figure 5b) plasma polymerization processes performed in “mild” operating condition.

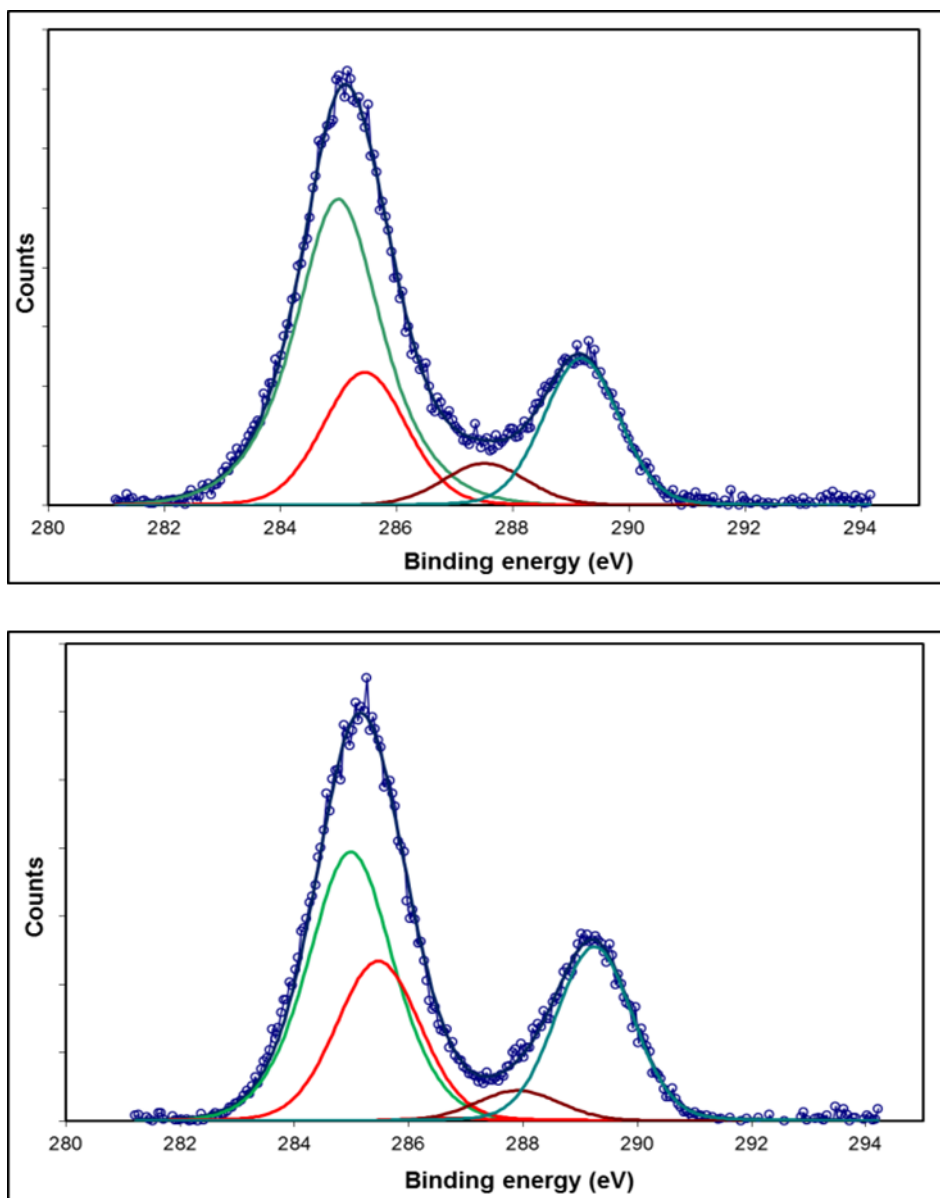


Figure 5. XPS deconvoluted C_{1s} peak of pPAA deposited on PVC substrate by means of AA plasma polymerization process performed in “mild” operating condition: 3 min (a) and 20 min (b) [1].

The C1s envelope of the deposited films can be deconvoluted into four distinct peaks: a peak at 285.0 ± 0.1 eV corresponding to C–C and C–H bonds, a peak at 285.5 ± 0.1 eV due to C–COOH functional groups, a peak at 286.8 ± 0.1 eV due to C–O bonds and finally, a peak at 289.1 ± 0.1 eV, attributed to carboxylic acid (–COOH) and/or ester (–COOR) groups. Furthermore, in the peak fitting of the C1s envelope of the 20 min deposited pPAA film, while the peak due to C–O bonds almost disappears, a peak at 287.8 ± 0.1 eV, attributed to C=O groups, is present.

Interestingly, as shown in Figure 5a and Figure 5b, no chlorine was detected in the C_{1s} envelopes of the deposited films. In light of this result, the thickness of the 3 min pPAA deposited film in “mild” operating condition can be supposed to be in the region between the XPS and ATR-FTIR sampling depth. Moreover, the results, presented in Figure 5 and Table 1, bring out that the increase of the plasma polymerization time from 3 to 20 min leads to (i) the increase of the C–COOH, –COOH and –COOR groups, (ii) the decrease of C–O and C–C functions, (iii) the appearance of C=O moieties in the chemical composition of the deposited film, (iv) the increase of O/C ratio from 0.44 to 0.59. In particular, as reported in Table 1, the increase of the amount of carboxylic groups from 22 to 26%, jointly to the appearance of the carbonyl ones, suggests that a greater retention of functional groups on the substrate can be accomplished by increasing the plasma polymerization time.

Table 1. Surface chemical groups concentration and O/C ratio after pPAA deposition by AA plasma polymerization processes [1].

Substrate	Operating condition	C-C	<u>C</u> -COOH	C-O	C=O	-COOH	O/C
		C-H			<u>O-C-O</u>	-COOR	
		285.0 eV	285.5 eV	286.8 eV	287.8 eV	289.1 eV	
PVC	3 min “mild” condition	48%	22%	8%	-	22%	0.44
PVC	20 min “mild” condition	43%	26%	1%	5%	26%	0.59
PE	20 min “mild” condition	44%	26%	0.5%	4.5%	26%	0.54
PE	20 min “strong” condition	32%	27%	9%	5%	27%	0.63

With the aim of gathering some fundamental and preliminary knowledge about the average thickness of the deposited pPAA, optical microscopy was used to investigate the thickness of the film after a 20 min plasma polymerization process in “mild” operating condition carried out on both PE and PVC

substrates. The preliminary obtained results showed that the pPAA coating deposited on the PE substrate had an average thickness of $42 \pm 15 \mu\text{m}$, while the one on the PVC substrate resulted to be $19 \pm 11 \mu\text{m}$ thick. Although the numerical values measured for the two analysed samples turn out to be rather different, they are both in the order of few tens of micrometers, in agreement with observations of the collected ATR-FTIR spectra. In order to give a representation of the thickness and the morphological aspect of the deposited coating, an image, focused at the interface between the pristine PE (properly covered by the mask during the polymerization process, as reported in the Experimental section) and the deposited pPAA, is reported in Figure 6.

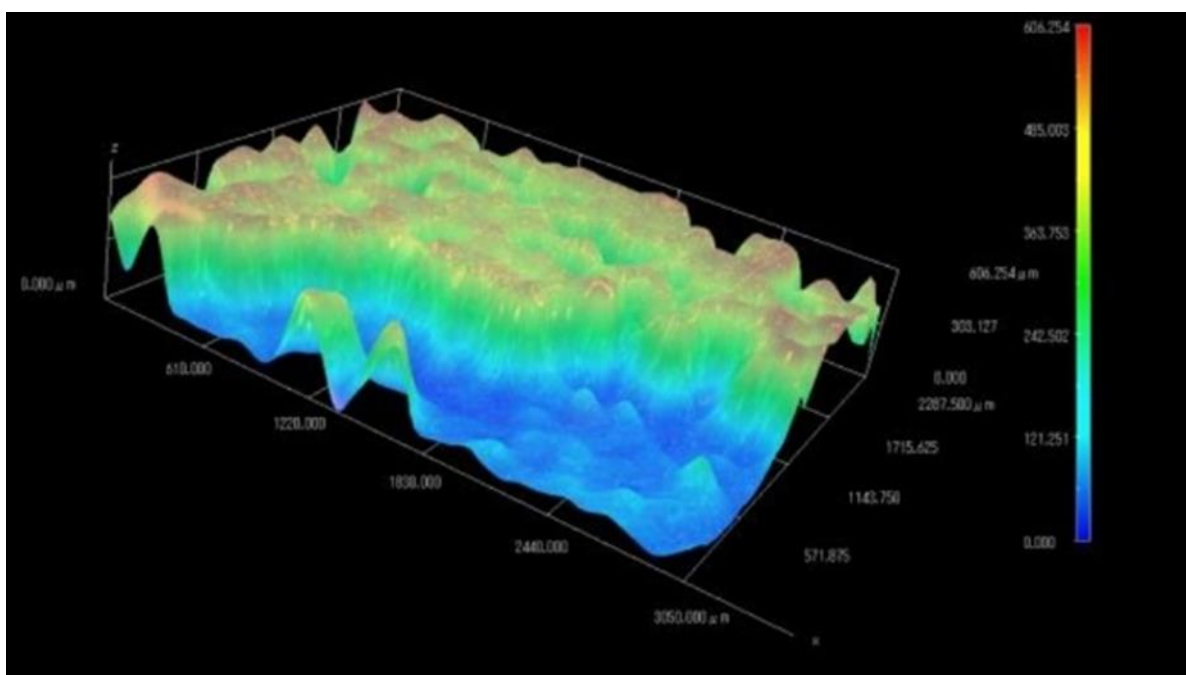


Figure 6. 3-D Optical microscope image at the interface between the masked area of PE and the area where the pPAA was deposited on the PE substrate (20 min “mild” condition) [1].

As noticeable, the film turns out to have a quite relevant roughness and not a constant thickness on the whole deposition area, in agreement with the results of previous work [15].

By applying “mild” operating conditions, the deposited film turned out to be highly water soluble and all peaks characteristic of pPAA were not detected in the ATR-FTIR spectra of the pPAA coated PE and PVC substrates dipped in distilled water for 30 s and air dried.

Therefore, “strong” operating condition (PV of 19.2 kV and a RR of 1000 Hz) was taken on to perform the AA plasma polymerization. The process in this conditions was carried out for both 5 and 20 min and, as reported in Figure 7, a comparison between the collected FTIR spectra of these samples

and the one obtained after 20 min “mild” condition process was performed for both PE and PVC substrates.

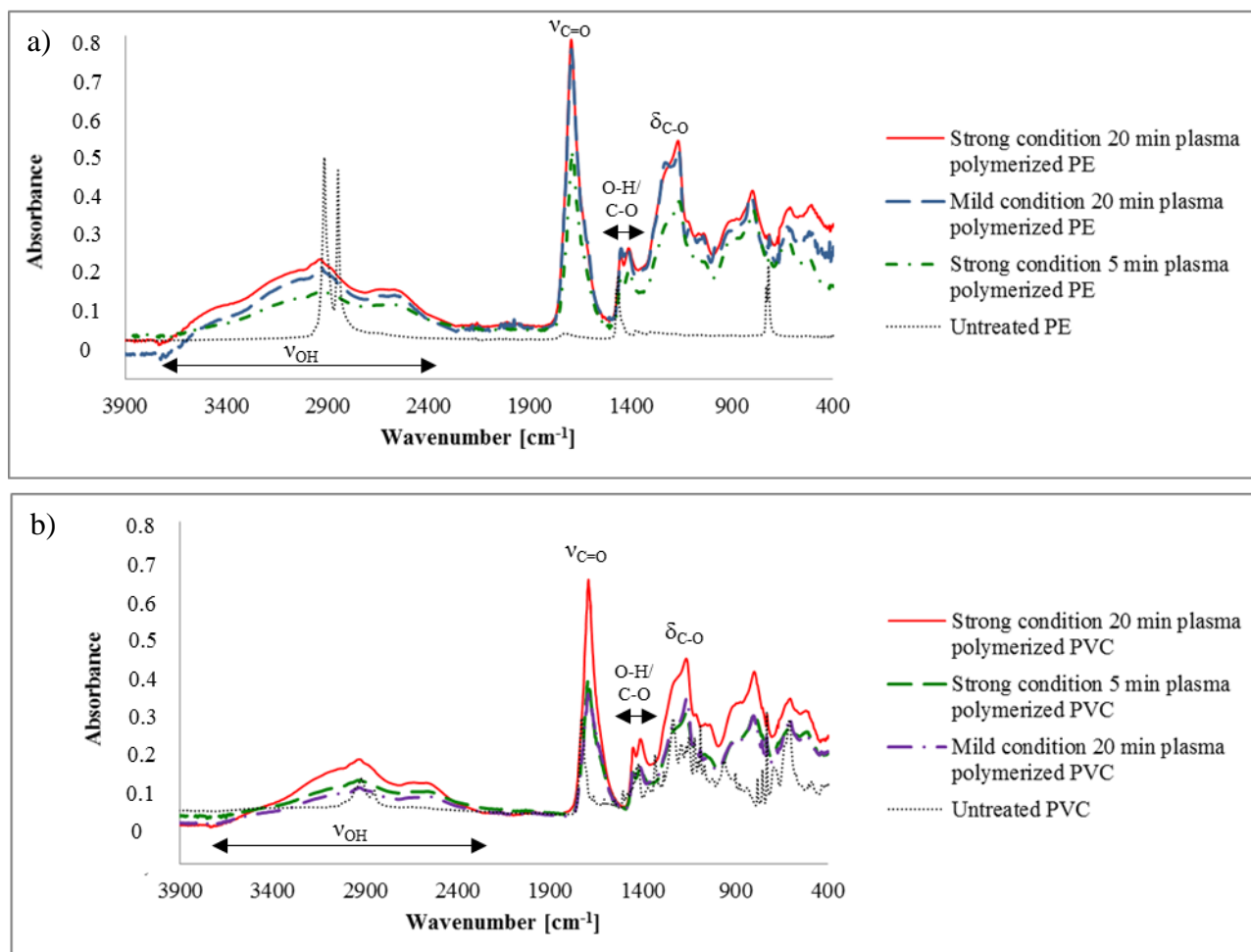


Figure 7. ATR-FTIR spectra of pristine PE and PE samples subjected to AA plasma polymerization process performed in “strong” operating condition: 5 and 20 min and in “mild” operating condition: 20 min (a); pristine PVC and PVC samples subjected to AA plasma polymerization process performed in “strong” operating condition: 5 and 20 min and in “mild” operating condition: 20 min (b) [1].

As observed for the “mild” condition, after 5 min plasma polymerization in “strong” operating condition the spectrum of the substrate cannot be detected anymore, while the pPAA spectrum results to be well defined. Interestingly, for the PE substrate, no relevant differences can be noted by comparing the spectra of the 20 min pPAA deposited in “mild” and “strong” conditions (Figure 7a). Conversely, in the case of PVC the pPAA spectra after 20 min “mild” condition process turned out to be very close to the one collected on the 5 min “strong” condition polymerized sample (Figure 7b). After the polymerization processes performed for 20 min in “strong” operating condition, the stability upon water contact of the pPAA films was tested by dipping the samples in distilled water for 30 s.

Although the drastic reduction of the absorbance of the pPAA characteristic peaks and the detectability of the spectrum of the underlying substrate, as shown in Figure 8, the pPAA film resulted not totally washed off after water dipping.

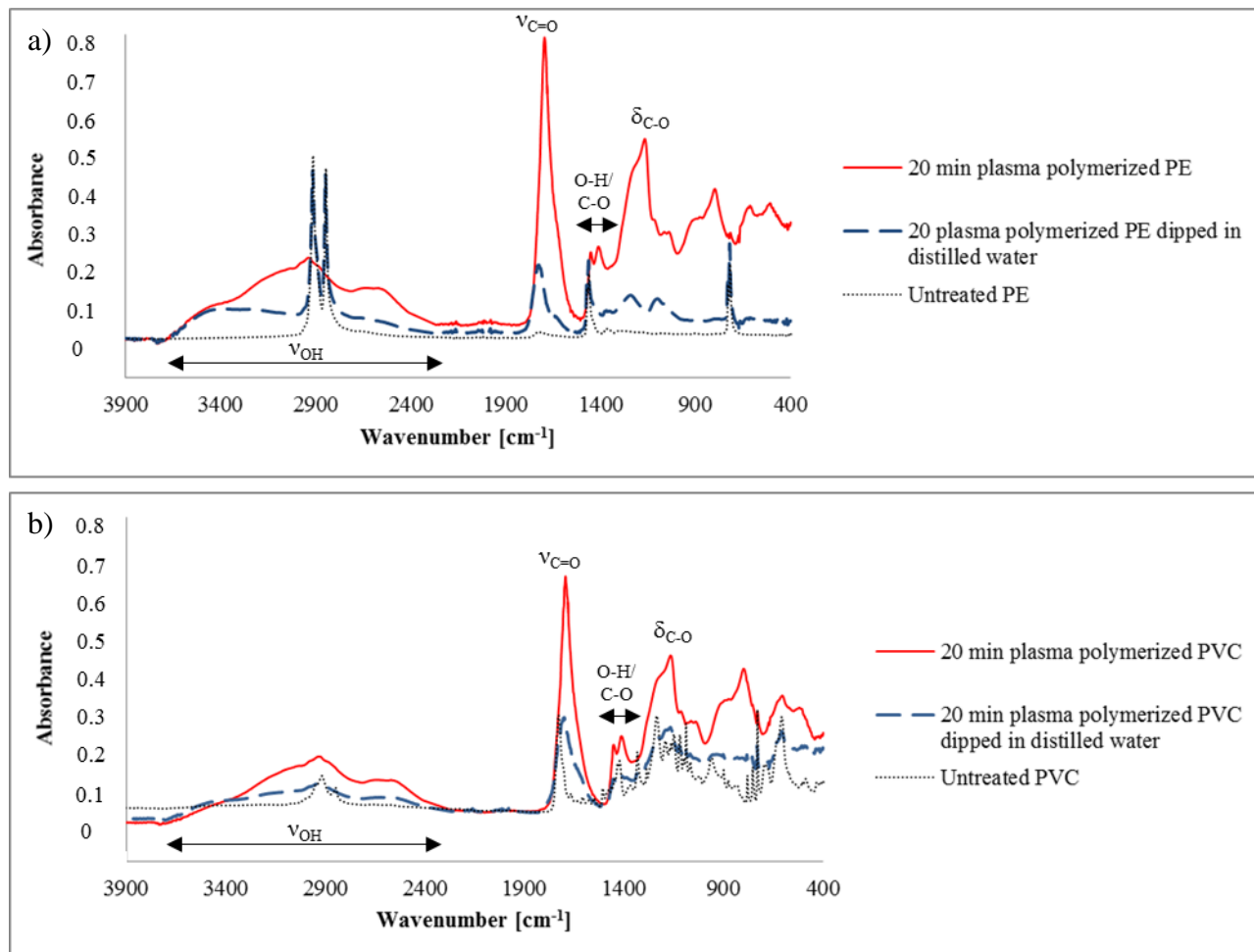


Figure 8. ATR-FTIR spectra of pristine PE and PE samples subjected to AA plasma polymerization process performed for 20 min in “strong” operating condition before and after being dipped in distilled water for 30 s (a); pristine PVC and PVC samples subjected to AA plasma polymerization process performed for 20 min in “strong” operating condition before and after being dipped in distilled water for 30 s (b) [1].

Since the deposited pPAA resulted partially insoluble upon water contact, an indicative water contact angle (WCA) measurement was performed in the region of the substrate subjected to the AA polymerization process, immediately after the polymerization process itself. While the measured WCA values were $71^{\circ}\pm 1^{\circ}$ and $73^{\circ}\pm 1^{\circ}$ for the pristine PE and PVC, respectively, indicative WCA values of $8^{\circ}\pm 1^{\circ}$ and $8^{\circ}\pm 3^{\circ}$ were obtained on the pPAA coated substrates after a 20 min plasma polymerization process in “strong” operating condition. The increased water wettability of the

plasma-polymerized surface provided further evidence for the presence of hydrophilic -COOH groups.

Since the pPAA deposited in “mild” condition was completely water soluble, the increase of the stability upon water contact after the “strong” condition process may be due to an increase of the degree crosslinking in the pPAA film, which is consistent with its higher water resistance properties. With the aim to get some confirmation to this hypothesis in terms of the chemical composition of the pPAA deposited film, the XPS analysis was performed on 20 min plasma polymerized PE samples both in “mild” and in “strong” operating conditions; a comparison between the C1s envelope obtained for the two kinds of sample is presented in Figure 9.

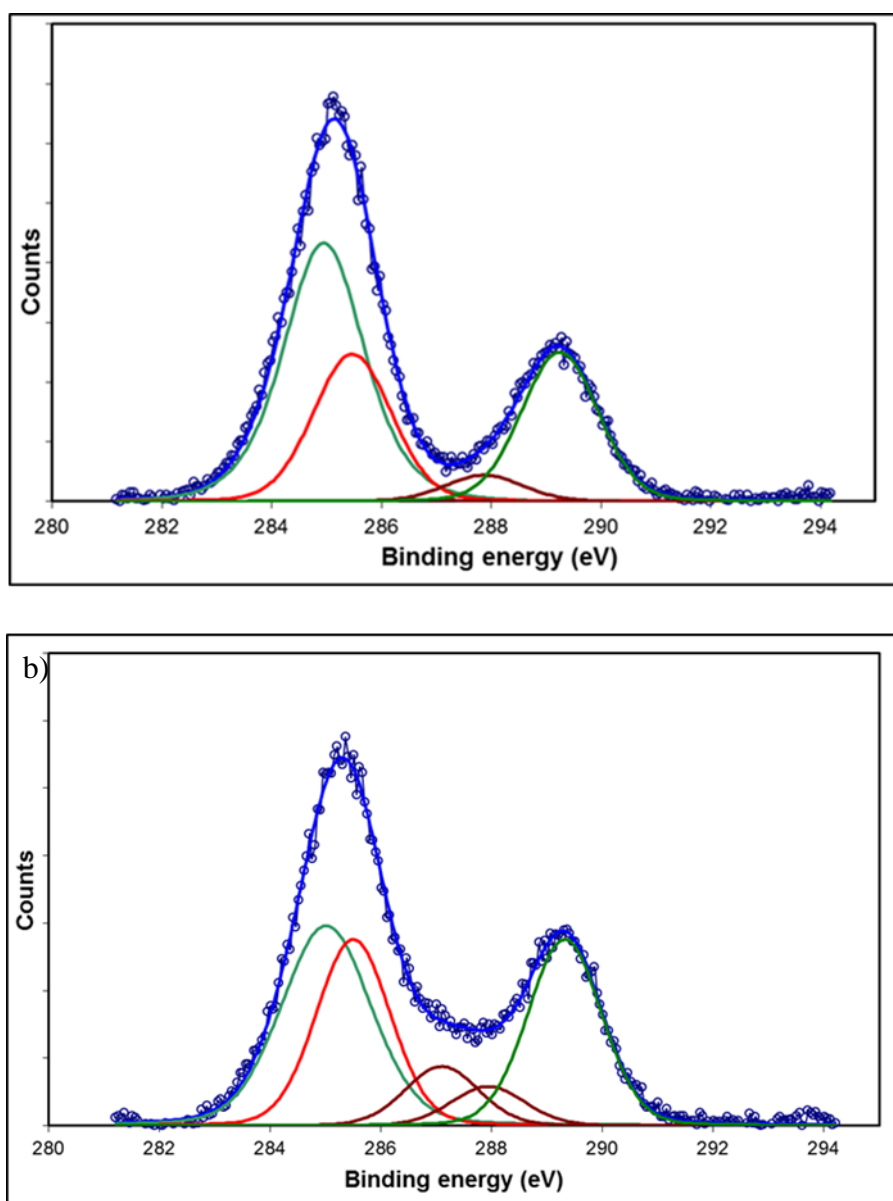


Figure 9. XPS deconvoluted C1s peak of pPAA deposited on PE substrate by means of AA plasma polymerization process performed for 20 min in “mild” operating condition (a) and in “strong” operating condition (b) [1].

By switching from “mild” to “strong” operating plasma polymerization conditions, while the amount of carbonyl and carboxylic functions slightly increases, a significant decrease of not oxidised carbon species in addition to a relevantly higher content of alcoholic, ether and peroxide functions, centred at 286.8 ± 0.1 eV, and to an increase of O/C ratio, was detected in the PE samples (Table 1).

Due to the assembly of various molecular fragments produced in the plasma region [16], the polyacrylic acid (pPAA) films obtained from the AA plasma polymerization process have been found to be generally more crosslinked than the ones produced from chemical processes. On this basis, the detected alcoholic, ether, peroxide and carbonyl functions, which are generally not or barely identified in the PAA chemical composition, can be associated to the occurred crosslinking during the AA plasma polymerization. In this regard, some works [17] have already demonstrated that plasma polymers obtained from the plasma polymerization of acrylate monomers are characterized by the same chemical composition of the conventional polymer, with additional peaks at the binding energies corresponding to the C=O and O-C-O moieties, possibly due to the loss of an ester carbon [17].

In order to better compare the effect of the operating conditions on the amount of the functional moieties of the deposited pPAA, the results of the XPS analysis are reported in Table 1. As demonstrated and already discussed, a great retention of –COOH and –COOR groups occurred independently on the employed operating conditions and on the treatment time. As evident in Table 1, by comparing the amount of functional groups evaluated on 20 min pPAA deposited in “mild” operating condition on both PE and PVC substrates, no significant difference can be noticed, suggesting that, in the limit of the XPS sampling depth, the pPAA chemical composition is independent of the underlying substrate on which it is deposited. Furthermore, it is worth pointing out that with the increase of the plasma polymerization time, carbonyl moieties are detected and, operating at “strong” condition, a relevant overall amount of C=O, O-C-O and C-O functional groups, jointly to an increase of O/C ratio, that could be attributed to a crosslinked chemical structure, is observed, conferring stability upon water contact to the film. As a last consideration on this aspect, since our studies on the plasma-induced mechanisms which lead to the crosslinking of the polymer chains are still ongoing, a resolving correlation between the plasma polymerization parameters and the amounts of both C=O, O-C-O and C-O functions cannot be proposed yet.

The 20 min plasma polymerization process in “strong” operating condition was also performed on PE and PVC substrates previously subjected to a 10 min long Ar plasma pretreatment, performed with a PV and RR of 12.7 kV and 500 Hz, respectively. As for the case in which the plasma polymerization process was performed without subjecting the substrate to the plasma pretreatment,

the area of the coating turned out to be 1 cm² and the area of the substrate interested by the plasma pretreatment can be assumed to coincide with the one of deposited coating. As reported in Figure 10, for this process, the pPAA deposited film turned out to be highly stable after 30 s water dipping for both the considered plasma pretreated substrates and no significant difference could be found by comparing the spectra collected before and after the samples water immersion.

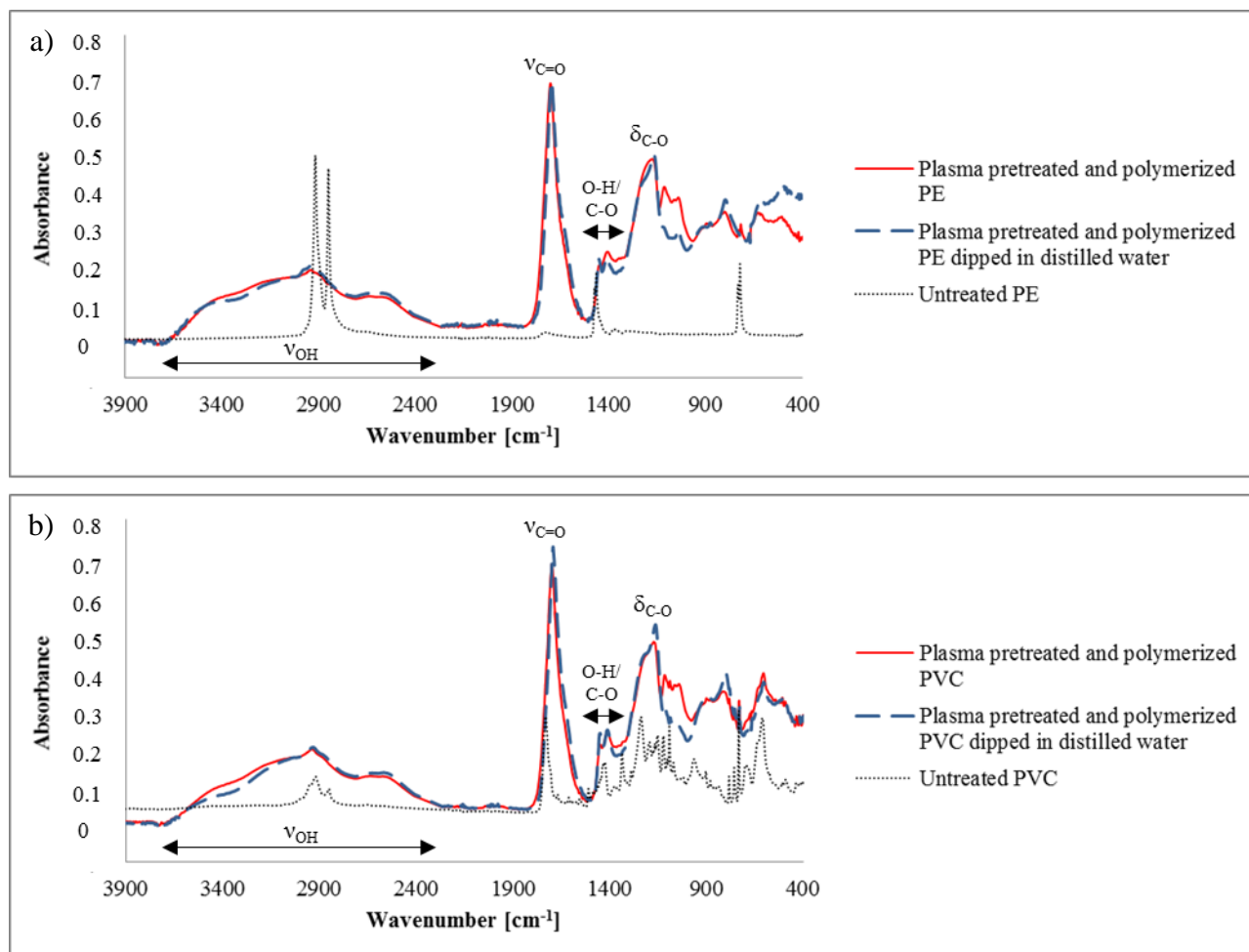


Figure 10. ATR-FTIR spectra of pristine PE and PE samples subjected to 10 min Ar plasma pretreatment and AA plasma polymerization process performed for 20 min in “strong” operating condition, before and after being dipped in distilled water for 30 s (a); pristine PVC and PVC samples subjected to 10 min Ar plasma pretreatment and AA plasma polymerization process performed for 20 min in “strong” operating condition before and after being dipped in distilled water for 30 s (b) [1].

Differently from the case in which the plasma pretreatment of the substrate was not performed, no great difference can be noticed by comparing the ATR-FTIR spectra collected before and after the water dipping. This result emphasizes that for the deposition of polymer coatings stable upon water contact, the adhesion of the polymer film to the substrate needs to be taken into account.

Finally, it is worth noticing that a very interesting work, reporting about the deposition of coatings from mixtures containing AA and ethylene by means of an atmospheric pressure DBD plasma jet, was recently presented by Bosso *et al* [18].

The paper highlighted that ethylene addition increased the deposition rate but also caused a slight reduction of the amount of the carboxylic groups retained in the deposited polymer with respect to the case in which only AA was plasma-polymerized. Interestingly, while thin films obtained without ethylene addition were unstable in water, coatings deposited from AA/ethylene mixtures were stable and did not show significant modifications even after 72 h of water immersion. In fact, the obtained results reported that the amounts of $-\text{COOH}/\text{R}$ detected by XPS before and after 72 h water immersion were almost unchanged, while the thickness loss after water dipping was around 7%. [18] Interestingly, the highest amount of $-\text{COOH}/\text{R}$ detected by XPS in the deposited coatings was around 9%, [18] which is significantly lower than the amounts (22-27%) here reported, further highlighting the potential of nanosecond high voltage pulses for the deposition of coatings with a high retention of functional groups.

6.3.2 pPAA/AgNPs coating co-deposition

Thickness and morphology of the AgNPs/pPAA coatings were investigated by means of SEM analysis. In particular, the coating thickness was measured to be around 30 μm from SEM images of the cross-sectional view of the co-deposited samples; a representative cross-sectional view of a sample coated with AgNPs/pPAA is shown in Figure 11.

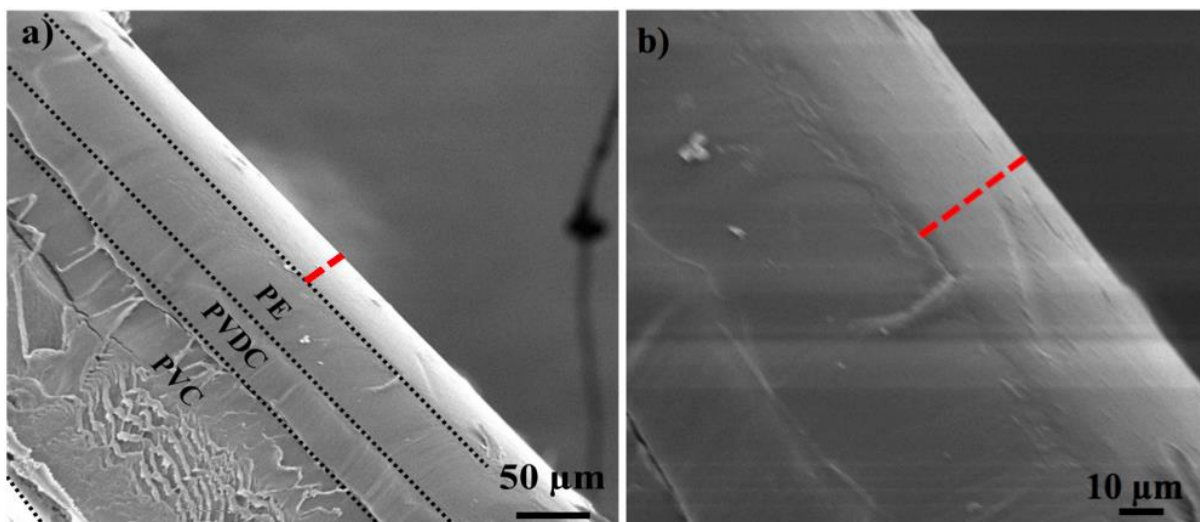


Figure 11. SEM images of the cross-sectional view of the AgNPs/pPAA coated PE; the coating thickness is indicated by the broken red line. Dotted black lines are drawn in Figure 2a in correspondence to the boundaries of the polymeric layers constituting the multi-layer film used as substrate. Magnification: 220 x (a), 810 x (b) [2].

This measured thickness is significantly higher than those achieved with other atmospheric pressure plasma sources. Indeed, Vogelsang *et al.* [15], in their work on the deposition of C:F coatings using a RF capillary microplasma jet, reported of a maximum coating thickness of 7.8 μm after 3 min of deposition; Chen *et al.*[19], reporting on the deposition of pPAA coatings with an atmospheric pressure glow discharge plasma jet, observed a thickness of around 300 nm after a 10 min deposition time. Bashir *et al.* [20], in their work on the polymerization of hexamethyldisiloxane using a DBD plasma jet, reported about an average thickness of the deposited coating of 662 ± 33 nm after a treatment time of 3 min. Finally, Bosso *et al.* [18] observed a maximum thickness of 300 nm for a pPAA coating deposited by means of DBD plasma jet (10 min deposition time).

SEM top views of the samples, reported in Figure 12, show that the co-deposited coating is characterized by an uneven surface, with bright regions in correspondence of polymer-coated AgNPs and aggregates (Figure 12b,d,f) similarly to what previously reported by Deng *et al* [21]; the dimension of these bright areas are almost coincident with the dimension of AgNPs particles and aggregates that can be observed on samples obtained by depositing only AgNPs (Figure 12a,c,e). The

highest resolution SEM top views (Figure 12e,f) underline the presence, in both the AgNPs/pPAA and AgNPs coatings, of AgNPs (having characteristic dimension around 100 nm) either isolated (marked as NP in Figure 12e,f) or organized in clusters (marked as NPc in Figure 12e,f) and sub-micrometric particles (having characteristic dimension of few hundreds of nanometers and marked as Sub μ P in Figure 3e,f); micrometric aggregates (circled by a broken yellow line in Figure 12e,f) are visible as well in the coating. The aggregation of nanoparticles during the co-deposition process was reported also by Deng *et al* [21].

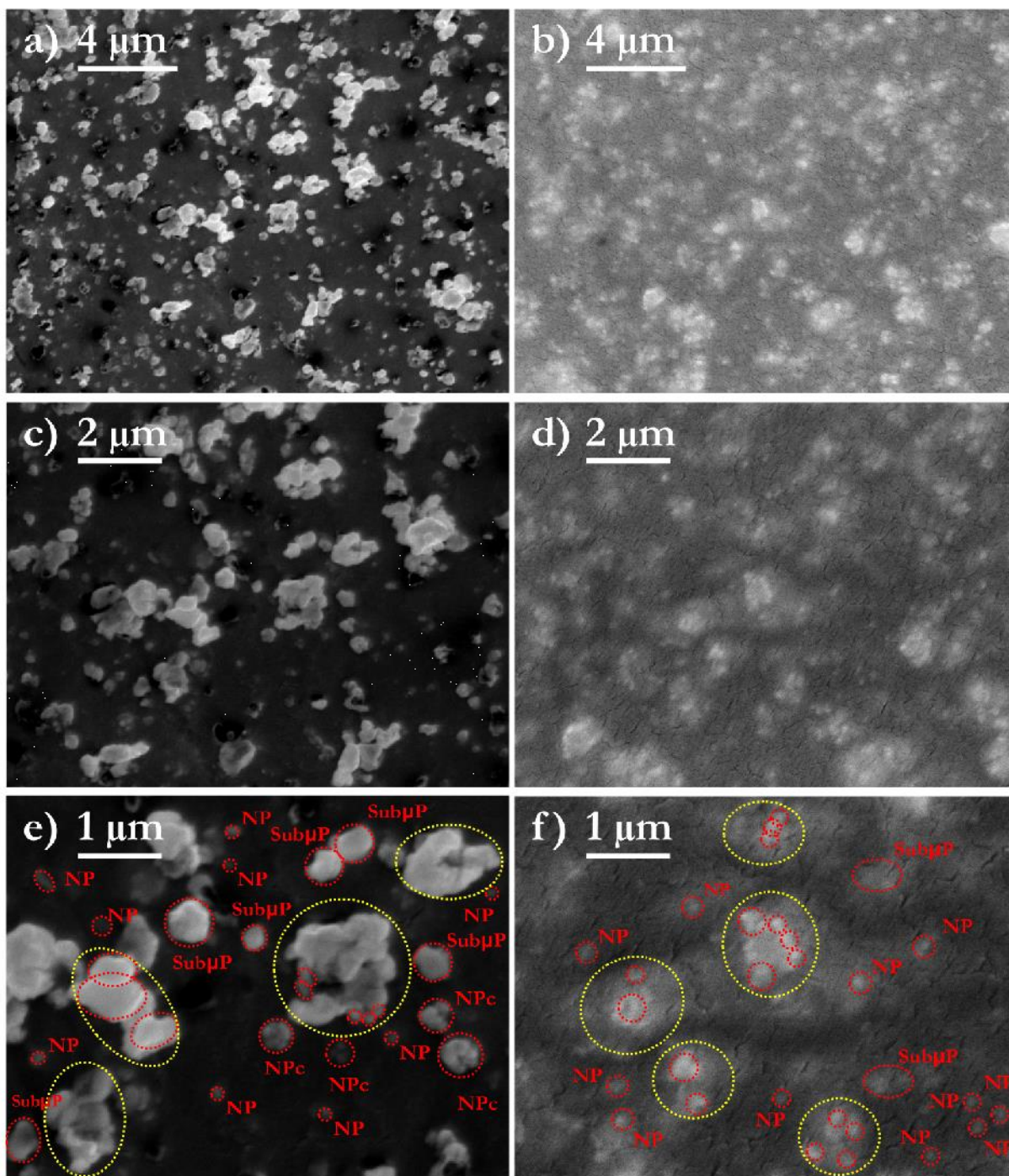


Figure 12. SEM images of the top views of the PE films coated with AgNPs (a, c, e) and AgNPs/pPAA (b, d, f). Magnification: 6000 x (a, b); 10000x (c, d), 20000x (e, f). Dotted yellow circles indicate micrometric aggregates; dotted red circles indicate AgNPs with characteristic dimension around 100 nm, either isolated (NP) or organized in clusters (NPc), and Ag sub-micrometric particles with characteristic dimension in the range of few hundreds nanometres (Sub μ P) [2].

The presence of Ag in the AgNPs/pPAA coatings is further confirmed by the collected EDS spectra shown in Figure 13; noticeable, the Ag characteristic peak is slightly lower in the AgNPs/pPAA coating than in the AgNPs one, as a consequence of the AgNPs being embedded in the polymeric matrix.

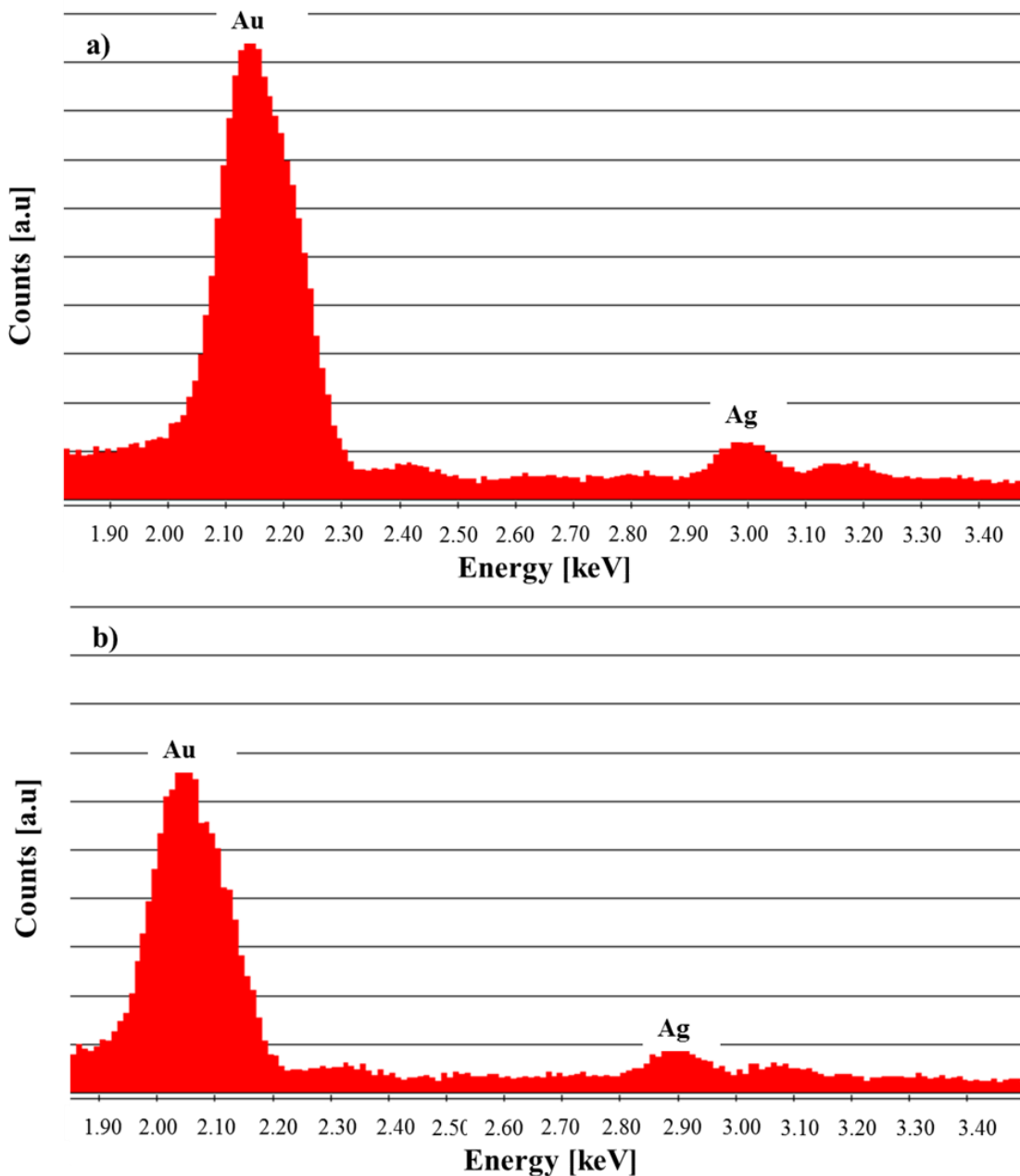


Figure 13. EDS spectra of PE films coated with AgNPs (a) and AgNPs/pPAA (b). Samples were sputter-coated with gold prior to examination [2].

ATR-FTIR analysis confirmed the successful deposition on the PE substrate of the pPAA matrix of the AgNPs/pPAA coating, as the collected spectrum, shown in Figure 14, is remarkably similar to other pPAA spectra previously reported in literature. Despite some works have indicated that ATR-FTIR might provide information about the molecular environment of the organic molecules on the surface of AgNPs [22,23] and thus lead to an indirect detection of the Ag in the coating through a slight shift of characteristic peaks of the spectrum [24], we could not observe any significant difference between AgNPs/pPAA and a typical pPAA coating, probably because the amount of Ag in our coating is below the sensitivity threshold of the technique.

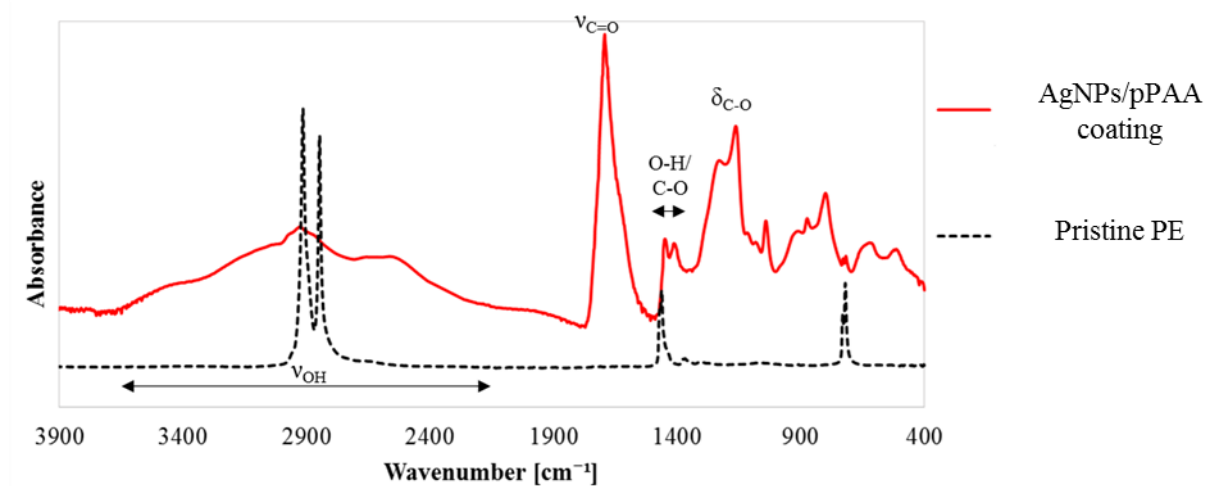


Figure 14. ATR-FTIR spectra of uncoated PE and of AgNPs/pPAA coated PE [2].

The XPS survey spectrum of the AgNPs/pPAA coating, reported in Figure 15, highlighted the presence of Ag, C, O and N through their corresponding XPS peaks (C_{1s} , O_{1s} , N_{1s} , Ag_{3d} and $Ag(A)$). The elemental concentrations in the nanocomposite coating, jointly with the atomic ratios, are reported in Table 2.

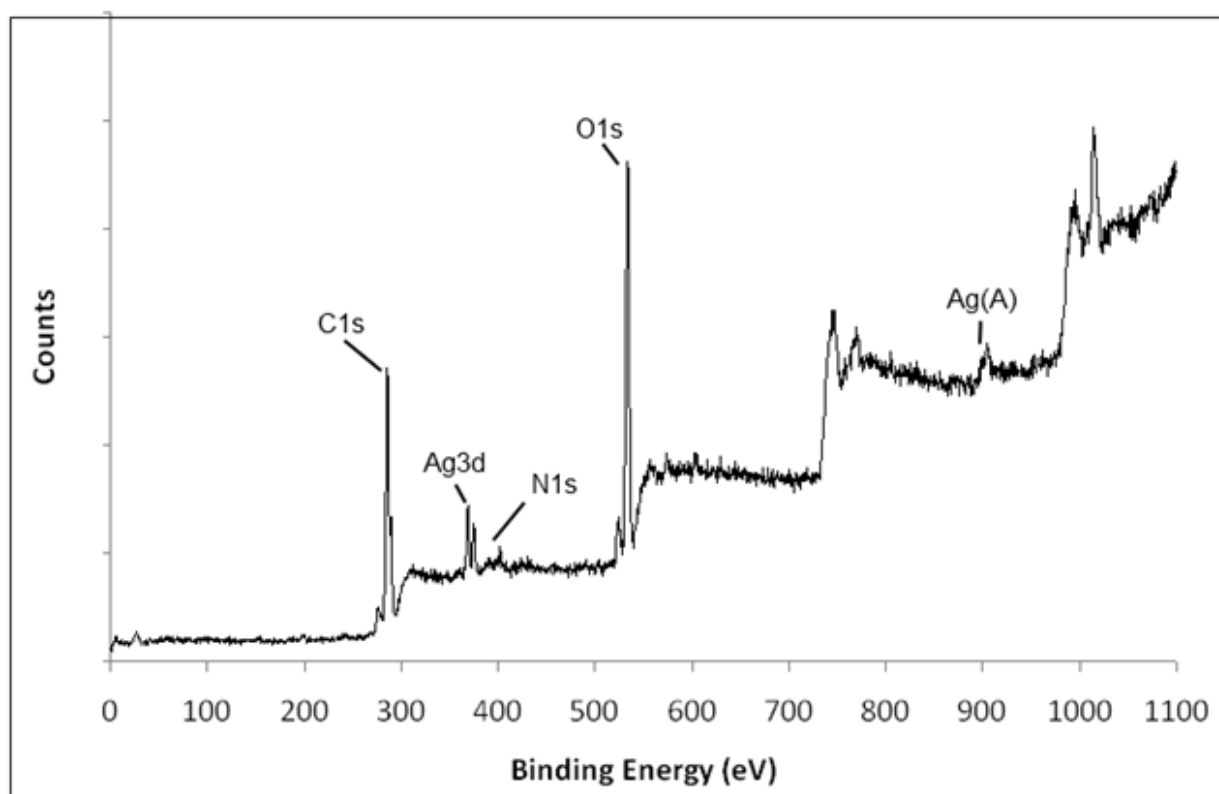


Figure 15. XPS survey spectrum collected for the AgNPs/pPAA coating [2].

Table 1. Elemental concentration and atomic ratios measured for the AgNPs/pPAA coating [2].

C	O	N	Ag	O/C	N/C	Ag/C
63.2%	34.2%	1.7%	0.9%	0.54	0.026	0.014

The presence of nitrogen in the XPS survey spectrum can be probably appointed to the interaction of AA, or the products of its plasma-polymerization, with vibrationally excited N₂ molecules, resulting from the mixing of the plasma plume with the surrounding air, as proposed by Bhatt *et al.* [25] for the case of plasma-polymerization of diethylene glycol dimethyl ether; indeed, they observed by means of optical emission spectroscopy the formation of OH, CH, N₂ and CN excited species when the monomer was introduced into the Ar plasma jet.

The curve fitting of the high-resolution C_{1s} peak, shown in Figure 16, provides useful information on the retention of carboxyl groups in the chemical structure of the pPAA matrix of the nanocomposite coating. Indeed, the C_{1s} envelope of the deposited nanocomposite coating can be deconvoluted into

four distinct peaks: a peak at 285.0 ± 0.1 eV corresponding to $\underline{\text{C}}-\text{C}$ and $\underline{\text{C}}-\text{H}$ bonds, a peak at 285.5 ± 0.1 eV due to $\underline{\text{C}}-\text{COOH}$ functional groups, a peak at 287.8 ± 0.1 eV due to $\text{C}=\text{O}$ bonds and, finally, a peak at 289.1 ± 0.1 eV, attributed to carboxylic acid ($-\underline{\text{C}}\text{OOH}$) and/or ester ($-\underline{\text{C}}\text{OOR}$) groups.

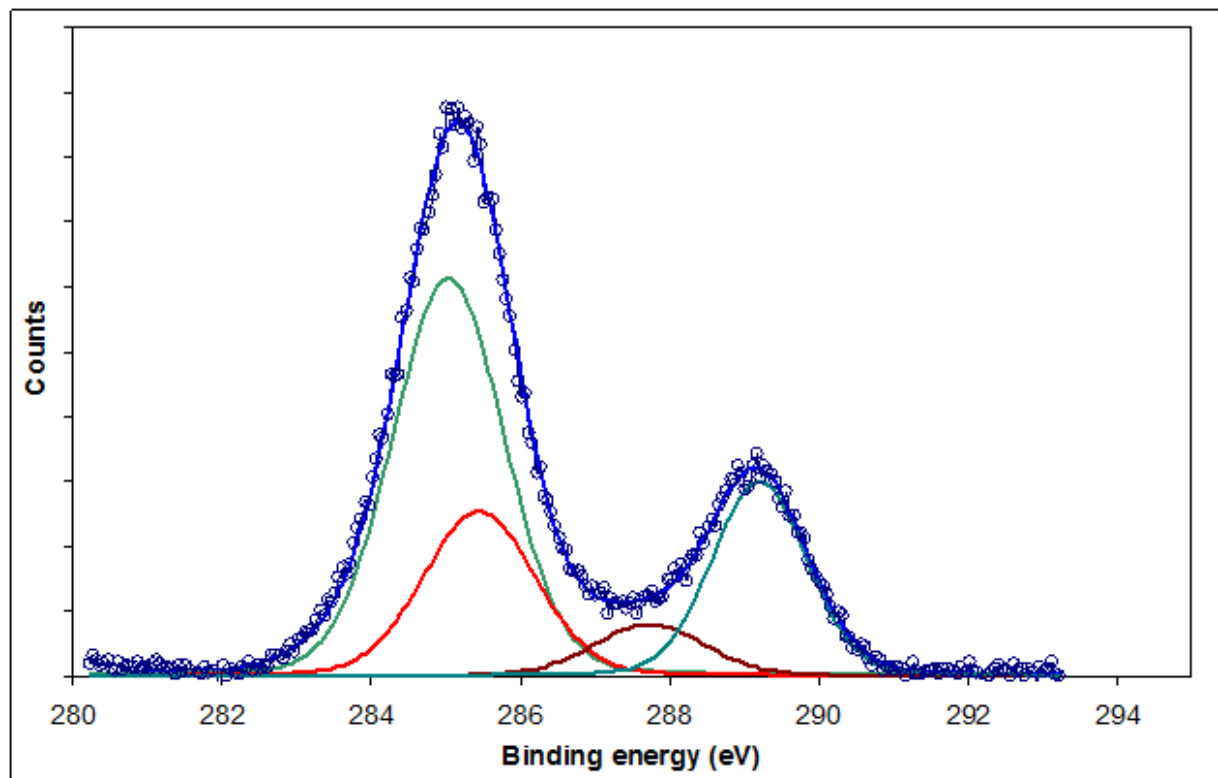


Figure 16. XPS deconvoluted C_{1s} peak of the AgNPs/pPAA coating [2].

Interestingly, as reported in Table 3, the AA plasma-polymerization carried out by means of the micropulsed CAP jet leads to a high retention of $-\text{COOH/R}$ groups (21%); this amount is fairly close to the one previously measured for pPAA deposited with the same plasma source, but driven by a nanosecond pulsed generator. This result can be probably attributed to the low value of duty cycle employed for the co-deposition process: in fact, as highlighted by Boscher *et al.* [26] in their work on the deposition of plasma-polymerized poly(glycidyl methacrylate) by means of DBD driven by ultra-short square pulses, the increase of the duty cycle leads to functional groups destruction and to the formation of a larger distribution of chemical bonds; conversely, films deposited using lower duty cycle conditions were found to be identical in terms of chemical composition to the ones obtained for conventionally polymerized poly(glycidyl methacrylate) [26].

Table 3. Surface carbon groups concentration of the AgNPs/pPAA coating [2].

C-C	C-COOH	C=O	-COOH
C-H			-COOR
285.0 eV	285.5 eV	287.8 eV	289.1 eV
52%	21%	7%	21%

High-resolution XPS spectra of the Ag_{3d} are reported in Figure 17 and indicate that the binding energies of the corresponding spin orbit splitting of Ag_{3d_{5/2}} and Ag_{3d_{3/2}} due to AgNPs are centered at 368.2 eV and 374.2 eV, respectively. Nonetheless, the binding energy positions of Ag_{3d} were not enough to identify the oxidation state of the Ag species, because the characteristic states of oxidized and metallic silver are close together. Nonetheless, partially oxidized AgNPs are known to exhibit better antibacterial activities than the zero-valent Ag, thus the kinetic energy (KE) in the Ag MNN region of the Auger transitions was measured and the modified Auger parameter (α') was used to characterize the chemical state of Ag. This parameter, originally proposed by Wagner [59, 60] and successively modified by Gaarenstrom *et al.* [27], is the sum of the kinetic energy of the Auger electron (in our case Ag M₄N_{4,5}N_{4,5}) and the binding energy of the core-level (Ag_{3d_{5/2}}) peak [28]. This parameter was independent of the charging, but still sensitive to the chemical state of silver and it was calculated as follow:

$$\alpha'(eV) = KE(Ag\ M_4N_{4,5}N_{4,5}) - KE(Ag_{3d_{5/2}}) + hv$$

where KE (Ag M₄N_{4,5}N_{4,5}) is the kinetic energy of the Auger transition, KE (Ag 3d_{5/2}) is the kinetic energy of the Ag 3d_{5/2} core-level and hv is the photon energy equal to 1253.6 eV.

The AgNPs/pPAA coated samples showed a photoelectron peak Ag_{3d_{5/2}} centered at 368.2 eV, and the M₄N_{4,5}N_{4,5} Auger peak centered at a kinetic energy equal to 355.3 eV. The α' parameter is therefore equal $355.3 + 368.2 = 723.5$. Based on the values reported by NIST Database and Wagner [29] this parameter value can be associated with the presence of AgO.

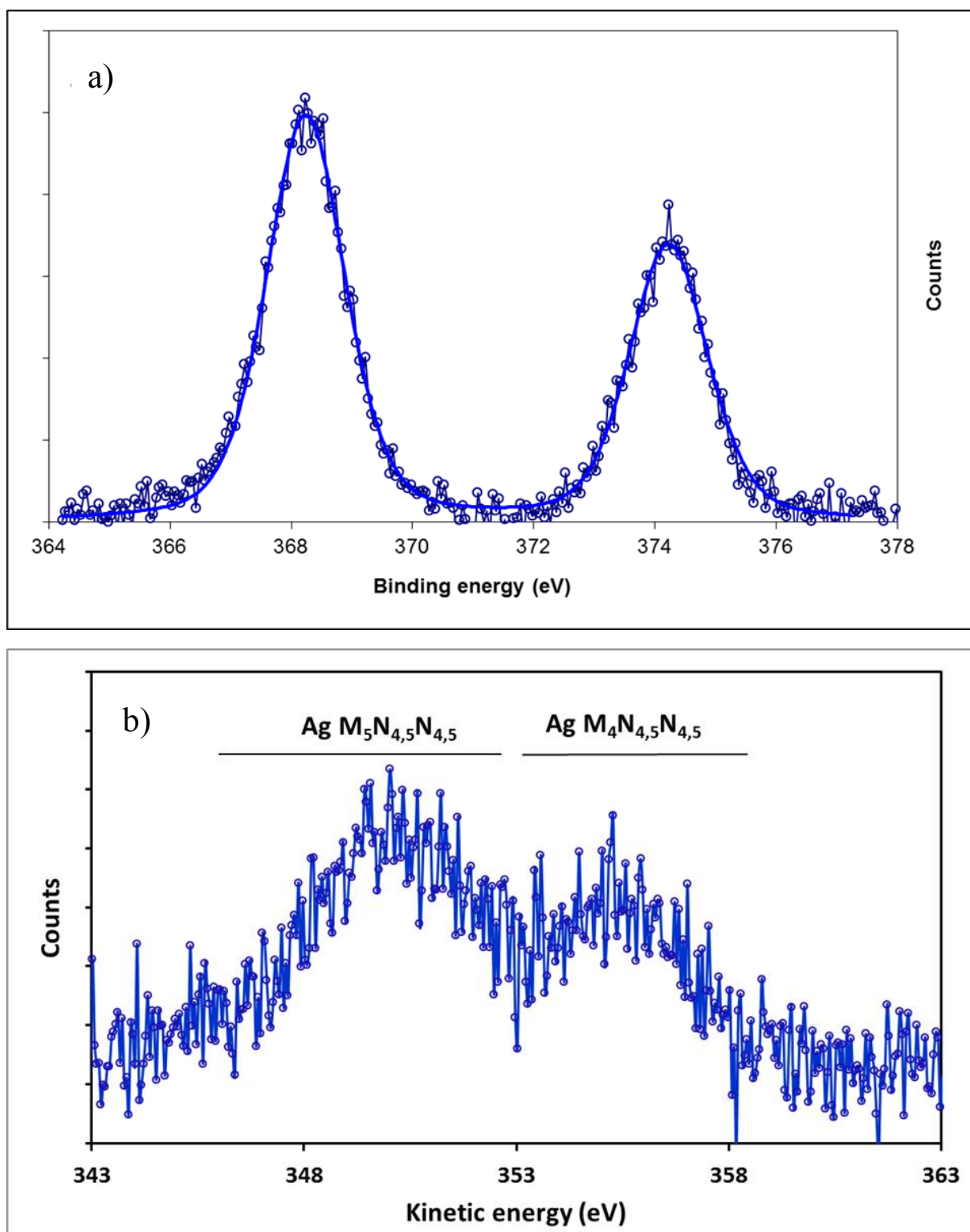


Figure 17. Ag3d core-level (a) and Ag MNN Auger transition spectra (b) of the AgNPs/pPAA coating [2].

As a last consideration on XPS results, it is worth reminding that XPS analysis provides information on the atomic abundance only at the outermost 4 nm of the coating. Since the characteristic dimension of the single AgNP or cluster encapsulated in the polymeric coating is higher than 100 nm, the Ag concentration detected by the surface analysis performed with the XPS cannot be considered as indicative of the bulk chemical composition of the coating, but it is expected to underestimate the Ag content as mentioned in previous works [30].

Results of agar disk diffusion tests to evaluate the antibacterial efficiency of the coatings are shown in Figure 18: while no growth inhibition area can be observed around the uncoated PE and pPAA coated PE samples, a clear zone with no bacterial growth can be clearly detected around the AgNPs/pPAA coated PE samples, similarly to what previously reported also by Sadeghnejad *et al.* [31]; this behavior is indicative of the action Ag ions, probably released from the Ag present either at the surface of the AgNPs/pPAA coating or made available for oxidation by some cracks in the coating, similarly to what previously proposed in literature [32, 33].

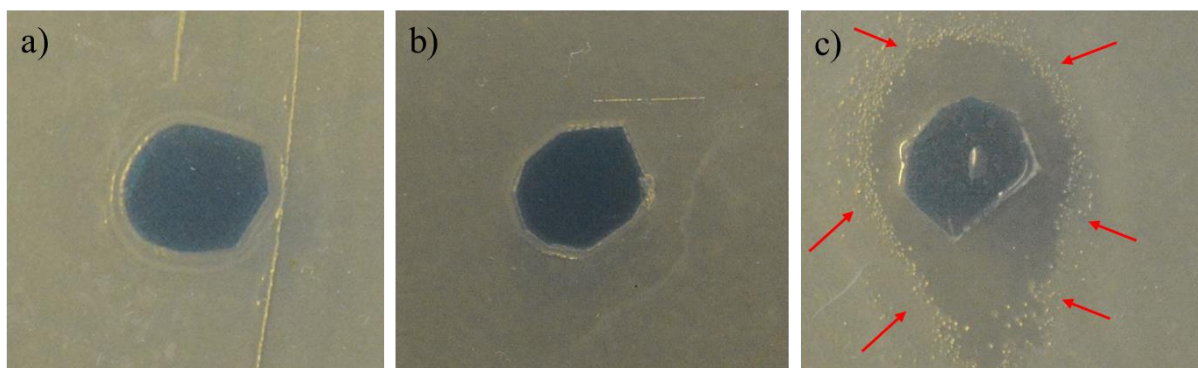


Figure 18. *E. coli* growth inhibition zones on TSA plates with uncoated PE (a), pPAA coated PE (b) and 5% AgNPs/pPAA coated PE (c) [2].

6.4 Conclusions

In this chapter, the results regarding the AA plasma-polymerization and the AgNPs/pPAA coatings deposition by means of a CAP jet have been presented.

Regarding the pPAA coating deposition, it has been observed that, in order to obtain the required characteristics, the operating conditions of the polymerization process need to be optimized. Results have shown that both the selected plasma-polymerization operating conditions (“mild” and “strong”), independently of the treatment time, enabled to obtain an amount of carboxylic acid moieties always higher than 22%, highlighting that the AA plasma-polymerization was successfully performed. However, despite the great amount of –COOH functional groups verified by both ATR-FTIR and XPS, coatings deposited in “mild” operating condition were found to be highly water soluble, probably due to the low crosslinking of pPAA chains. Switching from “mild” to “strong” operating conditions, the overall amount of the detected C=O and C-O functional groups, that could be attributed to pPAA crosslinking, became noticeable, with a parallel enhancement of the pPAA stability upon water contact, even though the coating turned out to be still partially soluble. The plasma treatment of the polymer substrate before the plasma-polymerization process has been demonstrated to reduce pPAA coatings solubility upon water contact, since no great difference between the ATR-FTIR spectra collected before and after water dipping can be observed.

The results obtained from the characterization of the chemical structure of the pPAA coatings allow pointing out that the plasma-polymerization process was successfully performed for all the investigated operating conditions and treatment times, since the high amount of typical pPAA functional groups detected on the substrates.

Furthermore, a preliminary but significant investigation of the morphology of the deposited coating, in terms of evaluation of its average thickness, was also performed by means of optical microscope and an average thickness of the coatings in the order of a few tens of micrometers after a 20 min plasma polymerization process was highlighted.

Regarding the single step AgNPs/pPAA coating co-deposition, the thickness of AgNPs/pPAA coatings co-deposited for 3 min was measured to be around 30 μm from SEM cross-sectional views of the samples. ATR-FTIR spectrum of the co-deposited AgNPs/pPAA coating was found to coincide with the spectrum of pPAA coating without AgNPs embedded. XPS results highlighted a significant

(21%) retention of carboxylic groups in the pPAA chemical structure, underlining that limited monomer fragmentation occurred during the process, and the presence in the coating of superficially oxidized AgNPs. Furthermore, the antibacterial efficacy of the co-deposited AgNPs/pPAA coatings was preliminary assessed with agar disk diffusion tests (using *E. coli*) and a growth inhibition area surrounding the samples, due to the release of Ag ions from the pPAA matrix, was clearly visible after incubation for 24 h at 37°C.

References

- [1] A. Liguori, A. Pollicino, A. Stancampiano, F. Tarterini, M. L. Focarete, V. Colombo, M. Gherardi, “Deposition of Plasma-Polymerized Polyacrylic Acid Coatings by a Non-Equilibrium Atmospheric Pressure Nanopulsed Plasma Jet”, *Plasma Process. Polym.* 2016, 13, 375, Copyright Wiley-VCH Verlag GmbH & Co. KGaA. Reproduced with permission.
- [2] A. Liguori, E. Traldi, E. Toccaceli, R. Laurita, A. Pollicino, M. L. Focarete, V. Colombo, M. Gherardi, “Co-Deposition of Plasma-Polymerized Polyacrylic Acid and Silver Nanoparticles for the Production of Nanocomposite Coatings Using a Non-Equilibrium Atmospheric Pressure Plasma Jet”, *Plasma Process. Polym.* 2015, DOI: 10.1002/ppap.201500143, Copyright Wiley-VCH Verlag GmbH & Co. KGaA. Reproduced with permission.
- [3] M. Boselli, V. Colombo, E. Ghedini, M. Gherardi, R. Laurita, A. Liguori, P. Sanibondi, A. Stancampiano, *Plasma Chem. Plasma Process.* 2014, 34, 4.
- [4] M. Boselli, V. Colombo, E. Ghedini, M. Gherardi, R. Laurita, A. Liguori, P. Sanibondi, E. Simoncelli, A. Stancampiano, *IEEE Trans. Plasma Sci.* 2015, 43, 3.
- [5] V. Colombo, D. Fabiani, M. L. Focarete, M. Gherardi, C. Gualandi, R. Laurita, M. Zaccaria, *Plasma Process. Polym.* 2014, 11, 247.
- [6] V. Colombo, E. Ghedini, M. Gherardi, R. Laurita, P. Sanibondi, D. Fabiani, M. Zaccaria, M.L. Focarete, C. Gualandi, *Proceedings of the 11th IEEE international conference on solid dielectrics—ICSD 11 2013*, 358.
- [7] D. Fabiani, M. Zaccaria, M. L. Focarete, C. Gualandi, V. Colombo, E. Ghedini, M. Gherardi, R. Laurita, P. Sanibondi, *Proceedings of the 11th IEEE international conference on solid dielectrics—*

ICSD 11 2013, 718.

[8] X. Zhu, F. Arefi-Khonsari, C. Petit-Etienne, M. Tatoulian, *Plasma Process. Polym.* 2005, 2, 407.

[9] R. Morent, N. De Geyter, S. Van Vlierberghe, P. Dubruel, C. Leys, E. Schacht, *Surf. Coat. Technol.* 2009, 203, 1366.

[10] D. T. Clark, H. R. Thomas, *J. Polym. Sci.: Polym. Chem. Ed.* 1977, 15, 2843.

[11] I. Onyshchenko, A. Y. Nikiforov, N. De Geyter, R. Morent, *Plasma Process. Polym.*, 2015, 12, 466.

[12] N. De Geyter, R. Morent, C. Leys, *Surf. Interface Anal.* 2008, 40, 608.

[13] G. Socrates, *Infrared and Raman Characteristic Group Frequencies—Tables and Charts*, 3rd edition, Wiley, West Sussex, UK 2001.

[14] D. L. Cho, P. M. Claesson, C. G. Golander, K. Johansson, *J. Appl. Polym. Sci.* 1990, 41, 1373.

[15] A. Vogelsang, A. Ohl, R. Foest, K. Schroder, K. D. Weltmann, *J. Phys. D Appl. Phys.* 2010, 43, 485201.

[16] T. R. Gengenbach, H. J. Griesser, *J. Polym. Sci. Part A Polym. Chem.* 1998, 36, 985.

[17] T. P. Kasih, S. I. Kuroda, H. Kubota, *Plasma Process. Polym.*, 2007, 4, 648.

[18] P. Bosso, F. Fanelli, F. Fracassi, *Plasma Process. Polym.*, 2015. DOI: 10.1002/ppap.201500005.

[19] G. Chen, M. Zhou, Z. Zhang, G. Lv, S. Massey, W. Smith, M. Tatoulian, *Plasma Process. Polym.* 2011, 8, 701.

[20] M. Bashir, S. Bashir, *Plasma Chem. Plasma Process.* 2015, 35, 739.

[21] X. Deng, C. Leys, D. Vujosevic, V. Vuksanovic, U. Cvelbar, N. De Geyter, R. Morent, A. Nikiforov, *Plasma Process. Polym.* 2014, 11, 921.

[22] P. Devaraj, P. Kumari, C. Aarti, A. Renganathan, *J. Nanotechnol.* 2013, 2013, 598328.

[23] T. Elavazhagan, K.D. Arunachalam, *I. J. Nanomedicine* 2011, 6, 1265.

[24] H. R. Humud, A. K. Abass, Z. Wheeb, *Asian J. Appl. Sci. Eng.* 2014, 3, 25.

[25] S. Bhatt, J. Pulpytel, S. Mori, M. Mirshahi, F. Arefi-Khonsari, *Plasma Process. Polym.* 2013, 11, 24.

- [26] N. D. Boscher, F. Hilt, D. Duday, G. Frache, T. Fouquet, P. Choquet, *Plasma Process. Polym.* 2015, 12, 66.
- [27] S. W. Gaarenstroom, N. Winograd, *J. Chem. Phys.* 1977, 67, 3500.
- [28] D. Briggs, M. P. Seah, *Practical Surface Analysis*, 2nd edition, John Wiley & Sons, New York 1992.
- [29] C. D. Wagner, W. M. Riggs, L. E. Davis, J. F. Moulder, G. E. Muilenberg, in *Handbook of X-Ray Photoelectron Spectroscopy*, Perkin-Elmer Corporation, Physical Electronics Division, Eden Prairie, MN 1979.
- [30] N. K. Vu, A. Zille, F. R. Oliveira, N. Carneiro, A. P. Souto, *Plasma Process. Polym.* 2013, 10, 285.
- [31] A. Sadeghnejad, A. Aroujalian, A. Raisi, S. Fazel, *Surf. Coating Tech.* 2014, 14, S0257.
- [32] C. Damm, H. Munstedt, *Appl. Phys. A* 2008, 91, 479.
- [33] X. Deng, A. Y. Nikiforov, T. Coenye, P. Cools, G. Aziz, R. Morent, N. De Geyter, C. Leys, *Sci. Rep.* 2015, 5, 10138.

CHAPTER 7

NON-EQUILIBRIUM ATMOSPHERIC PRESSURE PLASMA FOR CROSSLINKING OF BIOPOLYMERS

7.1 Introduction

Many crosslinking methods have been investigated to physically crosslink biopolymers, avoiding the use of chemical agents, and the fundamentals studies so far performed have greatly contributed to the understanding of the phenomenon. However, more effective technologies are demanded, since all the presented processes turn out to be very high time consuming and the final results are strongly dependent on the kind of biopolymers subjected to the process as well as to the characteristics of the environment in which the process is performed.

In this chapter, the research, carried out during my Ph.D activities and aimed at demonstrating the effectiveness of CAP in inducing crosslinking directly in the solid state, are reported and the obtained results are discussed. Wider descriptions of the studies carried out can be found in the two scientific works written on this topic [1, 2].

Briefly, the effectiveness of a CAP, generated by a dielectric barrier discharge (DBD) and operated in air, in successfully crosslinking water soluble pullulan, gelatin and genipin containing gelatin electrospun fibres was investigated. After being exposed to plasma, the fibres showed a remarkable capability to preserve structural stability and fibre morphology upon water exposure. For the pullulan mats, the gel fraction and the water absorption were quantified to evaluate the crosslinking efficiency of different plasma operating conditions, and ATR-FTIR characterization provided some insights into plasma-induced modification of pullulan chemical structure. For the gelatin and genipin containing gelatin mats, the mechanical properties were also evaluated, observing that mats preserved their morphology and stability upon solution contact, and displayed improved mechanical properties. Further stabilization was obtained through immersion in Phosphate Buffer Solution, due to the promoting action of the buffer both on genipin crosslinking reaction, which involves ϵ -amino groups, and on plasma induced crosslinks, most likely related to reactive species generated by plasma.

The results, reported in this chapter and thoroughly presented in the scientific papers [1, 2] were obtained by the IAP Group led by Prof. Colombo in collaboration with the groups led by Prof. Maria Letizia Focarete and Prof. Adrian Bigi, from the Department of Chemistry 'G. Ciamician', Alma Mater Studiorum - Università di Bologna.

7.2 Experimental part

In this session, the methods to fabricate electrospun mats, the non-equilibrium plasma source and the protocols adopted to induce crosslinking, jointly with adopted characterization techniques and methods are reported.

7.2.1 Fabrication of pullulan electrospun mats

Pullulan ($\eta = 15.0 \div 180.0$ mPa s, 10% in H₂O at 30°C) was purchased by TCI Europe. Pullulan solution for electrospinning was obtained by dissolving the polymer in MilliQ water at a concentration of 17% w/v. The solution was magnetically stirred at room temperature (RT) until complete polymer dissolution, in order to obtain a homogenous solution before electrospinning. The in-house built electrospinning apparatus was composed of a high voltage power supply, a glass syringe, a stainless-steel blunt-ended needle (inner diameter 0.84 mm) connected with the power supply and a grounded collecting plate. The polymeric solution was dispensed through a teflon tube to the needle, which was placed vertically on the collecting plate. The following electrospinning processing conditions were used: applied voltage = 19 kV, needle to collector distance = 20 cm, flow rate = 0.9 mL/h. The process was conducted at RT and relative humidity RH = 40 ± 5% and the meshes were kept under vacuum over P₂O₅ at RT overnight in order to remove residual solvent.

7.2.2 Fabrication of gelatin and genipin containing gelatin electrospun mats

The electrospinning apparatus, made in house, is composed of a high voltage power supply, a glass syringe, a stainless steel coaxial needle connected to the power supply electrode and a grounded aluminum collector (10 cm x 10 cm). The coaxial needle used in the present work enables to introduce a given amount of genipin in the fibres avoiding gelatin gelling. In brief, it is constituted by an inner needle (O.D.= 0.9 mm, I.D.= 0.6 mm) positioned concentrically to the outer needle (O.D.= 1.5 mm, I.D.= 1.2 mm). The tip of the outer needle protruded 10 cm below that of the inner needle. In addition, the tip of the inner needle wall presents twenty little holes of 0.5 mm in diameter organized in four lines distributed along the needle circumference. Each line contains five little holes 2 mm apart from each other. The solutions were individually dispensed at a controlled flow rate by using the syringe pumps through a Teflon tube to the outer and inner needles. The flow rate of the shell solution was set at 0.18 ml/h while that of the core solution was 0,09 ml/h. The coaxial needle was placed vertically to the collecting plate at a distance of 15 cm and the applied voltage was set at 21 kV. The shell solution was prepared by dissolving gelatin in AcAc:H₂O (60:40 V/V) at a concentration of 30% (w/V). To fabricate gelatin mats containing 18 % (w/w) of genipin (labeled GG), the core solution was prepared by dissolving genipin at a concentration of 12% (w/V) in AcAc. A reference mat not containing genipin (labeled G) was prepared by using a stainless steel blunt-ended needle (inner diameter 0.84 mm) connected to the power supply electrode. Electrospun mats were kept under vacuum over P₂O₅ at room temperature (RT) overnight in order to remove residual solvents.

7.2.3 Non-equilibrium atmospheric pressure DBD and crosslinking protocols

Crosslinking of pullulan, gelatin and genipin containing gelatin electrospun non-woven meshes was carried out by means of a controlled atmosphere DBD plasma reactor working at atmospheric pressure in static air. The DBD plasma source consists of two parallel aluminium-plate electrodes; the upper electrode, having a surface of $15 \times 10 \text{ cm}^2$ and a thickness of 0.13 mm, is connected to the high voltage generator, while the lower electrode, with a surface of $15 \times 9 \text{ cm}^2$ and a thickness of 0.13 mm, is grounded. As dielectric, a POM-C plate, having a surface of $19 \times 15 \text{ cm}^2$ and a thickness of 2.4 mm, covers the upper electrode surface. A gap of 1 mm between the grounded electrode and the POM-C plate was used for all the performed plasma treatments. The plasma source is enclosed in a volume having size of $21 \times 17 \times 3 \text{ cm}^3$ (LxWxH). Specific gases and gas mixtures can be introduced from the top of the plasma reactor through a tube connected to the gas flow meter; a bleed port is placed on a side wall of the plasma reactor for bleeding out the air during the initial flushing of the system and for keeping a constant pressure inside the close volume during the process. The crosslinking processes here described were performed using environmental air as the plasma gas, therefore no flushing phase was performed at the beginning of the process and no air flux was introduced during operation.

To crosslink pullulan electrospun mats, the DBD plasma source was driven by a HV Amplifier connected to a function generator capable of producing square wave voltage signals with microsecond rise time. In order to evaluate the effect of electrical parameters and treatment time on the crosslinking degree of the electrospun pullulan meshes, several operating conditions were tested, varying treatment time from 5 to 15 min, peak voltage (PV) from 10.5 to 15 kV and pulse repetition frequency (RR) from 300 to 500 Hz. A square wave voltage signal with microsecond rise time was used during the experiments. A simplified representation of the square waveform, PV and RR is reported in Figure 1.

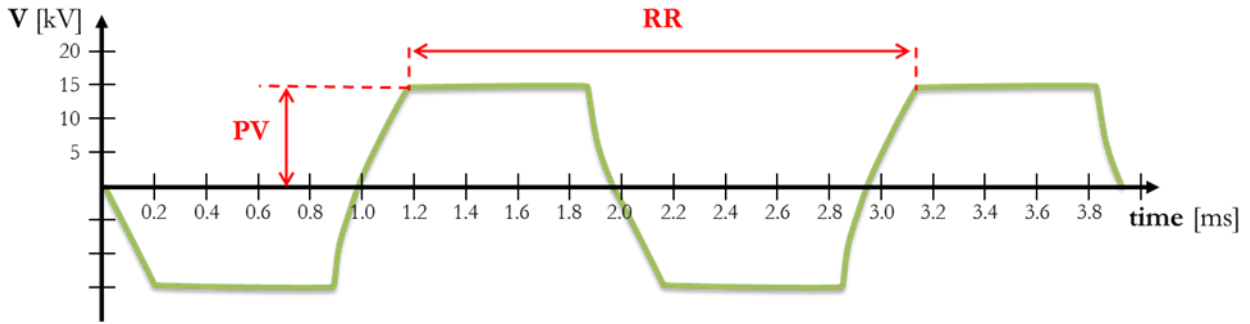


Figure 1. Simplified representation of PV and RR [1]

All the experimental operating conditions are reported in Table 1, together with the respective values of energy per pulse (E_p) and average dissipated power (P), calculated as follows:

$$E_p = \int_{\Delta t} V \cdot I dt$$

$$P = E_p \cdot RR$$

where V and I are the values of instant voltage and current, respectively, and Δt is the duration of a single pulse.

Table 1. Plasma operating conditions tested. Experiments were carried out in static air, using a square waveform with a $kv/\mu s$ rise rate and fixing the gap between the grounded electrode and the POM-C plate at 1 mm.

Treatment	RR (Hz)	PV (kV)	Treatment time (min)	E_p (mJ/pulse)	P (W)
T1	500	15	15	30	15
T2	500	15	10	30	15
T3	500	15	5	30	15
T4	500	10.5	15	16	8
T5	300	15	15	40	12
T6	300	10.5	15	14	4.2

The plasma generation was performed in static air with no introduction of additional gases inside the plasma reactor. The DBD plasma source was driven by a micropulsed generator, producing high voltage bursts (duration 7 ms) with a burst repetition frequency (BRF) of 125 Hz, during the bursts a 20 kHz sinusoidal waveform with 12 kV peak voltage is produced. In order to perform the plasma treatment on electrospun samples, mats were placed on the grounded electrode and directly subjected

to the plasma discharge. G samples were treated for different times (5, 10 and 20 minutes) and were labeled G_5, G_10 and G_20, accordingly, while GG samples were treated for 10 minutes (GG_10). After plasma discharge, parts of the treated samples were fixed to plastic rings and rinsed either in Double Distilled Water (DDW) or in Phosphate Buffer Solution (PBS) (pH 7.4 and Ionic Strength = 0.26M) for 20 seconds, in order to evaluate the effect of pH and Ionic Strength (I) on the morphological and structural stability of electrospun mats.

Depending on the soaking media, the samples were labelled either W (in the case of Double Distilled Water) or B (in the case of PBS). After immersion, mats were dried at RT. Samples differently treated were labelled as reported in Table 2.

Table 2. Labels of the samples before and after plasma treatment and immersion in DDW (W) or PBS (B). The numbers indicate the plasma treatment time (min).

As-spun samples	After plasma treatment	After soaking in PBS	After soaking in DDW
G	-	G_B	G_W
	G_5	G_5B	G_5W
	G_10	G_10B	G_10W
	G_20	G_20 B	G_20W
GG	-	GG_B	GG_W
	G_10	GG_10B	GG_10W

7.2.4 Characterization of pullulan crosslinked mats

The fibre morphology of the as-spun scaffolds and the one of scaffolds after the plasma exposure was analysed by using a Scanning Electron Microscope (SEM) at an accelerating voltage of 15 kV, on samples sputter-coated with gold. The distribution of fibre diameters was determined through the measurement of about 250 fibres by means of an acquisition and image analysis software and the results were given as the average diameter \pm standard deviation.

The infrared spectra of pullulan electrospun meshes were recorded by using a Agilent Cary 660 FT-IR spectrometer equipped with an attenuated total reflectance (ATR) sampling accessory. Spectra were acquired at RT in absorbance mode, from 4,000 to 400 cm^{-1} with a resolution of 2 cm^{-1} ; a total of 32 scans were recorded for each spectrum.

To evaluate the crosslinking degree, the gel fraction determination was carried out. Measurements were performed on square meshes (3x3 cm^2) having a thickness in the range of 30 \div 40 μm . After plasma treatment, each electrospun sample was dried overnight at 80°C under vacuum to constant

weight and immersed in deionized water for 24h at RT in a shaking bath; then, a washing step of 1h with fresh deionized water was performed. During water immersion, the sol fraction of pullulan is dissolved. The insoluble part (gel fraction) of each sample, retrieved from water, was dried overnight at 80°C under vacuum. The percentage gel fraction was calculated according to the following equation:

$$\text{Gel fraction(\%)} = \frac{W_f}{W_i} \cdot 100$$

where W_f is the final weight of the dried sample after the removal of the sol fraction and W_i is the initial weight of the dried sample after the plasma treatment. Three replicate specimens were run for each kind of plasma treatment and results were provided as average value \pm standard deviation (SD). The measurements of the water absorption were performed on square meshes ($3 \times 3 \text{ cm}^2$) having a thickness in the range of $30 \div 40 \text{ }\mu\text{m}$, previously immersed in deionized water for 24 h in order to remove the non-crosslinked sol fraction. The insoluble part (gel fraction) of each sample, retrieved from water, was dried overnight at 80°C under vacuum and weighted to constant weight. Each sample was then soaked in deionized water for 24h, by using a shaking bath at RT. The wet sample was gently blotted with a filter paper for few seconds to remove the excess of adsorbed water. Then, the wet sample was immediately weighted to avoid the effects of water evaporation. The percentage of water adsorption was calculated according to the following equation:

$$\text{Water Absorption (\%)} = \frac{W_w - W_d}{W_d} \cdot 100$$

Where W_d is the final weight of the dried sample after removal of the sol fraction and W_w is the weight of the wet sample. Three replicate specimens were run for each plasma treatment and results were provided as average value \pm standard deviation (SD).

7.2.5 Characterization of gelatin and genipin containing gelatin crosslinked mats

Morphological observations were carried out by SEM at an accelerating voltage of 15 kV, on samples sputter-coated with gold. The distribution of fibre diameters was determined through the measurement of about 200 fibres by means of an image acquisition and analysis and the results were given as the average diameter \pm standard deviation.

ATR-FTIR analysis of the electrospun mats was carried out using a spectrometer equipped with an ATR sampling device, using a diamond crystal as internal reflection element. Infrared spectra were acquired at room temperature in absorbance mode, from 3900 to 400 cm^{-1} with a resolution of 2 cm^{-1} ; a total of 32 scans were recorded for each spectrum.

The extent of crosslinking of gelatin mats was determined by a UV assay of uncrosslinked ϵ -amino groups before and after crosslinking treatment [3].

Electrospun samples of about 5 mg were incubated with 1 ml of a 4% (m/V) NaHCO_3 solution and 1 ml of TNBS solution at 0.5% (m/V) for 4 hours at 40°C . 3 ml of HCl 6 M were then added and the solution was maintained at 110°C for 24 hours. The absorbance of the diluted solution was measured at 346 nm in a Kontron Uvikon 931 spectrophotometer against a blank. The equation relating to the solution absorbance and moles of ϵ -amino groups per gram of gelatin is here reported:

$$\frac{\text{moles } \epsilon \text{ amino groups}}{\text{g}} = 2 \cdot \frac{A \cdot 0.02}{1.46 \cdot 10^4 \cdot bx}$$

where A is the measured absorbance, 0.02 l is the volume of the analysed solution, 1.46×10^4 ($\text{l} \times \text{mol}^{-1} \times \text{cm}^{-1}$) is the molar absorptivity of TNP-lys, b is the cell path length in cm, and x is the mat weight in g. The crosslinking degree is the ratio between the moles of free ϵ -amino groups in crosslinked gelatin and the moles of ϵ -amino groups in uncrosslinked gelatin.

Stress–strain curves of as-spun mats and of mats 24 h after the plasma treatment (specimen dimension: 5x20 mm, thickness measured by microcaliper) were recorded using an Instron Testing Machine 4465, with a cross-head speed of 1 mm min^{-1} , and the Series IX software package.

Samples were tested in a dry state: the Young's modulus (E), the strain at break (ϵ_b) and the stress at break (σ_b) of the strips were measured.

7.3 Results and Discussion

7.3.1 Crosslinking of pullulan electrospun mats

In order to evaluate the effect of electrical parameters and treatment time on the crosslinking degree of pullulan fibres, plasma treatment was performed for a wide range of operating conditions, reported in Table 1. Initially, the peak voltage (PV) and the pulse repetition frequency (RR) were fixed at 15 kV and 500 Hz, respectively, while the treatment time was varied. Then, for a given treatment time of 15 min, PV and RR parameters were changed independently (Table 1).

No significant variation in fibre morphology and fibre diameter was observed after all the performed treatments (Figure 2), indicating that no relevant damage or change of structure was induced by plasma.

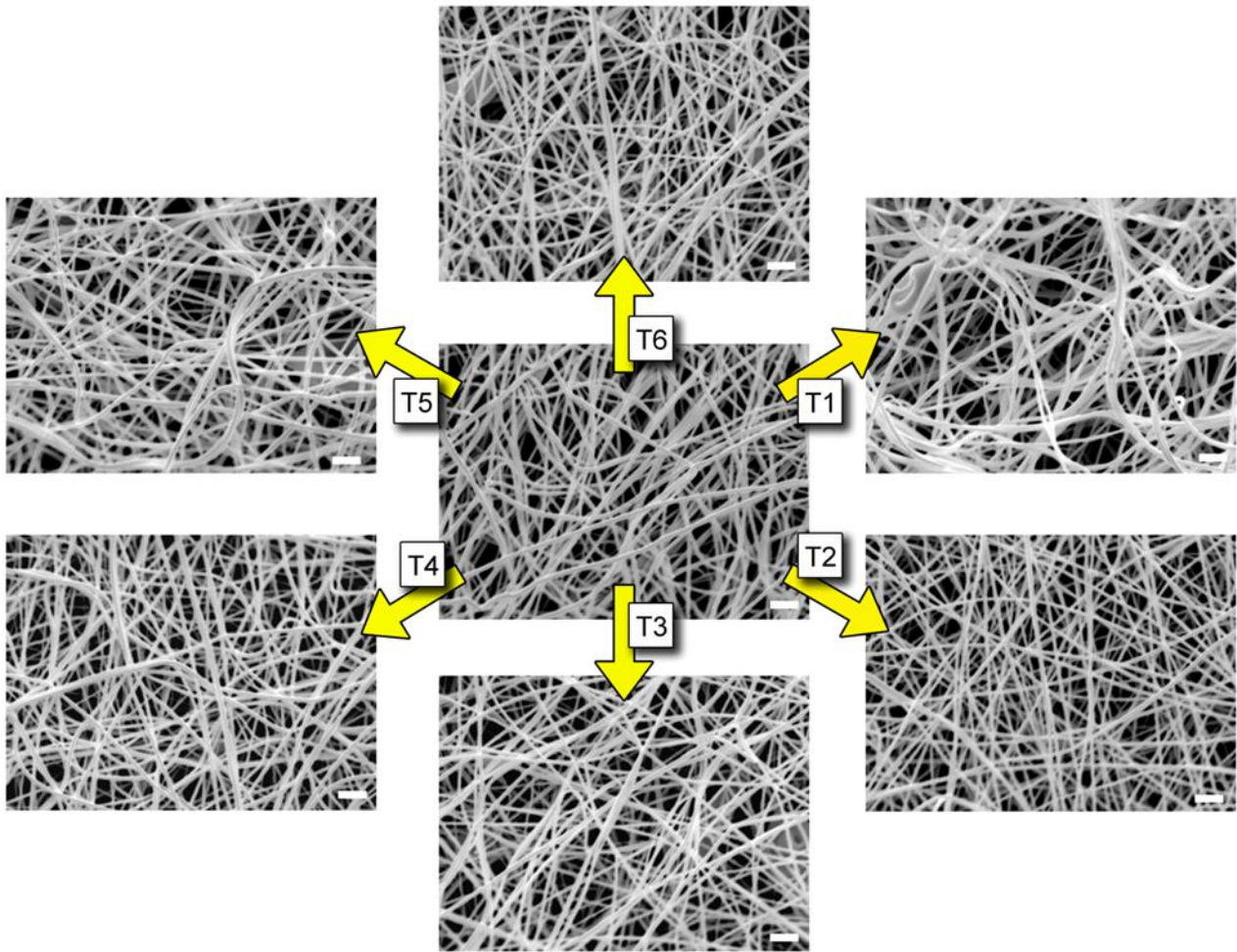


Figure 2. SEM micrographs of as-spun pullulan mesh (centre of the figure) and of pullulan meshes after the different plasma treatments, as indicated by the arrows [1].

As a first indication of the efficiency of the plasma induced crosslinking, the plasma-treated mats were immersed in water for 24 h in order to evaluate their capability to preserve both the structural stability and the fibre morphology upon water exposure. Figure 3 shows the pictures of the plasma-treated samples immersed in water, together with the SEM micrographs of the corresponding dried samples. As clearly depicted, mats showed a reduced structural and morphological stability with decreasing the treatment time from 15 to 5 min. In fact, while the treatments T1 and T2 allowed the mat to maintain a good and well-defined fibrous structure and a high porosity, after treatment T3 and water immersion the sample completely lost its original morphology and appeared as a continuous transparent film. Similar results were obtained with the treatment T6 when the lowest electrical parameters were used ($PV=10.5$ kV and $RR=300$ Hz). On the contrary, after the treatments T4 and T5, both the fibrous morphology and the sample integrity were retained. These results highlight that, in the right operating conditions, the plasma-mediated crosslinking approach enables to retain almost completely the fibrous structure of the constructs.

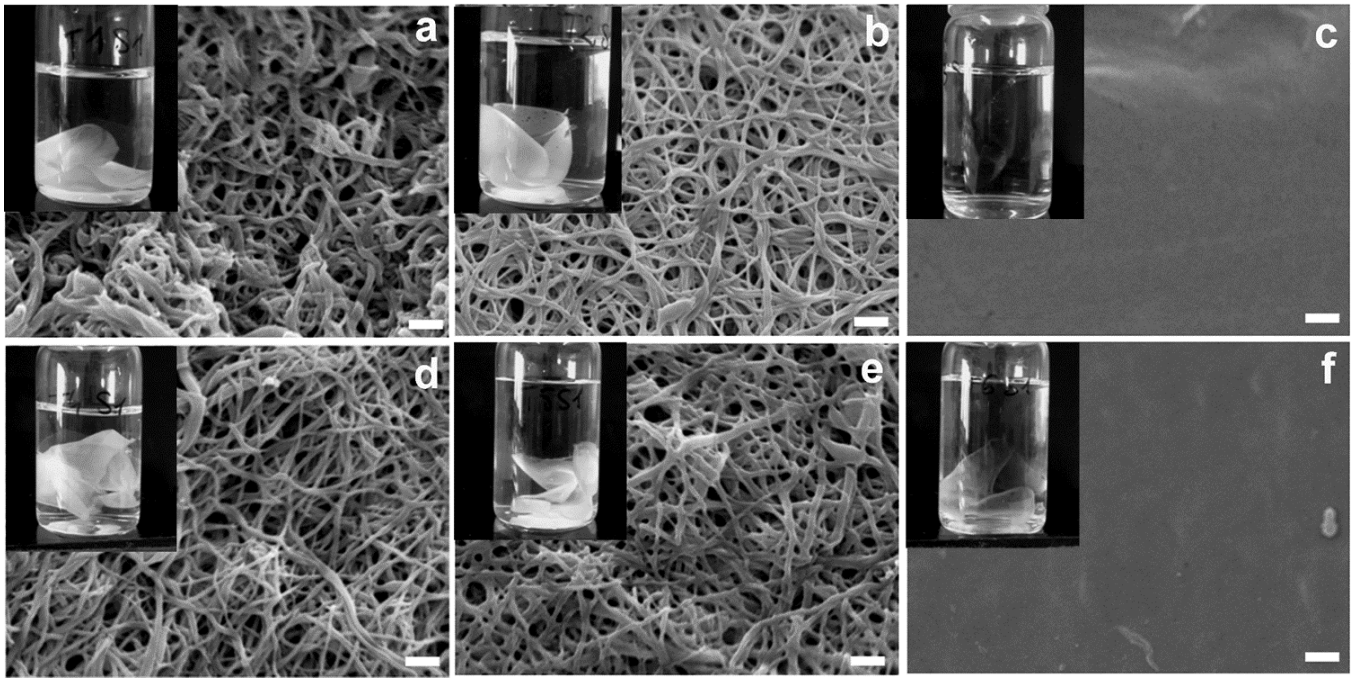


Figure 3. SEM micrographs of plasma treated pullulan electrospun mats after 24 h of water immersion. Insets: Images of plasma-treated samples soaked in water: (a) T1, (b) T2, (c) T3, (d) T4, (e) T5, and (f) T6. Scale bar: 2 mm [1].

In order to quantitatively assess the crosslinking efficiency of the different plasma treatments, the gel fraction and the water absorption were evaluated and the results are shown in Figure 4a and b, respectively. The gel fraction is related to the insoluble part of the sample, contrary to the sol fraction that is dissolved during water immersion, and it represents a measure of the crosslinking degree. As shown in Figure 4a, samples after the treatments T3 and T6 were highly water soluble, in agreement with the morphological observations reported in Figure 3c and f. Conversely, a greater water stability quantified by a higher value of the gel fraction ($>60\%$) was obtained for the pullulan mats after the treatments T1, T2, T4, and T5, which allowed mats to completely retain their fibrous structure.

These results were confirmed by the water absorption measurements (Figure 4b). Water absorption was very low when high crosslinking was achieved (i.e., for the optimized operating conditions T1, T2, T4, and T5) and it assumed higher values in the case of low crosslinking (i.e., for the treatments T3 and T6).

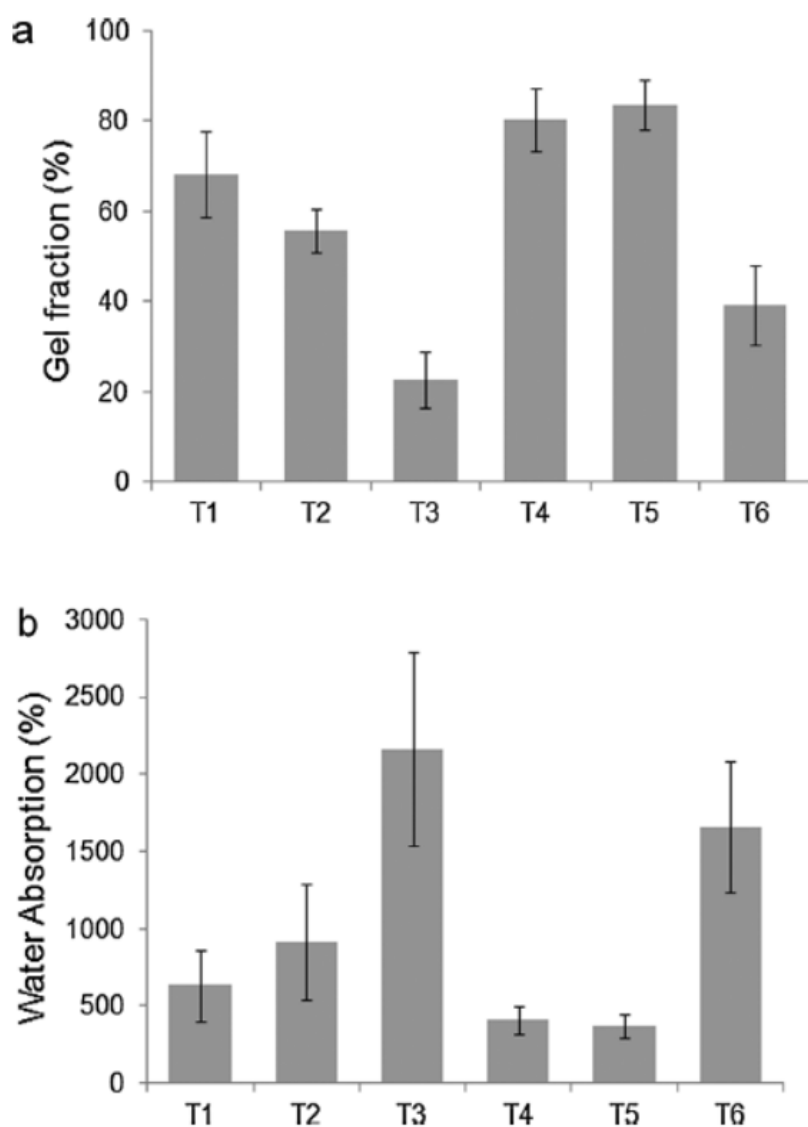


Figure 4. Gel fraction (%) (a) and water absorption (%) (b) of plasma-treated electrospun pullulan samples [1].

Attenuated total reflectance fourier transform infrared spectroscopy (ATR-FTIR) characterization, performed on selected samples (Figure 5), showed that in the chemical structure of the plasma treated samples, a new band appeared around 1700 cm^{-1} attributed to carbonyl and carboxylic moieties, that was absent in the pristine pullulan mat, whose intensity increased in line with the crosslinking efficiency of the plasma treatments ($T5 > T6 > T3$). Concomitantly, a parallel decrease of the broad band of hydroxyl groups (at $3200\text{--}3500\text{ cm}^{-1}$) was observed.

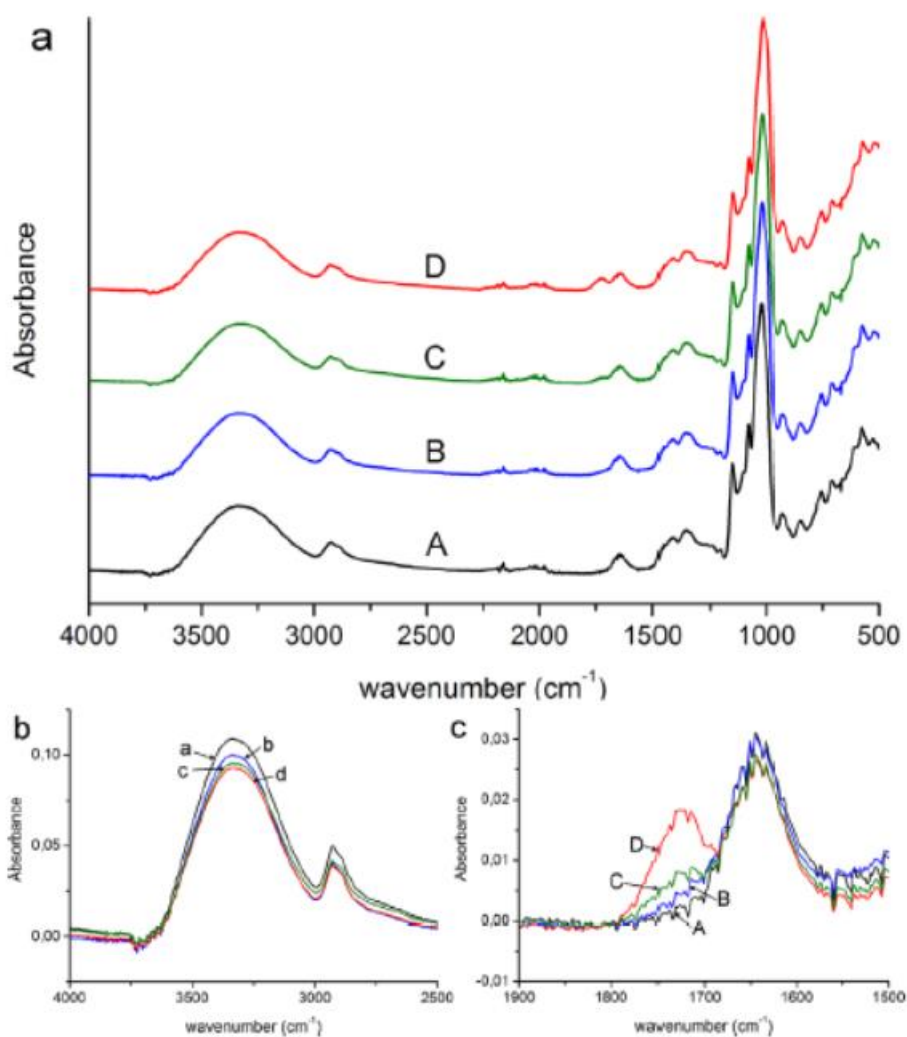


Figure 5. (a) ATR-FTIR spectra of pristine pullulan sample (A) and of sample after treatments T3 (B), T6 (C), and T5 (D). (b) and (c) enlargements of the two spectral regions of interest [1].

It is well known that plasma reactive species, such as electrons, ions, uncharged particles (metastables, neutral species, radicals), excited species, as well as ultraviolet photons, possess sufficient energy to induce scission of chemical bonds involved in organic structures, as well as dehydrogenation and oxidation reactions [4]. Moreover, the recombination of the reactive free radicals and new functional groups formed in the polymeric chains are recognized to generate highly crosslinked polymer chains. On the basis of very recent literature results on chitosan solution gelation by plasma [5], plasma treatment of pullulan macromolecules performed in air can be hypothesized to result in a complex series of reactions such as cleavage of the glycosidic bonds, as well as oxygenation of the glucopyranose ring and the dehydrogenation of primary hydroxyl ring groups, followed by a number of rearrangement reactions. The oxidation process, that can occur concomitantly with the cleavage of the glycosidic linkage, and that could also be due to post-treatment oxidation, might be

invoked in the formation of carbonyl and carboxylic groups observed in the ATR-FTIR spectra, which might crosslink inter- or intramolecularly with hydroxyl groups.

7.3.2 Crosslinking of gelatin and genipin containing gelatin electrospun mats

SEM images of as-spun G mats, shown in Figure 1a, display defect free and regular fibres. Figure 6d, g, j reports SEM images of G mats exposed to plasma for 5, 10 and 20 minutes, respectively. The images highlight that plasma does not provoke any appreciable alteration to the fibre morphology and diameter (Mean value = 320 ± 40 micron), independently from the adopted treatment time. In order to evaluate the capability of plasma treated mats of preserving fibre morphology upon liquid contact, immediately after plasma treatment G samples were fixed to plastic rings and rinsed in aqueous solution (DDW or PBS) for 20s. As shown in Figure 6b and 6c, the as-spun G mats dissolved immediately after immersion in DDW or in PBS, while plasma treated G mats better resisted to dissolution when the proper treatment time was selected.

In particular, it emerges that, by keeping constant the plasma operating parameters, the longer the treatment time the higher the water stability and fibre morphology preservation (compare Figure 6e, 6h and 6k and Figure 6f, 6i and 6l). This finding is in agreement with previous results obtained on plasma treated electrospun polysaccharides and demonstrates that there is a correlation between plasma treatment time and the extent of crosslinking degree.

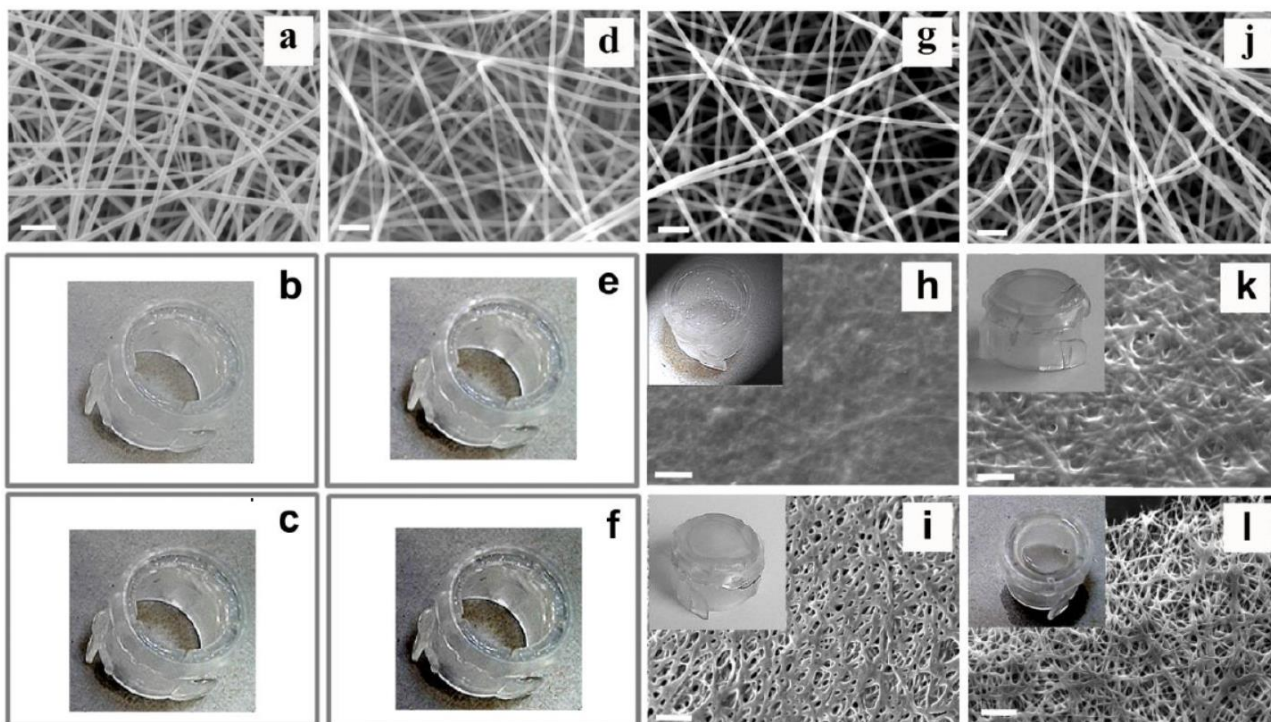


Figure 6. SEM images and pictures of gelatin as-spun mats, gelatin mats after plasma treatment and after immersion either in DDW (labelled W) or PBS (labelled B). a) as-spun G; b) G_W; c) G_B; d) G_5; e) G_5W; f) G_5B; g) G_10; h) G_10W; i) G_10B; j) G_20; k) G_20W; l) G_20B. Scale bars: a, d, g, j = 2 μm ; h, i, k, l = 5 μm [2].

In detail, 5 minutes plasma treated G mats (G_5) do not exhibit any relevant increased stability, being immediately dissolved when in contact with water (Figure 6e and 6f). Conversely, a treatment time of 10 min improves G mats stability and avoids its dissolution (Figure 6h and 6i) even if the fibrous structure is lost and the porous mat turned into a continuous film when immersed in DDW, whereas after soaking in PBS the porous structure is partially maintained. The increase of treatment time up to 20 min provides an improvement in mat stability and retention of fibre morphology after immersion in both DDW and PBS (Figure 6k and 6l), with a better preservation of the nanofibrous structure in PBS than in DDW.

In order to improve the stabilization of as electrospun mats, the natural crosslinker genipin was introduced in gelatin fibres during electrospinning. SEM images of electrospun GG mats before and after 10 min of plasma treatment are reported in Figure 7a and 7b, respectively. As for G samples, plasma treatment does not influence the morphology of the fibres, which exhibit a mean diameter of 355 ± 55 micron, not significantly different from that of G samples. In absence of plasma treatment, the genipin does not prevent the GG mats solubilization after immersion either in DDW or PBS, as shown in Figure 7b and 7c, respectively. On the contrary, when GG sample is subjected to plasma treatment for 10 minutes and then immediately soaked in PBS, the fibrous morphology is highly

preserved (see Figure 7f). It is worth noting that the presence of genipin in the fibres has a relevant role in maintaining the fibrous morphology, as shown by the reduced time of plasma treatment necessary to stabilize genipin containing mats. From these results, it can be deduced that plasma treatment activates genipin crosslinking of gelatin. Indeed, by comparing the SEM images of G_10B and GG_10B samples (Figure 7i and 7f) it emerges that the latter is more stable against water dissolution and swelling, being the fibrous morphology better retained.

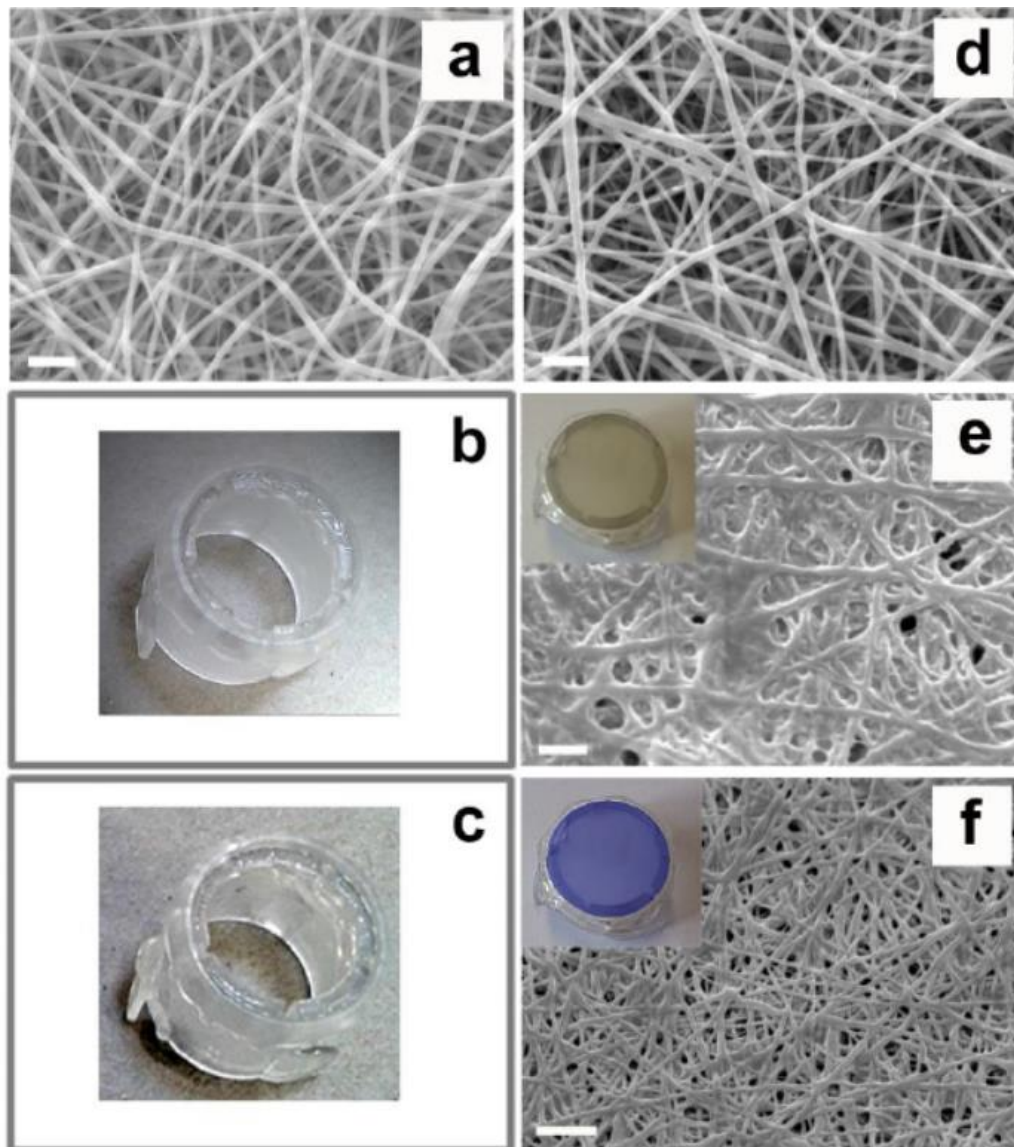


Figure 7. SEM images and pictures of genipin containing gelatin as-spun mats, genipin containing gelatin mats after plasma treatment and after immersion either in DDW (labelled W) or PBS (labelled B). a) as-spun GG; b) GG_W; c) GG_B; d) GG_10; e) GG_10W; f) GG_10B. Scale bars: a, d, e = 2 μm ; f = 5 μm [2].

Considering the above described results, further characterizations were carried out only on those samples that were better stabilized against dissolution after plasma treatment, i.e. on electrospun G and GG mats submitted to plasma treatment for 20 and 10 minutes, respectively.

The mechanical behaviour of as-spun G and GG samples was evaluated by tensile stress-strain measurements and compared with that of G_20 and GG_10 samples with the aim to investigate the effect of plasma treatment on sample mechanical properties (Figure 8). Table 3 reports the values of Young's Modulus, stress at break and strain at break obtained for the considered samples: the comparison between the mechanical behaviors of as-spun G and GG mats suggests that the presence of genipin does not have any remarkable effect on the mechanical parameters of the sample. The data also indicate that plasma treatment induces a slight increase of the elastic modulus (E) and of the stress at break (σ_b), associated with a significant reduction of the deformation at break (ϵ_b), for both the considered types of samples. In light of these results, the effects of plasma treatment on the mechanical properties of the mats turn out to be quite similar to the ones induced by the chemical crosslinking, which has been reported to increase mats rigidity [3].

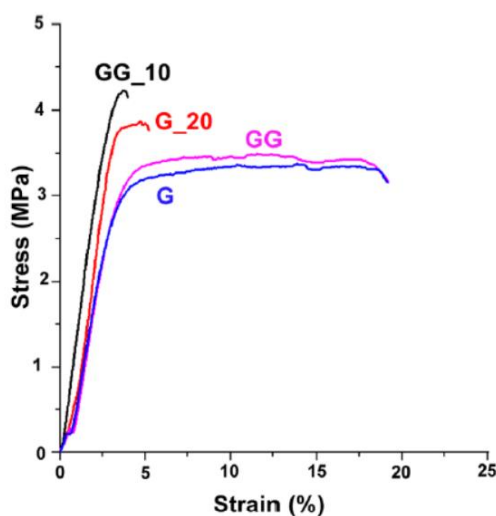


Figure 8. Typical stress-strain curves recorded from as-spun G and GG mats and from G_20 and GG_10 samples [2].

Table 3. Young's modulus, E, stress at break, σ_b , and strain at break, ϵ_b , of sample G and GG before and after plasma treatment.

Sample	E (MPa)	σ_b (MPa)	ϵ_b (%)
G	120±30	2.5±0.4	20±3
G_20	140±10	3.1±0.3	6±1
GG	120±20	3.1±0.4	18±4
GG_10	160±20	3.8±0.6	6±2

The extent of crosslinking of G and GG samples was determined for as-spun mats, for mats subjected to the plasma exposure and for the ones immersed in PBS after the plasma treatment, by using a method based on the evaluation of the moles of unreacted ϵ -amino groups per gram according to equation reported in the experimental part. The obtained values are reported in Table 4.

Table 4: Extent of crosslinking, expressed as percent of free ϵ -amino groups lost after crosslinking.

Sample	Extent of crosslinking (%)
G	0
GG	0
G_20	0
G_20B	61±4
GG_10	36±4
GG_10B	100±6

As expected considering the results of mat stability in water, as-spun G mat is not crosslinked and the simple addition of genipin within the fibres does not induce the formation of appreciable crosslinking bonds. This finding accounts for the similar mechanical behavior of G and GG mats and it is justified by the absence of chemical reaction between gelatin and genipin as a consequence of the relatively short time of contact during the electrospinning process. However, after plasma treatment, GG mats exhibited a 36% of crosslinking degree. This result is quite amazing, since it indicates that plasma is effective in initiating in the solid state crosslinking reactions that involve free ϵ -amino groups as those conventionally induced in the liquid phase by genipin.

On the contrary, G_20 mats did not present any evaluable decrease of ϵ -amino groups with respect to as-electrospun G mats. However, their stability in solution and mechanical properties turned out to be quite similar to those of plasma treated GG samples likely due to the fact that plasma treatment induces the formation of reactive groups able to create physical and/or chemical crosslinks that contribute to gelatin stabilization without involving ϵ -amino groups.

Moreover, immersion in PBS was demonstrated to have a great influence on the stabilization and on the enhancement of crosslinking degree. In fact, only 20 s of immersion in PBS were enough to increase the extent of crosslinking of GG_10 mats from 36% up to 100%. This result is in agreement with the reported positive contribution of PBS to the crosslinking reaction of genipin [6], which displays its maximum crosslinking activity at pH 7.4 [7]. However, also G_20 samples experienced a significant decrease of ϵ -amino groups after soaking in PBS, which yielded an increase of

crosslinking degree from 0% to 61%, suggesting that PBS promoted the formation of covalent bonds involving reactive groups originated by plasma treatment and ϵ -amino groups.

To elucidate the mechanisms of the plasma-induced crosslinking of gelatin nanofibres is not a simple issue, especially considering that there are few papers reporting of the application of plasma to a gelatin based material [8, 9]. Moreover, these studies used low pressure plasma and did not succeed in obtaining highly stabilized gelatin samples. Concerning our case, it is supposed that many of the active components of the air plasma are involved in the crosslinking of gelatin in the solid state. For instance, it has been demonstrated that the UV radiation induces the formation of radicals at specific residues in collagen (gelatin), leading to the scission and cross-linking of molecules [10]. Another reaction might be due to the increased number of crosslinking junctions through hydrogen bonding induced by hydroxyl compounds generated in gelatin by plasma treatment, as previously found by Fijitsu *et al.* [11] in gelatin gels. A further possibility is that the reaction mechanisms involve reactive species affected by H^+ concentration [12], which could account for the increased stabilization induced by PBS.

In order to evaluate if plasma treatment induced some structural changes on gelatin-based mats, we collected infrared spectra on samples G, G_20, GG and GG_10. Infrared spectra of as-spun materials, shown in Figure 9, presented some absorption bands corresponding to Amide I, II and III, as described elsewhere [3]. After plasma treatment, an increase of intensity has been detected between 1200 and 1500 cm^{-1} . Since C-O stretching and N-H bending vibrations of Amide III fall in this range, the increase of intensity might support the hypothesis of formation of H bonds among the reactive species created by plasma treatment.

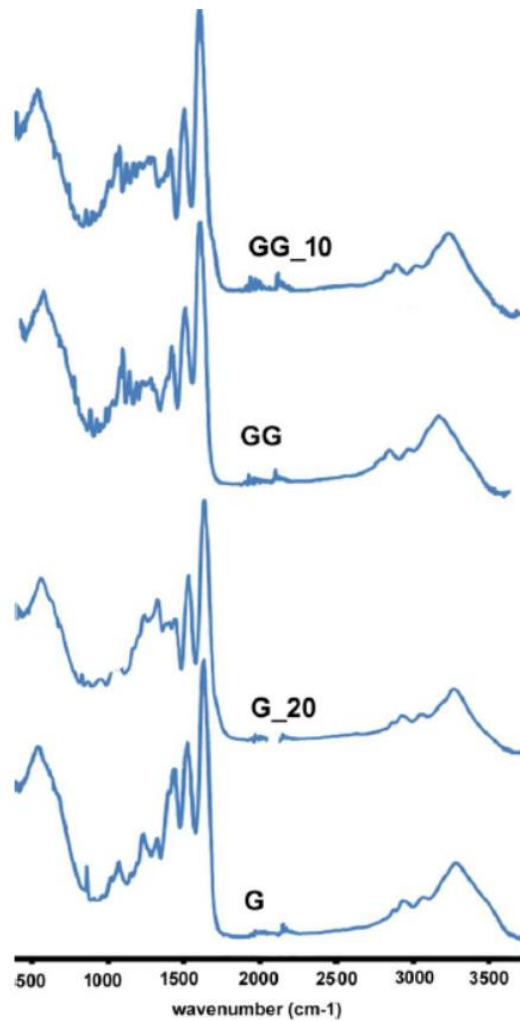


Figure 9. FTIR absorption spectra collected on samples G, G_20, GG and GG_10 [2].

Plasma treated polymeric materials and solutions are well-known to undergo a recovery of their chemical characteristics over storage time, probably due to a post-plasma oxidation processes caused by the radicals still present on the material surface or to the polymer chain rearrangements from the surface into the bulk of the materials [13, 14].

The effect of the ageing on plasma-treated electrospun mats was tested by dipping the samples in PBS after 15 days from their exposure to plasma. After few minutes of immersion, the samples were dried at RT and their morphology observed at SEM. The images recorded on the mats surfaces are shown in Figure 10a and 10b, respectively: it was evident that soaking GG_10 and G_20 in PBS 15 days after plasma treatment caused partial solubilization and loss of the nanofibrous morphology. On the other hand, the nanofibrous structure of samples GG_10B and G_20B was absolutely maintained (Figure 10c and 10d). The better retention of fibrous morphology with time shown by GG_10B and G_20B with respect to GG_10 and G_20, confirms that the immersion in PBS stabilizing solution immediately after plasma treatment turns out to be mandatory to prevent the loss of stability over

time. The chemical/physical interactions between the polymeric chains of the plasma-treated samples and the solution, which contribute to the gelatin structural stability, are probably due to the radicals and active sites generated by plasma in the polymeric chains of the mats during the treatment. The plasma-generated radicals and active sites can recombine with aging, which justifies the poor retention of fibre morphology observed for GG_10 and G_20. Conversely, PBS immersion stabilizes these interactions and prevent the recombination of the plasma-generated radicals and active sites over time.

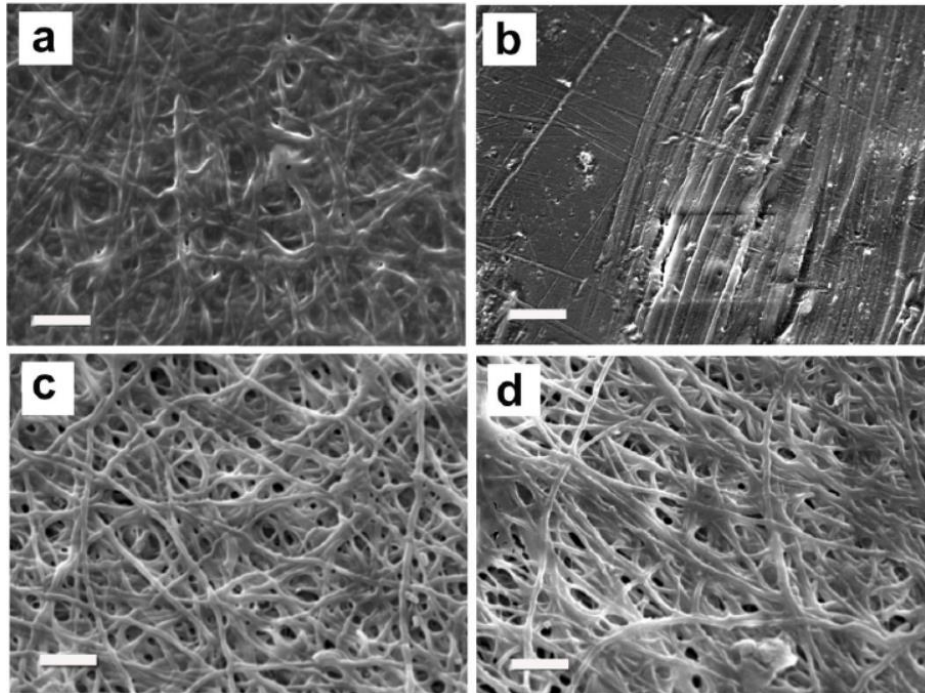


Figure 10. a) GG_10 and b) G_20 both immersed in PBS 15 days after plasma exposure; c) GG_10B and d) G_20B re-immersed in PBS 15 days after their preparation. Scale bars: a-d = 5 μ m [2].

7.4 Conclusions

The achieved results show that CAP treatment can successfully induce the crosslinking of pullulan, gelatin and genipin containing gelatin electrospun mats, directly in the solid state. The proposed method to crosslink water soluble biopolymer in the solid state definitely simplifies the crosslinking procedure, limits the use of solvents and chemicals, decreases the operational time and eases the scale-up of the method.

Interestingly, the studies carried out to crosslink gelatin mats highlight that 20 s soaking in PBS, performed immediately after plasma exposure, further stabilizes the mats and provides highly crosslinked materials that retain their stability over time.

References

- [1] A. Liguori, L. Paltrinieri, A. Stancampiano, C. Gualandi, M. Gherardi, V. Colombo, M. L. Focarete, “Solid-State Crosslinking of Polysaccharide Electrospun Fibers by Atmospheric Pressure Non-Equilibrium Plasma: A Novel Straightforward Approach”, *Plasma Process. Polym.* 2015, 12, 1195, Copyright Wiley-VCH Verlag GmbH & Co. KGaA. Reproduced with permission.
- [2] A. Liguori, A. Bigi, V. Colombo, M. L. Focarete, M. Gherardi, C. Gualandi, M. Oleari, S. Panzavolta, “Atmospheric Pressure Non-Equilibrium Plasma As A Green Tool To Crosslink Gelatin Nanofibres”, to be submitted.
- [3] S. Panzavolta, M. Gioffrè, M. L. Focarete, C. Gualandi, L. Foroni, A. Bigi, *Acta Biomater.* 2011, 1702.
- [4] T. Desmet, R. Morent, N. De Geyter, C. Leys, E. Schacht, P. Dubruel, *Biomacromolecules*, 2009, 10, 2351.
- [5] R. Molina, P. Jovancic, S. Vilchez, T. Tzanov, C. Solans, *Carbohydr. Polym.* 2014, 103, 472.
- [6] L. Solorio, C. Zwolinski, A. W. Lund, M. J. Farrell, J. P. Stegemann, *J Tissue Eng Regen Med.* 2010, 514.
- [7] M. T. Nickerson, J. Patel, D. V. Heyd, D. Rousseau, A. T. Paulson, *Int. J. Biol. Macromol.* 2006, 39, 298.
- [8] J. Ratanavaraporn, R. Rangkupan, R. Jeeratawatchai, S. Kanokpanonta, S. Damrongsakkula, *Int. J. Biol. Macromol.* 2010, 47, 431.
- [9] K. Sisson, C. Zhang, M. C. Farach-Carson, D. B. Chase, J. F. Rabolt, *Biomacromolecules* 2009, 10, 7.
- [10] R. S. G. da Silva, L. A. A. Pinto, *Food Eng Rev* 2012, 4, 165.
- [11] M. Fujitsu, M. Hattori, T. Tamura, *Colloid. Polym. Sci.* 1997, 275, 67.
- [12] Y. Li, G. Friedman, A. Fridman, H. F. Ji, *Clinical Plasma Med.* 2014, 2, 56.
- [13] L. S. Dolci, S. D. Quiroga, M. Gherardi, R. Laurita, A. Liguori, P. Sanibondi, A. Fiorani, L. Calzà, V. Colombo, M. L. Focarete, *Plasma Process. Polym* 2014, 11, 203.
- [14] C. M. Chan, T. M. Ko, H. Hiraoka, *Surface Sci. Rep.* 1996, 24, 1.

Part II

CHAPTER 8

CONVENTIONAL METHODS FOR THE SYNTHESIS OF NANOPARTICLES

8.1 Introduction

In order to get some insights on the suitability and the possible application fields of CAP technology for the production of nanoparticles in liquid environment, with respect to the already optimized methods, in the present chapter, a quick overview of the conventional methods for nanoparticles synthesis is reported.

The term nanoparticles refers to a broad family of nanomaterials characterized by a diameter less than 100 nm. These powders are particularly interesting since in the size range from the atomic level to around 100 nm materials may have different properties compared to bulk materials, mainly due to the increased volume specific surface area and the role played by quantum effects. Indeed, as the size decreases, the proportion of atoms at the surface of the material increases, leading to a greater surface area per unit mass. As the size decreases, quantum effects increasingly affect the properties of matter, determining optical, electrical and magnetic behaviour of materials. Depending on their size and material, nanoparticles have a wide range of potential applications, from catalysts to sunscreen creams, from batteries to nanomedicine; moreover, their size confers them ideal characteristics for applications in electronics and as composite additives.

Many processes have been developed for the production of nanoparticles, allowing accurate control of particle size, shape, crystallinity and surface composition. The usual classification divides these processes in top-down techniques, where nanoparticles are produced by progressively reducing the size of the raw material, and bottom-up techniques, where particles are assembled from smaller building blocks (atoms or molecules). A second classification may be done, based on the phase in which the process is carried out; while top-down processes are inherently solid-phase (milling, ablation, etc), bottom-up techniques may be either liquid-phase (co-precipitation, sonochemical reaction) or gas phase (flame and plasma synthesis). Typically, solid-phase and gas-phase processes are of great industrial interest for their higher productivity or higher purity, or both, with respect to liquid-phase processes; indeed, the latter have limited purity and require post-processing, but, in some cases, they are the only route available for the production of highly specific and tailored nanoparticles [1].

8.2 Top-down processes

The most important top-down processes, in terms of industrial impact, are ball milling, spark erosion and laser ablation [1].

During ball-milling the starting material is fractured by mechanical collision and friction in a ball mill [2, 3]. This process, especially attractive for the manufacture of thermoelectric materials [4,5], is characterized by high production rates, but, due to the equilibrium between the particles destruction and the aggregation forces, the minimum particles dimension is rather high, lying in the range 10-300 nm, in relation to the starting material. [6,7]. Furthermore, nanoparticle purity is limited due to oxygen inclusions, as well as of the material eroded from the milling device [8].

The process of spark erosion consists in the ignition of a spark between two electrodes, composed of the material to be vaporized due to the high temperatures reached in the discharge (around 20000 K [9]); the small amount of evaporated material nucleates and forms nanoparticles [10,11]. This method can be used to produce nanoparticles made of any conductive material, but is characterized by low productivity.

In the laser ablation, the base material is rapidly heated by a pulsed laser, thus micrometric and nanometric fragments are ablated from the substrate, as well as ions and molecules [12-14]. Due to the adopted operating parameters, the material is not directly vaporized, enabling the production of nanoparticles from materials that would otherwise decompose (mainly semiconductors and oxides); moreover, controlling the atmosphere under which the process undergoes, nanoparticles with specific composition may be produced [15]. The main disadvantage of this technique is its low productivity, limiting its application to the manufacture of high-added value materials.

8.3 Bottom-up processes

In bottom-up approach particles are created assembling together smaller building blocks, atoms or molecules; the main advantage with respect to top-down approaches is the reproducibility of the high quality of the resulting materials. These processes can be performed by means of wet methods and gas-phase methods. Chemical liquid-phase methods enable a fine control over particle size, morphology and composition [16-19], but they are generally difficult to upscale, mainly due to their low productivity output and to the high cost of the precursors, besides the relevant waste formation. In gas-phase approaches a supersaturated vapour is produced, starting from solid, liquid or gaseous precursors [20-22]. A steep rise in productivity is associated to gas-phase processes, which are progressively excluding liquid-phase approaches from the market. Among gas-phase processes, gas condensation, chemical vapour condensation, flame combustion synthesis and thermal plasma synthesis are worth mentioning for their large industrial employment.

In the gas condensation process, a solid-phase precursor, typically a metal, is evaporated inside a low pressure reaction chamber and is mixed with a flowing inert gas (usually He or Ar) [23-25]. When

this gas stream is cooled, either by being mixed with a cold quenching gas or by being exposed to a cooling surface [26], supersaturation occurs and the vapour starts to nucleate. This process is especially suitable for the production of composite nanoparticles; in a common configuration, two reaction chambers in series are used: a first precursor is evaporated and nucleates in the first reaction chamber, then flows into the second reaction chamber, where the second precursor is evaporated and condenses on the already formed nanoparticles [27, 28].

The process of chemical vapour condensation is carried out by introducing a gas-phase precursor in a heated reaction chamber (1300 – 1700 °C), where nucleation and condensation take place; the produced nanoparticles are then collected in a second chamber [29-31]. This process is strongly linked to the chemical vapour deposition (CVD), but nanoparticles are produced instead of a thin film by controlling gas flow rates, temperature, pressure and residence time in the reaction chamber. By introducing multiple precursors in the reaction chamber, this process enables the production of composite, ceramic and doped nanoparticles [32-35].

In the flame synthesis, a flame is used as a thermal source to induce pyrolysis reactions in a precursor injected in its core; thus, a supersaturated vapour is obtained, which then nucleates forming nanoparticles [36-40]. Typically, low pressures (30 mbar) are adopted to limit particle agglomeration; flame temperature, residence time, quenching, precursor feed rate and the use of additives are other key parameters.

Thermal plasma synthesis is a very suitable means for nanoparticle production, combining high temperatures (around 10^4 K) that enable the use of various precursors (Mo, W, Al_2O_3 , Si, SiO_2 , ...), high cooling rates offering precise control over nanoparticle size distribution, the possibility to work under inert or reactive atmosphere, high efficiency in nanoparticles production and scalability [41-43]. In this approach, plasma provides the heat for the vaporization of precursors (solid-, liquid-, vapour-phase, suspension and solution precursors) and its dissociation in atoms, radicals and ions [44]; once the vapour reaches supersaturation condition, typically as a consequence of the mixing with a cooling gas (quenching), nanoparticles are formed through nucleation.

Many thermal plasma technologies may be employed to produce nanoparticles, DC plasma arc and RF plasmas are the main ones [45].

DC plasma arc technology for nanoparticle synthesis relies on broad family of plasma sources, each with typical advantages and disadvantages. In some of these torches the discharge, with temperatures around 15000-25000 K, is ignited between a cathode located inside a tube shaped anode; when a cold gas flow is injected in the discharge region it is heated and exits from the plasma torch forming a gas jet, with temperatures up to 10000K. The precursor, introduced in the hot gas jet, first, is evaporated and then transformed into nanoparticles [46, 47]. In some cases, a subsonic expansion phase is

adopted to obtain uniform cooling rates and finer nanoparticles [46, 48]. Some other configurations are characterized by a reaction chamber, in which the jet, generated by the DC torch, can propagate: the synthesis of nanoparticles is performed by injecting the powders, at the outlet of the torch, in the jet expanding inside the chamber [49]. Furthermore, in the twin-torch DC system proposed by Tetronics, the torches are placed into a water-cooled chamber allowing atmosphere control [50]. The possibility of producing highly energetic plasmas makes this technology very suitable for industrial scaling-up, with the potential of production rates in the range of kg/h; several oxide nanoparticles have already reached commercial production with DC plasma technology [51, 52].

Although this technology has many advantages, a few issues still have to be overcome, mainly related to the erosion of the electrodes that can cause the contamination of the nanopowders as well as instabilities of the plasma jet, inducing inhomogeneity in the products.

RF inductively coupled plasmas (ICPs) technology is a versatile and flexible route for nanoparticle synthesis. The operating principle consists in injecting a solid, liquid or gaseous precursor inside the plasma region, where it undergoes evaporation because of the high temperatures (up to 12000 K in an RF ICP system). The produced vapour then becomes supersaturated and nucleation occurs, after which the nuclei then grow because of condensation and coagulation.

An ICP system for nanoparticle synthesis is composed of a plasma torch, a reaction chamber, mounted at the outlet of the plasma torch itself, determining the volume where nanopowders nucleate and grow and a filter to collect the produced materials. The precursor material is introduced axially in the ICP torch, directly in the high temperature plasma volume, by means of an injection probe; this characteristic is a strong advantage with respect to DC non-transferred arc thermal plasma technology, where the precursor is injected radially in the tail of the plasma due to the presence of the electrode. As a consequence, ICP technology offers higher evaporation rates, also due to the lower velocities and larger plasma volume; a second fundamental advantage over DC plasmas is the high purity of the products, enabled by the absence of the electrode [41].

References

- [1] M. Gherardi, Integrated analysis and design of optimization and up-scaling of inductively coupled plasma synthesis of nanoparticles, Ph.D Thesis, 2013.
- [2] J. Schilz, M. Riffel, K. Pixius K, H. J. Meyer, Powder Technology 1999, 105, 149.
- [3] L. Takacs, J. S. McHenry, J. Mater. Sci. 2006, 41, 5246.
- [4] T. Caillat, J. P. Fleurial, A. Borshchevsky, Proceeding of the International Conference on Thermoelectrics 1992, 1, 240.

- [5] B. A. Cook, J. L. Harringa, S. H. Han in CRC Handbook of Thermoelectrics (Ed:D. M. Rowe) Boca Raton FL USA 125-129, 1995.
- [6] K. Schoenert, Ullmann's Encyclopedia of Industrial Chemistry Vol. B2 VCH-Verlagsgesellschaft Weinheim Germany 5.1–5.14 3445–3451, 1998.
- [7] W. D. Schubert, A. Bock A, B. Lux, Int. J. Refract. Met. H. 1995, 13, 281.
- [8] B. S. Murty, S. Ranganathan Int. Mater. Rev., 1998, 43, 101.
- [9] R, Reinmann R, M. Akram, J. Phys. D: Appl. Phys. 1997, 30 1125.
- [10] N. Scoville, C. Bajgar, J. Rolfe, J. P. Fleurial, J. Vandersande, Nanostruct. Mater. 1995, 5, 207.
- [11] N. S. Tabrizi, M. Ullmann, V. A. Vons, U. Lafont, A. Schmidt-Ott, J. Nanopart. Res. 2009, 11, 315.
- [12] M. Ullmann, S. K. Friedlander, A. Schmidt-Ott, J. Nanopart. Res. 2002, 4, 499.
- [13] T. Yoshida, S. Takeyama, K. Yamada, K. Mutoh, Appl. Phys. Lett. 1996, 68, 1772.
- [14] A. V. Simakin, V. V. Voronov, N. A. Kirichenko, G. A. Shafeev, Appl. Phys. A 2004, 79, 1127.
- [15] G. P. Johnston, R. Muenchausen, D. M. Smith, W. Fahrenholtz, S. Foltyn, Journal American Ceramic Society 1992, 75, 3293.
- [16] C. B. Murray, C. R. Kagan, M. G. Bawendi, Annual Rev. Mater. Sci-2000, 30 545.
- [17] L. Manna, E. C. Scher, A. P. Alivisatos, J. Am. Chem. Soc. 2000, 122, 12700.
- [18] X. Wang, J. Zhuang, Q. Peng, Y. Li, Nature 2005, 437, 121.
- [19] O. Masala, R. Seshadri, Annual Rev. Mater. Res. 2004, 34 41.
- [20] M. Winterer, Materials Science Berlin Heidelberg: Springer, 2002.
- [21] M. Swihart, Colloid and Interface Science 2003, 8, 127.
- [22] F. E. Kruis, H. Fissan, A. Peled, J. Aerosol Sci. 1998, 29, 511.
- [23] A. Tasaki, S. Tomiyama, S. Iida, N. Wada, R. Uyeda, JPN J. Appl. Phys. 1965, 4, 707.
- [24] G. M. Chow, P. G. Klemens, P. R. Strutt, J. Appl. Phys. 1989, 66, 3304.
- [25] H. Hahn, R. S. Averback, J. Appl. Phys. 1990, 67, 1113.
- [26] C. G. Granqvist, R. A. Buhrman, J. Appl. Phys. 1976, 47, 2200.
- [27] A. Maisels, F. E. Kruis, H. Fissan, B. Rellinghaus, H. Zahres, Appl. Phys. Lett. 2000, 77 4431.
- [28] T. Ohno, J. Nanopart. Res. 2000, 4, 255.
- [29] M. L. Ostraat, J. W. De Blauwe, M. L. Green, L. D. Bell, H. A. Atwater, R. C. Flagan, J. Electrochem. Soc. 2001, 148, G265.
- [30] M. H. Magnusson, K. Deppert, J. O. Malm, J Mater. Res. 2000, 15, 1564.
- [31] A. G. Nasibulin, O. Richard, E. I. Kauppinen, D. P. Brown, J. K. Jokiniemi, I. S. Altman, Aerosol Sci. Techn. 2002, 36, 899.

- [32] R. Schmechel, M. Kennedy, H. von Seggern, H. Winkler, M. Kolbe, R. A. Fischer, X. Li, A. Benker, M. Winterer, H. Hahn, *J. Appl. Phys.* 2001, 89 1679.
- [33] R. A. Senter, Y. Chen, J. L. Coffey, L. R. Tessler, *Nano Letters* 2001, 1 383.
- [34] V. V. Srdic, M. Winterer, A. Moller, G. Miehe, H. Hahn, *Journal of the American Ceramic Society* 2001, 84, 2771.
- [35] S. H. Ehrman, M. I. Aquino-Class, M. R. Zachariah, *J. Mater. Res.* 1999, 14 1664.
- [36] M. R. Zachariah, M. I. Aquino, R. D. Shull, E. B. Steel, *Nanostruct. Mater.* 1995, 5, 383.
- [37] S. E. Pratsinis, *Progress In Energy And Combustion Science* 1998, 24, 197.
- [38] C. Janzen, P. Roth, *Combustion and Flame* 2001, 125, 1150.
- [39] D. Lee, M. Choi, *J. Aerosol Sci.* 2002, 33, 1.
- [40] H. K. Kammler, S. E. Pratsinis, P. W. Morrison, B. Hemmerling, *Combustion and Flame* 2002, 128, 369.
- [41] K. K. Ostrikov, A. B. Murphy, *J. Phys. D: Appl. Phys.* 2007, 40, 2223.
- [42] K. K. Ostrikov, U. Cvelbar, A. B. Murphy, *J. Phys. D: Appl. Phys.* 2011, 44, 174001.
- [43] J. H. Seo, B. G. Hong, *Nucl. Eng. Techn.* 2012, 44, 9.
- [44] M. Shigeta, A. B. Murphy, *J. Phys. D: Appl. Phys.* 2011, 44, 174025.
- [45] R. M. Young, E. Pfender, *Plasma Chem. Plasma Process.* 1985, 5 1.
- [46] N. Rao, S. Girshick, J. Heberlein, P. McMurry, S. Jones, D. Hansen, B. Micheel, *Plasma Chem. Plasma Process.* 1995, 15, 581.
- [47] R. G. Reddy, *Metallurgical and Materials Transactions B* 2003, 34, 137.
- [48] N. Rao, B. Micheel, D. Hansen, C. Fandrey, M. Bench, S. Girshick, J. Heberlein, P. McMurry, *J. Mater. Res.* 1995, 10, 2073.
- [49] K. Kim, *Met. Mater.* 2008, 14, 707.
- [50] S. Megy, S. Bousirh, J. M. Baronnet, E. A. Ershov-Pavlov, J. K. Williams, D. M. Iddles, *Plasma Chem. Plasma Process.* 1995, 15, 309.
- [51] <http://tetronics.com/>
- [52] <http://www.scanarc.se/>

CHAPTER 9

COLD PLASMA ASSISTED PROCESSES FOR THE SYNTHESIS OF NANOPARTICLES

9.1 Introduction

During my Ph.D activities, I had the opportunity to be involved in the COST Action TD1208, a consortium of European experts in the field of electrical discharge plasmas in contact with liquids. The aim of this Action is to improve the knowledge of basic processes responsible for initiating and sustaining discharges in/on liquids, by facilitating coordination and interdisciplinary exchange of knowledge and know-how between researchers from different scientific fields and countries. In order to achieve this aim, the COST Action also provided grants for short term scientific missions (STSMs) in institution or laboratory in foreign COST Country.

The STSM I performed during my Ph.D course can be placed in this frame. It was carried out in Prof. Mariotti's research group, which is part of the Nanotechnology & Bio-Engineering Research Centre – NIBEC at the Ulster University, Northern Ireland, UK, and it was aimed at broadening my knowledge on the interactions between CAPs and liquids for production of advanced nanomaterials, exploitable in several fields of applications, spanning from engineering to medicine.

In the present chapter, after an overview of the plasma sources and performed processes, reported in the state of the art and regarding the use of CAPs for the synthesis of nanostructures, the research activities carried out during my STSM and mainly concerning the synthesis of CuO quantum dots (QDs) in liquid environment are proposed.

9.2 Non-equilibrium atmospheric pressure plasma for nanomaterials fabrication

Besides the use of conventional technologies for nanomaterials fabrication, several approaches based on non-equilibrium plasma processes have been set up until now. However, most of the existent methods for nanomaterial synthesis are performed by means of low-pressure plasma processes. Since the spatial scale of the reaction volume involved in the low-pressure plasma systems is always large, leading to a difficult control of the temperature and residence time of particle, the products are commonly characterized by partial agglomeration and wide size distribution [1]. In addition, the surmised mechanism for non-equilibrium plasma assisted nanomaterial synthesis includes the collisions between radical moieties in the gas phase, which can be enhanced substantially at higher pressures [2]. Therefore, a plasma technology for high quality nanomaterial synthesis operated and controlled under atmospheric pressure is needed.

Recently, microplasmas, a special category of plasma confined within sub-millimeter (although the name refers to a micrometric geometry) length scale in at least one dimension [3, 4], have been widely employed for the synthesis of nanomaterials. In virtue of the increased surface-volume ratio and the decreased electrode spacing, microplasmas boast several key advantages compared with conventional

plasma: high-pressure operation, continuous-flow, sub-millimeter geometry and self-organization phenomenon [2].

Furthermore, microplasmas have been demonstrated to offer the possibility to preserve a strong non-equilibrium state in a wide range of gas mixtures [3, 5], allowing for high reaction rates [1, 3], although no resolute information have been so far reported concerning the throughput of the process.

Besides the synthesis of nanostructures, microplasmas have been employed for several kinds of applications spanning from the decomposition of volatile organic compounds (VOCs) [6] to biomedical applications, by testing their potentialities in biocidal tests [7, 8]. Microplasmas have been also used for surface functionalization of polymers and glasses [9, 10], thanks to the abundance of reactive species and radicals and for the deposition of hydrophobic coatings [11].

In the following paragraphs, the most employed microplasma systems for the synthesis of nanostructures, in the gas, solid and liquid phases, are briefly reported.

9.2.1 Microplasma systems

A relatively simple microplasma system used for nanomaterial fabrication is the hollow-electrode microcharges, which consists of two hollow metal capillary tubes separated by 1–2 mm, both connected to a DC power supply and acting as the cathode and the anode, respectively [3]. Meanwhile, they also function as precursor transporters, in which precursor vapours are introduced by a flow of inert gas such as Ar or He and are dissociated in the plasma area between two electrodes. The formed aerosol particles can be collected by an electrostatic precipitator or by a filter installed after the reactor (Figure 1).

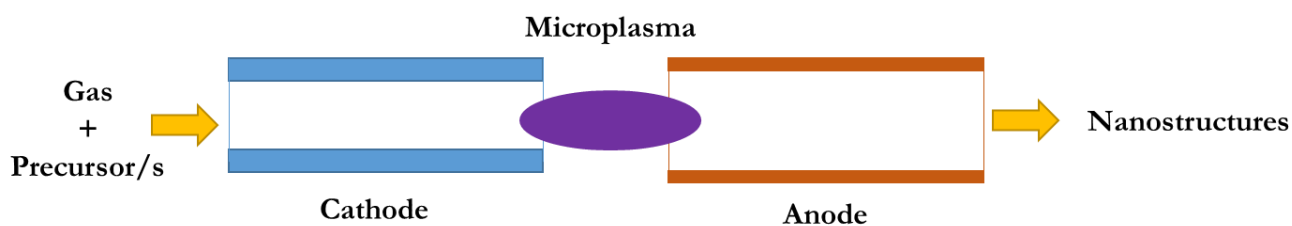


Figure 1. Schematic representation of a hollow-electrodes microcharges. (The schematic refers to the setup reported in [12])

In an emblematical hollow-electrode microcharge, the typical voltage and current used to prepare nanomaterials are at the level of hundred V and several mA, respectively and, therefore, the electrodes do not take part in the reactions [3, 12]. The method enables to produce ultrafine nanoparticles at atmospheric pressure and room temperature.

Besides the microplasma discharges, currently, various configurations of microplasma jets have been proposed and used as nanomaterial fabrication tools, with different types of power supplies (DC, RF or microwave) to ignite and sustain the plasma [3].

Concerning the microplasma jets, there are two main categories of systems, named microplasma jets with consumable wires as electrode and microplasma jets with tubes/external electrode [3].

Microplasma jets with consumable wires are generally composed by a metal wire, which acts as solid precursor for the synthesis of the desired nanostructures and it is inserted inside a capillary tube, as reported in Figure 2.

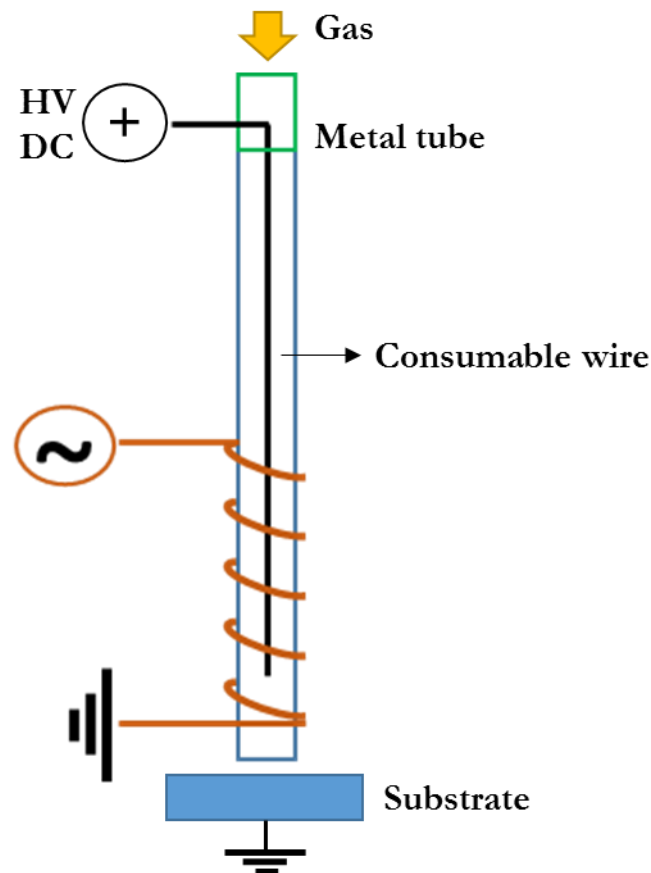


Figure 2. Schematic representation of a microplasma jet with consumable electrode. (The schematic refers to the setup reported in [13])

According to the different ways of coupling the power supply, metal/metal-oxide nanostructures could be obtained on the wire surface or on the substrate below the plasma jet [3, 14].

Regarding the microplasma jets with tubes/external electrode, a schematic representation is reported in Figure 3.

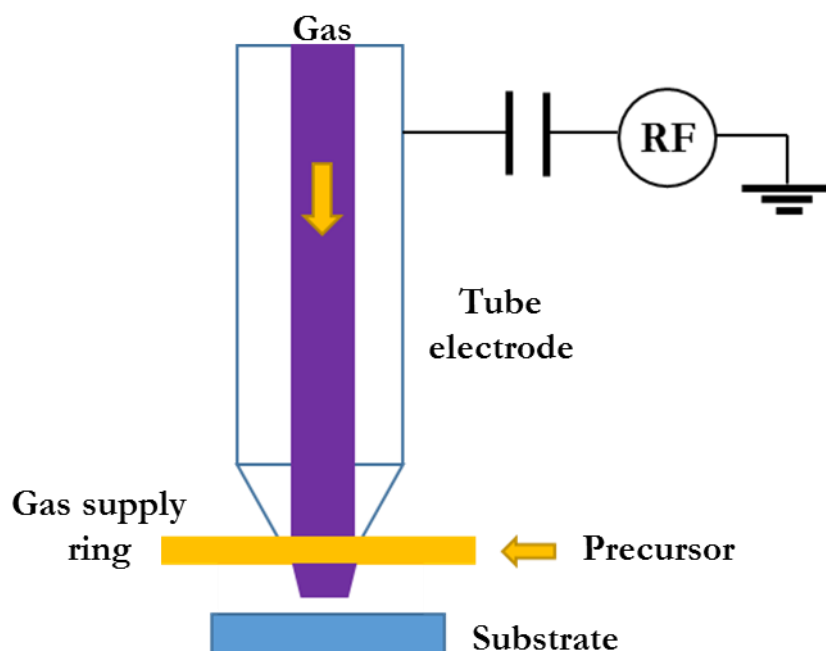


Figure 3. Schematic representation of a microplasma jet with tube used as cathode. (The schematic refers to the figure reported in [15])

For this kind of microplasma jets, some precursors such as CH_4 [16, 17], SiCl_4 [18], $\text{Ti}[\text{OC}_3\text{H}_7]_4$ [19, 20], $\text{Pd}(\text{hfac})_2$ [21] and $\text{Cu}(\text{hfac})_2$ [22] can be introduced at the outlet of the tube/electrode and used to synthesize the desired products [3].

Compared with the microplasmas using consumable wires as electrodes, this type of microplasma jet has a higher degree of flexibility in configuration. Indeed, there are more available ways to couple the power supply to the system and several kinds of process parameters could be tuned, such as the precursors ratio and the residence time.

9.2.2 Microplasmas for the synthesis of nanostructures in gas and solid phase

Gas-phase nucleation of nanomaterials in a microplasma from vapour precursors is a natural extension of previous studies with low-pressure plasmas [23, 24] and larger scale atmospheric plasmas and jets [23, 25, 26]. There are many different precursors, which can be non-thermally dissociated in a microplasma leading to the growth different types of materials (i.e. metals, semiconductors and oxides). The general mechanism for nucleation is to introduce the precursor in the microplasma and form reactive radical species. At the appropriate process conditions, these radicals can collide, react and nucleate small clusters. The clusters will then grow, by additional radical or vapour deposition on the particle surface, or agglomerate, through collisions with other particles. Finally, the particles will exit the plasma volume as an aerosol flow [23].

Compared with low-pressure plasma experiments [27], the particles synthesized by these routes are much smaller because of the shorter residence time experienced by the growing particles inside the reaction zone [23, 28]. Direct evaporation, sputtering or etching of solid materials is an alternative approach that has been explored via atmospheric-pressure microplasma synthesis [1, 13, 23, 29-39]. A critical challenge for this method is how to control the mechanism for particle nucleation and growth, which depends on many factors including the evaporation rate of the solid metal source. The mechanisms responsible for the surface reactions at the solid precursors are still not fully clear and further experimental studies are required. Nonetheless, there are significant advantages in using solid metals in terms of minimizing the amount of precursor and handling of dangerous gases or other chemicals [23, 40].

9.2.3 Microplasmas for synthesis of nanostructures in a liquid environment

Recently, the study of the interactions between plasma and liquids has raised a great interest and the generation of plasmas at the interface or inside liquids is under investigation for a wide range of applications [41-44]. In this frame, microplasmas have been widely demonstrated to be a suitable method to induce synthesis of nanostructures directly in liquid phase [44].

Mariotti *et al* designed a simple-to-use, one-step approach based on an atmospheric pressure microplasma which directly interacts with liquids to synthesize colloidal and electrostatically stabilized AuNPs [45, 46]. This synthesis technique does not need any added reducing and/or capping agents and only requires a water-based solution of the metal precursor. The synthesis was achieved by processing aqueous solutions with HAuCl_4 precursor at different molar concentrations by microplasma with different discharge currents.

The plasma was generated across a 0.7 mm gap between the liquid surface and a stainless steel capillary (1 mm external diameter and 0.25 mm internal diameter). Inside the capillary, He is flown at 25 standard cubic centimetres (sccm) so that the microplasma is largely formed in helium gas. The microplasma is sustained by a high DC voltage applied at the carbon rod, while the stainless steel capillary is grounded through a ballast resistor of 100 k Ω . The processing current is maintained constant (1–5 mA), while the applied voltage varies (due to changes in the solution conductivity) from about 2 kV at the start of the treatment down to about 800 V after 10 min processing.

The obtained results highlighted that the concentration of the gold precursor determines the size of the Au-NPs: increasing the concentration leads to an increase in average diameter. A possible explanation is that electrons injected in the solution induce the reduction of the Au-salt, forming Au^0 atoms; these come in contact with each other, leading to NPs nucleation and growth. At higher

precursor concentrations, the right average distance between the reduced Au⁰ atoms would therefore lead to larger particles.

Further experiments performed by the Authors, varying the processing current from 1 to 5 mA at different constant HAuCl₄ concentrations highlighted that at lower concentrations (0.05 and 0.1 mM), HAuCl₄ is quickly and completely reduced within a 10 min processing at any current value.

The colloidal Au-NPs produced with this technique are stable shortly after processing but they tend to aggregate over time.

In order to explain the mechanisms, which lead to the synthesis of AuNPs, the Authors interestingly processed water with the same microplasma set-up under the same operating conditions but without the gold precursor. After 10 min of plasma treatment of water, a drastic increase of the conductivity was observed, the pH decreased from 10 to 3 and H₂O₂ was formed. When the gold precursor is added to the aqueous solution, the overall chemistry of the solution is affected. However, as proposed in the work, the interactions of electrons with water molecules remain the same and Au-salt reduction becomes a competing reaction path for electrons, determined only by the concentration of HAuCl₄.

According to the mechanism suggested by the Authors, the synthesis of Au-NPs may be initiated by the reduction of the Au-salt, due to the presence of electrons in the liquid system. However, salt reduction may also result from “cascaded chemistry” by H[•] radicals [47], H⁻ anions or H₂O₂.

Following, gold atoms nucleate by collision and consequently grow into larger and larger NPs. The growing AuNPs are expected to leave the reaction zone just below the microplasma [47]. As they leave the reaction zone, Au-NPs will find a progressively lower concentration of Au⁰ atoms until the NPs growth is halted due to the absence of reduced HAuCl₄ [46, 47].

Du *et al* reported [48] a simple method based on the use of a microplasma to synthesize cuprous oxide (Cu₂O) NPs in NaCl-NaOH-NaNO₃ electrolytic system. Differently from the work previously reported, no copper containing salts were used. Microplasma acted as the cathode and a copper plate as the anode.

To carry out the synthesis, a stainless steel tube (0.7 mm inside diameter, 8 cm length) was positioned 3 cm away from the copper electrode with a gap of 2 mm between the tube end and the liquid surface. The stainless steel tube acted as the cathode and the copper sheet as the anode. The copper anode was polished and washed with distilled water, and then immersed into electrolytic solution containing 150 g/L NaCl, 1 g/L NaOH and 1.3 g/L NaNO₃ with the distilled water or H₂O–ethylene glycol as the solvent. At the end of the synthesis, the sediments were centrifuged and washed with deionized water and ethanol for several times. Subsequently, the obtained products were dried in a vacuum oven at 60 °C for 6 h.

The effects of electrolytic solution on the results of Cu₂O nanoparticles prepared by microplasma electrochemical method were firstly investigated. The XRD analysis underlined that when H₂O–ethylene glycol electrolytic system was used, the production of Cu₂O nanoparticles was observed, while for the distilled water electrolytic system also CuO and CuCl characteristic peaks were found. Furthermore, SEM images showed that lots of irregular shape structures were produced when pure water was used as solvent, while for H₂O–ethylen glycol mix solvent the Cu₂O exhibited a spherical shape with a diameter size ranging from 0.2 to 2 μm.

Regarding the mechanism for the Cu₂O particles formation, the Authors pointed out that the microplasma, being the cathode, produces electrons, which enable to initiate redox reaction in solution and the total reaction equation is here reported: $2\text{Cu} + \text{H}_2\text{O} = \text{H}_2 + \text{Cu}_2\text{O}$.

9.2.4 Microplasma for surface engineering of nanostructures in liquid phase

Even though not experimentally carried out during my Ph.D activities, some words have to be spent for the functionalization of nanoparticles in liquid phase by means of microplasmas, as it is another interesting application of this kind of plasma.

Mariotti *et al* have deeply investigated the surface engineering of SiNCs colloids by means of microplasma. The SiNCs were presynthesized by electrochemical etching of a silicon wafer and then subjected to mechanical pulverization [49-51]. SiNCs produced by this method are mostly hydrogen-terminated, however their properties in solution tend to degrade easily in contact with water or water vapour due to low temperature oxidation [50]. Therefore, the corresponding optical properties are also significantly affected. In order to avoid degradation, stable surface passivation is required.

The microplasma set-up was used in this case with a colloid of Si-NCs in ethanol. A nickel capillary with inner diameter of 0.7 mm and outer diameter of 1 mm was positioned 1mm above the surface of the Si-NCs colloid to provide Ar flow and a 5mm diameter carbon rod acted as counter electrode. The initial voltage was set at 2 kV until the current reached 1.5 mA and it was subsequently adjusted to keep the current constant at 1.5 mA. The treated colloids were made of 15 mg SiNCs in 20 mL of ethanol and only the supernatant part (10 mL) was extracted for processing immediately after the colloid was prepared.

The analysis of the Si-NCs, including Fourier transform infra-red analysis [49, 51] revealed that Si-NCs under microplasma processing have undergone a surface modification whereby Si–H bonds and other surface terminations have been removed and mostly replaced by Si–O–R terminations. Replacement of H-terminations was also seen in the PL measurements [50]. The improved passivation by Si–O–R contributes to the increase in PL intensity and the shift can be attributed to a

smaller band-gap that has been theoretically predicted when the surface of H-terminated Si-NCs is modified.

Mariotti *et al* also demonstrated the possibility to functionalize silicon nanocrystals (SiNCs) by direct current microplasma processing in water with poly(3,4-ethylenedioxythiophene) doped by poly(styrenesulfonate) (PEDOT:PSS), producing nanocomposites with enhanced optoelectronic performances [53]. The achieved results confirmed that SiNCs became stable in water with potential application impact for biorelated applications and that the microplasma processing in the presence of the polymer helps prevent the fast oxidation process over a longer period of time in comparison to the unprocessed sample. Interestingly, the proposed microplasma-based treatment turns out to enable the production of SiNCs/polymer nanocomposites that would be difficult to achieve otherwise due to the hydrophobic nature of H-terminated SiNCs in water [53].

To conclude, the proposed studies highlighted that plasma-induced liquid chemistry at atmospheric pressure represents a new and growing field that will challenge traditional wet chemical methods for nanomaterials synthesis. Furthermore, the impact of plasma-liquid interactions can be considered as a fundamental new approach to activating chemical reactions in liquids. However, further studies are still required to get insights on the throughput of the presented method, with aim to evaluate its suitability in industrial applications.

9.3 Atmospheric pressure DC microplasma for the synthesis of CuO QDs

The research activities carried out during my STSM in Prof. Mariotti's research group were mainly focused on the optimization of the experimental setup and investigation of the operating conditions for the plasma-assisted synthesis of cupric oxide (CuO) nanoparticles directly in liquid phase.

CuO is a versatile p-type material for energy applications capable of imparting diverse functionalities when the band-energy structure is manipulated, through quantum confinement, from 1.2 eV (bulk) to >2 eV [54-60]. This is an exciting opportunity, as it would make CuO a highly versatile and attractive material for a range of applications; for instance, it would be possible to use CuO nanoparticles with tuneable properties as absorber or transport/blocking layers in photovoltaic devices.

Various physical, chemical and physicochemical techniques have been employed for synthesizing CuO nanostructures [54, 56, 58, 61, 62]. However, these techniques suffer from numerous disadvantages including complex and time consuming steps, high temperatures, inert atmosphere, expensive source materials, toxic organic solvents and surfactants [63, 64]. The presence of surfactant or ligand chemistries is essential for minimising particle coalescence and agglomeration during

standard colloid synthesis; however, such chemistries impact significantly on the resultant nanoparticle optoelectronic properties and restrict the opportunity for bandgap tuning. Synthesis of non-agglomerated and pure CuO nanostructures is imperative for their successful integration in application devices [65, 66], and therefore developing an alternative, cheap and environmentally friendly synthesis method is highly desirable.

The plasma process for synthesis of CuO nanostructure, set up during the STSM in Prof. Mariotti's group, is a stable one-step approach for producing CuO quantum dots (QDs) from a bulk copper electrode in liquid. It is worth pointing out that no surfactant and/or capping agents or Cu containing salts were used in liquid phase.

The experimental setup and the characterization of the produced colloids and nanoparticles are here reported. A more thorough description of the results here reported and of those concerning the applications of the so-produced CuO QDs into third generation devices will be available after publication of our scientific paper "One-Step Rapid Synthesis of CuO Quantum Dots with Tailored Energy-Band Structure for All-Inorganic Solar Cells", recently submitted to Nature Communications [67].

9.3.1 Experimental part

For the synthesis of CuO QDs, an atmospheric pressure direct current (DC) microplasma (Figure 4) generated between a the tip of a Ni tube (0.7 mm internal diameter, 1 mm outer diameter) and 5 mL of ethanol was employed. A Cu foil, immersed by 5 mm in ethanol, was used as the anode and was placed at about 3 cm from the Ni tube which acted as the cathode. The distance between the Ni tube and the liquid surface was initially adjusted at 1 mm. Pure He was flown through the Ni tube and its mass flow rate was kept constant at 50 sccm. The voltage, applied to the Cu foil with the Ni tube grounded through a 100 k Ω ballast resistor, was initially set at 3 kV until the current reaches 0.5 mA. The current value was maintained constant throughout the whole process by progressively lowering the voltage from 3 kV to around 2 kV, in order to compensate the increase of the conductivity of the ethanol.

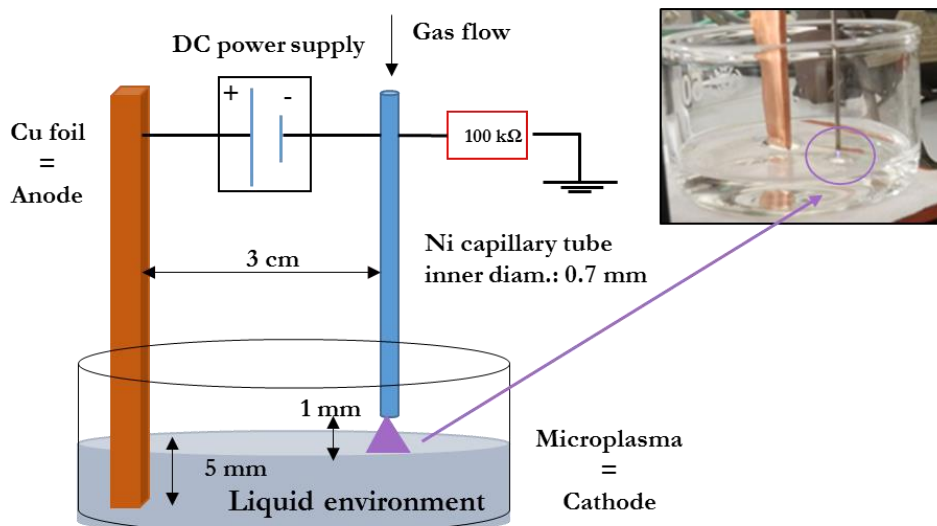


Figure 4. Experimental setup for synthesis of CuO QDs [67].

The synthesis initiated as soon as the microplasma was generated and after a few minutes the solution started turning yellow, due to the formation of QDs. The results reported here will relate to CuO QDs produced for a total of 30 min in 10 min consecutive processing steps. Figure 5 reports photos of the solution after 10, 20 and 30 min of plasma treatment and it clearly highlights the change of the colour of the solution turning into a colloid during the synthesis process.

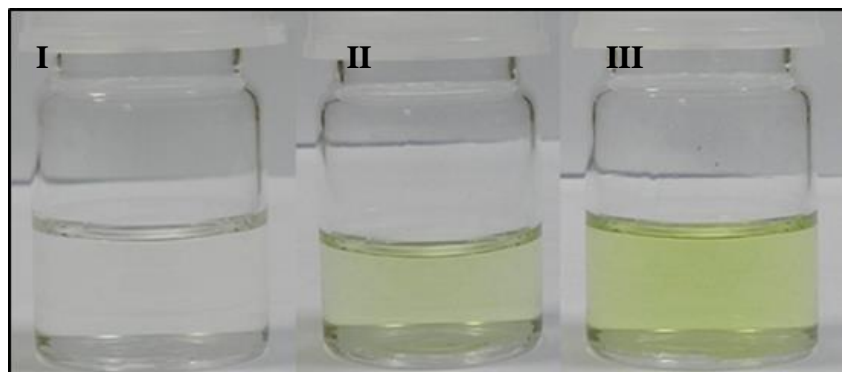


Figure 5. Photographs of the processed samples after (I) 10 min (II) 20 min and (III) 30 min processing [67].

Following the synthesis, the CuO QDs were characterized without any post-synthesis treatment. The morphology of the synthesis of QDs was investigated by means of the transmission electron microscopy (TEM; JEOL JEM-2100F) performed on samples drop-casted on carbon coated Au grids. The crystal structure was determined by transmission electron microscope (TEM) and X-ray diffraction (XRD, Bruker D8 Discover); XRD analysis was carried out on as-prepared colloids, which were spray-coated and dried on a silicon wafer. The chemical composition was assessed by X-ray photoelectron spectroscopy (XPS) with an Axis Ultra DLD spectrometer (Kratos Analytical, Japan) with monochromated Al K α X-rays source and by Fourier transform infrared spectroscopy (FTIR,

Thermo Scientific, Nicolet iS5, 4 cm⁻¹, resolution, totally scanned it for 50 times in N₂ atmosphere). Sample preparation for XPS was carried out by drop-casting the colloids on molybdenum foil and dried. FTIR analysis was carried out from as-prepared colloids, which were spray-coated and dried on a silicon wafer.

9.3.2 Results and Discussion

The TEM analysis of the produced QDs highlighted the presence of non-agglomerated QDs, as reported in Figure 6a. The analysis of hundreds of QDs indicated the presence of spherical particles with a diameter distribution that is closely fitted with a log-normal distribution (1.9 nm arithmetic mean and ± 0.49 nm variance) (Figure 6b).

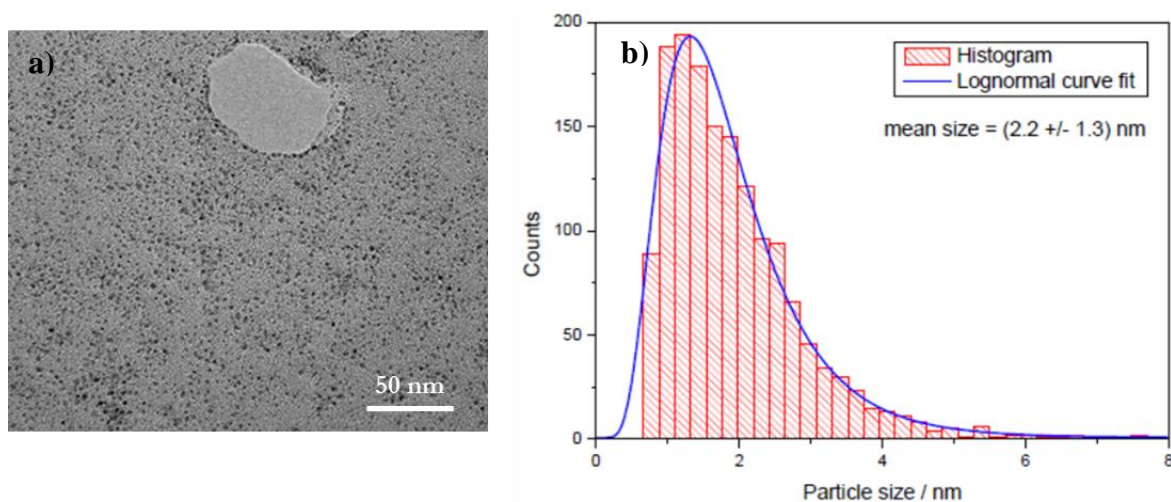


Figure 6. (a) Low magnification transmission electron microscopy image of CuO quantum dots and (b) corresponding diameter distribution with resulting arithmetic mean and variance [67].

The high resolution TEM (HRTEM) images, shown in Figure 7, clearly highlights the existence of atomic fringes indicating a crystalline structure.

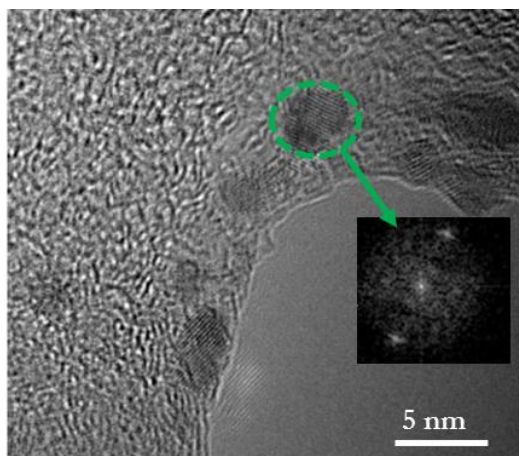


Figure 7. High resolution transmission electron microscope image of the CuO quantum dots and corresponding fast Fourier transform (FFT) image (insert) [67].

The XRD analysis, Figure 8, reported the presence of peaks corresponding to monoclinic CuO phase and the absence of other peaks suggesting a very high purity of the synthesis product; the high intensity peak around 70° originates from the Si substrate.

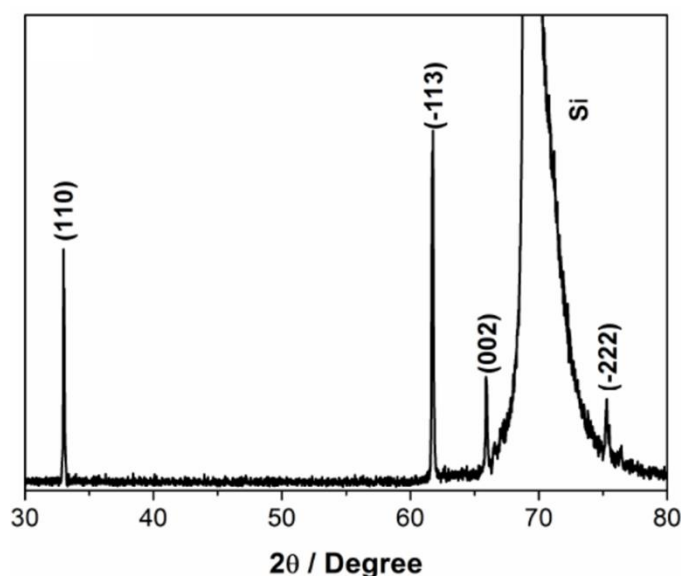


Figure 8. X-ray diffraction spectrum of the spray coated CuO quantum dots film on a silicon wafer [67].

Figure 9a reports the FTIR spectrum of the spray-coated CuO QDs onto Si wafer and details the assignment of the corresponding peaks. The absorption peaks from 420 cm^{-1} to 700 cm^{-1} belong to the CuO [54-56, 68]. In particular, the peaks at 428 cm^{-1} , 503 cm^{-1} and 536 cm^{-1} are characteristic stretching vibrations of Cu-O on monoclinic CuO, the absorption at 447 cm^{-1} represents the stretching mode of Cu-O [59, 68] and the absorption at 485 cm^{-1} is due to the Cu-O stretching along [101] direction [60]. Furthermore, the absence of the infrared-active modes at 610 cm^{-1} from the Cu_2O

phase confirms the purity of the CuO phase [59]. The XPS spectrum of the QDs is displayed in Figure 9b. The Cu 2p core level binding energies at 934.8 eV and 954.5 eV are attributed to the Cu 2p_{3/2} and Cu 2p_{1/2}, respectively [69].

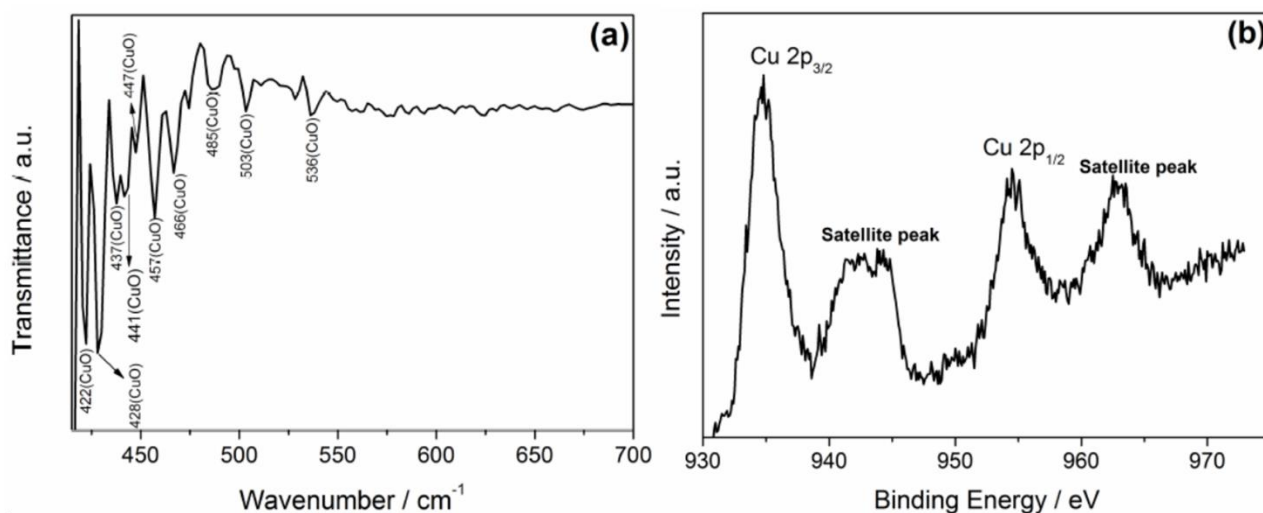
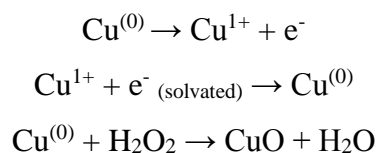


Figure 9. (a) Fourier transform infrared spectrum of spray-coated CuO quantum dots (QDs). (b) X-ray photoelectron spectra of Cu 2p core level for CuO quantum dots [67].

Despite much recent progress, many aspects that can lead to a description of this non-equilibrium and complex interface are still under debate. Nonetheless, hybrid plasma-liquid systems are producing important contributions to nanomaterial synthesis and surface treatment [48, 70, 71, 45, 46, 72-74]. With the current knowledge of plasma liquid-interactions, some mechanisms leading to the formation of the CuO QDs are hypothesized:



The first reaction is the result of passive anodic dissolution as expected due to the applied current [26], where the resulting electron closes the current loop into the copper electrode. Reduction of Cu-ions, from an oxidation state of 1 or 2 to Cu⁽⁰⁾, however, does not take place as in standard electrochemical cells due to the absence of a solid counter-electrode. On the contrary, at the plasma-liquid interface, solvated electrons [76] act as reducing agent producing atomic Cu⁽⁰⁾.

The plasma-ethanol interface is also known to produce radicals leading to the formation of H₂O₂ [46, 73, 77] and we have confirmed that also in our case hydrogen peroxide is produced and consumed [78]. The interaction of locally-produced (i.e. at the plasma-ethanol interface) hydrogen peroxide with reduced copper atoms then leads to the formation of CuO [79], where the very high reaction rates of solvated electrons and the non-acidic prevents the decomposition of hydrogen peroxide through

Fenton-like reactions with the Cu-ions [80, 81]. The size of the QDs is then determined by the local concentration of coalescing CuO.

9.3.3 Conclusions

In summary, although additional investigations are to be performed to evaluate on the throuput of the proposed method, it has been demonstrated that high quality and high purity CuO QDs can be synthesized with a simple and environmentally friendly one-step synthesis method, without requiring surfactant/capping agents or Cu-containing salts in liquid phase. Further investigations performed by Prof. Mariotti's groups demonstrated that the synthesized CuO QDs show quantum confined properties, which suggest the possibility of using Cu-based oxide for different applications and importantly with size-dependent functions in solar cell devices through appropriate energy-band structure engineering.

References

- [1] D. Mariotti, K. Ostrikov, *J. Phys. D. Appl. Phys.* 2009, 42, 092002
- [2] D. Mariotti, R. M. Sankaran, *J. Phys. D. Appl. Phys.* 2010, 43, 323001
- [3] L. Lin, Q. Wang, *Plasma Chem. Plasma Process.* 2015, DOI 10.1007/s11090-015-9640-y
- [4] T. Belmonte, G. Arnoult, G. Henrion, T. Gries, *J. Phys. D. Appl. Phys.* 2011, 44, 363001
- [5] D. Mariotti, *Appl. Phys. Lett.* 2008, 92, 3
- [6] T. Seto, S. B. Kwon, M. Hirasawa, A. Yabe, *Jpn. J. Appl. Phys.* 2005, 44, 5206
- [7] J. Mizeraczyk, B. Hrycak, M. Jasinski, *Przeegląd Elektrotechniczny* 2012, 88, 238
- [8] K. Becker, A. Koutsospyros, S. M. Yin, C. Christodoulatos, N. Abramzon, J. C. Joaquin, G. B. Marino, *Plasma Phys. Control Fusion* 2005, 47, B513
- [9] R. E. J. Sladek, E. Stoffels, R. Walraven, P. J. A. Tielbeek, R. A. Koolhoven, *IEEE Trans. Plasma Sci.* 2004, 32, 2002
- [10] K. Shimizu, H. Fukunaga, S. Tatematsu, M. Blajan, *Jpn. J. Appl. Phys.* 2012, 51, 11PJ01
- [11] A. Vogelsang, A. Ohl, R. Foest, K. Schroder, K. D. Weltmann, *J. Phys. D: Appl. Phys.* 2010, 43, 485201
- [12] W. H. Chiang, R. M. Sankaran, *Adv. Mater.* 2008, 20, 4857
- [13] T. Belmonte, G. Arnoult, G. Henrion, T. Gries, *J. Phys. D: Appl. Phys.* 2011, 44, 363001
- [14] D. Mariotti, A. C Bose, K. Ostrikov, *IEEE Trans. Plasma Sci.* 2009, 37, 1027
- [15] Z. Yang, H. Shirai, T. Kobayashi, Y. Hasegawa, *Thin Solid Films* 2007, 515, 4153
- [16] H. Shirai, T. Kobayashi, Y. Hasegawa, *Appl. Phys. Lett.* 2005, 87, 143112
- [17] S. Kona, J. H. Kim, C. K. Harnett, M. K. Sunkara, *IEEE Trans. Nanotechnol.* 2009, 8, 286

- [18] T. Nozaki, K. Sasaki, T. Ogino, D. Asahi, K. Okazaki, *Nanotechnology* 2007, 18, 235603
- [19] T. Suzuki, M. Kato, Y. Shimizu, *Int. J. Autom. Technol.* 2013, 7, 720
- [20] H. Yoshiki, T. Mitsui, *Surf. Coat. Technol.* 2008, 202, 5266
- [21] T. L. Koh, E. C. O'Hara, M. J. Gordon, *Nanotechnology* 2012, 23, 425603
- [22] Y. Shimizu, T. Sasaki, T. Ito, K. Terashima, N. Koshizaki, *J. Phys. D: Appl. Phys.* 2003, 36, 2940
- [23] D. Mariotti, R. M. Sankaran, *J. Phys. D: Appl. Phys.* 2011, 44, 174023
- [24] K. Ostrikov, *Rev. Mod. Phys.* 2005, 77, 489
- [25] N. Rao, S. Girschick, J. Heberlein, P. McMurry, S. Jones, D. Hansen, B. Micheel, *Plasma Chem. Plasma Process* 1995, 15, 581
- [26] R. P. Cardoso, G. Arnoult, T. Belmonte, G. Henrion, S. Weber, *Plasma Process. Polym.* 2009, 6, S302.
- [27] L. Mangolini, E. Thimsen, U. Kortshagen, *Nano Lett.* 2005, 5, 655
- [28] R. M. Sankaran, D. Holunga, R. C. Flagan, K. P. Giapis, *Nano Lett.* 2005, 5, 537
- [29] D. Mariotti, V. Svrcek, D. G. Kim, *Appl. Phys. Lett.* 2007, 91, 183111.
- [30] S. Stauss, Y. Imanishi, H. Miyazoe, K. Terashima K, *J. Phys. D: Appl. Phys.* 2010, 43, 155203
- [31] Shimizu Y, Koga K, Sasaki T and Koshizaki N 2009 *Cryst. Eng. Commun.* 11 1940
- [32] Y. Shimizu, A. C. Bose, T. Sasaki, D. Mariotti, K. Kirihara, T. Kodaira, K. Terashima, N. Koshizaki, *Trans. Mater. Res. Soc. Japan* 2006, 31, 463
- [33] A. C. Bose, Y. Shimizu, D. Mariotti, T. Sasaki, K. Terashima, N. Koshizaki, *Nanotechnology* 2006, 17, 5976
- [34] Y. Shimizu, T. Sasaki, C. Liang, A. C. Bose, T. Ito, K. Terashima, N. Koshizaki, *Chem. Vapor Depos.* 2005, 11, 244
- [35] Y. Shimizu, T. Sasaki, A. C. Bose, K. Terashima, N. Koshizaki, *Surf. Coat. Technol.* 2006, 200 4251
- [36] Y. Shimizu, K. Kawaguchi, T. Sasaki, N. Koshizaki, *Appl. Phys. Lett.* 2009, 94, 191504
- [37] Y. Shimizu, K. Koga, T. Sasaki, D. Mariotti, K. Terashima, N. Koshizaki, *Microprocesses and Nanotechnology*, 2007 Digest of Papers p 174
- [38] Y. Shimizu, A. C. Bose, D. Mariotti, T. Sasaki, K. Kirihara, T. Suzuki, K. Terashima, N. Koshizaki, *Japan. J. Appl. Phys. Part 1* 2006, 45, 8228
- [39] D. Mariotti, H. Lindstrom, A. C. Bose, K. Ostrikov, *Nanotechnology* 2008, 19, 495302
- [40] R. C. Flagan, M. M. Lunden, *Mater. Sci. Eng. A* 1995, 204, 113
- [41] P. Bruggeman, C. Leys, *J. Phys. D: Appl. Phys.* 2009, 42, 053001

- [42] D. O'Connell, L. J. Cox, W. B. Hyland, S. J. McMahon, S. Reuter, W. G. Graham, T. Gans, F. J. Currell, *Appl. Phys. Lett.* 2011, 98, 043701
- [43] N. Skoro, D. Maric, G. Malovic, W. G. Graham, Z. Lj, Petrovic, *Phys. Rev. E* 2011, 84, 055401(R)
- [44] S. Schneider, J.-W. Lackmann, D. Ellerweg, B. Denis, F. Narberhaus, J. E. Bandow, J. Benedikt, *Plasma Process. Polym.* 2012, 9, 561
- [45] D. Mariotti, J. Patel, V. Svrcek, Paul Maguire, *Plasma Process. Polym.* 2012, 9, 11-12, 1074
- [46] J. Patel, L. Nemcova, P. Maguire, W. G. Graham, D. Mariotti, *Nanotechnology* 2013, 24, 245604
- [47] K. Furuya, Y. Hirowatari, T. Ishioka, A. Harata, *Chem. Lett.* 2007, 36, 1088.
- [48] C. Du, M. Xiao, *Sci. Rep.* 2014, 4, 7339
- [49] I. Levchenko, K. Ostrikov, D. Mariotti, V. Svrcek, *Carbon* 2009, 47, 2379
- [50] D. Mariotti, V. Svrcek, J. W. J. Hamilton, M. Schmidt, M. Kondo, *Adv. Funct. Mater.* 2012, 22, 5, 954
- [51] V. Svrcek, A. Slaoui, J. C. Muller, *J. Appl. Phys.* 2004, 95, 3158
- [52] V. Svrcek, D. Mariotti, M. Kondo, *Appl. Phys. Lett.* 2010, 97, 161502
- [53] S. Mitra, S. Cook, V. Švrček, R. A. Blackley, W. Zhou, J. Kovač, U. Cvelbar, D. Mariotti, *J. Phys. Chem. C* 2013, 117, 23198
- [54] C. Yang, F. Xiao, J. Wang, X. Su, *J. Colloid Interface Sci.* 2014, 435, 34.
- [55] B. Balamurugan, B. R. Mehta, *Thin Solid Films* 2001, 396, 90.
- [56] M. U. A. Prathap, B. Kaur, R. Srivastava, *J. Colloid Interface Sci.* 2012, 370, 144.
- [57] W. Wang, L. Wang, H. Shi, Y. Liang, *CrystEngComm*, 2012, 14, 5914.
- [58] Y. Xu, D. Chen, X. Jiao, *J. Phys. Chem. B* 2005, 109, 13561.
- [59] K. Borgohain, J. B. Singh, M. V. R. Rao, T. Shripathi, S. Mahamuni, *Phys. Rev. B* 2000, 61, 11093.
- [60] S. P. Meshram, P. V. Adhyapak, U. P. Mulik, D. P. Amalnerkar, *Chem. Eng. J.* 2012, 204–206, 158.
- [61] Q. B. Zhang, K. L. Zhang, D. G. Xu, G. C. Yang, H. Huang, F. D. Nie, C. M. Liu, S. H. Yang, *Prog. Mater. Sci.* 2014, 60, 208.
- [62] A. S. Zoolfakar, R. A. Rani, A. J. Morfa, A. P. O'Mullane, K. K. Zadeh, *J. Mater. Chem. C*, 2014, 2, 5247.
- [63] H. He, J. Dong, K. Li, M. Zhou, W. Xia, X. Shen, J. Han, X. Zeng, W. Cai, *RSC Adv.* 2015, 5, 19479.
- [64] Q. Zhang, D. Xu, X. Zhou, X. Wu, K. Zhang, *Small*, 2014, 10, 935.

- [65] C. Y. Jin, M. Hu, X. L. Cheng, F. X. Bu, L. Xu, Q. H. Zhang, J. S. Jiang, *Chem. Commun.* 2015, 51, 206.
- [66] S. Dagher, Y. Haik, A. I. Ayes, N. Tit, *J. Lumin.* 2014, 151, 149.
- [67] T. Velusamy, A. Liguori, M. Macias-Montero, M. Gherardi, V. Colombo, P. Maguire, V. Svrcek, D. Mariotti, One-Step Rapid Synthesis of CuO Quantum Dots with Tailored Energy-Band Diagram for All-Inorganic Solar Cells, submitted to *Nature Communications*.
- [68] M. Huang, Y. Zhang, F. Li, Z. Wang, Alamusi, N. Hu, Z. Wen, Q. Liu, *Sci. Rep.* 2014, 4, 4518.
- [69] S. Sun, X. Zhang, Y. Sun, S. Yang, X. Song, Z. Yang, *ACS Appl. Mater. Interfaces* 2013, 5, 4429.
- [70] T. Yan, X. Zhong, A. E. Rider, Y. Lu, S. A. Furman, K. Ostrikov, *Chem. Commun.* 2014, 50, 3144.
- [71] C. Richmonds, R. M. Sankaran, *App. Phys. Lett.* 2008, 93, 131501.
- [72] T. Velusamy, S. Mitra, M. M. Montero, V. Svrcek, D. Mariotti, *ACS Appl. Mater. Interfaces*, 2015, (In Press), DOI: 10.1021/acsami.5b06577.
- [73] D. Mariotti, V. Svrcek, J. W. J. Hamilton, M. Schmidt, M. Kondo, *Adv. Funct. Mater.* 2012, 22, 954.
- [74] Y. Lu, Z. Ren, H. Yuan, Z. Wang, B. Yu, J. Chenab, *RSC Adv.* 2015, 5, 62619.
- [75] M. Datta, *IBM J. Res. Develop.* 1993, 37, 207.
- [76] P. Rumbach, D. M. Bartels, R. M. Sankaran, D. B. Go, *Nat. Commun.* 2015, 6, 7248.
- [77] S. Mitra, V. Svrcek, D. Mariotti, T. Velusamy, K. Matsubara, M. Kondo, *Plasma Process. Polym.* 2014, 11, 158
- [78] S. Pandija, D. Royb, S.V. Babu, *Mater. Chem. Phys.* 2007, 102, 144.
- [79] E. Vyhnánková, Z. Kozáková, F. Krčma, A. Hrdlička, *Open Chem.* 2015, 13, 218.
- [80] P. Rumbach, D. M. Bartels, R. M. Sankaran, D. B. Go, *Nat. Commun.* 2015, 6, 7248.
- [81] M. C. Kang, H. S. Nam, H. Y. Won, S. Jeon, H. Jeon, J. J. Kim, *Electrochem. Solid-State Lett.* 2008, 2, H32.

Acknowledgments

My dissertation will never be complete without thanking people who guided and accompanied me, making my Ph.D one of the most beautiful period of my life, always full of enthusiasm and motivations.

Maybe I would not have undertaken the Ph.D studies, if I had not met Prof. Vittorio Colombo, who, with his valuable teachings and advice, has had a fundamental importance in my growth as person and young researcher. I will never manage to thank him enough for all the opportunities he gave to me and I will always be grateful for the real privilege I have in learning from him and working in his group.

I absolutely must and want to especially thank Matteo for his friendship, for all the hours spent together in our conversations about science, for guiding me during the research activities, for his always worthy suggestions and helpful support. I consider myself very lucky to have the opportunity to work with him.

A great acknowledgment to Marco, Romolo, Augusto, Lele, Enrico and Anna, definitely the best friends of ever, for the countless hours spent together in lab, for the scientific and non-scientific discussions, for being always present when help is needed. Thank you for your sympathy, for your way of being, for your love for work and life.

Great thanks also go to Prof. Maria Letizia Focarete from the Chemistry Department at Alma Mater Studiorum-Università di Bologna, for her availability in sharing knowledge, for all the valuable teachings and the interesting research activities carried out together.

Many thanks to Prof. Davide Mariotti from Ulster University for welcoming me in his group during my short term mission, for the scientific conversations and the constructive collaboration we managed to set up.

A special acknowledgement goes to Prof. Lia Rimondini, Dr. Andrea Cochis and Prof. Barbara Azzimonti, from the University of Piemonte Orientale, for all the research activities performed together.

Thanks to Prof. Antonino Pollicino from University of Catania, for his great availability in collaborating with our group, for the valuable teachings and worthy suggestions.

An acknowledgment goes to Prof. Piero Favia from the University of Bari, for the instructive scientific conversations, and to the whole Scientific Community to which I proudly belong, for all the valuable scientific works, useful debates and talks, which contributed in widening my knowledge and in increasing my love for the scientific research activities.

Finally, a sincere acknowledgment goes to the Department of Industrial Engineering (DIN) and to the Advanced Mechanics and Materials, Interdepartmental Center for Industrial Research, Alma

Mater Studiorum—Università di Bologna. Many thanks go to AlmaPlasma srl, our spin-off, to which I wish all the best and a more than bright future, for all the fantastic, exciting and stimulating opportunities to put in practice the acquired knowledge.